

Functional Connectivity of the Visual Brain

and its Alteration by External Factors

Claire Beatriz Cécile Rosario Poullias (Linacre)

(claire.poullias@linacre.ox.ac.uk)

Department of Anatomy, Physiology and Genetics

University of Oxford

Supervisors:
Prof. Holly Bridge, Prof. Kristine Krug, Prof. Andrew J. Parker

Submitted: Hilary Term, 2023

Word Count: 47747

A dissertation submitted to the Department of Anatomy, Physiology and Genetics of the University of Oxford in partial fulfilment of the requirements for the degree of Doctor of Philosophy

To my grand-mother,

Rosario Jiménez Calvo,

for encouraging my curiosity

and pushing me to learn

as much as I could.

“El saber no ocupa lugar”

Acknowledgements

I would like to express my heartfelt gratitude to everyone who contributed to my journey toward completing this doctoral thesis. Regrettably but ultimately inevitably, I am certain that I will not manage to include everyone who has joined, supported, or briefly visited me on this long and eventful ride. To this end I can only hope those that I do not include below know that they were nonetheless appreciated and will forgive my momentary lapse.

First and foremost, I would like to thank my thesis supervisors for their invaluable insight and feedback. I would particularly like to thank Professors Kristine Krug for the opportunities she offered me and her support, notably during the COVID-19 pandemic, Holly Bridge for the persistently helpful conversations on MRI analysis and Andrew Parker for his patience, guidance and support, especially, though not exclusively, throughout the last year of my doctorate.

I am deeply grateful to the BBRSC and the ICase program for their generous financial support, without which I could not have undertaken my research. Their support allowed me to pursue my academic goals and opened up new avenues of knowledge and discovery.

I would be remiss if I did not acknowledge my colleagues and friends in both Oxford, where the doctoral journey began, and Magdeburg, where the final stages were realized. Their encouragement, feedback, and ideas have been invaluable. I would like to single out Drs Jackson Smith and Jérôme Sallet, both of whom dedicated substantial portions of their time to helping me as well as Andrew (Andy) Emberton for the support he provided in training the monkeys, and his work with Monkey Y specifically.

I want to express my heartfelt gratitude to my partner Michael. He has been my partner in

every sense of the word. I am deeply indebted to him for him willingness to proofread and edit my thesis. His unwavering support, patience, and understanding have been invaluable to me, and I could not have completed this work without him. Thank you for being a constant source of encouragement, for cheering me on during the challenging times, and for being my biggest champion. He has helped me stay organized, motivated, and focused, even when I felt overwhelmed or unsure of myself. I am incredibly fortunate to have him by my side, and I will forever be grateful for his love and support.

My sincere thanks also go out to my family. To my parents, Michel and Begoña, thank you for never questioning my (seemingly) crazy plans. They stood by my side through thick and thin, providing emotional and financial support, without question, whenever needed. Even in the face of their own challenges, they have always been there for me, cheering me on and offering words of both wisdom and comfort. To my sister, Laura, thank you for being my biggest fan and compiling of a list of the “best locations” in Paris for the past few years. I cannot wait to try all of them with you. I also want to thank my in-laws for their support, patience, and understanding. To Dr. Julia Spinthourakis, thank you for always being only a call away. My thoughts also go out to my late father-in-law, Dr. John Katsillis, for being a warm and loving presence in my life. I will always cherish the time we spent together, and I am forever grateful that you agreed to share your son with me.

I am grateful to Linacre College, for having been my home-away-from-home. I am particularly thankful for my friends from the Linacre College Bar; they were not only amazing to work with but also formidable peer supporters, in times of need. I am grateful to Dr. Raquel Maio for being a bubbly presence in my life and for regularly checking on my sanity. And, of course, I am grateful for the Linacre Ladies that Lift. They taught me I can always do better, reach

farther, and accomplish more than I think or anyone else assumes. They also reminded me that each failure is nothing more than a stepping stone on the path to success.

Finally, I would be remiss in not mentioning the three non-human primates that have been by my side, in a manner of speaking, for the last five years –despite their hard work not being part of this thesis, in the end. The animal technicians owe you (at least) an extra banana a piece.

Table of Contents

Acknowledgements i

Table of Contents iv

List of Figures ix

List of Tables xiii

Abstract xv

1 Introduction 1

1.1 Introduction and Statement of the Problem 1

1.2 Purpose and Significance of the Study 3

1.2.1 Primary Questions Examined in this Study 8

2 Methodology 10

2.1 Data Acquisition and MRI Sequences 10

2.2 MRI Preprocessing 11

2.3 Independent Component Analysis 11

2.4 Seed Based Correlation Analysis 21

2.4.1 From Seed Creation to Timeseries Extraction 21

2.4.2 Manual Seed Correction 24

2.4.3 Creating Functional Networks at the Individual Level 25

2.4.4 Higher Level Analysis 26

3 The Impact of Anaesthetic Agents on the Functional Brain 28

3.1 Introduction 28

3.2 Methods 31

3.2.1 Animals....31
3.2.2 Anaesthesia....31
3.2.3 Independent Component Analysis....35
3.2.4 Critical t-statistic Value....40
3.2.5 Criteria for Meaningful Significant Difference in Connectivity Strength....42
3.3 Results....43
3.3.1 Visual IC....44
3.3.2 Visual Association Networks....48
3.3.3 Non-Visual Networks....53
3.3.4 Statistical Comparison....63
3.4 Discussion....66
4 Effects of Isoflurane and Sevoflurane on Visual System Functional Connectivity....73
4.1 Introduction....73
4.1.1 Architecture of the Visual System....73
4.1.2 Functional Connectivity of the Visual System Under Anaesthesia....78
4.1.3 SBCA vs ICA in the Examination of Differential Localized Anaesthetic Effects..80
4.1.4 Impact of Statistical Significance Levels on Analysing Functional Connectivity in Visual System under Anaesthesia....81
4.2 Methodology....84
4.2.1 Animals and Anaesthesia....84
4.2.2 Seed Based Correlation Analysis (SBCA)....85

4.3 Results 88

4.3.1 Anesthetized Functional Connectivity of the Visual System Under Two Significance Levels 88

4.3.2 Comparison of the Visual System's Functional Connectivity Under Isoflurane Versus Under Sevoflurane by Visual Area 93

4.3.3 Statistical Comparison 102

4.4 Discussion 108

5 An Examination of Functional Connectivity in Macaque Visual Cortex Following Anatomical Damage Arising During Natural Developmental Processes 113

5.1 Introduction 113

5.1.1 The Central Role of V1 in Visual Processing 114

5.1.2 Lesions of V1 and Loss of Aware Vision 115

5.1.3 Thalamic Visual Pathways Circumventing V1 116

5.1.4 Resting State Functional Connectivity as a Tool to Study the Impact of a Natural Lesion of V1 120

5.2 Methods 122

5.2.1 Animals 122

5.2.2 Anaesthesia 129

5.2.3 Data Acquisition 129

5.2.4 Lesion Volume Calculation in the Lesion Animals 130

5.2.5 Seed Based Correlation Analysis (SBCA) 130

5.2.6 Connectivity Heatmaps 138

5.2.7 Comparison of Primary Visual Cortex Seed Connectivity Strength 141

5.3 Results 142

5.3.1 Lesion Description 142

5.3.2 Focal Impact of V1 Lesions over the Visual System Functional Connectivity 144

5.3.3 Functional Connectivity of the Calcarine vs the Operculum in Control Animals 176

5.4 Discussion 185

6 Summary, Conclusions, Limitations, and Recommendations 194

6.1 Summary 194

6.1.1 Method Summary 194

6.1.2 Comparison of Isoflurane and Sevoflurane Effects on the Whole Brain Functional Connectivity 195

6.1.3 Comparison of Isoflurane and Sevoflurane Effects on the Visual System Functional Connectivity 196

6.1.4 Exploring Changes in Functional Connectivity of the Visual System in Macaques with Natural Lesions of V1 196

6.2 Conclusions 199

6.2.1 The Practical Equivalence of Isoflurane and Sevoflurane in the Study of Functional Connectivity 199

6.2.2 Compensatory Pathways in V1 Lesioned Monkeys May Involve Strengthened Connections with the Remnants 200

6.3 Limitations 201

6.3.1 Limitations in Understanding the Impact of Lesions in V1 in Absence of Behavioural Data 201

6.3.2 Functional Connectivity Only Allows Limited Conclusions on Anatomy 205

6.3.3 The Challenges of Consistent and Reproducible Functional Connectivity Research Using Non-Human Primates 206

6.4 Recommendations 208

7 References 211

8 Appendices 265

8.1 Manual Seed Corrections 265

8.2 GLME Matrix Design 280

8.3 Noisy ICs 281

8.4 Group ICs 283

8.5 Group SBCA GLME Design Matrix 286

8.6 Whole Brain Level Functional Connectivity Differences 287

8.7 Functional Connectivity Comparisons Between the Calcarine Seeds: Part 1 291

8.8 Contrast Masking 292

8.9 Lesion Animal Functional Connectivity at z≥2.3 293

List of Figures

Figure 2.1 Independent Component Analysis Method.....15

Figure 2.2 Noisy IC Exclusion Criteria.....17

Figure 2.3 Obtaining Consistent IC Across Subjects for Group Comparison Through Dual Regression.....19

Figure 2.4 Seed Based Correlation Analysis (SBCA).....22

Figure 2.5 Seed Correction Example.....24

Figure 3.1 No Statistically Significant Difference Between Anaesthetic Agent Groups for Age, Delay Between Sedation and Data Acquisition, Median Systolic Blood Pressure, Expired CO2, Heart Rate, Respiratory Rate, Temperature, and Depth of Anaesthesia (Unpaired t-test).....35

Figure 3.2 Location of the Highest Correlated Voxel in the Group IC (Visual ICs).....45

Figure 3.3 Visual ICs Under Isoflurane and Sevoflurane.....46

Figure 3.4 Location of the Highest Correlated Voxel in Group IC (Visual Association ICs).....49

Figure 3.5 Visual Association ICs Under Isoflurane and Sevoflurane.....52

Figure 3.6 DMN Under Isoflurane and Sevoflurane.....53

Figure 3.7 Location of the Highest Correlated Voxel in Group IC (Somatomotor ICs).....54

Figure 3.8 Somatomotor ICs Under Isoflurane and Sevoflurane.....55

Figure 3.9 Auditory IC Under Isoflurane and Sevoflurane.....57

Figure 3.10 Insular ICs Under Isoflurane and Sevoflurane.....58

Figure 3.11 Location of the Highest Correlated Voxel in Group IC (Frontal ICs).....60

Figure 3.12 Frontal ICs Under Isoflurane and Sevoflurane.....61

Figure 3.13 Putamen IC Under Isoflurane and Sevoflurane.....62

Figure 3.14 Localised Significant Differences in Connectivity Strength.....65

Figure 4.1 Simplified Representation of the Visual System.....75

Figure 4.2 Visual Seed Locations.....86

Figure 4.3 Anesthetized Visual Resting State Functional Networks.....89

Figure 4.4 LGN's Functional Connectivity Under Sevoflurane and Isoflurane 94

Figure 4.5 V1 Functional Connectivity Under Sevoflurane and Isoflurane.....96

Figure 4.6 V2 Functional Connectivity Under Sevoflurane and Isoflurane.....97

Figure 4.7 V4DP Functional Connectivity Under Sevoflurane and Isoflurane 99

Figure 4.8 V5/MT Functional Connectivity Under Sevoflurane and Isoflurane.....100

Figure 4.9 FEF Functional Connectivity Under Sevoflurane and Isoflurane 102

Figure 4.10 SBCA Reveals Localized Differences Between the Visual Functional Connectivity Under Sevoflurane and Isoflurane.....107

Figure 4.11 Example of LGN Seed Placement in one Animal.....110

Figure 5.1 Structural Scan of the Lesion Animals Compared to the F99 Template.....114

Figure 5.2 Summary of Possible Alternative Visual Processing Pathways 119

Figure 5.3 Monkey Y's Performance Over Time on Odd One Out tasks.....127

Figure 5.4 Visual Seed Locations Outside the Primary Visual Cortex.....131

Figure 5.5 Location of the Primary Visual Cortex Seeds.....133

Figure 5.6 Visual Field Representation in V1 134

Figure 5.7 Obtaining Connectivity Heatmaps.....140

Figure 5.8 Structural Scan of Monkey S and Monkey Y, Compared to the F99 Template 143

Figure 5.9 Comparison Between the Functional Connectivity of the V1d Seed in the Lesion Animals Versus the Control Average 148

Figure 5.10 Comparison Between the Functional Connectivity of the V1v Seed in the Lesion Animals Versus the Control Average 150

Figure 5.11 Comparison Between the Functional Connectivity of the LGN in the Lesion Animals Versus the Control Average 154

Figure 5.12 Comparison Between the Functional Connectivity of the MT and FEF Seeds in the Lesion Animals Versus the Control Average 156

Figure 5.13 Comparison Between the Functional Connectivity of the Pulvinar in the Lesion Animals Versus the Control Average 161

Figure 5.14 Comparison Between the Functional Connectivity of the V2m and V2d Seeds in the Lesion Animals Versus the Control Average.....164

Figure 5.15 Comparison Between the Functional Connectivity of the V4DP and V4d Seeds in the Lesion Animals Versus the Control Average.....166

Figure 5.16 Comparison Between the Functional Connectivity of the V4v Seed in the Lesion Animals Versus the Control Average 167

Figure 5.17 Comparison Between the Functional Connectivity of the Superior Collliculus in the Lesion Animals Versus the Control Average 170

Figure 5.18 Difference in Connectivity Strength Between the Control Group and the Lesion Animals.....173

Figure 5.19 Functional Connectivity Differences Between Calcarine Seeds and V1d 178

Figure 5.20 Functional Connectivity Differences Between Calcarine Seeds and V1v 179

Figure 5.21 Comparison of the Operculum Seed Connectivity Strength Versus the Calcarine Seed.....183

Figure 8.1 GLME Matrix Design 280

Figure 8.2 Noisy ICs 281

Figure 8.3 Group IC 283

Figure 8.4 GLME Design Matrix for Group SBCA 286

Figure 8.5 Functional Connectivity Network of Isoflurane Compared to Sevoflurane in all Meaningful IC 287

Figure 8.6 GLME Design Matrix (1): Functional Connectivity Comparisons Between the Calcarine Seeds 291

Figure 8.7 Contrast Masking 292

Figure 8.8 Lesion Animal Functional Connectivity at z≥2.3 293

List of Tables

Table 3.1 Group IC Percentage of Explained Variance 37

Table 3.2 Bivariate Relationships Between Regressors of No Interest 39

Table 3.3 Contrasts Employed in the Group Analysis.....40

Table 3.4 Significant Difference Clusters location and Compliance with the Significance and Matching Network Criteria 64

Table 4.1 SBCA Contrasts.....87

Table 4.2 Significant Difference Cluster Location Summary.....106

Table 5.1 Seed locations outside the primary visual cortex.....132

Table 5.2 Contrasts Employed in the MLM Group Analysis for Differences Between the Functional Connectivity of the Calcarine Seed and the Operculum Seeds. 138

Table 5.3 AN.O.VA of Correlation Between Primary Visual Cortex and Visual and Subcortical Seeds 182

Table 8.1 Manual Seed Corrections for V5/MT 265

Table 8.2 Manual Seed Corrections for FEF.....266

Table 8.3 Manual Seed Corrections for V2m.....267

Table 8.4 Manual Seed Corrections for V2d 268

Table 8.5 Manual Seed Corrections for V1d 269

Table 8.6 Manual Seed Corrections for V1v 270

Table 8.7 Manual Seed Corrections for V4DP.....271

Table 8.8 Manual Seed Corrections for V4d 272

Table 8.9 Manual Seed Corrections for V4v 273

Table 8.10 Manual Seed Corrections for LGN.....274

Table 8.11 Manual Seed Corrections for Pulvinar 275

Table 8.12 Manual Seed Corrections for SC 276

Table 8.13 Manual Seed Corrections for V1Cal1 277

Table 8.14 Manual Seed Corrections for V1Cal2 278

Table 8.15 Manual Seed Corrections for V1C 279

Abstract

The brain's ability to receive and interpret visual inputs is supported by an ensemble of brain areas. Damage to any of these areas severely impacts the brain's ability to process visual information.

This study examines the case of two rhesus macaques (*Macaca mullatta*) with extensive, naturally occurring, bilateral lesions in their primary visual cortices (V1). V1 is essential to visual processing but these monkeys appear to have retained sight, suggesting their brains may have developed mechanisms compensating for these lesions. Abnormal functional networks, however, may indicate corresponding structural changes. The extent of these lesions strongly alluded to large disturbances to the lesion animals' visual systems' functional connectivity. Thus, the primary purpose of this study was to examine the functional connectivity of the visual system and how it is affected by different anaesthetics but also by the existence of lesions in the primary visual cortex.

Resting state connectivity is a measure of temporal correlation in spontaneous blood oxygen level–dependent (BOLD) signal, in at rest subjects. Temporally correlated areas are organized into resting state functional networks, which often have anatomic equivalents. Macaques' resting-state data are usually acquired under anaesthesia. Anaesthetics impact functional connectivity strength and network sizes. It is unclear if all anaesthetics have the same impact. Thus, before examining how V1 lesions affect the visual system's functional connectivity, we investigated the impact of two commonly used anaesthetics.

Independent component analysis was applied to data from 23 healthy animals (14 Isoflurane, 10 Sevoflurane) to examine differential anaesthetic effects at the whole brain level. Seed based correlation analysis (SBCA) was then used to examine the functional connectivity of the

visual system. The results of these analyses indicated broadly equivalent effects from the two anaesthetics that are, however, characterised by small, localized, statistically significant differences over both the whole brain and the visual system specifically.

Our examination of compensatory visual processing mechanisms was limited to the 14 subjects anaesthetized using isoflurane –the anaesthetic applied to the lesion monkeys. We employed SBCA to compare the lesion monkeys' V1 functional connectivity to that in the 14 healthy controls and to isolate variations in the functional connectivity of two thalamic pathways. We also examined the correlation between 12 regions of interest (ROI) in the lesion and control animals. Finally, we examined correlations between these ROI, the V1 calcarine, and V1 operculum in the 14 healthy subjects. Stronger connections may indicate structural connections –a baseline against which we were able to compare our lesion monkeys, seeking substantive insight into compensatory visual processing mechanisms.

The V1 lesions had surprisingly little impact on the aforementioned functional connectivity networks. There was increased connectivity strength between the lesion monkeys' V1 remnants and several areas of the visual cortex. Examinations of the healthy animals returned limited-but-compelling evidence supporting the existence of stronger connections between V1 calcarine and two of these areas. One of the two lesion monkeys also presented stronger correlations between two areas belonging to one of the thalamic pathways, potentially indicative of new structural connections supporting otherwise perplexingly persistent sight.

1 Introduction

1.1 Introduction and Statement of the Problem

The study of the brain is an endeavour both fascinating and exciting. Neurosciences are driven by the hope that a better understanding of the brain's architecture, function, connectivity, and topographic organization will lead to advancements in the treatment of neurological and psychological illnesses, but also to a comprehension of the human condition.

Visual Perception is perhaps the most tangible of brain functions; most of the world's population experiences it daily. Visual perception is defined as the brain's ability to receive and interpret visual stimuli. This process involves two main components. The visual receptive component and the visual cognitive component. The visual receptive component (or sensory function) retrieves and organizes information from the environment. In its purest form, this function is performed by the retina. The retina receives visual input which activates different retinal cell types (i.e., cones & rods), sorting visual information by characteristics (e.g., colours, dark/light contrast, etc.) (Masland, 2012). The visual cognitive component enables structuring and translating this information to ascribe meaning to it (i.e., to what is seen). From the retina towards the remainder of the visual system, processing of visual information progressively shifts from visual stimuli reception to visual cognition. Some low-level visual processing takes place as early as the lateral geniculate nucleus (LGN) (see review by Usrey & Alitto, 2015), which is the first cerebral nucleus to receive visual information. Thereafter, increasingly complex processing takes place in the visual cortex. The primary visual cortex (V1) is the first cortical relay of visual processing. V1 is primarily considered to be the area which refines edges and orientation (Hubel & Wiesel, 1959). In primates, V1 neurons also discriminate directions, spatial and temporal frequencies, binocular disparity, and colours (Cumming &

DeAngelis, 2001; DeAngelis et al., 1998; Horwitz & Hass, 2012; Movshon et al., 1978). Further refinement is then performed by the cortical visual areas of the ventral (i.e., colour, object recognition) and dorsal (i.e., motion, spatial tasks, visual-motor skills) pathways (Goodale & Milner, 1992; Ungerleider & Mishkin, 1982a). Both pathways end in visual association areas (e.g., TE,TEO, LIP, FEF, etc.), which perform the most specialised processing functions (Schall et al., 1995; Setogawa et al., 2021; Shadlen & Newsome, 1996; Ungerleider & Mishkin, 1982b). Visual perception, however, does not always function as intended.

Visual perception disorders are the result of the brain's failure to perform either one of the two aforementioned functions (see Ffytche et al., 2010; Girkin & Miller, 2001). Blindness is arguably the layperson's most familiar form of visual perception deficit. As recently as 2020, 49.1 million people worldwide were blind and 33.6 million more suffered from severe vision impairment (Bourne et al., 2020). On the individual level, blindness can often represent a substantial impact to quality of life. Although by no means universal, individuals can learn to deal with visual perception deficits to an astonishing level (Nyquist et al., 2016) and in some cases to have their vision partially restored (University of California, Irvine, 2022). On the group or even societal level, however, visual perception deficits represent a staggering economic burden. In the United Kingdom (UK), for example, 1.93 million people are affected by sight loss and blindness, corresponding to an estimated governmental expenditure of between £15.8 and £28.1 in 2013 (Pezzullo et al., 2018). This figure increased to £36.0 billion by 2019, and is expected to increase by a further £1.7 billion due to delays in treatment caused by the COVID-19 pandemic (Deloitte Economics, 2021, p. 19). From a certain point of view, to continue using the example of the UK, one could even argue that this fiscal burden returns to the individual level, via the taxes which fund the National Health Service (NHS) in their treatment and support of individuals with visual perception deficits. Regardless, while

healthcare systems, such as the NHS, play a vital role in supporting and treating individuals with visual perception deficits, they are far from able to effectively deal with many of these deficits and, indeed, struggle more, the more severe the deficit becomes. This is not to say that science has made no efforts to positively impact this area.

Attempts at developing visual prosthetics, a.k.a. electronic devices implanted into the visual pathway to restore some extent of sight, have been ongoing since Foerster (1929) discovered that stimulating a blind patient's visual cortex would make him perceive small bright dots, called phosphenes. Indeed, decades of experiments have shown that both humans (Bak et al., 1990; Bosking et al., 2017; Brindley & Lewin, 1968) and animals –most notably macaques (Bartlett & Doty, 1980; X. Chen et al., 2020; Tehovnik & Slocum, 2007)– can reliably perceive phosphenes, following cortical stimulation. Some headway has been made using retinal (Humayun S. et al., 2003; Stingl et al., 2013) and cortical implants (Dobelle, 2000; Dobelle et al., 1976) as visual prosthesis. Nevertheless, while current visual prostheses offer an undoubtedly welcomed alternative to the absolute lack of sight, however, they remain painfully inefficient. Indeed, no study has been able to go past the simple evocation of phosphenes to create complex precepts (e.g., a line). Therefore, it is necessary to further and refine our knowledge of the visual system.

1.2 Purpose and Significance of the Study

This study has is centred on an examination of the functional connectivity of the visual system in macaque monkeys. The functional connectivity of the brain reflects the anatomy of the brain. As a result, changes in functional connectivity often correspond to anatomical changes. We had access to two rhesus macaque (*Macaca mulatta*) monkeys with lesions in their primary visual cortices (the region of the brain most prominently associated with visual

processing). Despite missing substantial portions of their primary visual cortices, these two monkeys still appeared to possess the ability to see (to varying degrees). Taking this deviation from normal brain anatomy as a given, we are then interested in examining what effect it may have on the rest of the visual system. We accomplish this by examining the functional connectivity of the visual system in these atypical brains. Our findings regarding differences in the functional connectivity of the visual system may then correspond to the development of anatomical changes which correspond to compensatory mechanisms, allowing our lesion monkey subjects the ability to see (in a limited or otherwise capacity).

The majority of studies aiming to contribute to the development of cortical visual prosthetics target V1 for stimulation (see Cicmil & Krug, 2015). The preoccupation with V1 is, of course, understandable. The primary visual cortex is the cortical entry of visual information, receiving most of the inputs from the retina through the LGN, and V1, either directly or indirectly through the visual area 2 (V2), and sends afferences to all the subsequent visual areas (Felleman & Van Essen, 1991; Maunsell & Newsome, 1987). Its anatomic organization (Lund, 1973, 1988), retinotopy (Van Essen et al., 1984), and stimulus selectivity (Hubel & Wiesel, 1959, 1962) are also well described in the literature. Focusing on V1, however, contributes to the gap in knowledge hindering the development of efficient visual prostheses. Some blindness is, indeed, due to one or more lesions in V1 (Giaschi et al., 2003). There is, however, much to learn about how the *other* brain areas contribute to the processing of visual information and, potentially more importantly, how this information could be processed *without* V1.

Visual perception is supported by the visual system. Historically, the study of the visual system has primarily involved invasive methods, such as histology (Hendry et al., 1994) or

electrophysiology (Hubel & Wiesel, 1962). As a result of this and the obvious corresponding ethical connotations, the use of the animal model has proven instrumental as well as invaluable. Primates, such as rhesus macaques, have proven to be an excellent choice for studying vision. Their visual system has been extensively mapped (Felleman & Van Essen, 1991) and presents reasonably good equivalencies to the human visual cortex (Sereno & Tootell, 2005). Furthermore, macaques also experience vision the same way humans do (Ben-Haim et al., 2021; Jacobs, 1996).

The use of imaging methods such as functional Magnetic Resonance Imaging (fMRI) greatly facilitate the study of the visual system, most notably through the study of its functional connectivity. Resting state functional connectivity is extracted from datasets comprised of measurements from subjects who were in a relaxed/resting state. The resulting functional connectivity extracted from such data are specifically referred to as Resting State Functional Connectivity (Tippett & Keser, 2022). While a subject is at rest, it is possible to capture random fluctuations in the Blood-oxygen-level-dependent (BOLD) signal (B. Biswal et al., 1995; B. B. Biswal, 2012). These fluctuations can, in turn, be organized into resting state functional networks (Bukhari et al., 2017; Fox & Raichle, 2007; Vincent et al., 2007). The areas belonging to a functional network are assumed to be components of the same structural network. Thus, it is possible that deviations from a given normative functional connectivity network may reflect structural changes (Allen et al., 2007; Anand et al., 2009; Cauda et al., 2009).

In human studies, using subjects at rest presents several tangible benefits, above and beyond its non-invasive nature. These benefits include, though are not necessarily limited to, the absence of prerequisite subject training and the possibility to study heavily impaired patients (e.g., patients in a coma, with very low IQs, and those with motor disabilities) (Figueroa-Jimenez et al., 2021; Kaushal et al., 2017; Pugin et al., 2020). Animal models also employ

resting state connectivity studies. Indeed, using non-invasive methods on animals and especially primates (Hutchison & Everling, 2012), has proven useful in obtaining a deeper understanding of how certain pathologies can affect the functional network (e.g., in pre-/post-lesion examinations on the same subject), understanding neuronal mechanisms using a combination of imagery and an invasive methods (Logothetis et al., 2001), and in developing new research tools, before they are deemed safe for human use (Folloni et al., 2019).

Obtaining high quality resting state data from animals can be problematic, because of the difficulties in exerting behavioural control over such subjects. As a result, studies using non-human primates, such as the rhesus macaque, frequently acquire resting-state data under anaesthesia. This study is no exception, in this regard. It is, however, generally accepted that functional MRI scans of *anaesthetized animals* yield resting-state functional connectivity networks (RSN) that differ from the equivalent networks obtained from *awake resting animals* (Hudetz, 2012; Nallasamy & Tsao, 2011). A crucial step in providing a more comprehensive and meaningful description of the functional connectivity of the monkeys with lesions in the primary visual cortex is to address the impact of anaesthetics on the functional connectivity of the brain as a whole and the visual system in particular.

Anaesthetic agents' effects on functional connectivity in the resting state can be better understood in relation to bias(es) they might introduce into RSN analyses. Acquiring and enhancing this understanding is a prerequisite for establishing a framework that will enable us to minimize the impact of such bias(es). Isoflurane and sevoflurane are two inhalational anaesthetic agents routinely used in primate trials, which are notably perceived to be ostensibly interchangeable, based on comparisons between awake and anaesthetized states (e.g., Muta et al., 2022; Uhrig et al., 2018). This perception, however, is not based on the result of formal testing between the two anaesthetics but rather is the result of informed but

informal observational comparison between the effects of each on the resting vs awake states. Given the prevalence of isoflurane and sevoflurane in the collection of resting state data from primates, and the relative frequency of primate to human studies, formally testing for the existence of such differences seems not only advisable but, arguably, necessary. If one further extends the analogy to the significance of the visual system, it becomes apparent that a generalized examination of differences in resting state connectivity between the two agents, while necessary, may nonetheless be insufficient. Indeed, it is only knowing if such differences exist and, if they exist, where and to what extent, that we can then hope to meaningfully examine resting state functional connectivity data collected under the influence one or the other agent.

This knowledge has numerous potential applications. The prevalence of the two anaesthetic agents means that potential differentiations in their effects on the brain could have far reaching consequences for practical research considerations, including research comparability, animal welfare and, in a more mundane sense, costs. In the event that granular differences do exist, they may also inform research design for more specialized studies and procedures. Possessing the results of formal tests for differences between the effects of isoflurane and sevoflurane on resting state connectivity of the brain, both in general and the visual system in particular, may facilitate the extrapolation of meaningful information regarding the effect of lesions in sections of the brain associated with visual processing on visual functional connectivity. This, in turn, may offer greater insight into one or more of the compensatory mechanisms employed by the brain in an attempt to restore sight to subjects that should, by all accounts, be sightless. Indeed, while the plasticity of the brain could be argued to be both common knowledge and among its more intriguing aspects, the manner in which this plasticity expresses itself is largely unknown. As such, any information into the

underlying mechanisms of said plasticity would, by definition, represent a substantial and enthralling addition to the body of scientific knowledge in the field.

1.2.1 Primary Questions Examined in this Study

Any examination of the visual processing system, much less the brain as a whole, necessarily entails a plethora of questions. Three central questions, listed below, guide this study:

1. Is there a difference in the effect(s) of isoflurane and sevoflurane on the Functional Connectivity of the whole brain?
2. Is there a difference in the effects of isoflurane and sevoflurane on the Functional Connectivity of the visual system, specifically?
3. What compensation mechanisms explain the "blindsight" phenomenon resultant from substantial lesions in the primary visual cortex?

These three questions lead us from a general examination of the state in which we are examining subjects' brains, to the variations in their conditions as we examine the function of their visual processing systems, to specific examinations thereof. Isoflurane and sevoflurane are an important part of the majority of resting state network studies. Understanding their comparative functional profiles provides us with important theoretical and practical knowledge, while also enhancing our understanding of anaesthetics, the brain, and the effect of anaesthetics on the brain. An understanding of the differential effects, if any, of isoflurane and sevoflurane on the resting state functional connectivity of the visual system provides important insight into visual processing. Specific examinations of monkeys with lesions in V1 may expand our understanding of one or more compensatory mechanisms related to vision. This could, in turn, inform future research on blindsight, clinical trials for blindness, and

deepen our understanding on the processing of visual information outside the primary visual cortex.

The following chapters present:

a. the various methodologies employed in this study (see Chapter 2), followed by
b. the examination of the differences between the effects of isoflurane and sevoflurane on functional connectivity at the whole brain level (see Chapter 3),
c. the differences between the two agents on the functional connectivity of the visual system (see Chapter 4),
d. An examination of functional connectivity in macaque following a natural anatomical damage arising during natural developmental processes (see Chapter 5), and are completed in
e. a summary discussion, and a presentation of our conclusions, limitations, and recommendations for future research (see Chapter 6).

2 Methodology

This chapter discusses the consideration and procedures employed to collect and analyse resting state functional magnetic resonance imaging (fMRI) data in order to study functional connectivity.

Specifically, this chapter describes:

a. The data acquisition process and the MRI sequences used
b. A description of the benefit of running an Independent Component Analysis and its process
c. A description of Seed Based Correlation Analysis and the methodology employed to run it.

2.1 Data Acquisition and MRI Sequences

The MRI data at the core of this thesis was acquired in anaesthetized rhesus macaques (*Macaca mulatta*) in a 3T Siemens clinical MRI scanner[1]. The monkeys entered the scanner in a sphinx position (head first, laying on their belly, eyes closed). The animals' head was maintained raised and straight using a MRI-compatible stereotactic frame (Crist Instrument).

Data were collected using a four-channel phased-array radiofrequency coil in conjunction with a local transmission coil (H. Kolster, Windmiller Kolster Scientific, Fresno, CA). For each animal between one and three high-resolution (voxel size 0.5 mm x 0.5 mm x 0.5 mm) T1-weighted structural images were acquired using a 3D magnetisation-prepared rapid-acquisition gradient echo (MPRAGE) (TE = 4.04 ms; TR = 2500 ms; flip angle = 8°, 128 slices). If more than one structural scan for a given subject was acquired, scans were summed using

[1] For more details about the animals included and the anaesthesia procedure for each experiment, see Chapters 3.2.2, 4.2.1 and 5.2.2.

the FMRIB Software Library (FSL) (Fischl et al., 1999; Jenkinson et al., 2012; Reuter et al., 2012) *fslmaths* function. Resting state functional Magnetic Resonance Imaging (rsfMRI) data were acquired using a gradient-echo T2* echo planar imaging (EPI) sequence (2.0 mm x 2.0 mm x 2.0 mm resolution, 36 ascending slices, TR = 2.00 s, TE = 19 ms, flip angle = 90°).

2.2 MRI Preprocessing

Acquired functional and structural data were initially subjected to a visual quality check. Before further analysis, the data were pre-processed using tools from FSL (Fischl et al., 1999; Jenkinson et al., 2012; Reuter et al., 2012). First, non-brain structures were removed from both raw structural and raw fMRI resting state data using FSL's brain extraction function (BET) (Smith, 2002).

Next, resting state fMRI data were high pass filtered using the fslmaths function (hp_sigma:1, lp_sigma:5). The balance of fMRI data pre-processing was carried out using FSL's FEAT function first level analysis GUI (Woolrich et al., 2001). In FEAT, the first 6 volumes were removed to ensure radiofrequency excitation was consistent. Spatial smoothing (Gaussian 3mm FWHM kernel), intensity normalization, a high-pass filter cut off point set to the default suggested threshold adjustment (Woolrich et al., 2001) of 50s, and motion correction (McFLIRT) were applied. Registration was not carried out at this stage. Once image pre-processing was complete, either an Independent Component Analysis (ICA) or a Seed-Based Correlation Analysis (SBCA) could be applied to address the scientific questions posed in this thesis.

2.3 Independent Component Analysis

ICA is a signal processing method which separates a multivariate signal (e.g., BOLD), into

additive subcomponents (also referred to as factors, latent variables, sources, and Independent Components (IC)), each of which explains a percentage of the multivariate signal variance. ICA assumes that the source IC signals are (statistically) independent from one another and that their signal is non-Gaussian. The first assumption is a fundamental necessity for ICA to be possible so that the component source signals can be disambiguated into a set of statistically independent factors. The second assumption is made as a result of the mathematics of ICA and is based on the Central Limit Theorem (CLT). The mathematics that proves this, while interesting, has been presented rigorously by Hyvärinen and Oja (2000) and is beyond the scope of this thesis. In lay terms, however, as a result of the CLT, the distribution of aggregate variables will be approximately Gaussian, whether the component variables aggregated are Gaussian or not (and that their distribution will be increasingly more Gaussian, as the number of components increases towards infinity). It follows from this, that the distribution of aggregate variables will be more closely Gaussian than that of the components that comprise them. For obvious reasons, this second statement can only be true if none of the component variables that comprise the aggregate are, themselves, Gaussian. ICA combines this idea, along with measures of how far from Gaussian the distributions of potential component variables are (e.g. skew, kurtosis) and the independence assumption, to disambiguate them from the aggregate signal.

A classic example where such separation would be desirable is evident in what Cherry (1953) termed “the cocktail party problem”, wherein the researcher would attempt to ascertain the words of one individual (a single signal) amid the concurrent speech of several other individuals (the multivariate signal). To extend the analogy, here ICA was used to decompose the BOLD signal into isolated signals that originate in different areas of the brain but

nonetheless behave in the same way across time[2].

FSL's Multivariate Exploratory Linear Optimized Decomposition into Independent Components (MELODIC) (Jenkinson et al., 2012) tool makes ICA a relatively easy proposition. It decomposes four-dimensional (4D) datasets into ICs and excels at Blind Source Separation (BSS)[3](Cardoso, 1998). The researcher needs only input the data in MELODIC without having to make any hypotheses about it (i.e., without requiring a commensurate General Linear Model (GLM), postulations regarding brain area activity levels, overarching experimental design, etc.). As a consequence, ICA via MELODIC is an ideal vessel to perform a comprehensive, albeit initial, sweep of the data and obtain functional networks across the totality of the brain. The outcome should reveal potential relationships that can then be subjected to further hypothesis-based testing.

The ICA methodology employed in this study is illustrated in Figure 2.1. The first step in obtaining functional networks from the preprocessed rsfMRI data were to apply an ICA to each subject's functional images. The output of each single-subject ICA is reorganized in a space-by-time matrix. Individual-level ICA then decomposes this matrix into ICs (i.e., a set of spatial maps with their corresponding time course). In lay terms, it outputs the portions of the brain that behave similarly over time.

McKeon et al. (1998) suggest transforming the spatial maps to Z-score maps such that they have a zero mean and unit variance. They also recommend applying a preselected threshold (e.g., $|z| >$

[2] Such common signal behavior across time is often perceived to indicate the existence of a functional network. It should be noted, however, that for a functional network to meaningfully exist, the signal must also be neuronal in origin.

[3] BSS refers to the separation of a set of signals from a multivariate signal with the aid of little or no information about the individual signals or their mixing process (Cardoso, 1998).

2) when visualizing the Z-score maps to be able to discriminate "areas of activation" from background noise. The spatial maps, however, are the result of a signal decomposition by ICA and, as such, spatial intensities are by nature non-Gaussian. A simple transformation of the spatial intensities to voxel-wise Z-scores and the subsequent imposition of a threshold would result in a random false-positive rate (Beckmann & Smith, 2004). Thus, any voxels surviving the threshold (i.e., active voxels) could in fact be meaningless, since we would be inherently unsure if they were the result of false positives. To prevent this, MELODIC's contributors Beckmann and Smith (2004), propose a different approach in their toolbox. The residual noise in each voxel within the IC spatial map is estimated. They then convert the map to a z-score map by dividing it by the estimate of the standard deviation of the voxel-wise noise. From the z-score map, using an alternative hypothesis approach and a mixed Gaussian/Gamma model, a posterior probability map is established (i.e., a map of the probability of any intensity value to be background noise).

Posterior probability is a form of conditional probability, whose value results from updating pre-existing (or prior/ *a priori*) probabilities based on information obtained via an application of Bayes' theorem. In other words, it is a probability which is informed as a conditional probability based on prior knowledge (obtained under a Gaussian/Gamma model) of conditions assumed to be related to a voxel being truly active (or, inversely, to being a background noise artefact). In formal applications, where theoretical and/or mathematical examinations take place, the posterior probability of (one or more) parameters θ, given a body of evidence X, is denoted by $p(\theta|X)$. Unfortunately, in less rigorous applications, posterior probability is regularly symbolically represented by the same p as the probability of generalization error used in the examination of statistical significance. Of course, while the two should not be confused, their differentiation is often down to contextual cues.

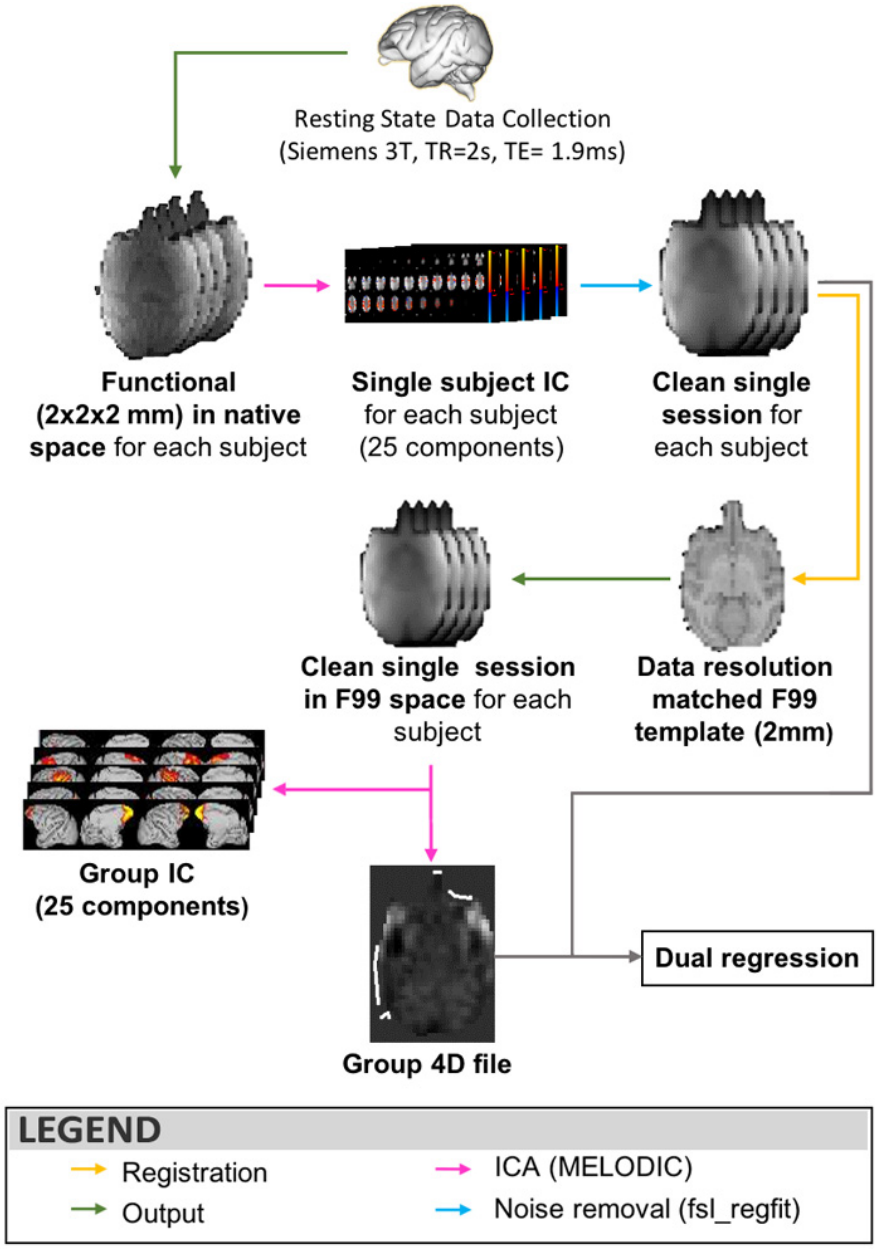


Figure 2.1 Independent Component Analysis Method

For each monkey, a functional scan was acquired under anaesthesia (Siemens 3T). The Independent component analysis ICA is a signal processing method which splits a multivariate signal into independent component that each explain a portion of the variance. After preprocessing the functional data, an ICA at the single subject level for each animal was run. Next the noisy components were manually excluded (fsl_regflit). The cleaned ICs were register from the functional space to a data resolution matched F99 template (2x2x2 mm) before running a group ICA (MELODIC). The group analysis outputs the IC at the group level along with a 4D image wherein each volume corresponds to a group IC. At this stage no difference between subject group was taken into account. To perform a group comparison, the group IC 4D file had to be entered into FSL's dual_regression, joined with the registered clean individual ICs, to employ a dual regression and statistical analysis.

The value of the posterior probability at which a voxel is deemed to be truly active or not is left to the researcher's discretion but is set, by default, to 0.50. This places equal importance

on false positives and false negatives and, lacking meaningful evidence supporting one or the other possibility, is indeed the suggested posterior probability threshold. Thresholded ICs, which can be visualized by the experimenter, are the result of the single subject ICA. Example special maps and the criteria used to exclude noisy ICs are presented in Figure 2.2.

By default, MELODIC outputs can contain exceedingly large numbers of ICs, increasing the risk of artificially splitting a real network into several, artificial, networks. This is not necessarily a problem unique to MELODIC as, indeed, ICA cannot inherently determine the true number of component signals. To avoid the potential for artificial network identification, studies run on humans have classically limited the allowable number of ICs from such analyses to between 20 and 30 (Abou Elseoud et al., 2011; Smith, 2002; Y. Chou et al., 2018). By this practice, the number of IC outputs was limited to a maximum of 25 statistically independent spatial maps and time-course couples for each subject. These maps cannot yet be called individual functional connectivity maps because, as noted previously, not all of them represent neural activity. Some of them are the result of noise artifacts, which can include, among other things, cardiac activity, head motion, and so on. They are therefore simply correlation structures in the data sets.

A visual inspection of the ICs was conducted, to isolate the individual functional connectivity maps from ICs resulting from noise artifacts for each animal. Noisy components were isolated based on their spatial map, time course, and power spectrum (Griffanti et al., 2017) (see Figure 2.2). An ideal signal IC spatial map (i.e., one that is not the result of noise artifacts) presents a limited number of large clusters of significant voxels ($p \leq 0.05$) overlapping the grey matter. In addition, its time course is fairly oscillatory and regular, and its power spectrum presents at least one strong peak within 0.01 – 0.10 Hz (Griffanti et al., 2017). Each subject's noisy ICs were excluded, using *fsl_regfit*, to obtain a 4D file including only the individual functional connectivity maps for each animal (i.e., the noisy ICs have been deleted). This 4D file can, in turn, be used in a group level ICA (see Figure 2.2).

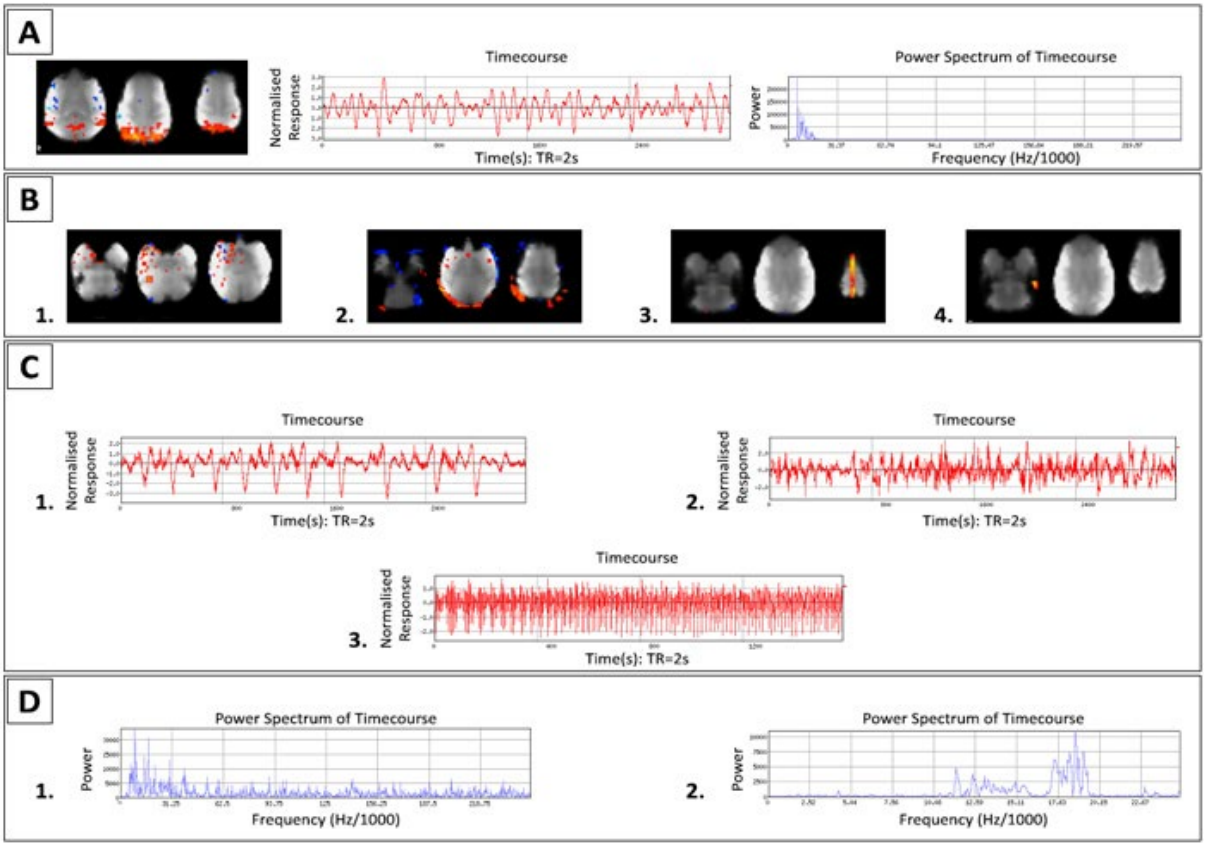


Figure 2.2 Noisy IC Exclusion Criteria

Panel A *presents an example of a spatial map, including a time course and a power spectrum for an ideal IC. The spatial map has large clusters of significant voxels (posterior probability >0.5) in the grey matter. Panels A and B present three transversal slices from spatial maps of five different IC obtained after running an individual ICA in three animals (Monkey Oct, Monkey Orc and Monkey Orv (A. Orc IC14; B: 1. Orv IC1 /2.Orv IC7/ 3.Oct IC4/ 4.Oct IC19)). The ideal timecourse is smooth. The power spectrum shows a neat spike in the low frequencies (at the beginning of the curve). B,C, and D show the most prevalent examples of noisy IC attributes in this thesis (see Salimi-Khorshidi et al.* (2014) *for other examples). IC possessing at least one of the presented attributes were classified as noisy and rejected.*

Panel B *presents noisy spatial maps (posterior probability p>0.5) -specifically: In (1) the IC is mainly unilateral and does not present uniform clusters of significant voxels in the grey matter. In (2) the IC forms a ring around the brain. This type of IC is traditionally associated to head motion but movements due to breathing is more likely here (anesthetized animals). (3) represents the sagittal sinus. In (4) all significant voxels are outside the brain.*

Panel C *presents noisy time courses In (1), the timecourse is overly regular which suggests it is due to cardiac activity, while (2) & (3) are examples of irregular time courses.*

Panel D presents noisy power spectrums. In (1) there is no clear spike at the beginning of the curve. In (2) the spike is in the high frequencies.

The group level ICA aims to isolate networks of activity that are common to all subjects within a given group. At this stage, the ICA is run across all the data as if it were a uniform ensemble (i.e., ignoring potential variations in experimental conditions). This is necessary as ICA cannot identify a uniquely correct ordering of the ICs it outputs. As a result, if one were to conduct two separate ICAs, for example under two discrete experimental conditions (e.g., under the

influence of isoflurane and sevoflurane), the ICs output by the two different group analyses would not be directly comparable. Thus, if the study aims to evaluate the potential impact of one or more experimental conditions over the functional network, it is then best practice to run the ICA on the data from all the subjects pooled together.

To run the group ICA, an affine registration was performed from each clean 4D file, to a "Data resolution matched" version of the F99 template, using FSL FMRIB's Linear Image Registration Tool (FLIRT) (Greve & Fischl, 2009; Jenkinson et al., 2002; Jenkinson & Smith, 2001). The "Data resolution matched" is down-sampled from the native resolution of the F99 template (0.5mm x 0.5mm x 0.5mm) to match the resolution of the functional images (2mm x 2mm x 2mm). Registration with FLIRT makes the output adopt the resolution of the reference image. Consequently, in the present case, using a resolution-matched template is more computationally efficient because does not change the resolution of the individual ICA outputs, the resolution at which the group ICA is going to be run. Next, the realigned, clean 4D files were inputted into MELODIC and a multisession temporal concatenation ICA was run on the overall dataset. Multisession temporal concatenation is the recommended approach "in cases where one is looking for common spatial patterns but cannot assume that the associated temporal response is consistent between sessions/subjects" (Griffanti, 2019, p. FSLwiki FSLwiki - MELODIC) . Each individual brain was realigned to F99 space, providing subjects in the group with a common spatial pattern. It is still, however, not possible to assume that the temporal response pattern is consistent across subjects for this kind of dataset because of the spontaneous nature of resting state activity.

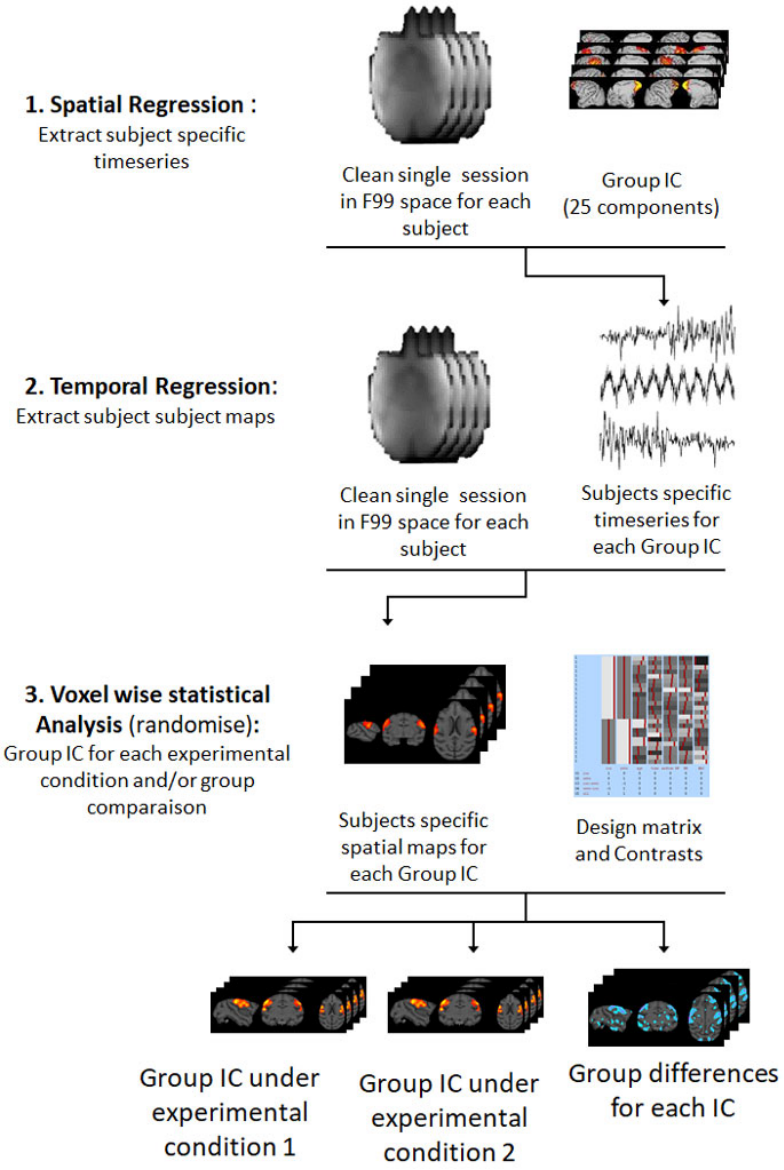


Figure 2.3 Obtaining Consistent IC Across Subjects for Group Comparison Through Dual Regression

To be able to compare group ICs across experimental conditions, each group IC must be consistent across experimental conditions. This is not the case if the ICA is run individually for each condition. The ICA must include all subjects, disregarding experimental conditions, and a dual regression used to obtain consistent group IC for each experimental condition. Here, the ICA outputs 25 group IC. The dual regression consists of two regression analyses. Initially, it spatially regresses each of the group-level ICs onto the clean, individual-subject's data, in order to extract subject-specific timeseries, for each group IC. These timeseries are then input into the temporal regression, to be regressed onto the clean, individual-subject's data, to obtain subject-specific spatial maps for each group. A common voxel-wise statistical analysis can now be employed. The subject-specific maps and a design matrix (a set of regressors and alternative hypotheses) are input into FSL's randomise function. This can then return the group average for each experimental condition and IC, the results of a group comparison, etc.

In the group analysis, the data from each animal are rearranged in a time-by-space matrix. Matrices are then concatenated along the time dimension and the ICA is run on all data simultaneously. The

ICA outputs a set of spatial maps and associated time courses. Here, however, the resultant ICs represent signals common to all of the subjects contained in the dataset. Here too, and for the same reasons, dimensionality was limited to 25 ICs. Thus, 25 spatial maps were obtained as the outcome of the group level ICA. The group level ICA also outputs a 4D file containing all the group ICs, that can be used as an input in FSL's dual regression function.

In order to visualize functional networks under a particular experimental condition (e.g., anaesthetic employed) or in a particular subject, a dual regression must first be run (see Figure 2.3). The dual regression evaluates the contribution of each subject to each of the group ICs. FSL's dual_regression (Nickerson et al., 2017) is performed in two steps. The first is a spatial regression which uses the group and individual clean IC 4D files for each subject. In other words, each of the group-level ICs is regressed onto the individual subject's data. This results in a subject specific time course for each IC of the group analysis. In the second step, all of the subject specific time courses for a given IC are fed into a temporal regression. The outcome of this regression is a subject specific spatial map for each group IC. In short, the dual regression transforms the data from a set of group IC to a set of subject specific IC for each of the aforementioned group ICs.

Now, the individual spatial maps can be used in a voxel-wise statistical analysis, to examine, among other things, variation between subjects along a –common IC dimension as a result of different experimental condition(s) and intersubject differences. This can also be achieved by dual_regression, which calls the FSL randomize function to perform the relevant non-parametric tests. This approach, which is employed later in this study, requires the researcher to input a design matrix and set of contrasts. The design matrix lists the regressors to be considered in the GLM or, more appropriately, in our case, the Generalized Linear Mixed-Effects

(GLME) model. The GLME is, functionally, an extension of the GLM for grouped data (e.g., into isoflurane and sevoflurane groups). The contrasts determine which hypothesis (or hypotheses) will be tested. The output of this analysis indicates the average spatial map for all subjects within an experimental group for each selected IC but also indicates where there are significant differences in shape and strength in the network between the various conditions.

All presented results presented in this study are oriented according to the radiological convention.

2.4 Seed Based Correlation Analysis

Seed Based Correlation Analysis (SBCA) is an hypothesis-based method which calculates the temporal correlation between a region of interest (a defined set of voxels referred to as a *seed*) and the remaining voxels in the brain's grey matter (B. Biswal et al., 1995; Fox et al., 2006). Therefore, it is particularly useful for testing if two brain areas may be involved in a same functional network. Results, however, are tied to seed size and location. It is, therefore, important to ensure that the chosen seed is properly located in the studied region of interest and only involves grey matter voxels. If the study involves a group analysis, the seed location and size must be consistent across subjects.

2.4.1 From Seed Creation to Timeseries Extraction

A visual guide to the process of SBCA is presented in Figure 2.4.

In order to set up SBCA, seeds must first be selected, then created. Seed selection varies from study to study and has been left to researcher discretion, dependent on subject matter and pre-existing empirical and theoretical literature.

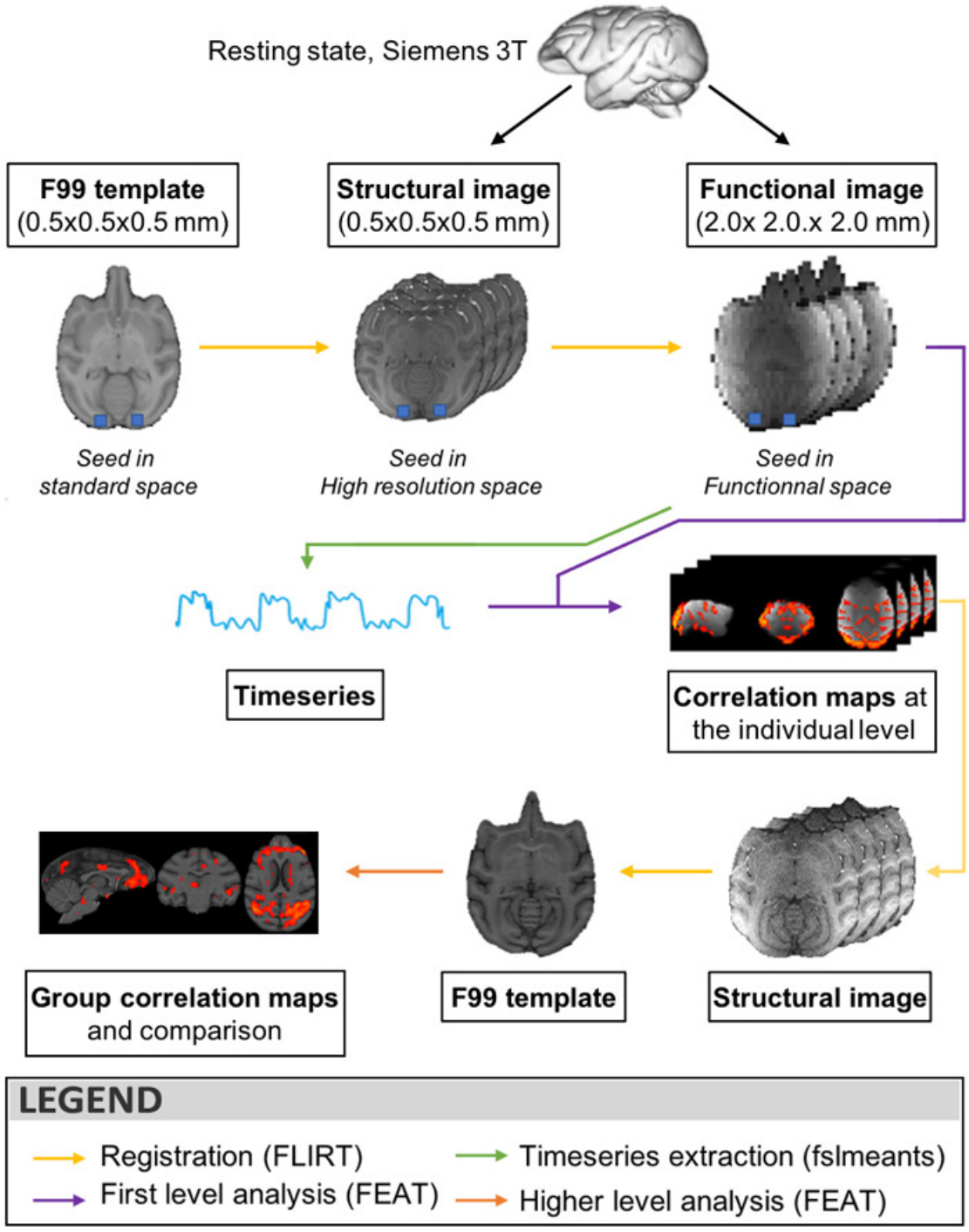


Figure 2.4 Seed Based Correlation Analysis (SBCA)

For each monkey a structural image and resting state functional data were acquired on a 3T scanner, under anaesthesia. SBCA is a useful method to calculate temporal correlation between a region of interest or seed, and the rest of the brain. To proceed, the seed's time series need to be extracted before calculating the temporal correlations. Seeds are first drawn on the F99 template before being registered to the animal's structural scan and then its functional data using FSL's function FLIRT. The timeseries at the seed location are extracted with fslmeants. The seed's timeseries is inputted in FEAT to calculate the temporal correlation between the seed and the rest of the brain and obtain the functional network for this seed and animal. The noise from the white matter and the cerebrospinal fluid is regressed out at this stage too. Next the individual maps are registered to the subject's structural before being aligned to the F99 template. The individual maps in standard space are now inputted in FEAT to run a higher-level analysis and obtain the group functional maps.

To ensure consistency across subjects, we first drew the various seeds on the F99 template (Van Essen, 2002) (resolution 0.5x0.5x0.5mm) using *A Combined MRI and Histology Atlas of the Rhesus Monkey Brain in Stereotaxic Coordinates 2nd Edition* (Saleem & Logothetis, 2006) as reference for location. Most seeds were 5x5x5 voxels large (15.6 mm^3); when the area of interest was too small to contain a seed this size, a 3x3x3 voxels (3.38mm^3) seed was used. The seeds were so their shape drawn to as close as possible from a cube while being contained within the bounds of the cortical thickness (either 125 voxels equally spread over 5 slices or 27 voxels over 3 slices).

The BOLD signal varies across time within each seed. The set of these various values, sampled over time, is one example of what is generally referred to as a *timeseries*. We must extract this timeseries at the seed's location, in order to calculate temporal correlations between the activity of the seed and the activity of the rest of the brain. Before we can extract the afore-mentioned timeseries, however, our seed must be correctly located/situated.

Each MRI image is acquired within a *reference space*. Several factors can influence the coordinates that correspond to a given region across different MRI images. These include but are not necessarily limited to the acquisition sequence's spatial frequency (in part responsible for image resolution) or subject's placement within the magnet. As a result of this, a seed created anywhere other than within a given subject's functional space, (i.e., a different space or, in this case, template), must be realigned to that subject's functional space.

Following FSL's recommended best practice, the seeds were first realigned from the F99 template to the subject's structural space (also called high resolution -or high res. space) with FLIRT.

The transformed seed in structural space for each animal was next realigned to their functional scan, again using FLIRT. The time series' values (or *eigenvariates*) were extracted at each seed location using *fslmeants*.

2.4.2 Manual Seed Correction

Rather unfortunately, FLIRT's automatic seed realignment proved to be not optimal for a majority of these animal brains (see Appendix 8.1). Often, the seed ends up being noticeably distorted or even outside the area of interest (see Figure 2.5, where the automatic process has placed the seed in the sulcus, spanning two anatomically distinct cortical areas). Because seed location is crucial, it became necessary to manually intervene to correct the seed. The results of each realignment were then visually inspected and, where necessary, further corrections (discussed below) were applied.

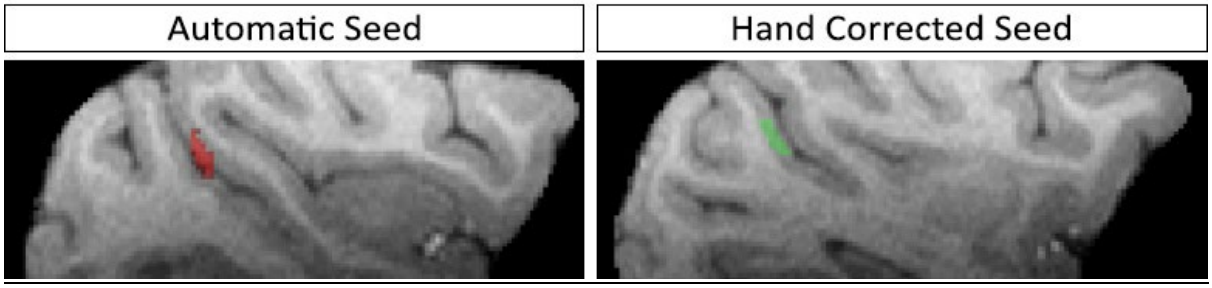


Figure 2.5 Seed Correction Example

Seed within V5/MT on Monkey Tu structural image. The automatic seed has been realigned from the F99 template to Monkey Tu's structural image. But the registration failed, and the automatic seed is mainly located in the sulcus and spreads over into MST. The hand corrected seed was created at the proper location using fsleyes editing tool. The hand corrected seed location was checked using A Combined MRI and Histology Atlas of the Rhesus Monkey Brain in Stereotaxic Coordinates 2nd Edition (Saleem and Logothetis, 2006). The size of the hand corrected seeds is 25 voxels per brain slice over 5 slices, consistent with the criterion given to the automatic selector. However, the revised set voxels are in the grey matter.

In those cases, which required further corrections when aligning seeds from the standard to the high resolution space (see Figure 2.4), the location on the structural image most closely matching the expected seed destination was identified using FSLeyes (FSL's image viewer). Then, using the editing mode in FSLeyes, a new seed was created at this location. The new seed consists of 5 slices of 25 connected voxels -or 3 slides of 9 connected voxels for smaller brain areas (e.g. pulvinar)- with no lacune voxels each. It was ensured that all included voxels belong

to the cortex and not to the white matter (WM) or the cerebrospinal fluid (CSF). Consequently, voxels belonging to the cortex were preferred over a general cubic shape for the seed.

In a handful of cases, seed registration from the structural space to the functional space failed, despite correction at the structural level. Incorrectly located functional seeds were hand corrected, in manner similar to the correction conducted at the structural level (discussed previously). The resolution of the functional images is low, making anatomical structures difficult to discern. As a result, each animal's structural image was aligned to the corresponding functional image using FLIRT. A structural image in functional space was obtained, that shared the same resolution with the functional image but where anatomical features where more easily discernible. The proper alignment of the two images was visually inspected before proceeding to the seed correction. The corrected seed was designed to keep a shape as close as possible to the original seed as long as voxels remained in the cortex and belonged to the brain area of interest. Hand corrected seeds were spread over 4 slices instead of 5 to account for the functional image resolution (2mm x 2mm x 2mm).

2.4.3 Creating Functional Networks at the Individual Level

Most of the fMRI signal is more strongly related to synaptic activity rather than generation of action potentials (Logothetis et al., 2001). And, while some glia-neuron Glutamate signalling happens in the white matter (Matute & Ransom, 2012), neuron to neuron synaptic activity happens exclusively in the grey matter (GM). Taken in concert, this means that the signal coming from white matter (WM), where no neuron's cell bodies are present, and from the CSF, which contains no cells at all, can be considered noise. Thus, temporal correlations between the seed and WM or CSF are a measure of the scanning quality and can be used as

a baseline for assessing seed-to-GM correlations. To remove this noise, I created a 6x6x6 voxel seed in WM and a 4x4x4 voxels seed in the CSF on the structural image of each subject. The locations for these non-GM reference points were matched across all animals. The time series or more precisely the first eigenvariates of the time series, at the seed's location were again extracted using *fslmeants*. The time series of the seed of interest, in conjunction with the time series of the WM's and CSF formed the design matrix that entered into FEAT for the first level analysis GLM. Times series from WM and the CSF were used as nuisance regressors. Nuisance regressors are regressors which are assumed to be contributing to the main the total signal variance but that were not experimental variable. They are included to reduce the error.

Analysing each GLM resulted in the functional network for a given seed and individual. The first level analysis was run with the prewhitening option turned on to remove autocorrelations.

2.4.4 Higher Level Analysis

Once the functional networks for a given seed have been created for all subjects, running a group (i.e., higher level) analysis is possible. Individual maps are initially registered from the functional space to the individual's structural space, then to the F99 template, using FLIRT. This step is performed as FEAT's built-in higher-level analysis functionality; it is, therefore, not necessary to take into consideration the resolution challenges faced by ICA as the particular function is built to solve them. These maps then describe a GLM (specifically, in this case, a linear regression) in FEAT. The simplified equation for an fMRI GLM is $\mathrm{Y} = \beta\mathrm{X} + \varepsilon$. Y represents the data vector (i.e., BOLD signal), X the design matrix (comprised of the regressors), β is the matrix parameter (i.e., effect size) and ε represents an error matrix

(representing the residual error). We employ this higher-level analysis in order to define networks, obtained from a (necessarily) limited sample of animals, from which we hope to infer to the macaque population.

There are two possible approaches to this particular inquiry: Fixed and Mixed Effects modelling. Fixed Effects only takes into account this average group effect. Mixed Effects incorporates both fixed (i.e., group-level) and random (i.e., subject-level) effects. Fundamentally, fixed (or group-level) effects describe how the group or population responds to a given treatment, while random (or subject-level) effects represent the variability among subjects (i.e., the declination between subjects and the group average). Fundamentally, the mixed effects approach allows for the existence of variance around the average group effect, due to between-subjects variance. This more comprehensive, higher-level GLM, the Mixed Methods model allows us to make more realistic, balanced predictions. The GLM employed for the Mixed Effect analyses are Generalized Linear Mixed Effects (GLME) models. The GLME is represented by the formula:

$$Y_k = X_k\beta_k + \varepsilon_k, \text{ where}$$

$$\beta_k = X_g\beta_g + \varepsilon_g$$

β_k: effect size; β_g: population effect size mean, ε_k: within subject variation, and ε_g: between subject variation in effect size.

The higher level analysis produces, among other things, the networks under each experimental condition and a comparison between said conditions. Again, results arepresented following the radiological orientation convention.

3 The Impact of Anaesthetic Agents on the Functional Brain

3.1 Introduction

Spatially organized low frequency (0.01-0.1Hz) fluctuations in the Blood Oxygenation Level Dependent (BOLD) signal are observed in fMRI data acquired from subjects at rest (i.e., subjects who are not performing any task). These fluctuations in the BOLD signal form structures, also referred to as a networks, which are consistent across healthy subjects (Damoiseaux et al., 2006). Because this specific type of network is observed in subjects at rest, it is referred to as a Resting-state Network (RSN). Areas that belong to the same RSN are temporally correlated. This phenomenon is referred to as "functional connectivity" (Aertsen et al., 1989; Friston et al., 1993). Resting-state functional connectivity has been used to study normal brain function as well as to identify biomarkers for diverse neurodegenerative (Allen et al., 2007; Lowe et al., 2002; Mohammadi et al., 2009; Seeley et al., 2009), neuro-developmental (Anand et al., 2009; Jafri et al., 2008; Monk et al., 2009; Zang et al., 2007), mental (Bluhm et al., 2009; Etkin et al., 2009), and neurological disorders (Cauda et al., 2009; Y. Liu et al., 2007; Vanhaudenhuyse et al., 2009).

In humans, good behavioural control makes the acquisition of resting state data relatively easy; it is a substantially more demanding undertaking in animals. Thus, studies in non-human primates (e.g. the rhesus macaque, one the most commonly used models of the human brain) regularly acquire resting state data under anaesthesia. It is widely accepted that resting state functional connectivity networks (RSN) extracted from functional MRI scans of anesthetised animals differ from similar networks extracted from at rest animals that are awake. Notable differences include: the full suppression of cross-hemisphere connectivity at 2% sevoflurane (Hudetz, 2012); the decrease and eventual complete absence of connectivity in the primary motor cortex,

sensorimotor cortex, and supplementary motor area, as well as in higher-order association areas (Nallasamy & Tsao, 2011). There is still some debate, however, regarding whether different anaesthetics impact RSNs in the same way. Understanding how anaesthetic agents influence the brain's functional connectivity is a crucial step in the process of describing that connectivity in a more comprehensive and meaningful manner. The better our understanding of the impact of anaesthetic agents on resting-state functional connectivity, the better our understanding of the bias(es) their use could introduce into analyses of RSN. Indeed, such comprehension is a necessary precursor to establishing a framework that will allow us to minimise the effect of such bias(es). Furthermore, any differences in RSN under different anaesthetics could help us better understand their effects on the central nervous system.

This chapter investigates potential differential effects of sevoflurane and isoflurane, upon the resting-state functional connectivity network. These anaesthetics are of particular interest, as they are routinely employed for the acquisition of non-human primate resting-state data. In clinical studies involving human subjects, they can have somewhat differential effects. In humans, sevoflurane produces more stable anaesthesia and requires a shorter recovery time than isoflurane (Frink et al., 1992). Both anaesthetics can be used for single-breath induction in humans –a way to obtain anaesthesia without using an injectable agent (e.g., Ketamine). Induction is smoother with sevoflurane, which is also characterized by a lower incidence of complications. Induction is also generally better accepted by human patients under sevoflurane (Sloan et al., 1996). Sevoflurane, however, is more expensive than isoflurane. As a result, isoflurane is often the preferred option in hospitals.

Using the waking resting-state as a reference, several studies have shown that the use of either sevoflurane or isoflurane generally decreases the functional connectivity, in a dose-dependent

manner (Hutchison et al., 2014; Jonckers et al., 2014; Martuzzi et al., 2010; Moeller et al., 2009). RSNs are smaller under anaesthesia: the networks involve fewer brain areas, or in some cases disappear entirely, and the relevant temporal correlations between areas within them are weaker (Deshpande et al., 2010; Paasonen et al., 2018; Peltier et al., 2005; Wu et al., 2016). Despite the similarity between sevoflurane or isoflurane with regard to their impact on RSN, there appears to be no rigorous comparison of the two agents and their effects on specific brain networks. As a result, it is possible that one may preserve functional connectivity better than the other.

The existence of differences could also imply that sevoflurane and isoflurane induce unconsciousness through different neural mechanisms. Indeed, the underlying mechanisms by which anaesthetics achieve unconsciousness is still much discussed, both at the molecular (Denomme et al., 2019; Sonner et al., 2003) and functional level (U. Lee & Mashour, 2018). From a functional standpoint, better knowledge of the precise effect of each anaesthetic across the brain could substantively help future researchers' considerations of the balance between scientific interest and animal welfare. Informed anaesthetic agent selection facilitates targeted research, while considering the safest possible method of anaesthesia and the smoothest recovery for the animal.

Resting-state functional data were acquired from 23 adult rhesus macaques. Ten animals (6 Females and 4 Males, 3.38-11.21 years old, 4.4-14.38 kg) were scanned under sevoflurane (median expired concentration anaesthetic: 1.8 – 3.0 %) and fourteen monkeys (3 Females and 11 Males, 3.66-9.69 years old, 4.87-12.8 kg), among which one male was also included in the sevoflurane group, were scanned under isoflurane (median expired: 0.8 – 1.6%). From the resulting dataset, RSNs under each anaesthetic were obtained using Independent Component Analysis (ICA). ICA (see Chapter 2.3) is an efficient way to obtain networks at the whole brain

level requiring limited *a priori* assumptions (Beckmann & Smith, 2004; S. Chen et al., 2008; Hutchison et al., 2012). The resulting Independent Components (ICs) under isoflurane were compared to the equivalent ICs under sevoflurane to highlight potential differences.

3.2 Methods

3.2.1 Animals

This study involved 23 healthy rhesus macaque (*Macaca mulatta*) monkeys, 9 females and 14 males (age range: 3.38-11.21 years, weight range: 4.4-14.38kg). The animals were purchased from the Centre for Macaques, a breeding centre at Porton Down (UK). The monkeys were socially housed in a facility using a 12:12 light:dark cycle. All procedures related to this study complied with the Animals Scientific Procedure Act (1986) under a number of different licences from the UK's Home Office, complying with the EU Directive 2010/63/EU (European Union, 2010).

Data collection was conducted within the framework of a large set of routine scans, whose purpose was the production of a database to be used in several concomitant studies. The non-study-specific nature of the original data collection *de facto* resulted in our data having a number of otherwise unexpected characteristics -the most salient of which are presented and discussed below. The present study included all suitable animals or datasets available at the time of observation or analysis. No animals were preselected for participation. Data collection and analyses were non-blinded to the experimental conditions.

3.2.2 Anaesthesia

rsMRI data were acquired under general anaesthesia. Sedation was first induced via an

intramuscular injection of ketamine (7.5 mg/kg), xylazine (0.125-0.25 mg/kg), and midazolam (0.1 mg/kg). The animals also received meloxicam intravenously (0.2 mg/kg) and atropine intramuscularly (0.05 mg/kg). The animals were intubated prior to scanning. To prevent head motion during the scan, they were placed in a stereotaxic frame (Crist, Hagerstown, USA).

The anaesthetic agent was either inhalational sevoflurane or inhalational isoflurane. Muscle relaxation and reflexes were inspected before each MRI scan to make sure the animal was at the correct level of anaesthesia. Data collection under inhalation anaesthesia took place on average 280 minutes (range: 112-455 minutes) after the initial ketamine injection. In other words, all rsMRI data were collected after the clinical ketamine peak time point, which occurs 30 minutes after injection (Mion & Villevieille, 2013; West et al., 2014; Winterborn et al., 2008). The range of time-delays between ketamine injection and resting state functional data acquisition was one result of this study's data collection originally occurring without a specific study in mind.

Resting state data was typically acquired at the tail end of the scanning session, following the acquisition of a number of other scans of interest (including though not limited to stimuli presentation). Anaesthetic agent concentration was maintained relatively constant within each session, however, and physiological parameters, such as subject heart and respiration rates, were rigorously monitored. We therefore have no reason to believe that the quality of the resting state functional data was impacted by the delay in or order of data acquisition.

The Minimum Alveolar Concentration (MAC) is the necessary concentration of a given anaesthetic agent required to prevent motor response in 50% of subjects, in response to a surgical incision (Miller et al., 2015; Welsh, 2009). The MAC has been the standard measure of potency for volatile anaesthetic agents since its introduction in 1965 (Lobo et al., 2022). Its

measurement of a quantitative characteristic, immobility, has made the MAC both useful and reproducible across both human and animal subjects (Lobo et al., 2022).

Comparing the depth of anaesthesia across subjects (of the same species) is relatively straightforward, given we possess knowledge of those characteristics that could influence the effectiveness of our anaesthetic agent of choice (here: primarily weight). Thus, comparisons between subjects exposed to different anaesthetic agents are made relative to their anaesthetic's MAC value. The MAC for each anaesthetic is different. For example, MAC for isoflurane is 1.3% of expired anaesthetic (Steffey et al., 2015), while MAC for sevoflurane is 2.3% of expired anaesthetic (Bertrand et al., 2017). Thus, we cannot meaningfully compare directly against isoflurane and sevoflurane values; rather, we report depth of anaesthesia relative to the MAC. The concentration of exhaled anaesthetic is used to measure the depth of a given subject's anaesthesia, within a common anaesthetic group. By dividing the concentration of exhaled anaesthetic for a given subject by the MAC for their given anaesthetic agent (see Equation 1), we derive the depth of the anaesthesia, relative to the MAC, what we refer to for clarity as the "individual MAC value" (MAC_i). This gives the median concentration (MAC) of expired anaesthetic relative to the minimum alveolar concentration of the anaesthetic agent they have been administered, providing a measure that is directly comparable between anaesthetic groups within the same species (Soma et al., 1995; Steffey et al., 1994).

$$MAC_i = \frac{\%\ of\ expired\ anaesthetic}{MAC_{anaesthetic}}$$

Equation 1 Equation for the calculation of individual MAC value for each subject

The individual MAC value (MAC_i) is the expression of each subject's percentage of exhaled anaesthetic standardized against the MAC value for the particular anaesthetic agent they subjected to.

Data under sevoflurane anaesthesia (median expired concentration anaesthetic: 1.8 – 3.0 %) were collected from ten animals. Data under isoflurane anaesthesia (median expired concentration anaesthetic: 0.8 – 1.6 %) were collected from fourteen animals. One monkey that had more than one MRI scan was a member of both anaesthetic groups. For isoflurane, the monkeys' average individual MAC_i value was 0.94 and for sevoflurane the average MAC_i value was 1.01. In addition to the depth of each animal's anaesthesia, the animal's age, the time delay between sedation and fMRI data collection, median systolic blood pressure, percentage of expired CO_2, heart rate, respiratory rate and rectal temperature were also recorded during the scanning session. The averages of each of these parameters were compared between the anaesthetic groups with a series of unpaired t-tests (see Figure 3.1); no statistically significant differences were observed between the two groups.

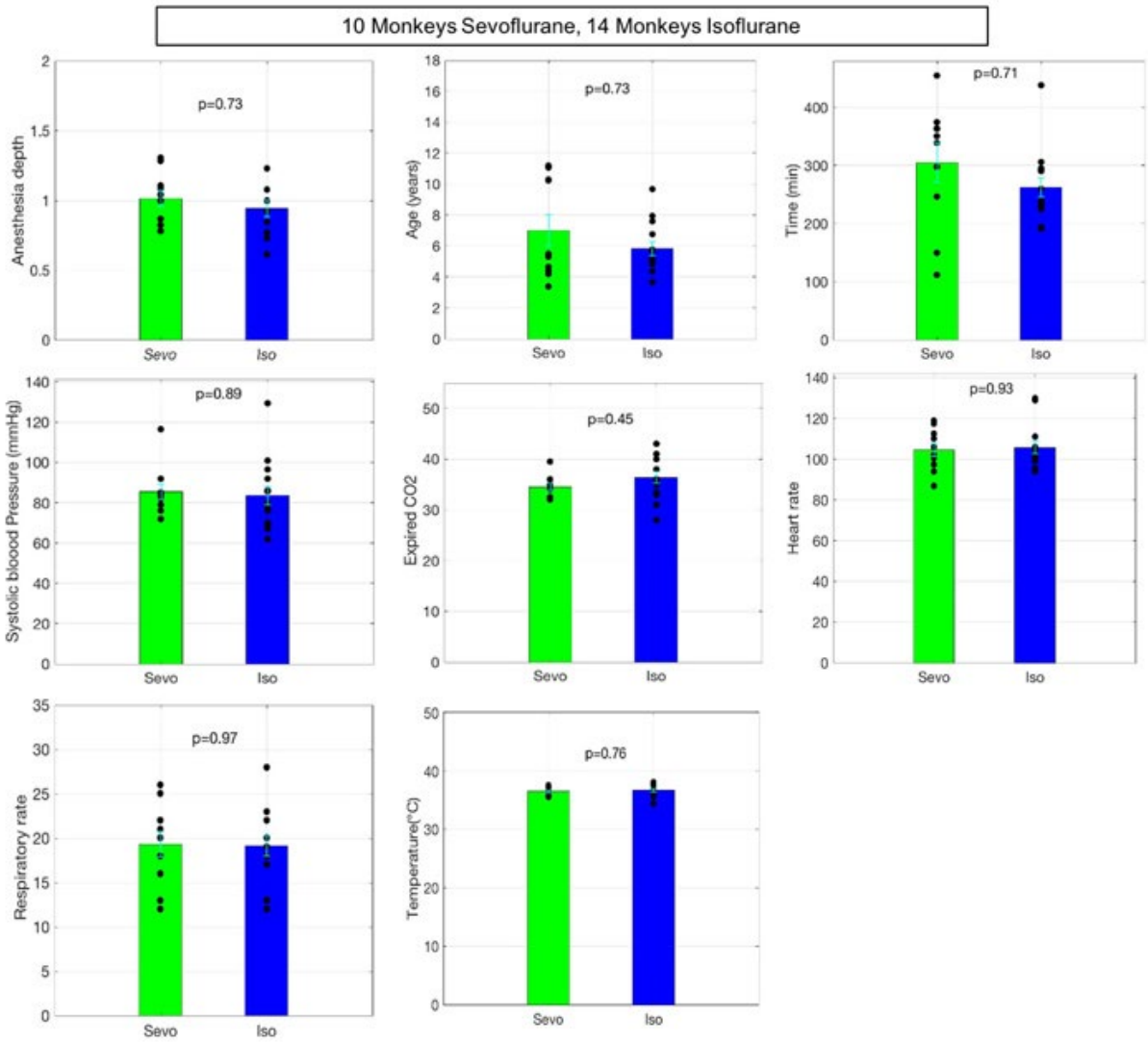


Figure 3.1 No Statistically Significant Difference Between Anaesthetic Agent Groups for Age, Delay Between Sedation and Data Acquisition, Median Systolic Blood Pressure, Expired CO2, Heart Rate, Respiratory Rate, Temperature, and Depth of Anaesthesia (Unpaired t-test)

23 rhesus macaque were included in our study. There was no difference between groups in average age (average 7 years for sevoflurane, 5.9 years for isoflurane), delay between sedation and data collection (Time) (average isoflurane: 305.4; average sevoflurane: 262.4 min), systolic blood pressure (average sevoflurane: 85.5 mmHg; average sevoflurane: 83.7 mmHg), expired CO2 (average sevoflurane: 34.55 mmol/L, average isoflurane: 39.4 mmol/L), Heart Rate (average sevoflurane: 104.6 bpm, average isoflurane: 105.6 bpm), respiratory rate (sevoflurane average: 19.3; isoflurane average: 19.14) and rectal temperature (average sevoflurane: 34.5 °C; average isoflurane: 36.8 °C), and anaesthesia depth value (p=0.73; average sevoflurane: 1.01 MAC, average isoflurane: 0.94MAC). Anaesthesia depth was measured as the concentration of expired anaesthetic agent divided by the relevant MAC value (sevoflurane: 2.3%, isoflurane: 1.3%). The MAC value is the minimum concentration of inhaled anaesthetic necessary to prevent skeletal movement in 50% of the subjects.

3.2.3 Independent Component Analysis

rsMRI functional data and structural scans were acquired under general anaesthesia, following the method described in Chapter 2.1 and preprocessed (see Chapter 2.2). Functional scans

consist of 800 or 1600 volumes per run, corresponding to a 20min or 40min scan. The variance in scan length is another result of the non-study-specific nature of the original data collection. Indeed, the data was collected over the course of several years. As a result, scan length, including the number of volumes collected, was adapted across the acquisition process, to coincide with what was considered best practice at the time of acquisition. Both despite and as a result of this, the scan quality of the two sets of data was visually inspected, compared, and deemed similar enough to be merged after preprocessing[4] (for more about the preprocessing step, see Chapter 2.2).

The effects of sevoflurane and isoflurane upon the resting-state functional connectivity were compared at the whole-brain level by means of an ICA (for a discussion of ICA, see Chapter 2.3). ICA divides whole-brain resting-state functional data into components which, are spatially and temporally independent for each other. Most of the extracted ICs are thought to have a neuronal origin and, as such, each can be considered equivalent to a functional network. Some ICs, however, can be related to circulatory activity or signal coming from the white matter or the cerebro-spinal fluid. For the purposes of treatment as RSN exploration, these ICs are considered physiological noise (as defined by Beckmann & Smith (2004)). For details on how neuronal-based RSNs were discriminated from physiological noise, see Chapter 2.3.

ICA of the functional scan acquired from the 23 monkeys involved in this study resulted in 25 group ICs.

[4] The number of volumes in a given session is a functional component of the process of scan preprocessing. While the number of volumes does not affect, for example, the quality of a session's preprocessing, incorrectly declaring a session to have, again, for example, 400 instead of 800 *would*. Special attention was given to the different numbers of volumes in each session, at the requisite points in our analyses.

The percentage of explained variance for each of the 25 group IC is presented in Table 3.1.

Table 3.1 Group IC Percentage of Explained Variance

Group IC	% of Explained Variance
IC1	5.87
IC2	5.85
IC3	5.47
IC4	5.45
IC5	5.18
IC6	5.17
IC7	4.95
IC8	4.47
IC9	4.03
IC10	3.99
IC11	3.80
IC12	3.78
IC13	3.67
IC14	3.54
IC15	3.54
IC16	3.45
IC17	3.38
IC18	3.25
IC19	3.29
IC20	3.12
IC21	3.12
IC22	3.07
IC23	2.92
IC24	2.88
IC25	2.83

Having acquired the ICs, the goal was to examine whether there was a differential effect between isoflurane and sevoflurane over the RSN at the whole-brain level. First a dual regression (see Chapter 2.3 and Figure 2.3), using FSL function *dual_regression* (Beckmann et al., 2009), was run on the 25 group ICs. The dual regression creates a subject-specific version of each group IC. It then implements a GLME (see Chapter 2.3), by calling FSL's randomise[5] FSL's

[5] FSL's randomise function employs permutation for statistic map thresholding, where the null distribution is unknown and allows modelling and inference using standard GLM design setup (Winkler et al., 2014).

function (500[6] permutations) (*Randomise/UserGuide - FslWiki*, 2019; Winkler et al., 2014), a "tool for nonparametric inference on neuroimaging data" (*Randomise/UserGuide - FslWiki*, 2019). It generates permutations of the subject-specific ICs estimated during the dual regression and design matrix (see Appendix 8.2) and contrast files to perform a cross-subject analysis. The design matrix is comprised of the GLME regressors. For this analysis, the anaesthetic groups (iso: isoflurane, sevo: sevoflurane), the animal's age (AGE), delay between anaesthesia induction and data acquisition (TIME), the subject's median blood pressure (MEDIAN BP), heart rate (HR), and individual MAC value (MAC) were used as regressors. AGE, TIME, MEDIAN BP, HR and MAC are employed as regressors of no interest.

Each of the variables included in the GLM as regressors of no interest are known to be associated with the variation in the BOLD signal across time. Their relationship to each other is also important, not only to better understand their function but also because too strong a relationship between any two may introduce issues of collinearity into our estimations. We calculated the correlations between each of the regressors of no interest using SPSS (*IBM SPSS Statistics for Windows (Version 27.0)*, 2020) (See Table 3.2). None of the relationships between the variables included in the GLM was statistically significant but, given the small sample size and especially its commensurate increased propensity for Type I errors, there is nevertheless merit in examining such relationships as may exist within the bounds of the sample. All but one of the relationships examined, however, were weak ($r_{Pearson} < 0.300$). The exception, the relationship between subjects' Median Blood Pressure (MBP) and Heart Rate (HR), was of average strength ($r_{Pearson} = 0.371$). There is little consensus as to the precise magnitude of a correlation that implies collinearity but the most conservative

[6] FSL employs 500 permutations by default. Lacking specific reason to do otherwise, we kept this figure.

interpretation is that any "strong" linear relationship ($r_{Pearson} \geq 0.600$) is problematic. Even by this measure, however, there are no such problems in our dataset (see Table 3.2).

Table 3.2 Bivariate Relationships Between Regressors of No Interest

		AGE[1]	TIME	MBP	HR	MAC
AGE	Pearson's R	1.000	-0.262	0.005	-0.159	-0.280
	Sig.(2-tailed)	0.000	0.264	0.983	0.503	0.231
	N	20	20	20	20	20
TIME	Pearson's R		1.000	0.102	0.029	0.010
	Sig. (2-tailed)		0.000	0.667	0.903	0.968
	N		20	20	20	20
MBP	Pearson's R			1.000	0.371	-0.214
	Sig. (2-tailed)			0.000	0.107	0.366
	N			20	20	20
HR	Pearson's R				1.000	-0.013
	Sig. (2-tailed)				0.000	0.957
	N				20	20
MAC	Pearson's R					1.000
	Sig. (2-tailed)					0.000
	N					20

[1.] *Age: Age of the subject at time of data collection; Time: Time between Ketamine injection and image recording; MBP: Median Blood Pressure (mmHg); HR: Heart Rate; MAC: Minimum Alveolar Concentration*

The GLME aims to determine how much each regressor contributes to the group IC before comparing these contributions to each other. The matrix parameter is estimated by FSL and contains parameter weights for each regressor for each voxel. Hypotheses regarding which parameter weights contribute to the test statistic must be formed and input as a set of Contrasts[7], contained in the contrast file and are presented in Table 3.3.

In all four Contrasts, all parameters other than the anaesthetic group are used as regressors of no interest. In practice, they may contribute to the BOLD signal, but they were not manipulated during this study.

[7] For all intents and purposes, the term Contrast, employed by FSL, is functionally equivalent to an Alternative Hypothesis.

Table 3.3 Contrasts Employed in the Group Analysis

Contrast	*Contrast Description*
Isoflurane group average	*Tests the null hypothesis that mean isoflurane group effect ($\mu_{(\beta_ISO)}$) is equal to zero. In lay terms, this outputs the mean correlation across the isoflurane subjects.*
Sevoflurane group average	*Tests the null hypothesis that the mean sevoflurane group effect ($\mu_{(\beta_SEVO)}$) is equal to zero. This contrast outputs the mean correlation across the sevoflurane subjects.*
Isoflurane - Sevoflurane	*Corresponds to the hypothesis test:* *H_0: There is no difference between the mean isoflurane and sevoflurane group effects, or $\mu_{\beta_ISO} - \mu_{\beta_SEVO} = 0$.* *H_a: The mean isoflurane group effect is greater than the mean sevoflurane group effect, or $\mu_{\beta_ISO} - \mu_{\beta_SEVO} > 0 \leftrightarrow \mu_{\beta_ISO} > \mu_{\beta_SEVO}$.*
Sevoflurane - Isoflurane	*Corresponds to the hypothesis test:* *H_0: There is no difference between the mean isoflurane and sevoflurane group effects, or $\mu_{\beta_SEVO)} - \mu_{\beta_ISO} = 0$.* *H_a: The mean isoflurane group effect is greater than the mean sevoflurane group effect, or $\mu_{\beta_SEVO} - \mu_{\beta_ISO} > 0 \leftrightarrow \mu_{\beta_SEVO} > \mu_{\beta_ISO}$.*

Randomise outputs one t-statistic maps per Contrast. Meaningfully creating and, moreso, interpreting such maps is a relatively complex process. As a result, researchers employ *dual_regression* to compare populations and threshold-free cluster enhancement (TFCE) (Smith & Nichols, 2009), to statistically compare between the two groups. This approach, however, is conservative and is, therefore likely poorly suited (i.e., lacking in sufficient power) to the detection of differences in small populations. Given the small number of animals in both groups (and particularly in the sevoflurane group), we lack said statistical power (Geuter et al., 2018) and elected to forego TFCE (for a longer discussion of this choice, see Chapter 3.4).

3.2.4 Critical t-statistic Value

Comparisons on each t statistic map outputted by *randomise* are undertaken against a critical t-statistic value. In other words, we conduct the appropriate t-test, from which we derive a specific t-statistic score, which we then compare to the relevant critical t-statistic value. In

the Result section (see Chapter 3.3), the astute observer will note that the isoflurane and sevoflurane IC are examined using two different critical t-statistic values. The explanation for this is relatively simple.

When examining large samples (which is generally accepted to mean $N \geq 30$) the t-statistic functionally follows the standard Normal distribution (or the distribution of the z-statistic). Until this point however, the distribution of the t-statistic and thus the *critical value of t* are both *dependent on the degrees of freedom*. Smaller sample sets will have t-distributions which are more leptokurtic (i.e., with fewer values "grouped" around the distribution mean and with heavier tails), while larger sample sets will be progressively more platykurtic (i.e., with more values grouped around the distribution mean and lighter tails), until they eventually become functionally indistinguishable from the z-distribution.

In lay terms, what this means is that sample sets with lower degrees of freedom (or, all other things being equal, *smaller* sample sets) have a higher probability of extreme values, while sample sets with higher degrees of freedom (or *larger* sample sets) will correspond to lower probabilities of extreme values. The level of statistical significance, α, corresponds to the *a-priori* defined acceptable possibility of finding a result as "extreme" as the one observed in our test, given that the sample was drawn from a population where the test's null hypothesis is true. Thus, the *same* level of statistical significance (i.e., the *same probability*) will correspond to different critical t-values depending on the degrees of freedom of a given sample set. Sample sets with lower degrees of freedom will correspond to higher critical values of the t-statistic, while sample sets with higher degrees of freedom will correspond to lower critical values of the t-statistic.

Indeed, this is mirrored in our examples, where, at the $\alpha = 0.001$ level of statistical

significance, the isoflurane group, with 12 degrees of freedom, has a critical t-value of $t_{crit(ISO)} = 4.32$ and the sevoflurane group, with 8 degrees of freedom, has a critical t-value of $t_{crit(SEVO)} = 5.04$.

3.2.5 Criteria for Meaningful Significant Difference in Connectivity Strength

The *Isoflurane - Sevoflurane* and *Sevoflurane-Isoflurane* contrasts (see *Table 3.3*) are differential contrasts. They are obtained by deducting the average group effect for one of the anaesthetics agents from the other. The differences are calculated as the simple algebraic difference ($\Delta\mu_{iso-sevo} = (\mu_{ISO} - \mu_{SEVO})$ and $\Delta\mu_{sevo-iso} = (\mu_{SEVO} - \mu_{ISO})$, respectively). Thus, it is possible for the difference between two, on average, negative correlations, to be net positive. If this net positive difference is sufficiently greater than that expected due to random chance, it will return a significant result to the test being conducted and appear as a significant difference on the relevant map.

While there is much debate surrounding the meaning of negative correlations in the context of functional connectivity *(Buckner et al., 2009; Giove et al., 2009; Meunier et al., 2009; Skudlarski et al., 2008)*, there is no clear consensus on their meaning and nuanced interpretation. An examination of the theoretical or practical meaning attributable to these otherwise perplexing relationships is, however, outside the purview of this particular inquiry. Our goal is, among other things, to examine and interpret the existence, locations, and overall networks comprised of positive correlations within the brain. In this sense, therefore, contrasts such as those discussed above represent a rather unique form of “false positive” (or TYPE I error) –due to conceptual, rather than statistical limitations.

To prevent incorrectly interpreting the presence of a significantly different cluster, there are,

fundamentally, two criteria which can be employed to substantially curtail the probability that these results represent false positives:

1. The clusters of voxels representing significant differences for the "Isoflurane-Sevoflurane" contrast (H_0: $\Delta\mu_{iso-sevo} > 0$) must be present in the tested IC's isoflurane network and those representing significant differences for the "Sevoflurane-Isoflurane" contrast (H_0: $\Delta\mu_{sevo-iso} > 0$) must be present in the tested sevoflurane network (heretofore referred to as the criterion of "Matching Network"). It should be noted that clusters representing negative correlations are excluded from consideration when examining the existence of a given cluster in an IC.
2. The isoflurane, sevoflurane and Difference RSNs must be compared at the same level of statistical significance (heretofore the criterion of "Significance"). For the purposes of this examination, the level of significance is fixed at $\alpha = 0.001$.

3.3 Results

An ICA was undertaken to evaluate the resting-state functional connectivity network under isoflurane and sevoflurane, then to compare them to identify potentially differential effects of the two anaesthetics. Isoflurane and sevoflurane are both fluorinated ethers used as inhalational anaesthetic agent. As such, it would be expected that they act on the brain following similar molecular mechanisms and would therefore have similar consequences over the resting-state network. ICs were obtained from 10 adult rhesus macaques anesthetized with sevoflurane and 14 anesthetized with isoflurane (3T MR scanner, TR 2s, 800 or 1600 volumes). The following section highlights a trend where most ICs appear to be better

preserved under isoflurane than under sevoflurane.

The ICA was set to output 25 ICs. Of these, 3 were excluded as noise (to see theses IC and read about the exclusion criteria, see Appendix 8.3). In order to label the 22 remaining ICs, the location of the strongest correlation was found in each group IC (see Appendix 8.4) by artificially increasing the lower threshold until only a cluster of voxels remained. Following this method 7 different IC categories were identified: Visual, Visual associated, Somatomotor, Auditory, Insular, Frontal and Putamen.

The following section will describe the remaining ICs under each anaesthetic (contrast "Isoflurane group average" and "Sevoflurane group average"), before considering whether there is a significant difference between the effect of isoflurane and sevoflurane on the functional connectivity ("Isoflurane - Sevoflurane and "Sevoflurane – Isofurane").

3.3.1 Visual IC

Visual areas are cortical areas involved in visual processing, belonging either the ventral or the dorsal pathway. The primary visual cortex (V1), secondary visual cortex (V2), V4 (which is part of the ventral pathway) and MT, the last relay of the dorsal pathway, are located in the occipital cortex (Felleman, 2009). Eight of the 25 group ICs (see Figure 8.3 in Appendix 8.4) resulting from the ICA had their strongest correlated point in a visual area (see Figure 3.2); these ICs can be classified as visual networks (see Figure 3.3).

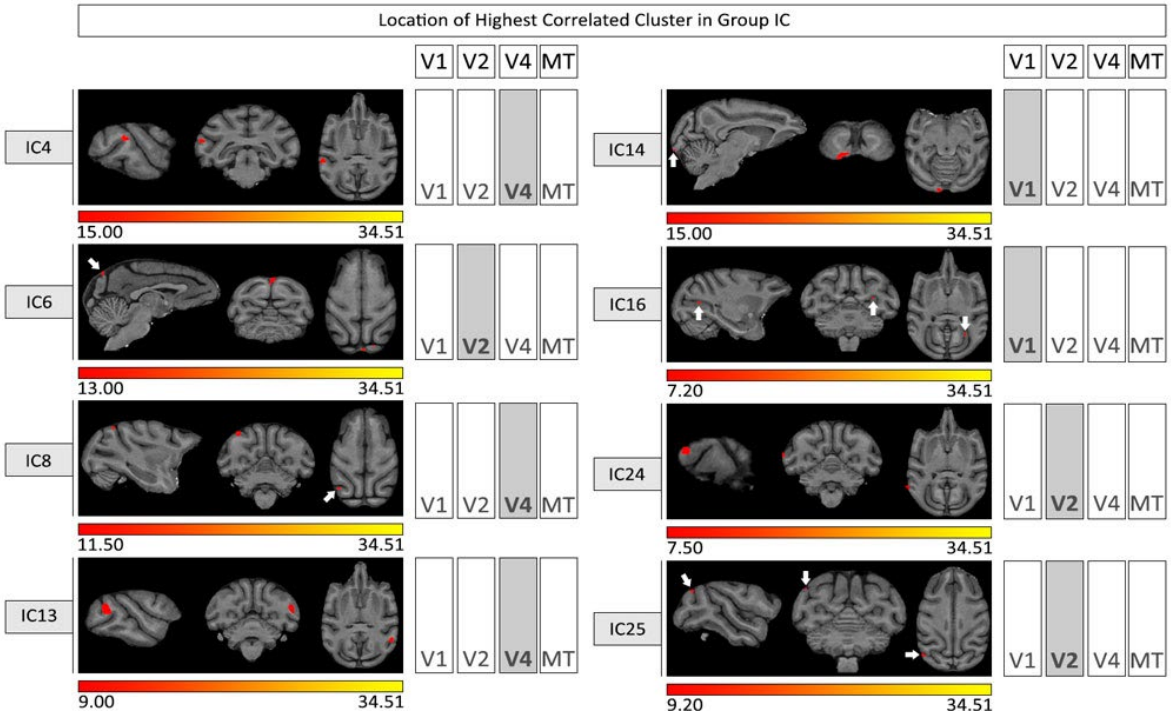


Figure 3.2 Location of the Highest Correlated Voxel in the Group IC (Visual ICs)

The location on the F99 template of the cluster containing the highest z-value voxel in the group IC. The associated table indicates (grey) in what brain area this cluster is located. Networks were classified as a visual area if the highest voxel cluster was located in a visual area. The colourbar represents the range of z values from the threshold where no other significant cluster other than the one presented above was visible to the highest value of z across all 25 IC. White arrows highlight the smaller clusters.

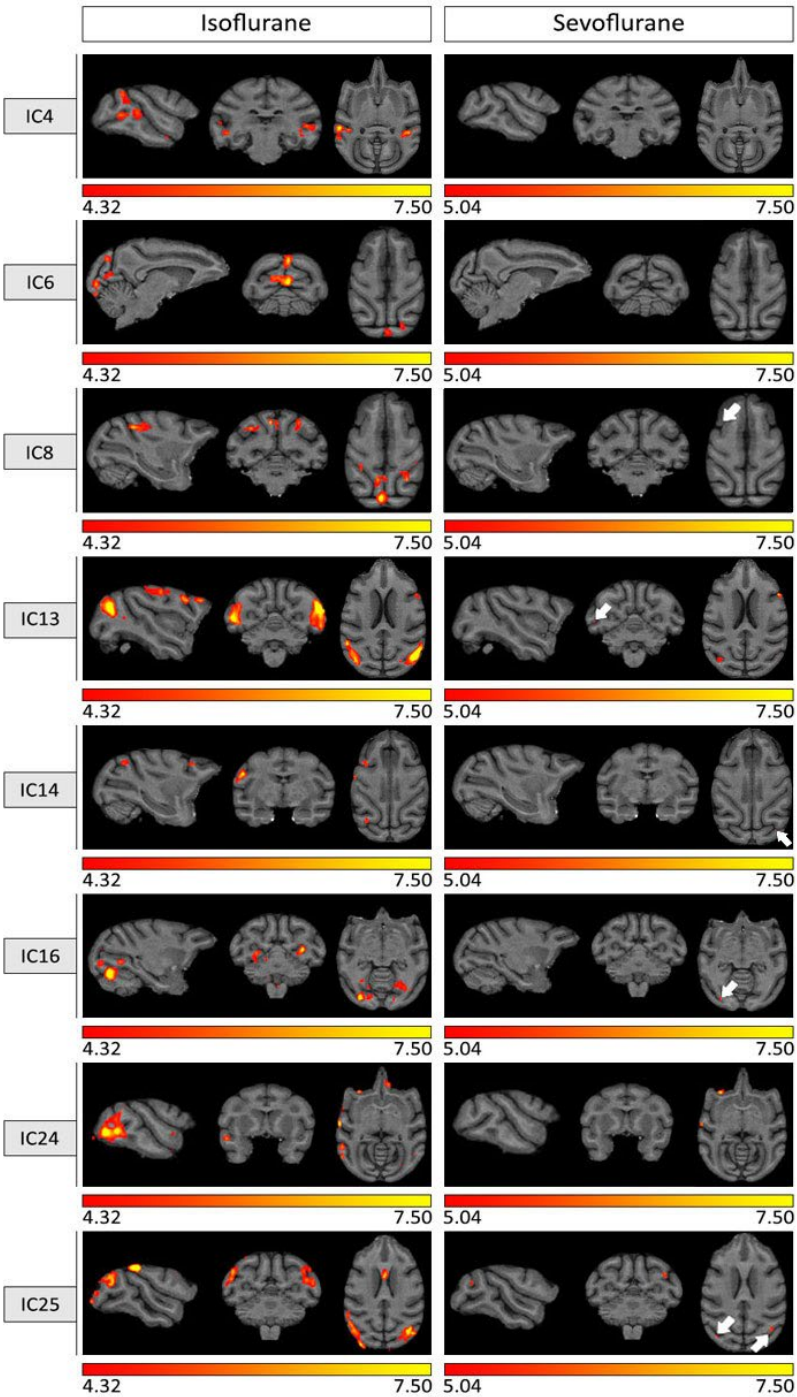


Figure 3.3 Visual ICs Under Isoflurane and Sevoflurane

An Independent Component Analysis run on resting-state fMRI data (Siemens 3T, TR=2S, TE=19ms, 800 or 1600 volumes) from 23 adult rhesus macaques (9 under sevoflurane, 13 under isoflurane, one in both group). This figure presents the results of the dual regression subsequent to the ICA: t-statistics maps for each Visual IC under sevoflurane and isoflurane.

The correlations maps are presented thresholded at the significance level α=0.001 (isoflurane: t≥4.32, sevoflurane: t≥5.04) on the F99 template. The colour bar represents the range of the values of t from the significance level. Voxels with t value over 7.50 were grouped under same colour (yellow) to allow for easier direct comparisons. ICs were classified as visual ICs if the voxel in the group IC correlation map (see Figure 8.3) with the highest correlation score was located in a visual associated area.

White arrows point toward significant clusters the reader might otherwise miss.

3.3.1.1 Visual IC Under Isoflurane

Under isoflurane (see Figure 3.3), IC4 includes significant ($p \leq 0.001$) bilateral correlations in TEO and V4, right IPa, right V3v. The isoflurane IC6, is centred on the median line but it also includes significant clusters in V1 and V2. Under isoflurane, IC8 involves small clusters in V4 and a unilateral cluster in the right V2. Significant correlations are also evident in the visual association areas most notably in the intraparietal cortex. Bilateral correlations are present the LIP, VIP and MIP (small left cluster) and unilateral cluster are found in the right MST, right AIP, and the right superior parietal area. IC8 also includes significant correlations in the right PCC. IC13 bilaterally involves V2, ventral V3, dorsal V3, V3A, and V4. There are some unilateral correlations in IC13 present in the left hemisphere in the somatosensory cortex, the motor, the premotor cortex (F5) and the ventrolateral prefrontal cortex. The isoflurane IC14 is only constituted of unilateral significant clusters. In the left hemisphere, significant correlations are evident in area TG, TE and V2. Three visually-related clusters are located in the right V4, the right V3A and the right FEF but its largest cluster encompasses the right somatosensory areas 3a and 3b, and the motor cortex. IC16 involves the ventral parts of the visual areas V2 ventral V3. Significant correlations are also evident in the calcarine portion of V1. The only non-visual correlation is a unilateral cluster in the right premotor cortex (F4). IC24's largest cluster is unilateral and overlaps with the right ventral V2, V3, V4 and TEO. Smaller unilateral clusters are also present in the left V1, the left FEF, left V3v the left orbitofrontal area and in the right temporal pole and right auditory cortex. IC25's strongest correlations are located in V1 and V2. The network also includes a bilateral cluster in V4, and unilateral clusters in right putamen right 7a/Opt, in the left medial prefrontal cortex, as well as a cluster in the left IPA.

3.3.1.2 Visual IC Under Sevoflurane

Visual ICs under sevoflurane appear smaller than their isoflurane counterparts (see Figure 3.3). They not only contain fewer brain areas but the significant clusters that do exist also cover fewer voxels. As a matter of fact, IC4, IC6 and IC8 show no significant clusters under sevoflurane. The IC14 sevoflurane is reduced to a single voxel in the right V2. Similarly, the sevoflurane IC16 only involves a small cluster in the right ventral V2. The sevoflurane IC24 includes correlations in the left orbitofrontal area, and the right auditory cortex that were previously observed in its isoflurane equivalent. However, the large ventral visual cluster observed in the isoflurane IC24, does not exist under sevoflurane, although a small significant cluster is present in TEO. IC25 under sevoflurane is also constituted of a galaxy of small significant clusters located in the left V3A, the left medial prefrontal area, the right V1, and right V2. No large clusters are observed as it was the case under isoflurane.

IC13, although also substantially smaller than its isoflurane equivalent, is the better-preserved network among the visual ICs. The only bilateral clusters remaining in the sevoflurane IC13 is located in V2. Significant correlations in V4 and V3d are only found in the left hemisphere. Of the non-visual areas that were part of the isoflurane IC13 network, only a small cluster in left F5 remains. Nevertheless, significant correlations with the left FEF are evident in the sevoflurane network. This was not the case under isoflurane.

3.3.2 Visual Association Networks

Visual association areas are those that receive inputs from the visual areas, whose function is relevant to vision (e.g., eye movement), and which perform higher cognitive tasks. FEF, for example, is involved in eye movements and attention and receives inputs from MT (Schall, 2009). Area 7a

receives inputs from the dorsal pathway (Fattori et al., 2017) and controls saccadic and oculomotor movements (Bremmer et al., 1997). TEO, involved in object categorisation (Setogawa et al., 2021), receives major output from V4 (Ungerleider et al., 1984). Four ICs had their most highly correlated voxels in a visual association area (see Figure 3.4 and, for a more detailed presentation, Figure 8.3 in Appendix 8.4) and were, as a result, classified as visual associated ICs (see Figure 3.5).

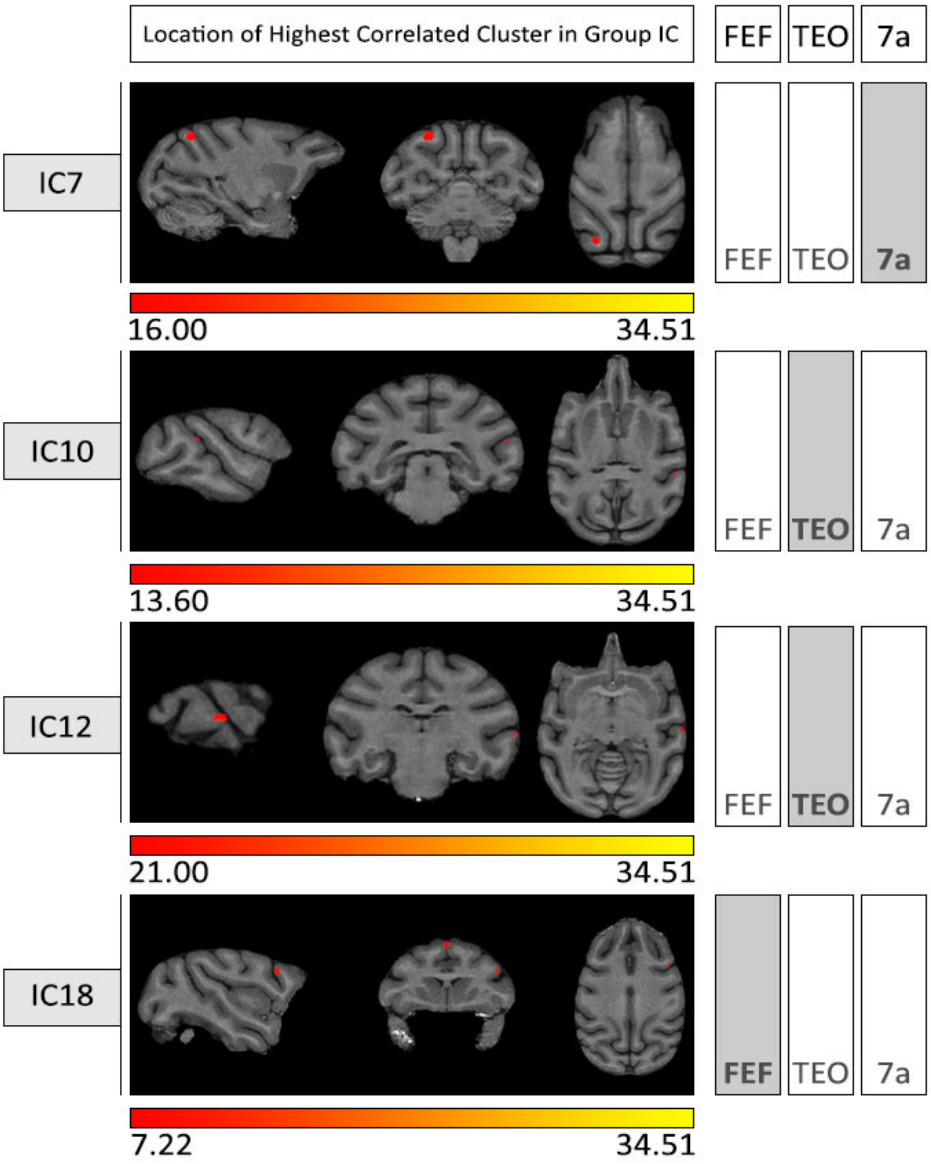


Figure 3.4 Location of the Highest Correlated Voxel in Group IC (Visual Association ICs)

Cluster containing the highest z-value voxel in the group IC on the F99 template. *The location of this cluster in the brain is shown (in grey) in the accompanying table. If the highest voxel cluster in a network was situated in a visual* association *area, the network was categorized as a visual* association network. *The colo*urbar *bar shows the range of z values between the point where no other significant cluster except the one shown above was seen and the* highest *value of z across all 25 ICs*.

3.3.2.1 Visual Association IC Under Isoflurane

IC7 under isoflurane, presents significant correlations (α =0.001) in the occipital cortex with the dorsal portion of V2, in V4, in dorsal V3 and V3A. The network also includes correlations in areas involved in eye movements (Shadlen & Newsome, 1996) or arm/eye/head coordination (Bosco et al., 2010; Fattori et al., 2017). Bilateral significant cluster is evident in area 7a/Opt and MIP. Unilateral correlations with other portions of the intraparietal sulcus are also evident in the left LIP, and right PIP. A significant cluster is also found in the left FEF. Isoflurane IC7 additionally includes bilateral significant correlations in the parieto-occipital area and a unilateral cluster is present in the left lateral parieto occipital area, both involved in object recognition (Grill-Spector et al., 2001). Other significant correlations are located in motor areas or areas processing motion. A bilateral cluster of significant voxels in the premotor cortex (F2 and F5) are evident. In the right hemisphere, correlations are present in MST and FST. Additionally, bilateral significant correlations are evident in dorsolateral prefrontal cortex and the entorhinal cortex, which both play a role in working memory (Curtis & D'Esposito, 2003; Vann et al., 2009).

IC10 is a mostly temporal network. Its largest cluster is centred on TEO and TE. Significant correlations are evident along the superior temporal sulcus (STS). A bilateral cluster is present bilaterally in the STS dorsal bank area (PGa), the STS fundus area (IPa) and area TPO. Unilaterally, significant correlations are found in the right floor of the superior temporal area (FST), the left area TPO, the left temporal pole. Still in the temporal lobe, a significant correlation is found in the left auditory cortex. In the parietal and frontal cortex unilateral correlation are present in the left FEF, left ventrolateral prefrontal cortex, the right caudal inferior lobule area (7a/Opt), the right premotor cortex (F5), and the right motor cortex.

IC12 under isoflurane bilaterally includes area TE and the auditory cortex. Bilateral

correlations are also present in TEO and V3a, although clusters size was noticeably smaller in one of the hemispheres than the other (right for TEO, left for V3a). The network also contains a number of unilateral significant correlations. In the left hemisphere correlations are present in V2, AIP, and the somatosensory 3 a/b (cluster a few voxels large). In the right hemisphere correlations with LIP, 7a/Opt and temporo-parietal area (tpt) are found.

The isoflurane IC18 comprise significant bilateral correlation in two areas related to motor functions, area 7a and the ventral premotor cortex. Otherwise, the network involves unilateral correlations. Unilateral clusters are found in visual association areas such as the left LIP, the right MST, the right temporal pole. Unilateral correlations with some visual areas are also present. A small cluster is found in the left V4 and another is present in the left calcarine portion of V1. Clusters in parieto-frontal areas unilaterally are evident in the left somatosensory area 3/b, the left small cluster in Tpt (temporo-parietal area), the right motor cortex, and the right dorso-lateral prefrontal area.

3.3.2.2 Visual Association IC Under Sevoflurane

Similarly, to the visual ICs, the visual association sevoflurane networks involve fewer brain areas and present sent smaller clusters compared to their Isoflurane counterpart. IC10 and IC12 are the most reduced networks, compared the number of areas their isoflurane equivalent involves. IC10 presents no significant (α=0.001) correlations under sevoflurane. And the IC12 network is reduced to a couple of voxels in the right V3d. IC18 is also remarkably reduced in size. Significant correlations are only evident in the right orbital prefrontal area (10m), the left ventral prefrontal cortex, and the right 7a area.

IC7 is the better-preserved IC of among the sevoflurane visual association IC. It presents visual

correlations already described in the isoflurane network. Bilateral correlations are evident in V3A and V2. Nevertheless, the V2 clusters are only a few voxels wide. Visual correlations are also present in V3d but the correlations are only found in the left hemisphere while the cluster was bilateral under isoflurane. This is also the case for the correlations in MIP and the ventral premotor cortex, which are only present in the right hemisphere.

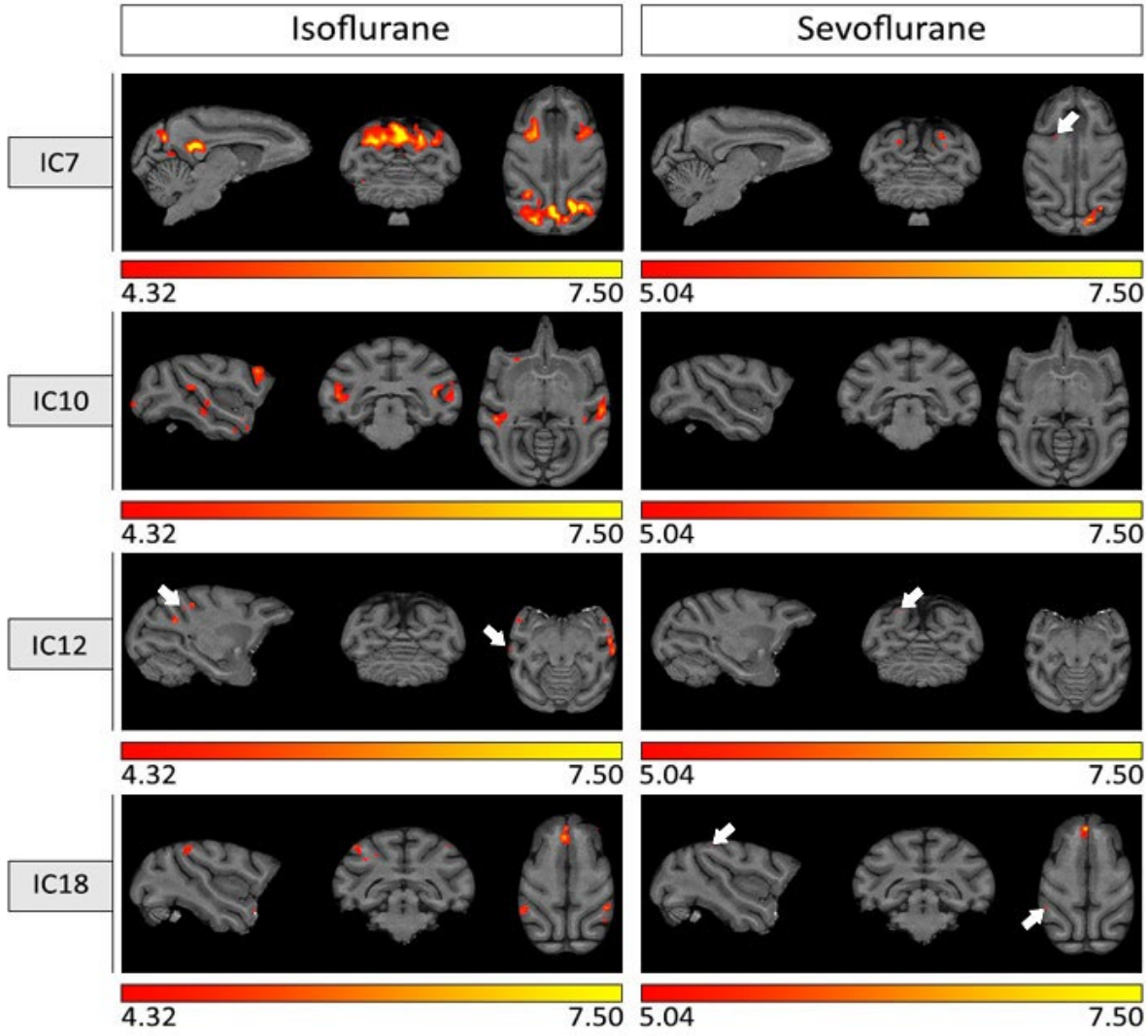


Figure 3.5 Visual Association ICs Under Isoflurane and Sevoflurane

t-static map resulting from the dual regression following the ICA for each Visual association IC under isoflurane (14 monkeys) and sevoflurane (10 monkeys).
The t-statistics maps are presented on the F99 template with a significance level of α=0.001 (isoflurane: $t \geq 4.32$, sevoflurane: $t \geq 5.04$). The colourbar represents the range of values of t from significance. To aid direct comparisons, voxels with values superior to 7.50 are grouped under the same gradient colour (yellow). White arrows point toward significant clusters the reader might otherwise miss.

3.3.3 Non-Visual Networks

3.3.3.1 Default Mode Network

The Default Mode Network (DMN) is a large scale network comprised of several high-level cognitive areas that remain active when the subject is at rest (Mantini et al., 2011) or anesthetized (Arsenault et al., 2018). Typically, the DMN in macaques contains prefrontal and medial parietal regions, including areas 9/46d, 31 and 8b, as well as the ACC and the PCC (Mantini et al., 2011). IC5 under isoflurane (see Figure 3.6) includes the right dorsolateral prefrontal area (8b), the left prefrontal areas 46v and 46d, the left dorso-medial prefrontal area and, bilaterally, ACC, PCC (small cluster), and the dorso-lateral prefrontal area (9d).

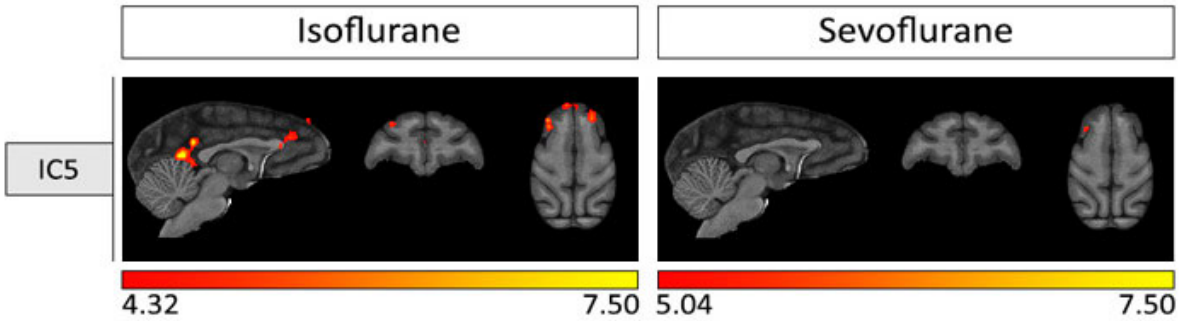


Figure 3.6 DMN Under Isoflurane and Sevoflurane

Output of the dual regression following the ICA the DMN IC under isoflurane (14 monkeys) and sevoflurane (10 monkeys). The t-statistics maps are presented on the F99 template with a significance level of α=0.001 (isoflurane: $t \geq 4.32$, sevoflurane: $t \geq 5.04$). The colourbar represents the range of values of t from significance. To aid direct comparisons, voxels with values superior to 7.50 are grouped under the same gradient colour (yellow).

Under isoflurane (see Figure 3.6), IC5 presents small significant correlations with areas not traditionally associated with the DMN. Significant clusters are present in the left premotor cortex (F2, F5), the somatosensory area 1-2, and the right retrosplenial cortex.

However, most clusters are located in DMN area. Significant correlations are evident in the ACC and the PCC bilaterally. A significant cluster is also evident in the right FEF. In the dorsolateral prefrontal cortex, correlations with the areas 46d and 46v, 9d right 8Bs and bi 8bd, bi 9d.

The sevoflurane network is reduced to a cluster a few voxels large, in the left dorsolateral prefrontal cortex in 9d.

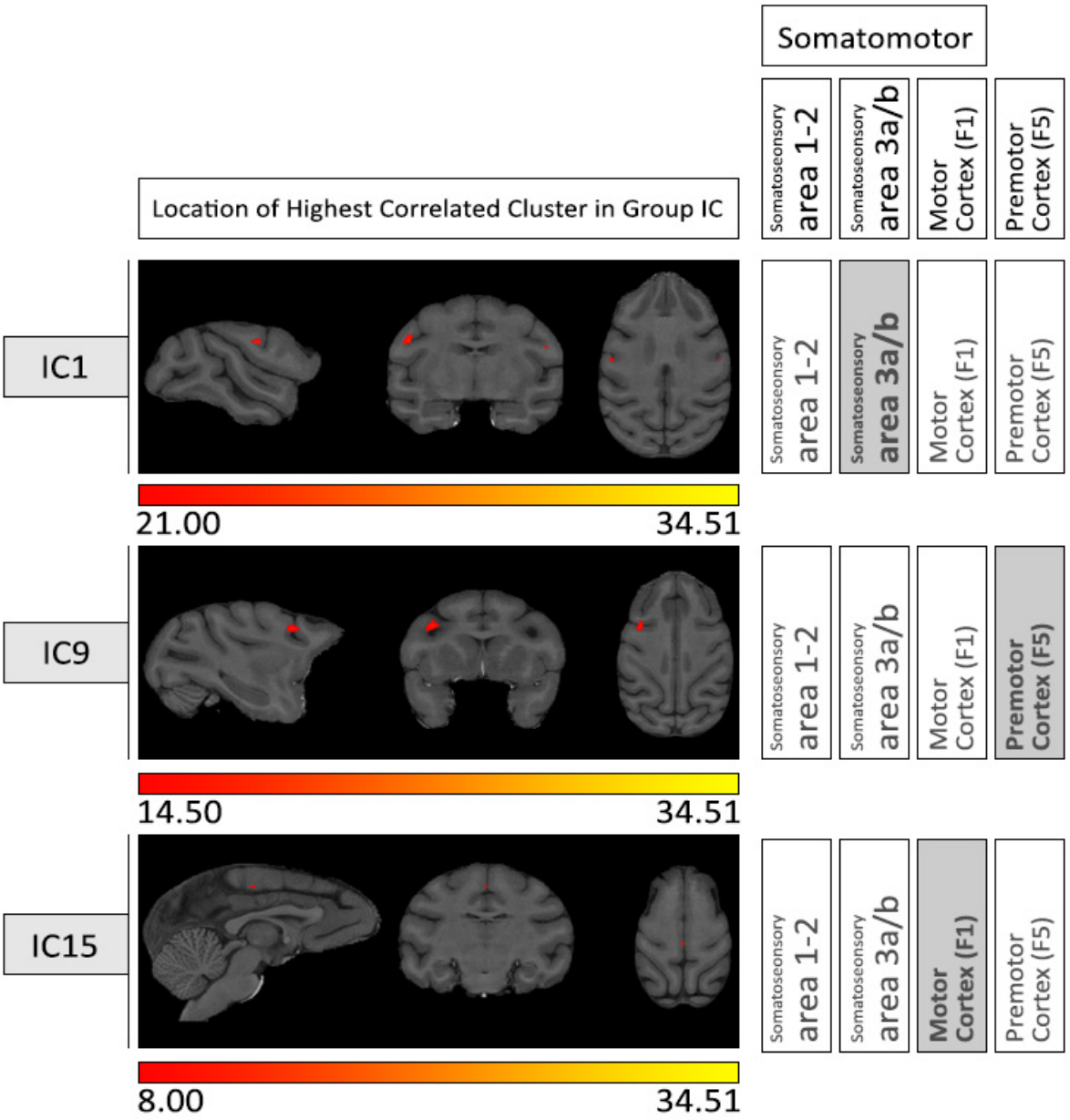


Figure 3.7 Location of the Highest Correlated Voxel in Group IC (Somatomotor ICs)

Location of the highest z-score voxel in the group IC. The associated table shows (in grey) which brain area this cluster is located in. If the highest voxel cluster in a network was located in a somatosensory or a motor area, the network was classified as a somatomotor IC. The colourbar depicts the range of z values from the threshold where no other significant cluster other than the one shown above was visible to the highest z value across all 25 ICs.

3.3.3.2 Somatomotor

Somatomotor group ICs (see Figure 8.3 in Appendix 8.4) have their strongest correlation in either the somatosensory cortex or the motor cortex. IC1, IC9 and 15 all met this criterion (see Figure 3.7).

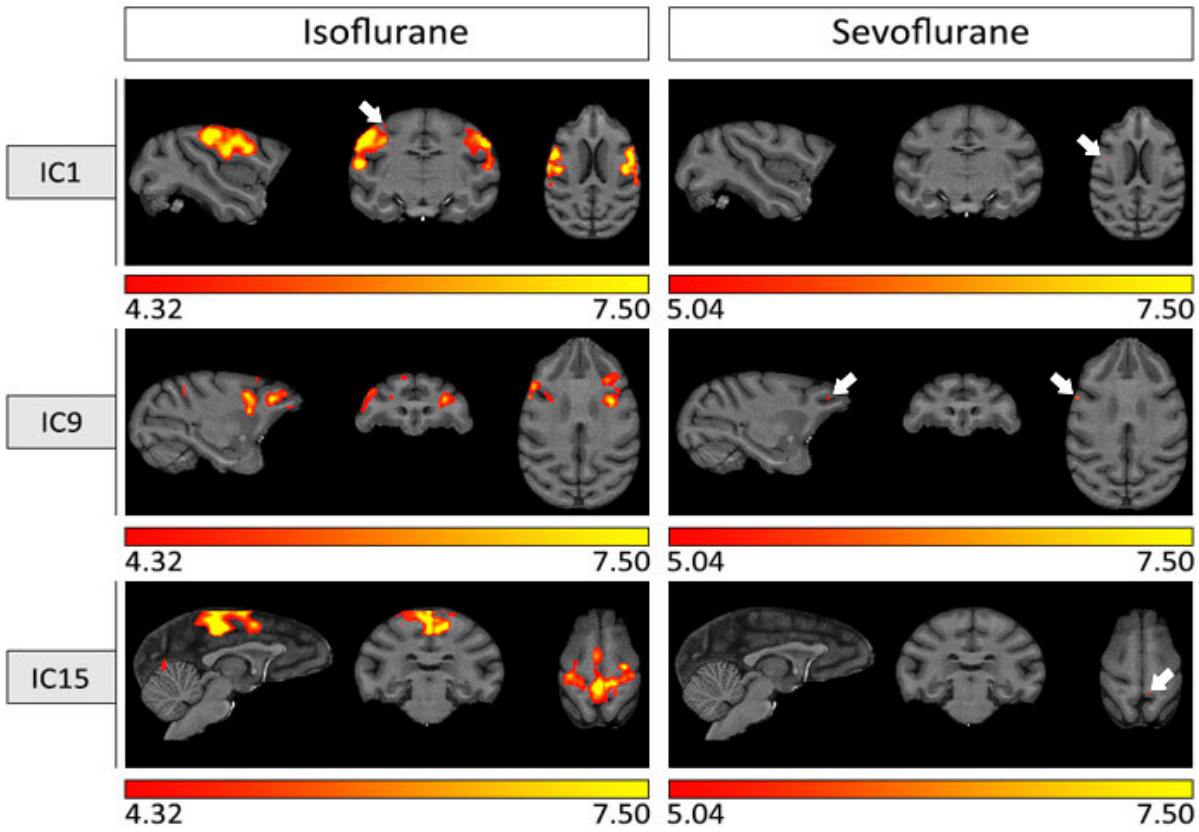


Figure 3.8 Somatomotor ICs Under Isoflurane and Sevoflurane

Output of the dual regression following the ICA the Somatomotor networks under isoflurane (14 monkeys) and sevoflurane (10 monkeys)
The t-statistics maps are presented on the F99 template with a significance level of α=0.001 (isoflurane: $t \geq 4.32$, sevoflurane: $t \geq 5.04$). The colourbar represents the range of values of t from significance. To aid direct comparisons, voxels with values superior to 7.50 are grouped under the same gradient colour (yellow). White arrows point toward significant clusters the reader might otherwise miss.

3.3.3.2.1 Somatomotor IC Under Isoflurane

The isoflurane IC1 (see Figure 3.8) is centred on the somatosensory cortex and includes the somatosensory areas 1, 2, 3a and b, as well as the secondary somatosensory cortex. IC1 also overlaps with the motor cortex and the ventral premotor cortex (F4 bilaterally and F5 in the right hemisphere). Interestingly, IC1 also includes three areas which are strongly activated in

macaques when they observe someone grasp an object: PFG, AIP and LIP (Nelissen et al., 2011). The premotor cortex (F2, F5 and left F4) is also included in IC9. A bilateral significant correlation cluster is evident in 7a/Opt, although the cluster in the right hemisphere is noticeably smaller. In the frontal cortex, the network involves FEF, the ventrolateral prefrontal cortex (areas right 46v, 46d, 45b and left 44), and the dorsal prefrontal cortex (right 8Bs). Unilateral correlations are also found in the left orbital prefrontal area 12m and the right Insula.

IC15's main cluster is located on the somatosensory areas 3a and 3b, and expands to the somatosensory areas 1 and 2. IC15 also includes clusters of significant voxels are present in motor areas such as the motor cortex (F1), the ventral premotor cortex (F2 and left F4) and the right superior parietal lobule area PE. Some non-sensorimotor areas also belong to the IC15 network. Significant correlations are found in the anterior cingulate cortex (ACC) and the posterior cingulate cortex (PCC) and in the visual areas V2 and the left V3v.

3.3.3.2.2 Somatomotor IC Under Sevoflurane

Under sevoflurane (see Figure 3.8), all the somato-motor ICs are reduced to the point of only involving a handful of voxels. The IC1 network is constituted of a 2 voxels large cluster located in the white matter. IC 15 under sevoflurane comprises one significant voxel in the left V2 and the sevoflurane IC9 only involves a cluster in the right ventral premotor cortex (F4).

3.3.3.3 Auditory

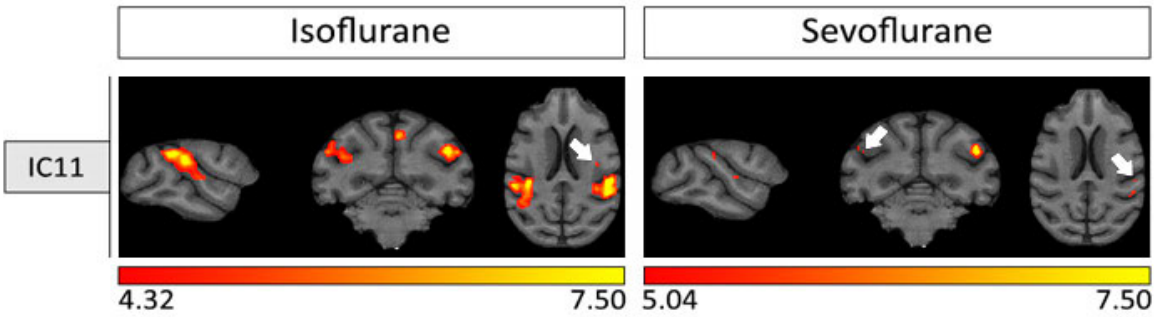


Figure 3.9 Auditory IC Under Isoflurane and Sevoflurane

t-static map produced by the dual regression following the ICA for the auditory IC under isoflurane (14 monkeys) and sevoflurane (14 monkeys) (10 monkeys).
The t-statistics maps are displayed on the F99 template with a significance level of α=0.001 (isoflurane: t≥4.32, sevoflurane: t≥5.04). The colourbar represents the range of values of t from significance. To aid direct comparisons, voxels with values superior to 7.50 are grouped under the same gradient colour (yellow). White arrows point toward significant clusters the reader might otherwise miss.

IC11 (see Figure 3.9) is a mostly auditory IC. Under isoflurane, it includes large portions of the auditory cortex and the temporo-parietal area (TPT). Significant clusters are also present in the motion processing areas MT and MST. Small unilateral clusters are also present in the right parietal opercular area (7op), the right area PE, the right FST, the left PGa and the left PCC. Bilateral correlations are also present in the dorsal portion of V4 and the claustrum.

IC11 under sevoflurane network, while being noticeably smaller than its isoflurane counterpart, still involves several of the areas described above. Significant correlations are present in the auditory cortex. A cluster is present in the right caudomedial area (CM), the left auditory area I (A1) and a few significant voxels are found in rostromedial region of the auditory cortex (R/RM). A larger cluster of significant voxel is also evident in the left hemisphere. It overlaps several temporal areas to include TPt, TPO, MST, and 7a/Opt.

3.3.3.4 Insular

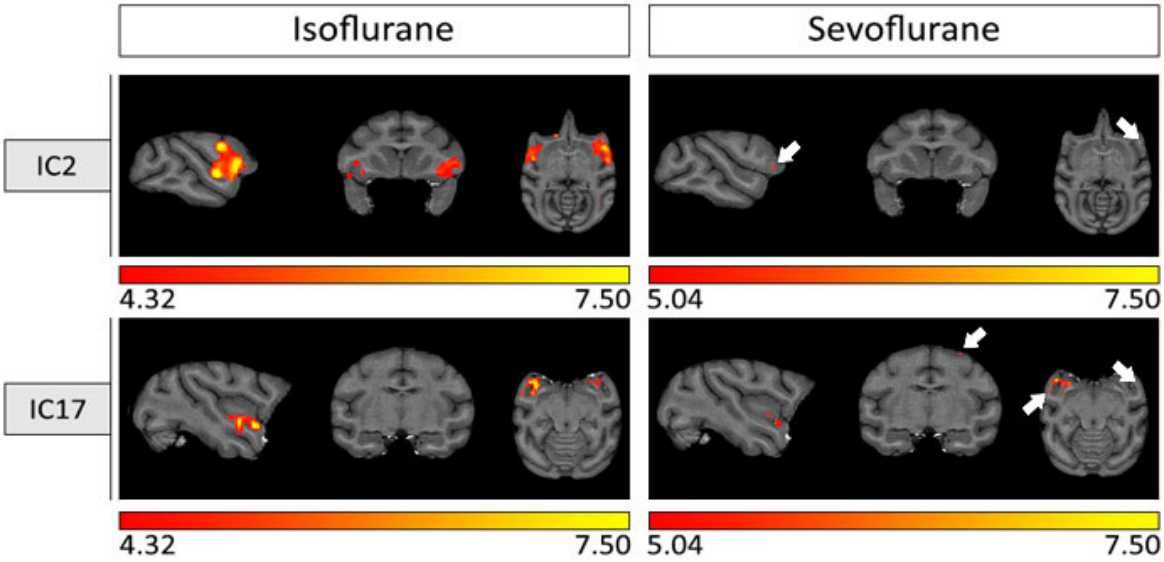


Figure 3.10 Insular ICs Under Isoflurane and Sevoflurane

t-statistic maps for each Insular IC under sevoflurane (10 monkeys) and isoflurane (14 monkeys)
The t-statistics maps are displayed on the F99 template with a significance level of α=0.001 (isoflurane: $t \geq 4.32$, sevoflurane: $t \geq 5.04$). The colourbar represents the range of values of t from significance. To aid direct comparisons, voxels with values superior to 7.50 are grouped under the same gradient colour (yellow). White arrows point toward significant clusters the reader might otherwise miss.

The strongest correlation in the group IC2 and IC17 groups is located in the insula and therefore these two groups were labelled as insular ICs (see Figure 3.10).

3.3.3.4.1 Insular IC Under Isoflurane

Under isoflurane (see Figure 3.10), IC2 is a bilateral IC, which sits over the anterior part of the Insula, the Secondary somatosensory cortex and the somatosensory area 1-2. It also includes the gustatory cortex, the auditory cortex and the motor cortex (F1).

The isoflurane IC17 network is arguably a small unilateral network located in the right hemisphere. Indeed, significant correlations are present in the left hemisphere around the piriform cortex but this area neighbours the middle cerebral artery. It is consequently difficult

to exclude the observed correlation are due to the strong circulatory activity in the region. The network in the right hemisphere is centred around the ventral portion of the right insula and right parainsular areas but also includes significant correlations in the auditory cortex. Significant correlations are present in the rostrotemporal region (RT/RTp), A1, the anterior lateral region (AL). A small significant cluster is also present in the right V4.

3.3.3.4.2 Insular IC Sevoflurane

Under sevoflurane (see Figure 3.10), IC2 presents unilateral correlations, whereas there was only bilateral clusters were present in the isoflurane IC. All the sevoflurane clusters are also very small. A few significant voxels are present in the left F5, the left ventro-lateral prefrontal area (12r), and the somatosensory area 3a/b (one voxel). The insular correlations are only found in a handful of voxels in the right insula.

In the sevoflurane IC17, similarly to its isoflurane counterpart, most significant correlations are found in the right hemisphere. Significant clusters are evident in the right claustrum, the right claustrum the right auditory cortex (RTp), the right TPO and the right insula. A few significant voxels are also found in the left hemisphere

3.3.3.5 Frontal

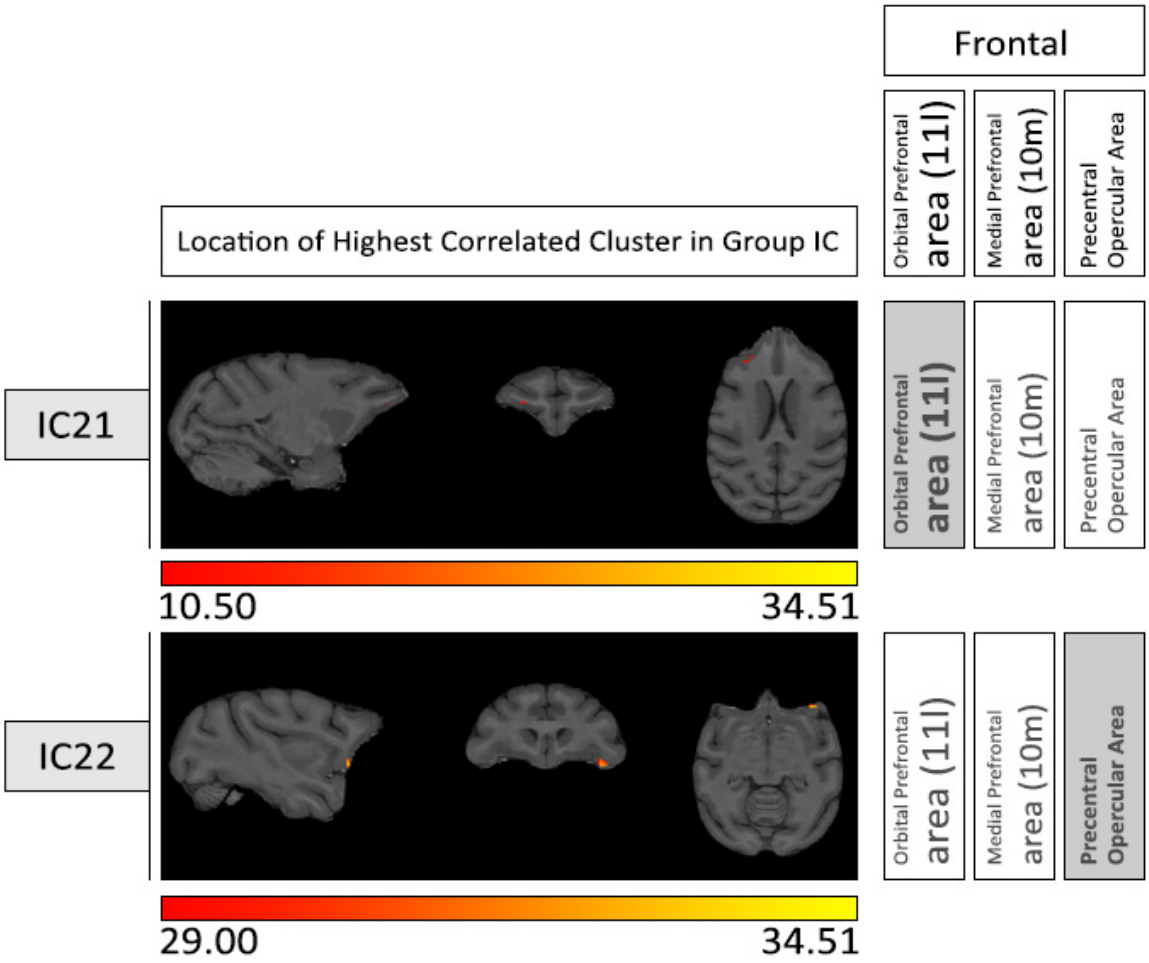


Figure 3.11 Location of the Highest Correlated Voxel in Group IC (Frontal ICs)

Location of the highest z-score voxel in the group IC. The adjacent table shows (in grey) which brain area this cluster is located in. If the highest voxel cluster in a network was located in a frontal area, the network was classified as a frontal IC. The colourbar depicts the range of z values from the threshold where no other significant cluster other than the one shown above was visible to the highest z value across all 25 ICs.

ICs were classified as Frontal if their highest correlated voxel was located in a frontal or prefrontal area. IC21's voxel with the highest correlation was located in the orbital prefrontal area. IC22's highest correlations were located in the medial prefrontal and the Precentral opercular area.

3.3.3.5.1 Frontal IC Under Isoflurane

Under isoflurane, IC21 (see Figure 3.12) only bilateral cluster is located in TE although the

right cluster is substantially larger than its left hemisphere counterpart, as it extends in area TG. Small clusters of significant voxels is present in the orbital prefrontal cortex in the left area 13l, and the right area 12r. A last significant cluster is found in the right precentral opercular area (PrCO), which is large in size relative to the other clusters of the network.

Similarly, in the IC22 isoflurane network (see Figure 3.12), a few significant voxels are present in the left medial prefrontal area (10mr) and the left orbito-frontal area (13m). In the right hemisphere, slightly larger clusters of significant voxels are evident in the right motor cortex (F1), the right medial prefrontal area (10m), and the right TPO.

3.3.3.5.2 Frontal IC Under Sevoflurane

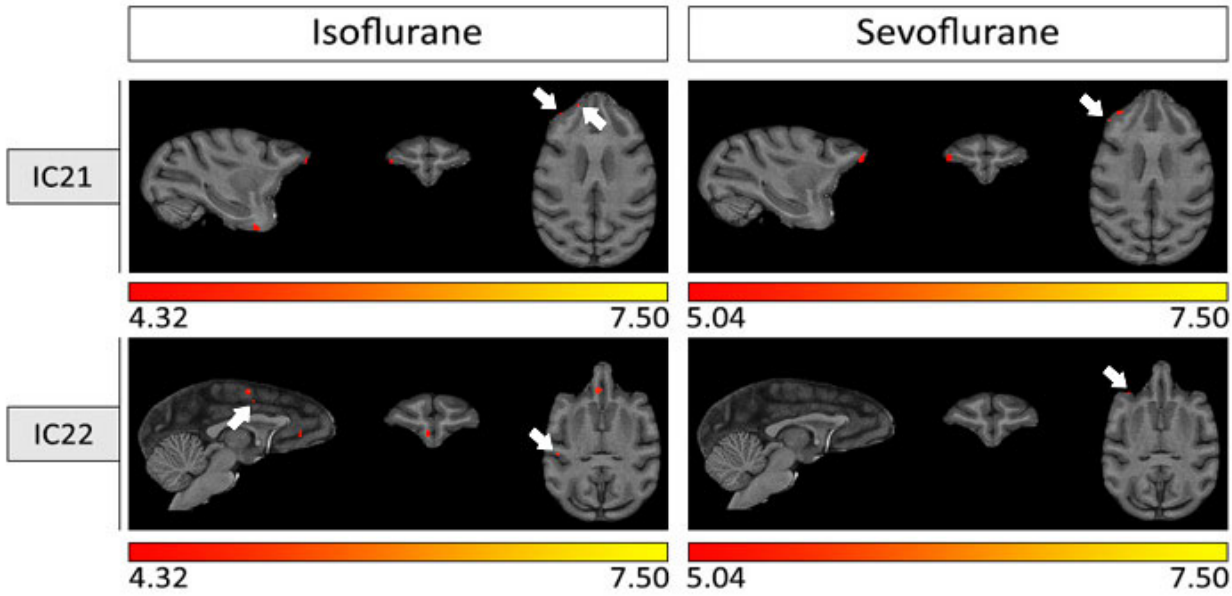


Figure 3.12 Frontal ICs Under Isoflurane and Sevoflurane

Results of the dual regression subsequent to the ICA for each frontal IC under sevoflurane (10 monkeys) and isoflurane (14 monkeys).
The t-statistics maps are presented on the F99 template with a significance level of α=0.001 (isoflurane: t≥4.32, sevoflurane: t≥5.04). The colourbar represents the range of values of t from significance. To aid direct comparisons, voxels with values superior to 7.50 are grouped under the same gradient colour (yellow). White arrows point toward significant clusters the reader might otherwise miss.

The cluster size in IC21 under sevoflurane (see Figure 3.12), are similar to the ones of the

equivalent isoflurane network, only its involves unilateral correlations. A small correlation cluster in the left PrCO- absent from the isoflurane network- is the only cluster in the left hemisphere. In the right hemisphere, other correlations absent from the isoflurane IC21, are found in the orbitofrontal 13b, in the Anterior olfactory nucleus (AONI) and in the ventro-lateral prefrontal area 12l. A significant cluster centred on the right orbitofrontal area 12r and significant is nevertheless present in both networks. This is also the case for the right TE but no correlations in the left TE are found in the sevoflurane network.

IC22 under sevoflurane, however, is almost inexistent. Only a few significant voxels are found in the orbitofrontal are 12o.

3.3.3.6 Putamen

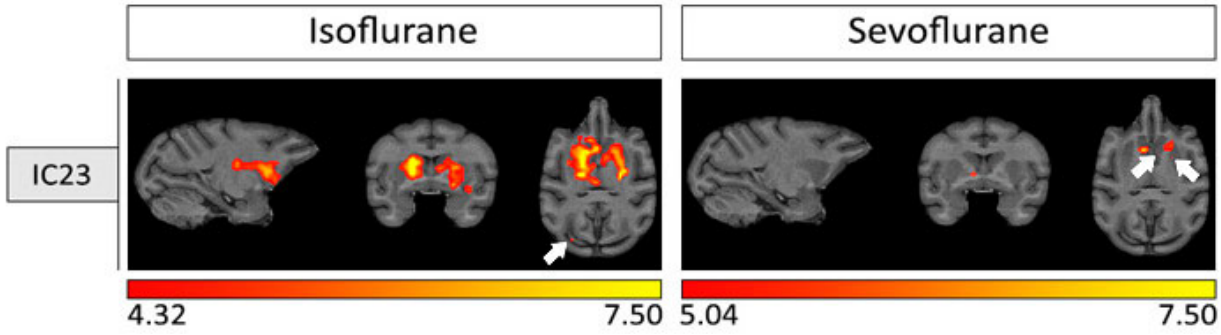


Figure 3.13 Putamen IC Under Isoflurane and Sevoflurane

Results of the dual regression subsequent to the ICA for the putamen IC under sevoflurane (10 monkeys) and isoflurane (14 monkeys).
The t-statistics maps are presented on the F99 template with a significance level of α=0.001. The colour bar represents the range of t-values from significance (isoflurane: t≥4.32, sevoflurane: t≥5.04). To aid direct comparisons, voxels with values superior to 7.50 are grouped under the same gradient colour (yellow). All maps are corrected for multiple comparisons. The white arrows draw attention to small but significant clusters.

Both IC23 (see Figure 3.13) network consists primarily of bilateral cluster including the putamen and caudate nuclei. Nevertheless, the clusters are smaller in the sevoflurane network. Contrarily to the sevoflurane network, the isoflurane IC23 also includes unilateral

significant correlations in the right hemisphere in the Thalamus, the ACC, V1 and V3.

3.3.4 Statistical Comparison

The results described in the previous section show a trend of ICs under isoflurane involving more brain areas than their sevoflurane counterparts. The clusters within isoflurane ICs are also larger, in the way that each cluster involves more voxels than in their sevoflurane IC counterparts.

These results indicate that isoflurane is better at preserving the integrity of the functional connectivity network than sevoflurane. This conclusion, however, needs to be nuanced by rigorous statistical testing. Indeed, the final stage of FSL's *dual_regression* is to run a permutation test to test the null hypothesis that for a given IC there are no differences between the isoflurane and sevoflurane mean group effects. Examination of the comparison maps output by FSL's randomise function (see Figure 8.5 in Appendix 8.6 for results in all 22 IC) indicate that differences between the effect of isoflurane and the effect of sevoflurane over the functional connectivity are found in 9 networks over 22 (see Figure 3.14). These significant differences, all unilateral, are detailed in Table 3.4.

As interesting as these results may be, however, they should be approached with caution. It is often the case that significant differences clusters are located in brain areas that did not belong to the corresponding IC and anaesthetic functional network (e.g., IC1 functional network under isoflurane). As a result, it is possible (although by no means guaranteed) that they could not be meaningful (see Chapter 3.2.5). It may only be possible to speak with conviction regarding the existence of differential effects for brain areas that were included in the original network for the corresponding seeds and anaesthetics (see Figure 3.14).

Table 3.4 Significant Difference Clusters location and Compliance with the Significance and Matching Network Criteria

		Isoflurane -Sevoflurane		*Sevoflurane-Isoflurane*	
		Significant difference cluster location[1]	**Complies with Matching Network criteria[1]**	**Significant difference cluster location[1]**	**Complies with Matching Network criteria[1]**
Visual	*IC7*	N/A	N/A	Left ACC	Left ACC
	IC13	• Brain stem (medial long. fasciculus) • Right V4v	N/A	N/A	N/A
	IC24	• Left Auditory cortex (CM) • Left PGa	Left Auditory cortex (CM)	N/A	N/A
Visual Association	*IC12*	Brain stem	N/A	N/A	N/A
Somatomotor	*IC9*	N/A	N/A	Right orbital prefrontal area (13a)	N/A
Auditory	*IC11*	Left TG	N/A	Right somatosensory 3a/b	N/A
Insular	*IC17*	N/A	N/A	White matter	N/A
Frontal	*IC21*	Left PGA	N/A	• Right Anterior olfactory nucleus (AONI) • White matter	Right Anterior olfactory nucleus (AONI)
	IC22	N/A	N/A	Right V1	N/A

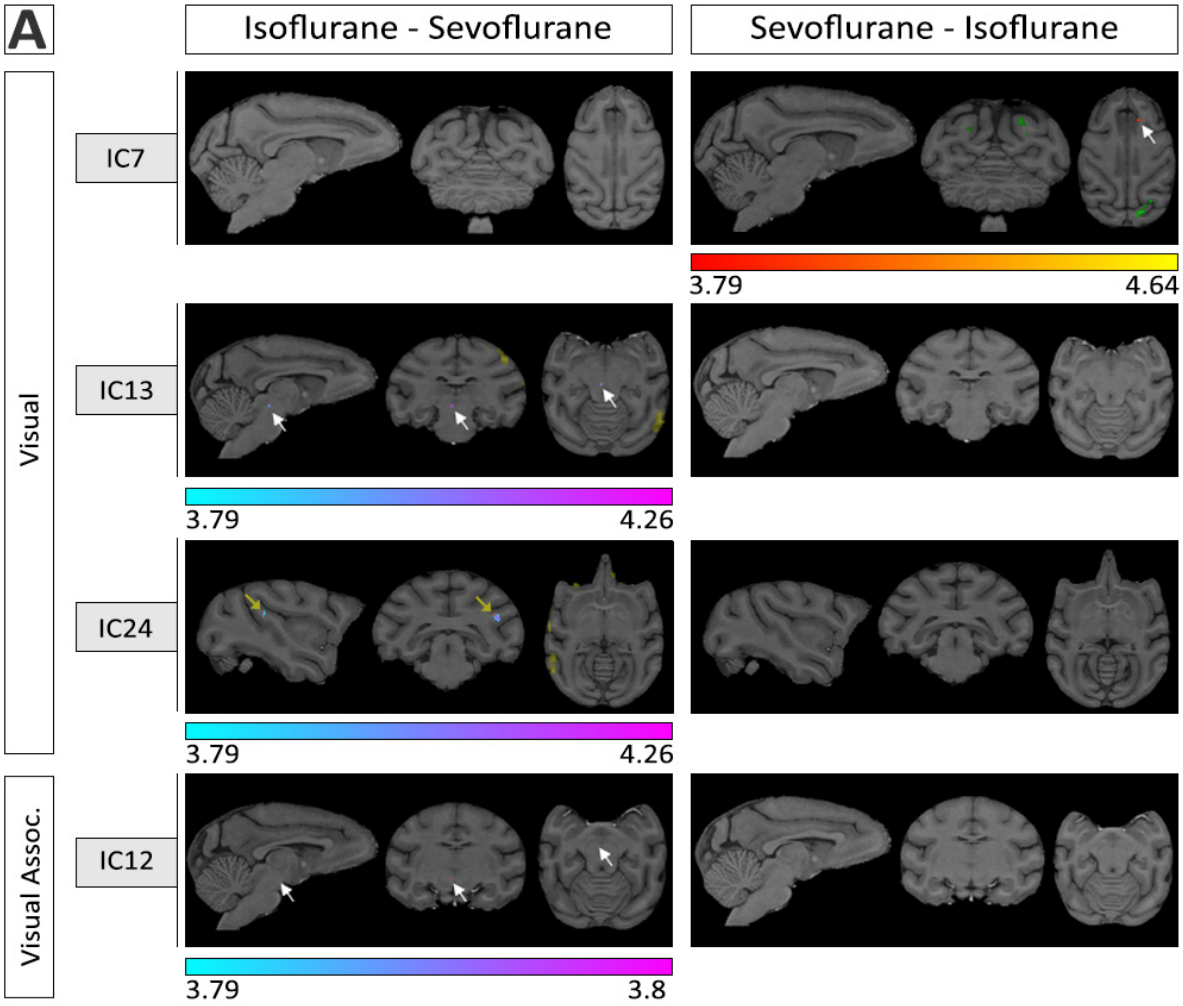
1. p≤0.001

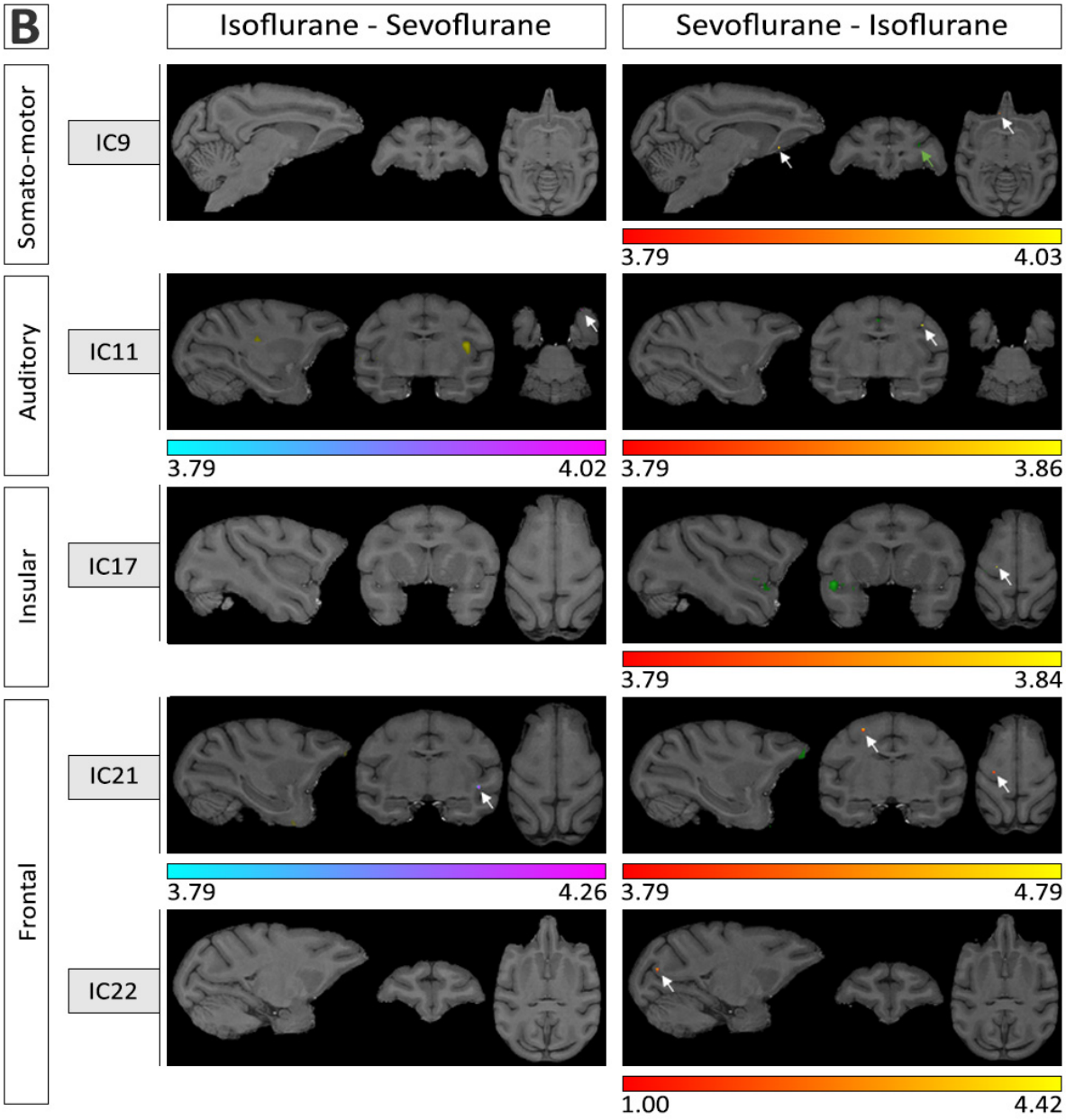
Of the 9 IC where significant differences have been isolated only 3 present significant differences that also satisfy the significance and the matching network criteria (see Table 3.4). In the visual network IC24, stronger correlations under isoflurane than sevoflurane are found in the left Auditory cortex. Inversely the frontal network IC21, stronger correlations under sevoflurane then isoflurane are present in the right AONI. Similarly, stronger correlations under sevoflurane exist in the left ACC for the visual network IC7. It is worth noting, however, that the size of these three difference clusters is very small, involving only a handful of voxels.

Figure 3.14 Localised Significant Differences in Connectivity Strength

Results of the test for H_0: There is no difference between the mean isoflurane group effect and the mean sevoflurane group effect are represented by a t-value map. Column 1 shows the result obtained with contrast Isoflurane - Sevoflurane while column 2 presents the result obtained with contrast sevoflurane) > mean (group isoflurane). The level of statistical significance for both tests was α=0.001 (corresponding to t=3.79).
Only the IC where significant differences were found are presented here. All difference maps are presented in Appendix 8.6. Results are displayed on the F99 template. Colourbars represent the range of t-values from significance to the highest possible t-value in the map. White arrows draw the reader's attention towards significant difference clusters they may otherwise miss.
In the first column, yellow clusters represent the tested IC under isoflurane at t ≥4.32. Yellow arrows point towards small but significant clusters of the isoflurane network. In the second column, green clusters represent the tested IC under sevoflurane at t≥5.04. Green arrows point towards small but significant clusters of the sevoflurane network

For legibility, Figure 3.14 is divided into four parts:
***A.** Figure 3.14 part 1: Visual and Visual Association (Visual Assoc.) IC* ***B.** Figure 3.14 part 2: Somatomotor, Auditory, Insular and Frontal IC*





3.4 Discussion

22 identifiable ICs were obtained by running an ICA on functional resting-state brain data acquired in 10 macaques anaesthetized with sevoflurane and 14 macaques anaesthetized with isoflurane. Many of the isolated ICs are supported by previous research. Moeller et al.'s (2009) reference study found 20 ICs in an awake macaque that was being shown a movie. The authors report 8 visual ICs, also present in the absence of visual stimuli, which echo the visual

ICs described in this chapter. Indeed, these visual ICs align with our understanding of the anatomy of the visual system (Celesia & DeMarco, 1994). IC4, which involves both V4 and TEO, is consistent with the ventral pathway. The visuo-motor IC9 links areas FEF, F5 and ventrolateral prefrontal cortex, which are all involved in visually guided grasping behaviours (Howells et al., 2020). The insula and the somatosensory, involved in IC2, support pain processing (Hu et al., 2015).

Auditory correlations, also reported by Moeller et al.(2009), were present in IC11. It is difficult to conclude if this strong auditory representation is meaningful or due to auditory stimulation related to the loud MRI environment. Future research, employing silent techniques, such as Electroencephalography (EEG) or Magnetoencephalography (MEG), could be valuable in exploring this question further.

Numerous studies show the impact of either isoflurane or sevoflurane on the resting-state functional connectivity compared with the awake state (Peltier et al., 2005; Wu et al., 2016). No studies, however, have compared of the impact of these different anaesthetics on the functional connectivity network. The ICA results, which allow us to observe the RSN as a whole, seem to indicate a trend in which isoflurane appears better at preserving the RSN than sevoflurane. The statistical analysis, however, shows significant differences between the isoflurane and sevoflurane maps for just three of the 22 meaningful ICs.

These findings are surprising, given the findings of previous research employing a MAC-matched sevoflurane/isoflurane Human dataset in Electroencephalography (EEG), which indicates that these anaesthetics change the power spectrum in a similar way (Schwender et al., 1998). Dynamic resting-state analysis work suggests that the functional connectivity network is not fixed across time but is instead comprised of a constant formation and

dissolution of functional connectivity patterns, also called brain states (Deco et al., 2013). Barttfeld et al. (2015) identify 7 brain states repeated across time in awake macaques. Each state appears at a different frequency. When the subject is awake, the more prevalent states are the ones that are the furthest from anatomy (low rank). When the animal is anesthetized, the most frequently found state is the closest to the anatomy (high rank), which is to say the brain state closest to the default mode network. A later study (Uhrig et al., 2014), found the shift from low to high rank observed under anaesthesia happens regardless of the employed anaesthetic (e.g., propofol, ketamine and sevoflurane). In other words, regardless of the molecular mechanism by which unconsciousness is achieved, all anaesthetics should affect the functional connectivity in an overall similar way.

It is worth noting that all of the meaningful significant difference clusters (i.e., those that do not result from negative functional connectivity) are both unilateral and fairly small. As a result, there is a question of significance over substantive import. While statistically significant (i.e., probabilistically present in the study's population), these spatially limited differences, however, which are only present in a minority of networks, are likely to be of little consequences at the scale of most functional connectivity studies.

Isoflurane and sevoflurane are both fluorinated ethers. Both are gamma-aminobutyric acid (GABA) agonists (Jenkins et al., 1999) and interact with the $GABA_A$ receptors. Sevoflurane and isoflurane may however differ in their ability to interact with other receptors and ion channels. It has, for example, been established that in several mammal species, including humans and rats, that fluorinated ether anaesthetics decrease the capacity of the carotidal glomus cells to detect hypoxia (Gaudy et al., 1993; Knill et al., 1983; Ponte & Sadler, 1989). This effect is dose dependent, but its magnitude is not uniform across all inhalational

anesthetics. Sevoflurane, for example, has a minimal effect on the glomus cells' response to hypoxia, while isoflurane and halothane have greater impacts (Hudson et al., 2013). Hypoxia signaling in glomus cells involves potassium ion channels, hyperpolarizing the cell, which triggers an influx of calcium ions inside the cell, through the activation of voltage dependent calcium channels (Lopez-Barneo et al., 2001). Isoflurane and halothane increase the activity of the potassic channels compared to regular hypoxic conditions, which in turn decreases the internal calcic concentration (Pandit et al., 2010). The inhibition of potassium channels in endothelium and vascular smooth muscle cells further contributes to hypoxia regulation by causing vasoconstriction. Hypoxic pulmonary vasoconstriction is attenuated by isoflurane and Halothane but their effect is counteracted by a potassium channel inhibitor (R. Liu et al., 2001). The decrease in internal calcic concentration in the glomus cells remains minimal under sevoflurane, compared to halothane (Pandit & Buckler, 2009). The sevoflurane induced attenuation of hypoxic pulmonary vasoconstriction is also unaffected by potassium channels inhibitors (R. Liu et al., 2001). This differential effect suggests that sevoflurane may interact with potassium channels in a manner different to isoflurane or halothane. Potassium and calcium channels are essential to neurotransmission (Tetzlaff et al., 1993). Potassium channels have notably been suggested to have a central role in neurons' excitability and arousal state regulation (Alkire et al., 2009). The role of ion channels in consciousness loss is unclear but it is conceivable that a differential effect of isoflurane and sevoflurane over potassic channels' activity could result in a differential effect over neural activity.

The primary limitation of this study, the small sample size(s), led us to eschew TFCE. TFCE is used to accentuate clusters in data (Smith & Nichols, 2009). It transforms "raw" statistical data (like the t-statistic maps presented in this chapter) into a continuous function which re-weights every point based on the strength of the underlying activation of it and its

neighboring points. It is usually considered an efficient way to increase cluster sensitivity. Despite using all the animals available to us at the time of the study, however, our sample size remains small (Geuter et al., 2018). Obtaining strong effect sizes with a small number of subjects is difficult. As intimated above, TFCE favors regions of data which effect sizes are largest. Indeed, by creating region-dependent weighted averages, TFCE can and often does miss regions of medium and small effect sizes (Noble et al., 2020), by smoothing them out to the point of insignificance. This smoothing is a feature of TFCE, which attempts to differentiate stronger activations from signal noise. Indeed, all test statistics (χ^2, F, z, and t) are intrinsically tied to the magnitude of the phenomena they correspond to. The t-statistic is defined as the measure of the difference between observed effect (or mean, difference, correlation, etc.) and hypothesized value, divided by the standard error of said effect. In a simplified sense, the t-statistic tells us how much larger the effect is than what would conventionally be deemed "random". Corrections of statistical power (e.g., for multiple comparisons) are generally perceived as adjustments of α, the level of statistical significance, or p-values or, somewhat oversimplified, of the probability of encountering effects as extreme as those observed in our results. In either case, these corrections impose more conservative thresholds, meaning we must find results that are more unlikely (i.e., that have smaller corresponding p-values). These probabilities, however, are inversely related to the magnitude of our test statistics. Thus, as we correct for multiple comparisons, we impose a requirement for more improbable results, which is to say larger effect/difference sizes. TFCE, by favoring stronger activations, imposes a requirement for higher t-statistic values (which is to say, greater statistical power). This, in concert with the reduced statistical power in our sample(s), made TFCE a precarious "correction", at best. Not employing TFCE, however, means that we must approach determinations of the existence of significant difference

clusters comprised of only a handful of voxels with increased caution. One such cluster, for example, was observed in the sevoflurane IC 12 (see Chapter 3.3.2.2).

TFCE may also have substantially impacted our comparison of the effects of isoflurane and sevoflurane on the whole brain functional connectivity. Precisely how they would have been impacted is difficult to predict, without direct comparison. On the one hand, clusters we now consider significant may have nonetheless not corresponded to strong enough activations, resulting in their being average-weighted into "insignificance". On the other hand, since TFCE does not impose a firm significance threshold (like the one employed in this chapter) we may also have found larger/wider clusters, providing less meaningful information on specific regions of activation.

It is also worth discussing the inclusion of nuisance regressors in the independent component analysis presented in this chapter, which is also salient to their inclusion in later analyses in this study. When comparing the average of the two groups on the characteristics one at a time, there was no statistically significant difference between the two. This, however, is not sufficient grounds for their exclusion from subsequent statistical models, for a number of reasons. Our tests did not, for example, examine the lack of difference between the two groups on all of the characteristics *concurrently*, a fundamental component of the simplest stage of subsequent analyses. The ICA and SBCA which follow are not simply one-off linear regressions and these characteristics may also affect other aspects of our models. ICA is comprised of a dual regression which creates subject-specific versions of each group IC, which are then permutated (through FSL's randomize function) and contrast files for inclusion in the GLME. The relationship between these permutated, subject-specific ICs (and contrasts) and the nuisance regressors is unknown (and, outside of the model, would provide us with little

meaningful information, regardless). Statistical modelling, however, is not, and should not be, driven by statistical significance alone. Regressors, nuisance or otherwise, are included on the basis of theoretical importance –in this case, the previous research that supports their effects on the BOLD signal. On a practical level, the lack of statistical significance is not necessarily indicative of a lack of substantive significance, especially in the context of a limited sample. For that matter, given the complexity of our modelling strategies and the limited size of our sample (and, for that matter, most sample sizes in such research), relying solely on statistical significance is precarious, given the de facto increased risk of TYPE II error (i.e., false negatives) which increase as sample size decreases and variability increases. There are some methodological approaches which ameliorate these concerns to various extents, usually in higher-level analyses. These include non-parametric approaches (such as FSL's randomize feature[8]) and mixed effects modelling (such as the implementation of FLS's FLAME, which will be discussed in the next chapter). Thus, however, while there are some reasons to disregard regressors that are not statistically significant, there are more (and arguably more important) reasons to retain them.

[8] In conjunction with corrections for multiple comparisons. As (Nichols & Holmes, 2001, p. 6) note, the p-values resulting from these non-parametric permutation tests "are *uncorrected P*-values. Type I errors must be controlled overall, such that the probability of falsely declaring any region as significant is less than the nominal test level α. Formally, we require a test procedure maintaining strong control over *image-wise* Type I error, giving *adjusted P*-values, *P*-values *corrected* for multiple comparisons".

4 Effects of Isoflurane and Sevoflurane on Visual System Functional Connectivity

4.1 Introduction

Whole-brain level analyses, such as those presented in the previous chapter are, undoubtedly, interesting. The more focused the examination, however, the less a priori knowledge we possess, and thus both our examinations and our findings hold the promise of greater interest. Localized differentiations of isoflurane and sevoflurane networks, coupled with a general trend wherein isoflurane networks were larger than their sevoflurane counterparts hint at the potential for the existence of more meaningful differences, when examining the effects of the two anaesthetics in a more granular fashion. Thus, in this chapter, we focus our attention on the examination of the effects of isoflurane and sevoflurane on the Visual System's resting state functional connectivity. To do so, we must understand the architecture of the visual system, how anaesthetics affects the functional connectivity of (here, specifically, visual) areas of the brain in the resting (as opposed to awake) state, and employ an appropriate analytical methodology for the questions we wish to answer and the areas we wish to examine. The introductory section of this chapter addresses these three requirements before proceeding to the actual analysis in the body of the chapter proper, concluding in a discussion thereof.

4.1.1 Architecture of the Visual System

The visual system (see Figure 4.1), is one of the best described sensory systems. The early hierarchical architecture characterizing the visual system in macaques is well mapped, consisting of a series of brain areas which are hierarchically organized based on their interconnectivity (Van

Essen & Maunsell, 1983). At the early levels, they are homologous (R. B. H. Tootell et al., 2003). The Lateral Geniculate Nucleus (LGN), located in the thalamus, is the first relay of visual sensory input in the brain (Conley & Fitzpatrick, 1989; Hubel & Wiesel, 1972). It projects to the primary visual area (V1) (Perkel et al., 1986). V1 is arguably the most extensively studied of the visual areas (Hubel et al., 1977; Hubel & Wiesel, 1962). It is located in the posterior pole of the occipital cortex in mammals and is where the first cortical level of visual processing takes place. Across the left and right hemispheres, V1 contains a complete representation of the visual field. In primates, V1 neurons discriminate orientations, directions, spatial and temporal frequencies, binocular disparity, and colours. V1 sends feedback efferents to the LGN (Briggs & Usrey, 2007; Fitzpatrick et al., 1994; Lund et al., 1975) and strong feedforward connections to the secondary visual area (V2), among others (Huff et al., 2022).

V2 possesses many commonalities with V1. V2 also contains the full representation of the visual field and its neurons are tuned to many of the same visual properties as V1. V2 neurons, however, show comparatively greater ability to detect contours and textures (Anzai et al., 2007; Marcus & Van Essen, 2002). Most V1-V2 connections are direct, although the pulvinar acts as a relay in some cases (Kaas & Lyon, 2007) . V2 projects to the third visual area (V3), the fourth visual area (V4), and the middle temporal visual area (V5/MT) (Anderson & Martin, 2002; Gattass et al., 1997; Kaas & Lyon, 2007). V3 is an occipital visual area, located immediately anterior to V2. Neuroscientists have been debating the function of V3 for at least half a century (see, e.g., Hubel & Wiesel, 1962), and seem to persist into contemporary debates (for an extended debate on the issue, see Lyon & Connolly, 2012). Van Essen et al. (1986) found that neither ventral nor dorsal V1 project to ventral or dorsal V3, respectively. New World Monkey data prompted a theory to explain this by proposing a novel area (DM) adjacent and anterior to V2 (see Allman & Kass, 1975; Jeffs et al., 2013; Rosa et al., 2005). This competed with the V3 model (Brewer et al., 2002; Burkhalter & Van Essen, 1986),

which proposed a multi-component structure for V3.

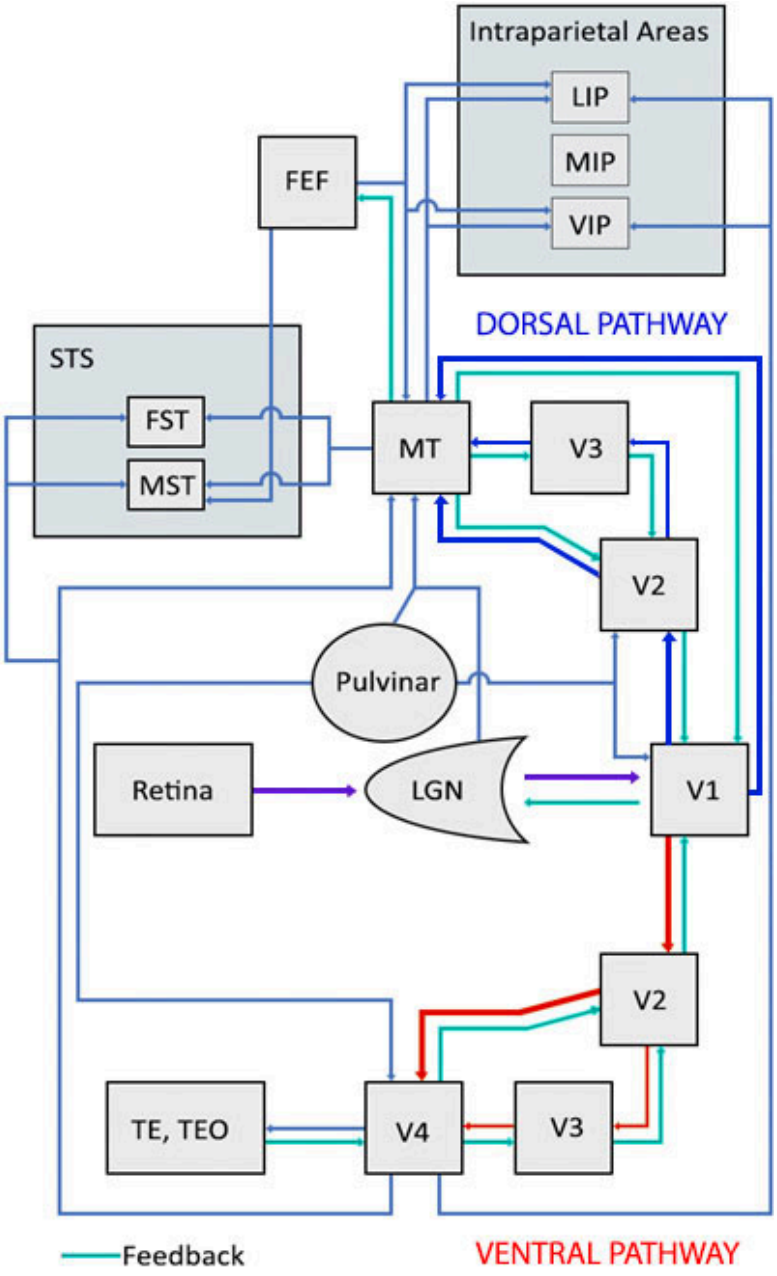


Figure 4.1 Simplified Representation of the Visual System

Adapted from Gattass et al.(1997), *Gilbert & Li* (2013), *Riecanský* (2004), *Ungerleider et al.* (2008), *and Ungerleider & Desimone* (1986). *The larger arrows represent the pathway classically considered as the main visual processing pathway. The pathway coming from the Lateral Geniculate Nucleus (LGN) splits after the primary visual area (V1) into the dorsal pathway (dark blue) and the ventral pathway (red). Feedback connections are represented in teal. For a clearer illustration the secondary visual area (V2) and the third visual area (V3) have been separated in two blocks. This does not correspond to the anatomic reality. Other abbreviations: MT: middle temporal areas, V4: fourth visual area, TE: area TE, TEO: area TEO, FEF: frontal eye field, STS: superior temporal sulcus, FST: floor of superior temporal area, MST: medial superior temporal area, VIP: ventral intraparietal area, MIP: middle intraparietal area, LIP: lateral intraparietal area.*

Van Essen et al. (1986) argue that V3 should actually be split into two independent areas, each containing a portion of the visual field. While consensus seems to be that V3 as a unified -but not uniform- entity does, in fact, exist, there appears to be only limited evidence regarding its precise function (Lyon & Connolly, 2012). Studies by Lyon and Kaas (2001) and Felleman et al. (1997) seem to indicate that it functions in a manner commensurate to V2. Electrophysiological recordings in macaques show that the majority of cells in ventral V3 (V3v) are colour sensitive (Burkhalter & Van Essen, 1986). Reports on dorsal (V3d) vary but is seems that a larger proportion of V3d's cells is motion/orientation sensitive while a smaller proportion of the neurons are colour sensitive (Felleman & Essen, 1987; Gegenfurtner et al., 1997). Other studies only find motion sensitive cells (Baizer, 1982; S. M. Zeki, 1978). Huff et al. (2022) describe visual processing from V2 onward as a visual processing pathway, which feeds to V3-V5, bifurcating into ventral (object recognition) and dorsal (spatial tasks and visual-motor skills) streams (Krubitzer & Kass, 1990).

In macaques, V4 is anterior to V2, in the occipital lobe, before the posterior infratemporal gyrus. V4 neurons are sensitive to simple geometric forms and colours. Like V4, the dorsal prelunate area (DP) is located in the prelunate gyrus (May & Andersen, 1986). This area's role in visual preprocessing is unclear but it is generally considered part of the dorsal stream, as it projects to the parietal visual association areas LIP and VIP (Baizer et al., 1991). DP also receives inputs from dorsal V4 (Ungerleider et al., 2008). The boundary between Dorsal V4 and DP in the crown of the prelunate gyrus is yet to be firmly defined. One study places it at the end of the superior temporal sulcus (Gattass et al., 1988), while others position it much more ventrally (e.g., Stepniewska & Kaas, 1996; Youakim et al., 2001). Additionally, the lower quadrant of the visual field representation in V4 is thought to extend from the anterior bank of the lunate sulcus, across the crown of the prelunate gyrus, and into the posterior bank of

the superior temporal sulcus that overlaps with what some studies consider to be DP (e.g., Youakim et al., 2001). Therefore, atlases like *A Combined MRI and Histology Atlas of the Rhesus Monkey Brain in Stereotaxic Coordinates 2nd Edition* (Saleem & Logothetis, 2006), taken as a reference in this thesis, often choose to introduce a transition area between dorsal V4 and DP. Heretofore, we will refer to this area as V4DP. V5/MT is located in the superior temporal sulcus (STS). It receives strong inputs from V1, V2, the dorsal part of V3, as well as some minor inputs from the LGN and the pulvinar (Ungerleider et al., 1984). V5/MT neurons are tuned for motion direction, binocular disparity, and speed (Born & Bradley, 2005; Dubner & Zeki, 1971; Maunsell & Van Essen, 1983). In both old and new world monkeys, V5/MT projects to a large number of areas implicated in the analysis of optic flow and the generation of eye movements (Riecanský, 2004; Ungerleider & Desimone, 1986).

V5/MT projects to several areas, including the fundus of the superior temporal area (FST), the medial superior temporal area (MST), ventral intra-parietal area (VIP), lateral intra-parietal area (LIP), and the frontal eye field (FEF) (Abe et al., 2018; Maunsell & Newsome, 1987). The FEF is located in the frontal cortex. While not strictly part of the "visual cortex" FEF plays an essential part in saccadic eye movements (Schall et al., 1995) and spatial attention (Thompson et al., 2005). In addition to V5/MT, FEF has connections with several areas involved in eye movements and saccades: the thalamic nuclei lateral mediodorsal (MD), medial ventral anterior nucleus (VA), medial pulvinar, LIP, the supplementary eye field (SEF), the dorsolateral prefrontal cortex (dlPFC), and area 7m in the medial parietal lobe (Lynch et al., 1994; Lynch & Tian, 2006). It also projects to the ipsilateral superior colliculus (SC), caudate nucleus, and putamen (Huerta et al., 1986; Künzle & Akert, 1977; Leichnetz et al., 1981; Lynch et al., 1994; Lynch & Tian, 2006; McFarland & Haber, 2002). Reciprocal connections also exist between FEF and V2, V3, V4, MT, MST, LIP, TEO, and TE (Stanton et al., 1995).

4.1.2 Functional Connectivity of the Visual System Under Anaesthesia

The studies cited above make up only a small portion of the literature (and corresponding research that has greatly contributed to our understanding of both how visual information is processed and how the visual areas interact with each other and the rest of the brain. Unfortunately, obtaining these results requires (to date) the use of invasive methods such as tracer injections, cortical and subcortical electrophysiology recordings, and electrical neurostimulation. This prerequisite renders this type of study nearly impossible in humans. Indeed, ethical considerations make the use of non-invasive methods, such as MRI, the standard approach in human studies.

The study of functional connectivity is one of most widely employed ways to establish connections between two areas of interest in the brain. There are two ways to examine connections within the brain: *physical* (also referred to as *structural*) *connectivity* and *functional connectivity*. As one might expect, anatomical connectivity refers to the physical connection between two brain areas. There are multiple means of discerning the existence of anatomical connectivity. It can, for example, be evidenced via Histology or imaging techniques, such as Diffuse Tensor Imaging (DTI). Histological tracing involves the injection of a tracer agent into nervous tissue, sacrificing the animal and then discerning the location and path taken by said agent through the examination of brain slices (Bentivoglio et al., 1980; Kristensson & Olsson, 1971). DTI is a non-invasive technique, employed to divine, among other things, neural connections (Alexander et al., 2007; Basser et al., 2000; Jones et al., 1999). Diffusion MRI, the more general family of techniques to which DTI belongs, measures the in-vivo, non-invasive, signal attenuation of water molecule diffusion (Le Bihan & Breton, 1985). DTI, in particular, can be used to map three dimensional molecule diffusion to determine spatial location (Alexander et al., 2007) to, among other things, map the structure

of the white matter, is also a good predictor of Histology (Girard et al., 2020).

Functional connectivity can be measured in humans as correlations of BOLD signal changes between different areas over time -the underlying idea being that if activity-over-time in one area is correlated with activity-over-time in another area, the two areas are probably connected to each other, which is to say one area is either *influencing* the other area, *being influenced by* the other area, or *the two areas share a common input*. Indeed, since the functional connectivity of a brain area is generally similar to its anatomical connectivity (Damoiseaux & Greicius, 2009; Wang et al., 2013), the existence of such a relationship, in turn, indicates the potential existence of an anatomical link between the two areas of the brain. It is, however, difficult to obtain perfect behavioural control over an awake animal. Consequently, many animal resting studies are done under anaesthesia. This, too, however, is less than ideal. In mammals, compared to the awake state, anaesthetics can impact the cerebral blood flow (Slupe & Kirsch, 2018), the BOLD response to a stimulus (Aksenov et al., 2015; Dueck et al., 2005; Martuzzi et al., 2010) and change the functional connectivity of brain areas in a dose dependant manner (Giacometti et al., 2021; Hutchison et al., 2014; Martuzzi et al., 2010; Peltier et al., 2005).

In marmosets and macaques, isoflurane decreases the strength of the functional connectivity across all tested networks (visual system included) (Hori et al., 2020; Lv et al., 2016). Similar results are found in the human Default mode network with sevoflurane (Deshpande et al., 2010). Although, still in humans, the functional connectivity of the posterior cingulate is increased under propofol sedation (Mhuircheartaigh et al., 2010; Stamatakis et al., 2010). In addition, electrophysiology studies have found that anaesthetics affect the activity of the visual system. In macaques, for example, ketamine decreases the firing rate of LGN neurons in response to a visual stimulus (Alitto et al., 2011). Sufentanil anaesthesia, moreover, produces

spontaneous synchronized firing in V1 that is absent in the awake monkeys (Ecker et al., 2014).

4.1.3 SBCA vs ICA in the Examination of Differential Localized Anaesthetic Effects

ICA of the whole-brain resting state functional connectivity (see Chapter 3) showed a trend wherein resting state functional networks under isoflurane are larger than equivalent networks under sevoflurane. A more diligent statistical analysis indicated the existence of both meaningful and statistically significant differential effects of isoflurane and sevoflurane on the connectivity strength in two brain areas. While ICA is a strong analytical tool and one well suited to initially examine such differences, it is neither the only method available to us, nor the most granular. As we discuss below, however, there is some research of the effect of anaesthetics at the cellular level that suggest a greater differential effect may exist at the local network level.

Despite isoflurane, sevoflurane, and other agents from the same family of anaesthetics giving the impression of functional commonality, in a broader sense, studies persist in identifying finer differences between them. Using extracellular recordings in cats' V1, Villeneuve and Casanova (2003) showed that, under anaesthesia with isoflurane-NO_2, visual cells' response to visual stimuli was decreased compared to Halothane-NO_2 (another inhalational anaesthetic). Visual evoked potential in rats under Ketamine-xylazine had a longer latency (i.e., the time between a visual stimulus and its detection by the visual cortex) and a higher amplitude than it did under sevoflurane (Castoldi et al., 2021). Aksenov et al. (2019) showed that sevoflurane is more likely to suppress single neuron activity in rabbits than isoflurane. In local field potentials, the same study also found that, while both anaesthetics decrease slower delta oscillations and reduce gamma oscillations, only isoflurane decreases beta oscillations.

Consequently, it is possible that a more detailed approach than ICA, for example in the form of a Seed Based Correlation Analysis (SBCA), could still reveal local differences.

SBCA calculates a linear correlation between the timeseries of a ROI chosen by the experimenter and the rest of the voxels of the brain. It is a particularly appropriate method to study the functional connectivity of a specific area or particular system (e.g., the visual system) in the brain. A seed based approach in mice showed that isoflurane had a different impact on the connectivity of the visual system than Avertine, Ketamine-Xylazine or Urethane (Xie et al., 2020). Building on these foundations, we will employ SBCA will to extract the resting state functional network under anaesthesia from several seeds relevant to the visual system. For each seed the network is then separately obtained under both isoflurane and sevoflurane. Finally, a statistical analysis of the networks under each anaesthetic condition is conducted, to isolate potential local differential effects of the two anaesthetics.

4.1.4 Impact of Statistical Significance Levels on Analysing Functional Connectivity in Visual System under Anaesthesia

The apparent discrepancy in network sizes between isoflurane and sevoflurane observed in the results of the ICA (see Chapter 3.3) could be due to a lack of statistical power. Indeed, in any given statistical test, the determination of the existence of a statistically significant difference (or effect, or relationship) is dependent on finding sufficient evidence that the magnitude of the difference, effect, or relationship, is sufficiently greater than what might be expected, due to random chance. The "sufficient" level of evidence is what is commonly referred to as the "level of statistical significance" (α) and is determined *a priori* based on logic, careful practical considerations of sample size, tests' statistical power, and expected loses to TYPE I and II

error. More often than not, however, the selection of a particular level of statistical significance is based on established practice (i.e., the collective considerations and resulting observations of previous researchers) in a given field's literature. Obviously, the higher (i.e., more conservative) the level of statistical significance we select, the more difficult it is to conclude the existence of statistically significant differences, effects, or relationships.

Generally speaking, it is precarious to surreptitiously select levels of statistical significance less conservative than those established in the literature. The realities of practical research, however, often necessitate adaptation with regards to several aspects of formal inquiry. In other words, it is equally precarious to blindly follow the dictates of precedent when faced with evidence that it may be less-than-ideally suited to the realities of one's current inquiry.

In the case of this research and, for that matter, the majority of research involving live subjects, sample sizes are almost guaranteed to be small. All things being equal, smaller sample sizes correspond to lower statistical power. This study examines live subjects that were unrelatedly (and thus uncontrollably) grouped by anaesthetic agent. Thus, there is a certain amount of lack of statistical power imposed on the tests conducted in the study.

The prevalence of TYPE II errors (or false-negatives, i.e., failing to reject null hypotheses that are actually false) is proportional to the burden of evidence required to reject said hypotheses. Lower statistical power also results in greater difficulty in rejecting null hypotheses, which are actually false. In other words, lower statistical power results in greater frequency of TYPE II errors.

It is therefore possible to offset a known and unavoidable structural lack of statistical power by employing a less conservative level of statistical significance. In the previous chapter, we employed the level of statistical significance $\alpha=0.001$, recommended by Woo et al. (2014). The authors argue that using a more liberal level of statistical significance hinders spatial

specificity –especially when statistical power is low. The results of Chapter 3, however, seem to indicate that, in the present study, this level of statistical significance may be too conservative. As a result, a less conservative level of $\alpha=0.01$ may be necessary to offset the increased likelihood of TYPE II error in our analyses. Using a lower significance level also facilitates applying corrections for multiple comparison, what was not the case in the precious chapter, increasing spatial specificity.

With this in mind, a SBCA is employed in order to:

- Study of the functional connectivity of the visual system under anaesthesia across animals, without taking into account what anaesthetic agent was employed. This is undertaken at both the established $\alpha=0.001$ ($z\geq3.1$) significance level and the less conservative level $\alpha=0.01$ ($z\geq2.3$), also currently used in functional connectivity studies (Berken et al., 2016; Eickhoff et al., 2010; Sawaya et al., 2015) , to examine how, in light of the considerations listed above, choosing one or the other could impact our conclusions.
- Investigate the existence of more localized differences between the functional networks of the six visual areas (LGN, V1, V2, V4DP, V5/MT, FEF), under sevoflurane and isoflurane

4.2 Methodology

4.2.1 Animals and Anaesthesia

This study involved the 23 healthy anesthetized rhesus macaque (*Macaca mulatta*) group described previously (9 females and 14 males) (see Chapter 3.2.2). The data used in this examination was the same as in the previous chapter's ICA (see Chapter 3.2.2, Figure 3.1) and was also preprocessed using the method described in Chapter 2.2. As previously noted, all relevant sessions available at the time of analysis were included.

Although it was described previously, given the nature of the examination being undertaken here, it seems reasonable to restate that a similar anaesthesia protocol was followed for all animals. After induction with an intravenous injection of ketamine (7.5 mg/kg), xylazine (0.125-0.25 mg/kg), and midazolam (0.1 mg/kg), 10 of the animals were maintained with sevoflurane and 14 were maintained with isoflurane (see Chapter 3.2.2). One animal was included in both anaesthetic groups. Data acquisition for rsMRI took place after the time point of clinical ketamine peak -at, on average, 280 minutes after the initial ketamine injection. Resting state functional and structural MRI data were acquired on a Siemens 3T scanner for each subject in the dataset.

On average, the isoflurane dosage was 0.94 MAC and the sevoflurane dosage 1.01 MAC. At these values, no burst suppression –which is to say "a continuous alternation between high-voltage slow waves [...] and depressed (or suppressed) electrographic activity" (Amzica, 2015)– or isoelectric signal –electrophysiological silence– can be observed in EEG in humans (Eger, 1981; Niu et al., 2017). In lay terms, while preserving behavioural anaesthesia, the neuronal activity at this dosage is closer to that of the wakeful state than that of a total loss of consciousness (e.g., coma) and one can consider that much of the neural activity is preserved.

4.2.2 Seed Based Correlation Analysis (SBCA)

SBCA is a method allowing the extraction of temporal correlations between a region of interest (seed) and the rest of the brain (see Chapter 2.2 and Figure 2.4). As a consequence, it is a good way to observe how different brain areas that contribute to visual processing are involved in a functional connectivity network. SBCA also facilitates examination of the possibility that sevoflurane and isoflurane differentially affect resting state functional connectivity between specific areas of the brain.

Six brain areas were selected because of their key roles in visual processing and their locations in the brain, in order to best illustrate the visual functional connectivity networks. They were initially bilaterally drawn on the F99 template, in:

- the lateral geniculate nuclei (LGN) (seed location in F99 coordinates: [96 88 48; 45 88 47) in the thalamus,
- the primary visual area (V1) ([106 25 73; 34 25 72]),
- the secondary visual area (V2) ([75 34 74; 67 35 74]) in the occipital cortex,
- the first relay of the ventral stream, visual area 4 (V4DP) (V4DPF99: [111 50 90; 31 46 90]),
- the middle temporal visual area (V5/MT) (112 58 76; 30 56 77]) in the occipital lobe, and
- the Frontal Eye Fields (FEF) ([111 128 84; 29 130 82]) in the frontal cortex.

With the exception of the LGN, seeds were 5x5x5 voxels (15.63 mm^3) in size. Because of the small size of the LGN, a 3x3x3 (3.38mm^3) voxel seed was preferred.

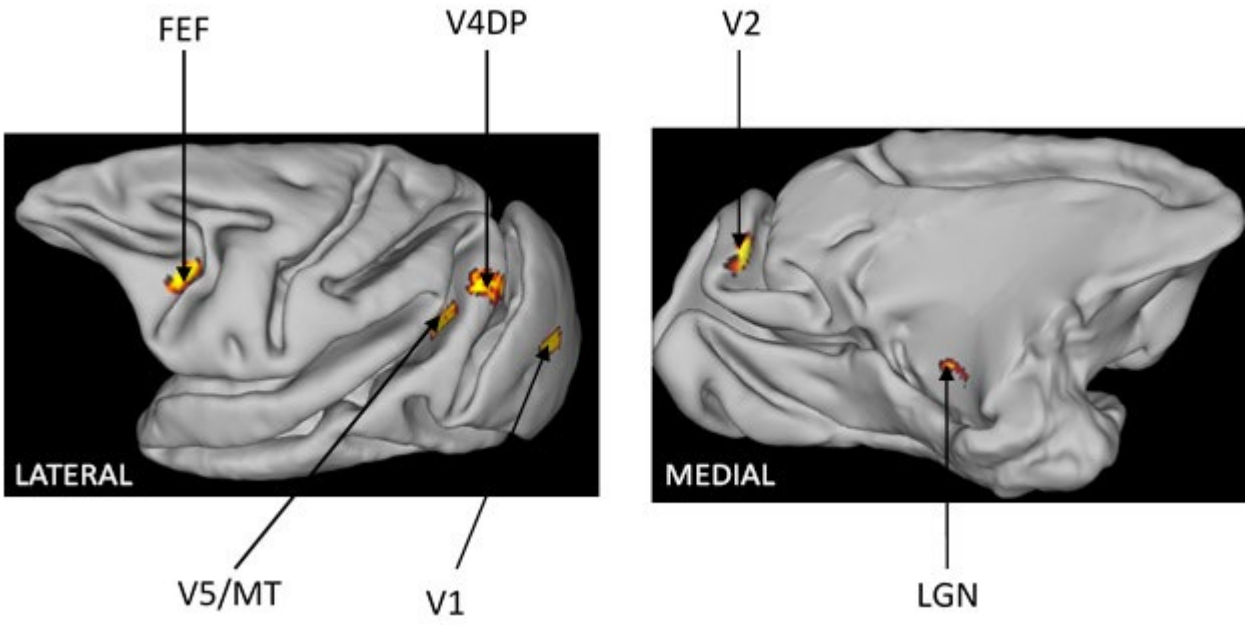


Figure 4.2 Visual Seed Locations

Seeds are bilateral regions of interest. They have been drawn on the F99 template before being realigned to the animal. The left hemisphere seeds are displayed on the semi-inflated F99 template.
V1: Visual area (5x5x5 voxels), V2: secondary visual area (5x5x5 voxels), V4DP: Visual area 4 (5x5x5 voxels), FEF: Frontal Eye Field (5x5x5 voxels), MT: Middle temporal visual area/V5 (5x5x5 voxels), LGN: lateral geniculate nucleus (3x3x3 voxels)

Following first level analysis for each seed, a functional network between the seed and the rest of the grey matter was obtained for each animal. All individual RSNs for a given seed were then entered into FEAT to undertake a higher-level analysis. The higher-level analysis produces the functional networks under each anaesthetic condition as well as a comparison between experimental conditions (i.e., the sevoflurane network, the isoflurane network, the isoflurane-Sevoflurane Comparison, and the Sevoflurane-isoflurane Comparison) using a GLME (see Appendix 8.5 for the design matrix). The anaesthetic group (iso: isoflurane, sevo: sevoflurane) was used as the main regressor of interest. In addition, the animal's age (AGE), delay between anaesthesia induction and data acquisition (time), the subject's median blood pressure (median BP), heart rate (HR), and individual MAC value (MAC), were used as nuisance regressors. A set of four Contrasts (see Table 4.1) was employed for the SBCA:

Table 4.1 SBCA Contrasts

Contrast Description	
Isoflurane group average	*The mean isoflurane group effect.* *This hypothesis examines whether the temporal correlation of the seed timeseries with the timeseries of a given (i,j) voxel is greater than the average temporal correlation across the whole brain, averaged across the isoflurane anaesthetic group. In this instance, the null hypothesis* H_0*:*$[(\overline{z_{(i,j)}})]_{ISO}$*=0 means that on average across the isoflurane group, the temporal correlation within the (i,j) voxel did not vary from the average temporal correlation across the entire brain.*
Sevoflurane group average	*The mean sevoflurane group effect.* *This hypothesis examines whether the temporal correlation of the seed timeseries with the timeseries of a given (i,j) voxel is greater than the average temporal correlation across the whole brain, averaged across the sevoflurane anaesthetic group. In this instance, the null hypothesis* H_0*:*$[(\overline{z_{(i,j)}})]_{SEVO}$*=0 would mean that, on average across all subjects, the temporal correlation within the (i,j) voxel did not vary from the average temporal correlation across the entire brain.*
Isoflurane - Sevoflurane	*The mean isoflurane group effect is greater than the mean sevoflurane group effect (*H_0: $\left[\left(\overline{z_{i,j}}\right)\right]_{ISO} - \left[\left(\overline{z_{i,j}}\right)\right]_{SEVO} > 0$*).*
Sevoflurane - isoflurane	*The mean sevoflurane group effect is greater than the mean isoflurane group effect (*H_0: $\left[\left(\overline{z_{i,j}}\right)\right]_{SEVO} - \left[\left(\overline{z_{i,j}}\right)\right]_{ISO} > 0$*)*
All	*This contrast examines whether the temporal correlation within a given (i,j) voxel is greater than the average temporal correlation within the whole brain, averaged across all animals regardless of the anaesthetic group.*

A higher-level analysis was run for each seed of interest using mixed effects Multi-Level Modelling for Group Analysis. FMRIB's Local Analysis of Mixed Effects (FLAME) employs both between-subject and within-subject variability to provide accurate parameter estimates which, in turn, allows us to infer from our findings to the population of our study (i.e., from which our sample was drawn). FLAME is particularly powerful for at least three reasons. It carries enables easy modelling and estimation of different variances for different groups, within the same model. It employs the first level (fixed effect) variance in higher level analyses, rather than attempting to decrease it (often resulting in negative variances in other applications) and FLAME is applicable to groups with uneven sizes.

All the obtained correlation maps are corrected for multiple comparison using a cluster-based approach (cluster P threshold set at 0.05).

4.3 Results

In this chapter we tested 6 different visual seeds using SBCA. We obtained an isoflurane and sevoflurane network for each seeds. These networks were then qualitatively examined, in search of evident trends in the function of the two anaesthetic agents. Those trends were then examined rigorously, using a series of GLMs. The results of these analyses are presented below.

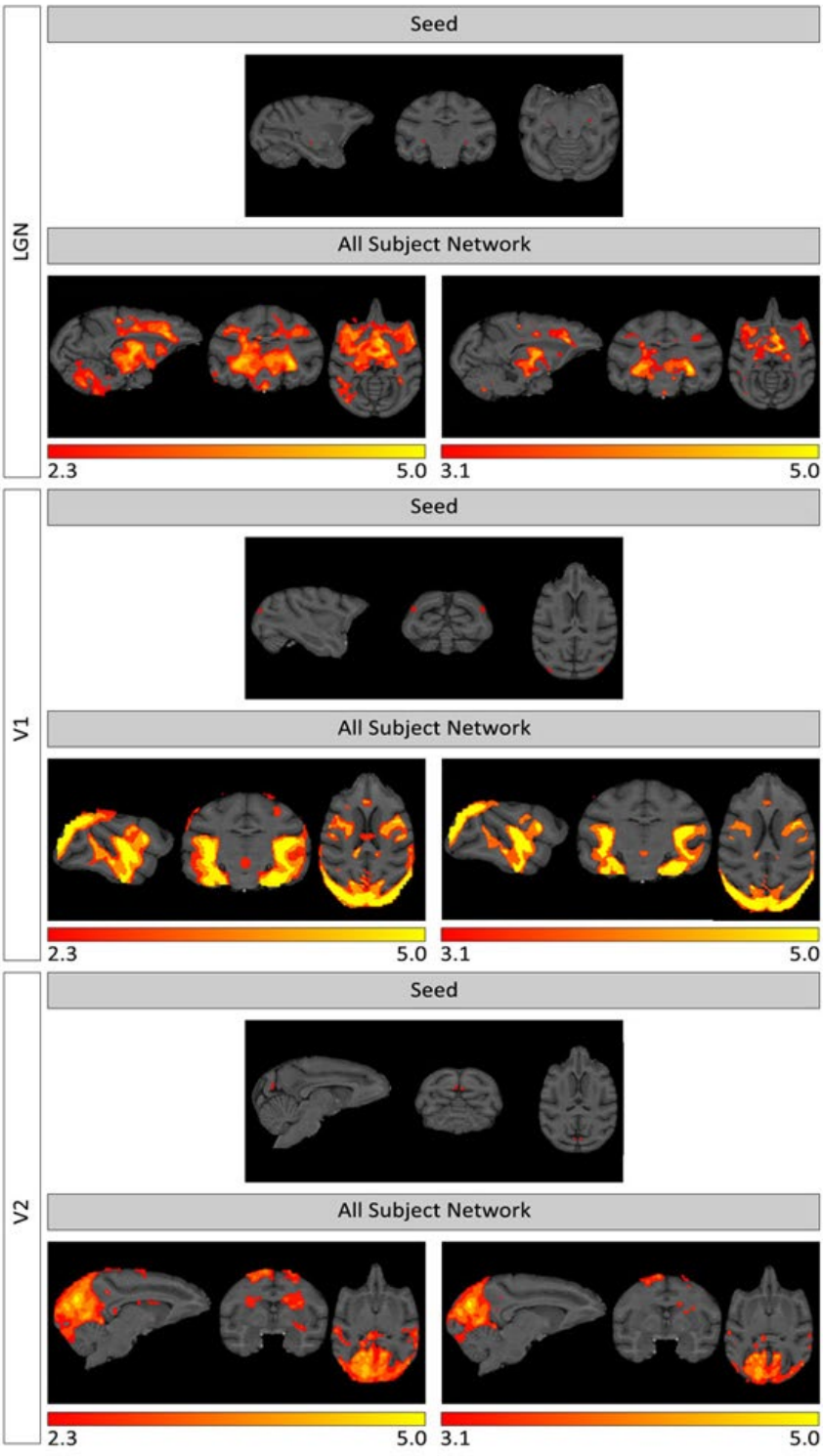
4.3.1 Anesthetized Functional Connectivity of the Visual System Under Two Significance Levels

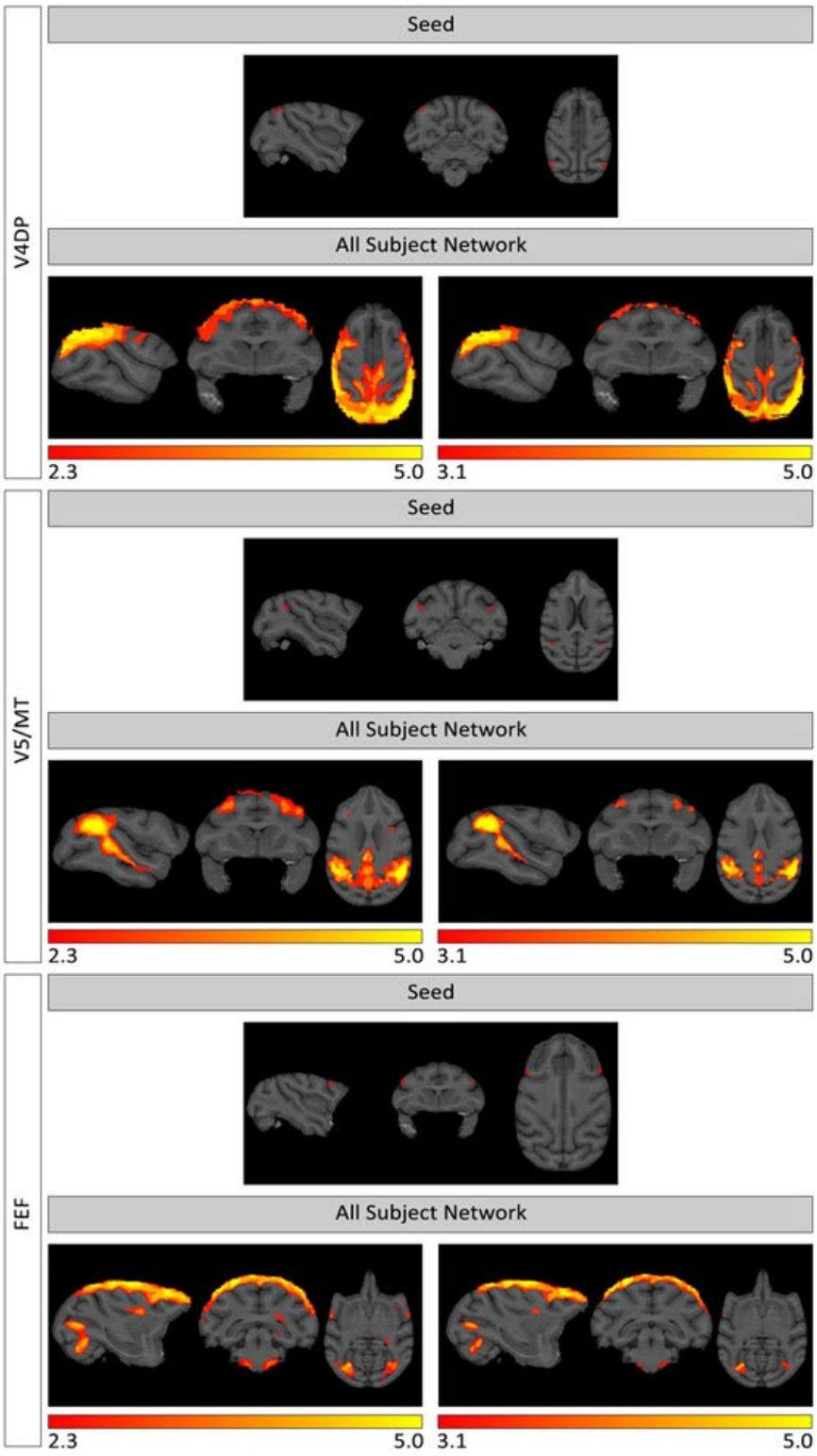
In this section, we discuss the networks obtained with the "All" contrast (see Chapter 4.2.2), where all the study's animals are examined concurrently, without consideration of anaesthetic agent, to obtain a "generic" anaesthetized network for each seed. The resulting networks are described under two significance levels: $\alpha = 0.01$ $(z \geq 2.3)$ and $\alpha = 0.001$ $(z \geq 3.1)$.

Each of the seeds tested is functionally connected to at least one other visual area (for z≥3.1). The LGN seed's network (z≥3.1) (see Figure 4.3) only presents localized correlation with the visual system, in V1 (calcarine), right V3v, right V3A, the right V2, V4 and the right TEO. At the less conservative threshold of z≥2.3, these clusters are larger and significant correlations can be found with TE and the left ventral V4.

Figure 4.3 Anesthetized Visual Resting State Functional Networks

Results obtained with Contrast "All".
SBCA on 23 animals (13 under isoflurane, 9 under sevoflurane, 1 in both groups), without consideration of anaesthetic conditions. Networks were obtained for 6 bilateral visual and visual-associated seeds: Lateral Geniculate Nuclei (LGN) (3x3x3 voxels), the primary visual area (V1) (5x5x5 voxels), secondary visual area (V2) (5x5x5 voxels), visual area 4 (V4DP) (5x5x5 voxels), the middle temporal visual area (V5/MT) (5x5x5 voxels), and the Frontal Eye Field (FEF) (5x5x5 voxels).
The networks are displayed on of the F99 template. The results are shown thresholded for z≥2.3 (α=0.01) and then for z≥3.1 (α=0.001). The colour bar illustrates the gradient of z-values from the significance level to an upper threshold of z=5.0. This upon bound has been applied to facilitate visual comparison All maps are corrected for multiple comparisons.
For illustration purpose the figure was split in two parts.





The V1 anaesthetised functional network (see Figure 4.3) shows significant correlations between the V1 seed and the visual and visual association areas. Bilateral significant correlations are evident

in V2, V3d, V3A, V4, TE, and 7a/opt under both significance levels. For z≥2.3, the visual association areas TEO and superior parietal lobule area are also included in the V1 network. No significant correlations can be found in the LGN, under either significances level (see Figure 4.3).

The V2 network (see Figure 4.3) includes the striated area V1, and the extrastriate areas V3, V4, and left-hemisphere-MT (bilateral at z≥2.3), as well as the visual association areas LIP, MIP and the lateral occipital parietal area. V2's network also involves the superior temporal sulcus (STS) fundus area (IPa) and the STS fundus dorsal area (PGa) –bilaterally at z≥2.3 but only in the left hemisphere at z≥3.1. Significant correlations clusters are evident in FEF at z≥2.3 but not at z≥3.1.

The V4DP network is very similar at both significance levels (see Figure 4.3), involving the visual areas V1, V2, and V3d for both. Significant correlations between V4DP and the visual association areas LIP, MIP, TEO, and the parieto-occipital area (PO/V6) are also found under both significance thresholds.

The V5/MT anaesthetised network (see Figure 4.3) includes significant (z≥2.3) correlations with V1 outside of a cluster centred on the midline, an area of the brain with strong circulatory activity. For z≥3.1, this V1 cluster is reduced to a few voxels around the midline. A second V1 cluster is found in the right hemisphere in the calcarine, both at z≥2.3 and z≥3.1. Significant correlations with V2 are found in the right hemisphere at both significance levels, although here, too, the cluster is greatly reduced in size, for z≥3.1. A large significant cluster overlaps with V4 and V3A, at both z≥2.3 and z≥3.1. The V5/MT anaesthetised network also involves visual association areas such as MST, FST, 7a/opt, LIP, MIP, and the lateral occipital parietal area. These clusters are found at both significance levels, but are again smaller in size for z≥3.1. Significant correlations with V5/MT are also evident in TEO, although they are bilateral z≥2.3 and unilateral (left hemisphere) at z≥3.1.

The FEF anaesthetised network (see Figure 4.3) includes several visual areas. Significant correlations are evident in V4, the left V2, V1, and the right V3v, for z≥3.1. For z≥2.3, the V2 and V3v correlations are bilateral and significant correlations are also evident in V3d and the left V3A. At both levels, significant correlations are present in the visual association area 7a and the superior parietal lobule area. Nevertheless, the FEF anaesthetised network primarily consists of fronto-parietal areas. Large significant correlation clusters are present at both significance levels in the somatosensory cortex, the motor and premotor cortices, the supplementary motor area, and the dorsolateral and ventrolateral prefrontal cortices. Subcortical correlations are also present in the putamen at z≥3.1, and in the left pulvinar at z≥2.3.

The inclusion of non-visual areas is not limited to FEF. Indeed, all of the previously discussed seeds' networks also included non-visual areas. Some of LGN's strongest functional connections are located in the insular cortex and subcortical areas, such as the other nuclei in the thalamus and the putamen (see Figure 4.3). At both levels, the LGN anesthetized functional network also includes large clusters of significant correlations with the basal ganglia, the hippocampus and the amygdala. For z≥3.1, subcortical significant correlations clusters are also evident in the hippocampus and the putamen in the V1 network and the left putamen in the V2 network (see Figure 4.3). For z≥2.3, V2 network includes the caudate nucleus and the putamen cluster is bilateral.

The observed functional networks also involved motor areas. The LGN network (see Figure 4.3) includes the motor cortex and the visuomotor area AIP, for z≥2.3. The premotor cortex is included in the V1, V2 (F2, right F5), V4DP (F4) and the V5/MT (F2, F5, right F4) networks, for z≥3.1. For z≥3.1, the premotor cortex cluster in the V2 network (see Figure 4.3) includes bilateral correlations in F4 and F7. For z≥2.3, bilateral significant correlations are apparent in

the motor cortex, in the V2 anaesthetized network.

Significant correlations are also found the ventrolateral prefrontal cortex (44 and left 45a) in the LGN network, for z≥2.3 (see Figure 4.3). The V1, V4DP, and V5/MT networks present significant correlations with the prefrontal cortex (46v and 46d), although they are unilateral in the V1 network. The V1 unilateral cluster is smaller but still present, for z≥3.1.

The somatosensory cortex is also represented in the LGN, V1, V2, and V4DP anaesthetised networks (see Figure 4.3). The somatosensory cluster in the V1 functional network (see Figure 4.3) includes both the somatosensory area 3a/b, the secondary somatosensory area, and the left somatosensory area 1-2, at z≥2.3. For z≥3.1, only the significant correlations in the somatosensory area 3a/b and the left secondary somatosensory area remain. The V2 and V4DP anaesthetised functional networks both present significant correlations in the somatosensory area 1-2 for both z≥2.3 and z≥3.1, although the cluster is reduced to a few voxels n the V2 network, at the more conservative 3.1 level.

Significant correlation clusters are present in the auditory cortex of the V1 and MT anesthetized networks under for both z≥2.3 and z≥3.1.

In short, at the more conservative z≥3.1 level, networks were smaller with regard to the number of voxels they involved but also the number of areas they included.

4.3.2 Comparison of the Visual System's Functional Connectivity Under Isoflurane Versus Under Sevoflurane by Visual Area

A resting state functional network was obtained for each of the six visual seeds (LGN, V1, V2, V4DP, V5/MT, FEF) under isoflurane ("Isoflurane" contrast) and under sevoflurane ("Sevoflurane" contrast), via SBCA. In the following sections we describe the functional

connectivity of the visual system under each anaesthetic condition. Brain areas, which show evidence of meaningful, statistically significant differential effects of isoflurane and sevoflurane over the functional connectivity strength are then isolated.

4.3.2.1 LGN

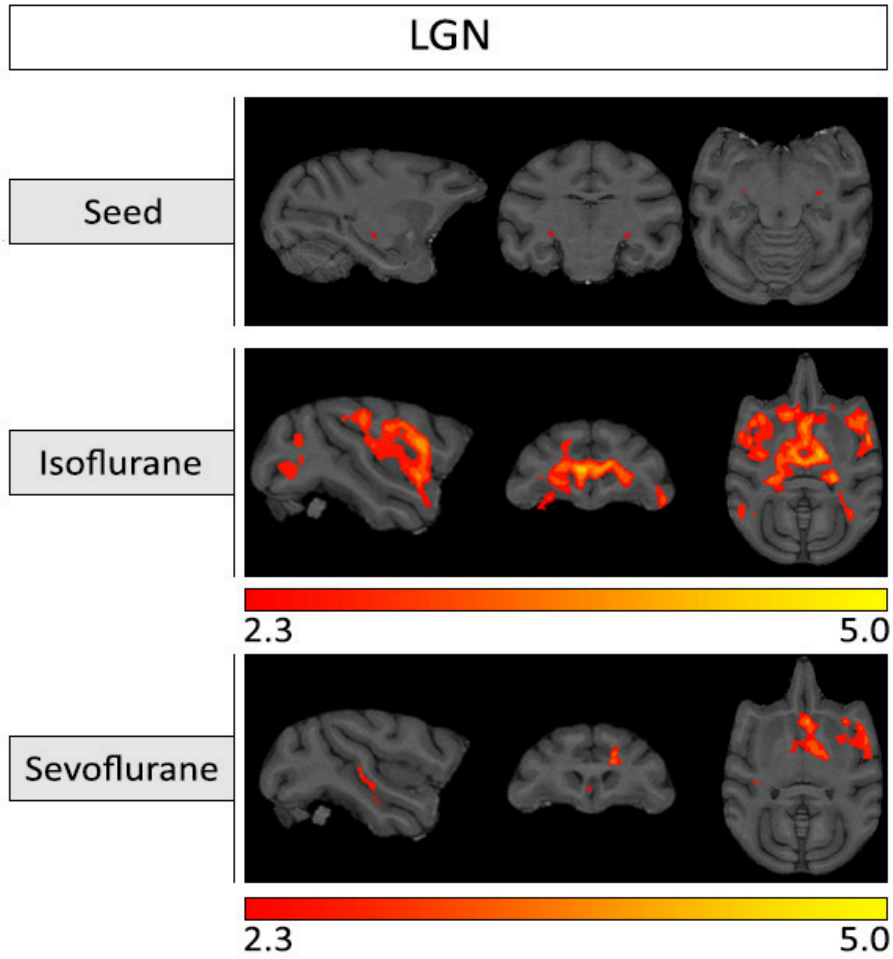


Figure 4.4 LGN's Functional Connectivity Under Sevoflurane and Isoflurane

Results of SBCA to extract temporal correlations between the 3.4 mm3 bilateral LGN seed (first line) and the rest of the grey matter. White arrows indicate the seed's location.
The Z-maps obtained in the isoflurane and the sevoflurane group are displayed on a semi-inflated version of the F99 template (Left: left hemisphere, Right: right hemisphere). The maps are thresholded to z≥2.3 (α=0.01)
The colourbars represent the range of z-values from the level of statistical significance (α) to the highest correlation value. All maps are corrected for multiple comparisons.

The isoflurane LGN functional connectivity network (see Figure 4.4) includes significant

(z≥2.3) correlations with the early visual areas. Indeed, bilateral clusters of significant voxels are present in calcarine V1, V3d, V3v, and, although the left cluster is small, V2. The network also comprises visual associated areas in the temporal pole, a high level visual processing area ensemble (Herlin, Navarro, and Dupont 2021) and in AIP.

In addition, the LGN appears to have functional connections with non-visual structures. In the parietal cortex, significant clusters are present in the insular cortex, the secondary somatosensory cortex, and the motor cortex. In the frontal cortex, correlations are present in the ventrolateral prefrontal cortex (11l, left 12l, right 13m/13l). Correlations are also present in subcortical areas, such as the hippocampus and other nuclei in the thalamus, more notably the pulvinar, putamen, and caudate nucleus.

Under sevoflurane, the size of the LGN network (see Figure 4.4) is substantially reduced. No connectivity with the early visual areas or the frontal cortex remains. In the temporal cortex, no significant correlations can be found in the temporal pole or the auditory cortex. But a unilateral correlation with the right IPA/PGa (right) can be found. Unilateral significant clusters in the left hemisphere are present in the secondary somatosensory cortex, the somatosensory area 3a/b and the insula. Regarding the subcortical areas, the sevoflurane LGN network includes bilateral significant correlations with the ventral nucleus of the thalamus, the amygdala (Ld/Lv), the caudate and a small cluster in the left putamen.

4.3.2.2 V1

The isoflurane V1 functional network (see Figure 4.5) includes both the early visual processing area V2 and the higher visual processing area V4. A cluster of significant voxels is also present in the left MT. The network includes bilateral correlations in TE and TEO. There are no

significant correlations with the LGN.

Outside the visual correlations, V1 activity over time correlates with several temporal areas: the TPt, the insula, auditory cortex, TPO, and IPA/PGA. One bilateral cluster is also present in the putamen and another in the hippocampus. The V1 network under isoflurane also encompasses a cluster in the ventral premotor cortex (F5).

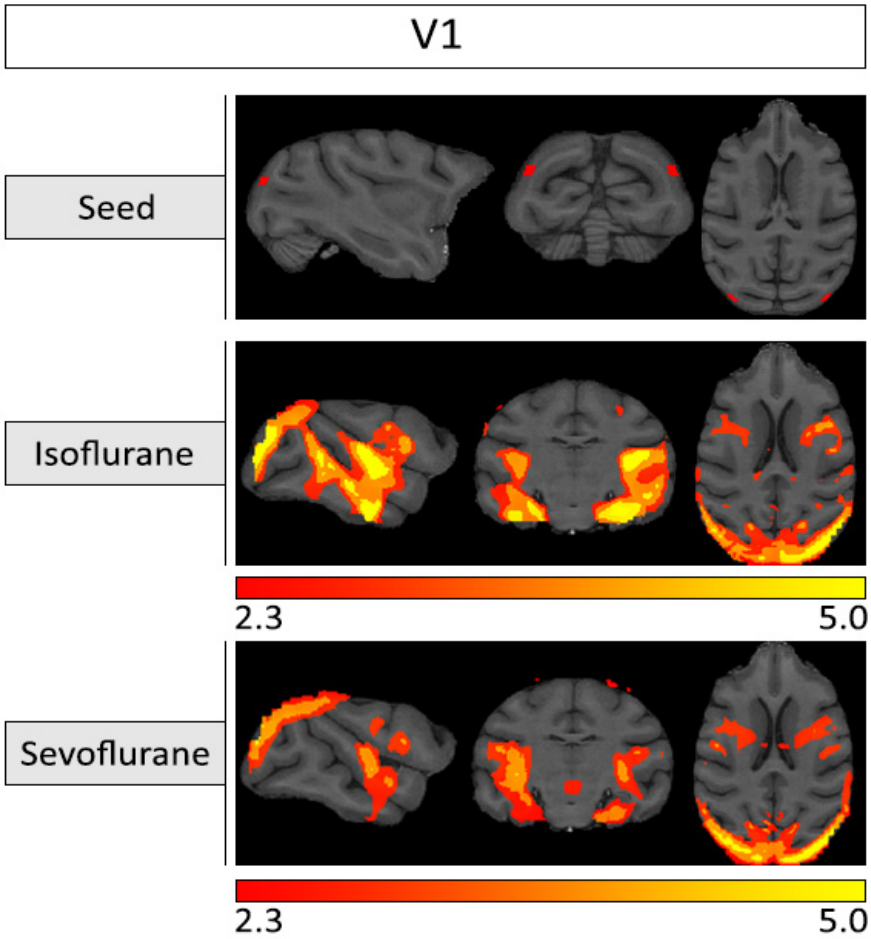


Figure 4.5 V1 Functional Connectivity Under Sevoflurane and Isoflurane

Results of group SBCA with a 15.6 mm3 seed in V1 (first line).
Z-maps were obtained for the isoflurane and sevoflurane groups. The maps are displayed on the F99 template and thresholded to z≥2.3 (α=0.01). To aid in direct comparisons, an upper threshold of z=5.0 was used. The colourbars represent the range of z-values from the significance level to z=5.0. All maps are corrected for multiple comparisons.

The sevoflurane V1 functional network (see Figure 4.5), is of similar size to its isoflurane counterpart. Most of the correlations present in the isoflurane V1 network are also present

in the sevoflurane network, although there are a few differences. The correlations observed in V4 and TPt are only present in the left hemisphere. In the somatosensory cortex, there is a small but bilateral cluster located in the somatosensory area 3 a/b, while the correlation was only present in the right hemisphere in the isoflurane network.

4.3.2.3 V2

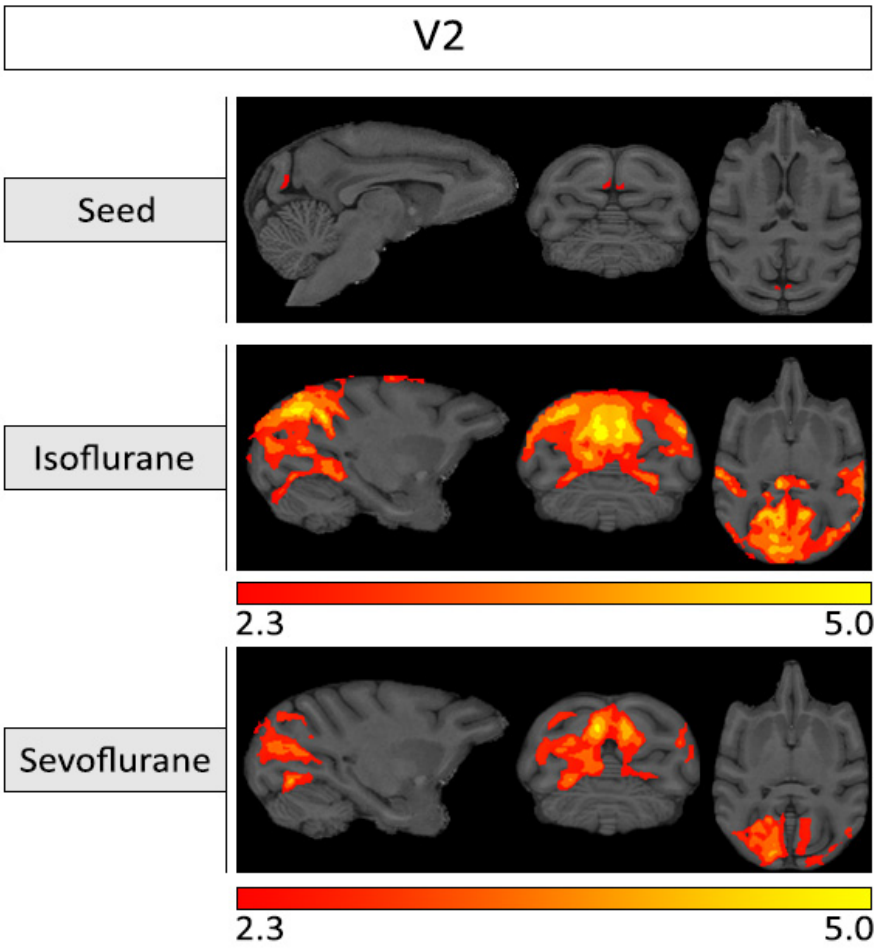


Figure 4.6 V2 Functional Connectivity Under Sevoflurane and Isoflurane

Results of the SBCA with a 15.6 mm3 seed in V2 for the sevoflurane and isoflurane groups. A z-map was created for each anaesthetic group. The maps are displayed on the F99 template and thresholded at z≥2.3 (α=0.01). An upper threshold of z=5.0 was used to facilitate direct comparisons. The colourbars represent the range of z-scores from the level of significance to the upper threshold. All maps are corrected for multiple comparisons.

The V2 isoflurane network (see Figure 4.6) is a large, mostly occipital network. It encompasses all

of the cortical visual areas (i.e., V1, V3d, V3A, V3v, V4, and MT (at z≥2.3)). A significant cluster is also present in the left FEF. V2's functional network also involves areas in the superior temporal sulcus (STS): the IPa and the STS fundus dorsal area (PGa) as well as FST.

V2 is also correlated with fronto-parietal areas. Significant correlations are evident with the intraparietal areas (LIP, MIP, PIP) and the lateral occipital area (LOP). Small significant correlations clustes are present in the right somatosensory area 1-2 and the dorsal premotor cortex (F2).

Like the sevoflurane LGN network (see Figure 4.6), the V2 sevoflurane (see Figure 4.6) network is greatly reduced in size compared to its isoflurane counterpart. The only significant correlations outside of V2 are located in V1 and V3. The V3 cluster includes a small bilateral correlation with V3d and unilateral correlations with the right V3v.

4.3.2.4 V4DP

The isoflurane and sevoflurane (see Figure 4.7) functional networks for the V4DP are similar in many regards. In both cases, V4DP is functionally connected to the visual areas V1 and V2 and the parieto-occipital area (PO/V6). In the temporal cortex, the networks include a cluster in the motor (F1), and ventral (F5) and dorsal (F2) premotor cortices are present in both networks. Nevertheless, the left hemisphere motor and dorsal premotor cortices clusters are much larger under sevoflurane. This is also the case for the significant correlations cluster located in the posterior cingulate cortex (PCC). Each anaesthetic condition z-maps for include significant correlations with the PCC but the clusters involve more voxels under sevoflurane.

Some clusters present in the isoflurane maps are absent from the sevoflurane map. An additional cluster is present in the left V3d and V3v in the isoflurane network. In the intraparietal area, the isoflurane V4DP network overlaps with the right lateral intraparietal cortex (LIP), while no

correlations in LIP are visible in the sevoflurane maps. The isoflurane z-map also involves frontal clusters in the FEF, and the right ventro-lateral prefrontal cortex. In the left STS, there are significant correlations in TPO, the TE and IPa/PGA. These STS and frontal clusters are not present in the sevoflurane network, however. Similarly, the isoflurane network include a unilateral significant correlations cluster in the left hippocampus that does not exist in the sevoflurane network.

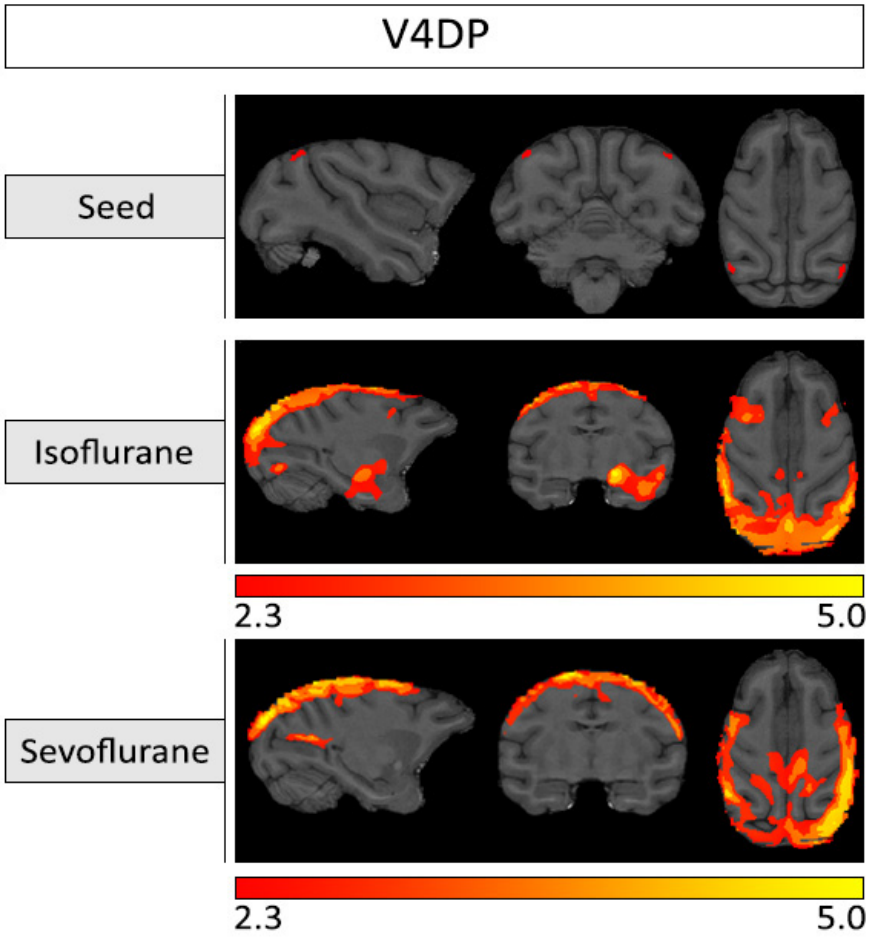


Figure 4.7 V4DP Functional Connectivity Under Sevoflurane and Isoflurane

Sevoflurane and isoflurane groups' group SBCA results with a 15.6 mm35 seed in V4DP (first line).
A z-map was created for each anaesthetic group. The maps are displayed on the F99 template and thresholded at z≥2.3 (α=0.01).To aid in direct comparisons, an upper threshold of z=5.0 was used. The colourbars represent the range of z-values from the significance level to z=5.0. All maps are corrected for multiple comparisons.

4.3.2.5 V5/MT

The V5/MT isoflurane RSN (see Figure 4.8) includes most the cortical visual processing areas

(i.e., V1, V2, V3d, V3A, and V4), as well as bilateral clusters in MIP, LIP, FEF, FST, MST and the retrosplenial cortex. It involves motor connections with significant correlations in the dorsal premotor cortex and the left ventral premotor cortex. Under isoflurane, V5/MT is additionally connected to the dorsolateral prefrontal cortex (area 46). A large cluster is also present in the STS, involving the TPO, TE and IPA/PGA.

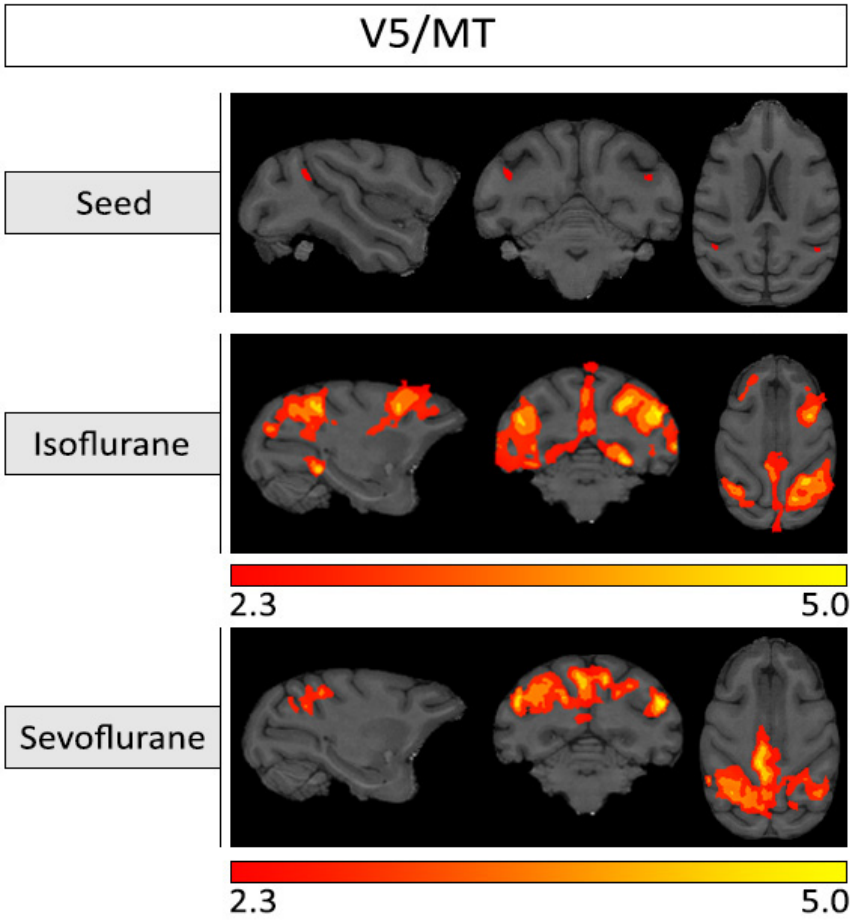


Figure 4.8 V5/MT Functional Connectivity Under Sevoflurane and Isoflurane

SBCA results with a 15.6 mm3 seed in V5/MT for sevoflurane and isoflurane groups.
A z-map was created for each anaesthetic group. Maps are displayed on the F99 template, thresholded at z≥2.3 (α=0.01). To enable direct comparisons, an upper threshold of z=5.0 was applied. The range of z-scores from the level of significance to the upper threshold is shown by the colorbars.All maps are corrected for multiple comparisons.

The V5/MT sevoflurane network (see Figure 4.8) is noticeably smaller than its isoflurane equivalent. Significant correlations are retained in a handfull of voxels located in V4; a small cluster is found in

V3d/V3A. Clusters in the LIP, the retrosplenial splenial, and MST are also present in the sevoflurane map, as well as the right MIP. A cluster in V6 /PO which was in the right hemisphere in the isoflurane map, is now found in the left hemisphere under sevoflurane. In both anesthetics V5/MT network significant correlations with the PCC are evident but they are larger under sevoflurane. However, the sevoflurane V5/MT network does not include significant frontal and STS clusters.

4.3.2.6 FEF

The FEF network under isoflurane (see Figure 4.9) appears to be functionally connected with more fronto-parietal areas than the other tested seeds. The network does include significant temporal correlations in the dorsal portion of V4, although the left hemisphere is larger than in right hemisphere. The isoflurane network also includes localized correlations in V2 and the right V1 (calcarine). Larger clusters are present in LIP, the insula, the somatosensory cortex area 1-2, the motor cortex (F1), the dorsal premotor cortex (F2 and F4), the dorsolateral prefrontal cortex and the ventrolateral prefrontal cortex. The FEF also correlates with the left pulvinar.

The FEF sevoflurane RSN (see Figure 4.9) is again similar to its isoflurane counterpart –to the extent that it involves the same parietal and frontal areas, with the exception of the left insula, where no significant correlation are found. All the clusters found in the visual areas described in the isoflurane network (i.e., V1, V2, and V4) are also present in the sevoflurane map but they are smaller. The V4 cluster is bilateral but this time, the right hemisphere cluster is larger than the left hemisphere's. The V2 correlations are unilateral, located in the left hemisphere, under sevoflurane. Interestingly the V2 cluster also includes ventral correlations which were absent under isoflurane. The V1 cluster is located in the right calcarine, while it was in the left calcarine under isoflurane. There are no significant correlations with LIP or the pulvinar under sevoflurane. Nevertheless, all the other

parieto-frontal clusters mentioned above are present in both FEF networks.

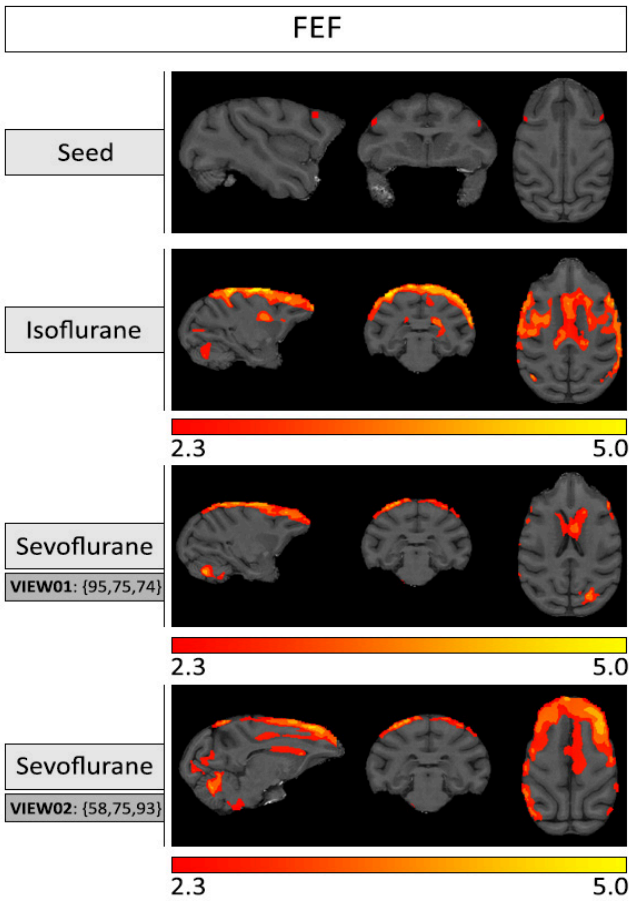


Figure 4.9 FEF Functional Connectivity Under Sevoflurane and Isoflurane

Group SBCA results with a 15.6 mm^3 bilateral FEF seed (first line).
A z-map was created for each anaesthetic group. The maps are displayed on the F99 template and thresholded at z≥2.3 (p=0.01). Here, to better describe the sevoflurane network, two view of this network (In F99 space, {95,75,74} and {58,75,93}) are represented. An upper threshold of z=5.0 was used to facilitate direct comparisons. The colourbars represent the range of z-scores from the level of significance to the upper threshold. All maps are corrected for multiple comparisons.

4.3.3 Statistical Comparison

The functional networks obtained with each of the tested visual seeds (see Figure 4.4 through Figure 4.9) appear to confirm the trend suggested by the results of the ICA (see Chapter 3.3). In general, the sevoflurane networks are smaller than their isoflurane counterparts. This is particularly true for the sevoflurane LGN, V2, and MT networks. A visual inspection indicated that, while the sevoflurane V1, V4DP and FEF networks were (relatively) close in size to their isoflurane counterparts, they still

involved fewer areas. This remains, however, is a purely descriptive conclusion, based on a visual inspection of the results. It would be premature to conclude regarding the validity of such claims, without employing more rigorous analysis. To this end, a GLM was run, testing the null hypothesis that there are no differences between the mean effect of the isoflurane group and the sevoflurane group (for details and an exposition of the alternative hypotheses this was tested against, see Chapter 4.2.2). The results of the GLME model (see Figure 4.10) provide more nuanced information. Indeed, they seem to indicate the existence of localized differential effects of isoflurane and sevoflurane on visual system resting state functional connectivity.

In a fundamental sense, the first alternative hypothesis (Isoflurane - Sevoflurane), corresponds to the mean effect of the isoflurane group being greater than the mean effect of the sevoflurane group. With regard to functional state connectivity, these effects are expressed as (clusters of) correlations. For some of the seeds –which is to say the LGN (see Figure 4.10), the FEF (see Figure 4.10) and V2 (see Figure 4.10)– no significant (i.e., $z<2.3$ in all cases) clusters were found where this was the case. In the V1, V4DP and MT network (see Figure 4.10), however, the mean correlation is statistically significantly stronger (i.e., $p<0.01$, or $z\geq2.3$) under isoflurane than sevoflurane, in several visual areas. All three networks show stronger correlations under isoflurane in V2, although this is only the case in the left hemisphere for V1 and MT, and in the left V3v. The V4DP and MT isoflurane networks present stronger correlations in V1 than their sevoflurane counterparts. Significantly stronger correlations in MT and ventral V4 are found in the isoflurane V1 network. Significant difference clusters are also found in visual association areas. Correlations are stronger under isoflurane in the left parieto-occipital area for MT, the left TEO and Left TE for V4DP, and the left FST and left TEO for V1.

The second alternative hypothesis (Sevoflurane - Isoflurane), is that the mean effect of the

sevoflurane group is greater than the mean effect of the isoflurane group. No statistically significantly stronger correlations were found for the LGN and V1 networks under sevoflurane. The sevoflurane networks present stronger correlations than their isoflurane counterpart in motor areas. The V4DP, MT and V2 present significant differences in favour of sevoflurane, in the ventral premotor cortex (only in the left hemisphere for V4DP). A significant cluster of differences is also evident in the motor cortex for V4DP (left hemisphere) and V2. The Sevoflurane - Isoflurane differential maps also show stronger correlations under sevoflurane in visuospatial and visuomotor areas. The V4DP map includes the left AIP, the FEF map includes the left MIP. The MT map presents unilateral differential clusters in the right hemisphere for LIP, VIP, MIP, the PGm, the superior and inferior parietal lobule area and MST. The V2, V4DP and MT sevoflurane networks all present stronger correlations in the somatosensory cortex than their isoflurane counterparts. Stronger correlations under sevoflurane are also evident in several frontal areas. The V4DP and MT Sevoflurane – Isoflurane maps show significant differences in the orbito-prefrontal area (V4DP: 12o, 13l; V5/MT: 12o, 13m) and left ventrolateral prefrontal area. In the FEF networks, the sevoflurane networks show stronger correlations in the left V1 and the left V2 than their isoflurane equivalents.

As interesting as these results may be, however, they should be approached with caution. Indeed, as discussed in Chapter 3.2.5, only positive correlations are meaningful in this context. Therefore, it is often the case that significant differences clusters observed in the differential maps obtained with the Isoflurane - Sevoflurane and the Sevoflurane - Isoflurane contrasts are located in brain areas that did not belong to the corresponding seed and anaesthetic functional network (e.g., the V1 functional network under isoflurane). These clusters result from the algebraic difference between two negative correlations and must be excluded (see

Chapter 3.2.3). Thus, "Matching Network" and "Significance" criteria must be applied to ensure that the observed difference clusters are meaningful (see Figure 4.10 and Table 4.2).

1. Matching Network: The clusters of voxels representing significant differences for the "Isoflurane-Sevoflurane" contrast (H_0: $\Delta\mu_{iso-sevo} > 0$) must be present in the tested seed's isoflurane network and those representing significant differences for the "Sevoflurane- Isoflurane" contrast (H_0: $\Delta\mu_{sevo-iso} > 0$) must be present in the tested sevoflurane network.
2. Significance: The isoflurane, sevoflurane and Difference RSNs must be compared at the same level of statistical significance. For the purposes of this examination, the level of significance is fixed at z>2.3 ($\alpha = 0.01$)

The significance level is *de facto* satisfied, since we are only comparing maps thresholded at z≥2.3. The Matching Network criteria is somewhat less ideal but still frequently satisfied (see Table 4.2). None of the clusters found with the sevoflurane (Sevoflurane-Isoflurane) in the V2 network satisfy it. On the contrary, all significant difference clusters found in the FEF Sevoflurane – Isoflurane network also belonged to the sevoflurane network. And, for other networks such as the isoflurane and sevoflurane V4DP and V5/MT and the isoflurane V1, only a portion of the clusters satisfy the "Matching Network" criteria. This necessarily curtails any substantive conclusions to the existence of differential effects to those networks where the Matching Network criterion is satisfied (see Table 4.2).

Table 4.2 Significant Difference Cluster Location Summary

	Isoflurane - Sevoflurane		Sevoflurane - Isoflurane	
Network	**Satisfies Matching Network criteria (z>2.3)**	**Does not satisfy Matching Network criteria (z>2.3)**	**Satisfies Matching Network criteria (z>2.3)**	**Do not satisfy Matching Network criteria (z>2.3)**
LGN	*No Difference Found*	*No Difference Found*	*No Difference Found*	*No Difference Found*
V1	Left TEO Left MT Left FST Left V2	Left V4v Left V3v	*No Difference Found*	*No Difference Found*
V2	*No Difference Found*	*No Difference Found*	N/A	premotor cortex, motor cortex, somatosensory cortex, secondary somatosensory cortex, insula, hypothalamus, right caudate, right putamen, right LGN
V4DP	left V1 left V2 left TE left auditory cortex left TPO left subfield of the hippocampus	left TEO left V3v	left ventral premotor cortex (F2, F4) left motor cortex left somatosensory 1-2 left AIP left superior parietal area	ventro-lateral prefrontal cortex (12l, 46), rostral superior temporal area, dorsal temporal pole, ventral premotor cortex (bilateral F5) left ventrolateral prefrontal area orbito-prefrontal area (12o, 13l) right caudate
V5/MT	V1 V2 Left parieto-occipital area	Left V3v	Right inferior parietal lobule area Right LIP Right VIP Right MIP Right PGm Right retrosplenial cortex Right PCC Right superior parietal lobule area. Right V3A Right MST	orbito prefrontal cortex (12o, 13m) left rostral superior temporal gyrus left TE left dorsal temporal pole ventral premotor cortex (F5 and right F4) left ventro lateral prefrontal area (12m, 12r)
FEF	*No Difference Found*	*No Difference Found*	left V2 left V1 left MIP	N/A

For each seed, this table lists the brain area were the null hypothesis "there are no significant differences between the mean effect of the isoflurane group and the mean effect of the sevoflurane group" was rejected.
***Isoflurane - Sevoflurane**: the mean effect of the isoflurane group is greater than the mean effect of the sevoflurane group*
***Sevoflurane - Isoflurane**: the mean effect of the sevoflurane group is greater than the mean effect of the isoflurane group*
Matching network criterion: The clusters of voxels representing significant differences for the first test (H_0: $\Delta\mu_{iso-sevo}>0$) must be present in the tested seed's Isoflurane network and those representing significant differences for the second test (H_0: $\Delta\mu_{sevo-iso}>0$) must be present in the tested seed's sevoflurane network (heretofore referred to as the criterion of "Matching Network". The areas in the column "Does not satisfy Matching Network criteria (z>2.3)" are areas were a significant difference between the functional connectivity of each anaesthetic have been found but which cannot be considered meaningful because they result from negative correlations.

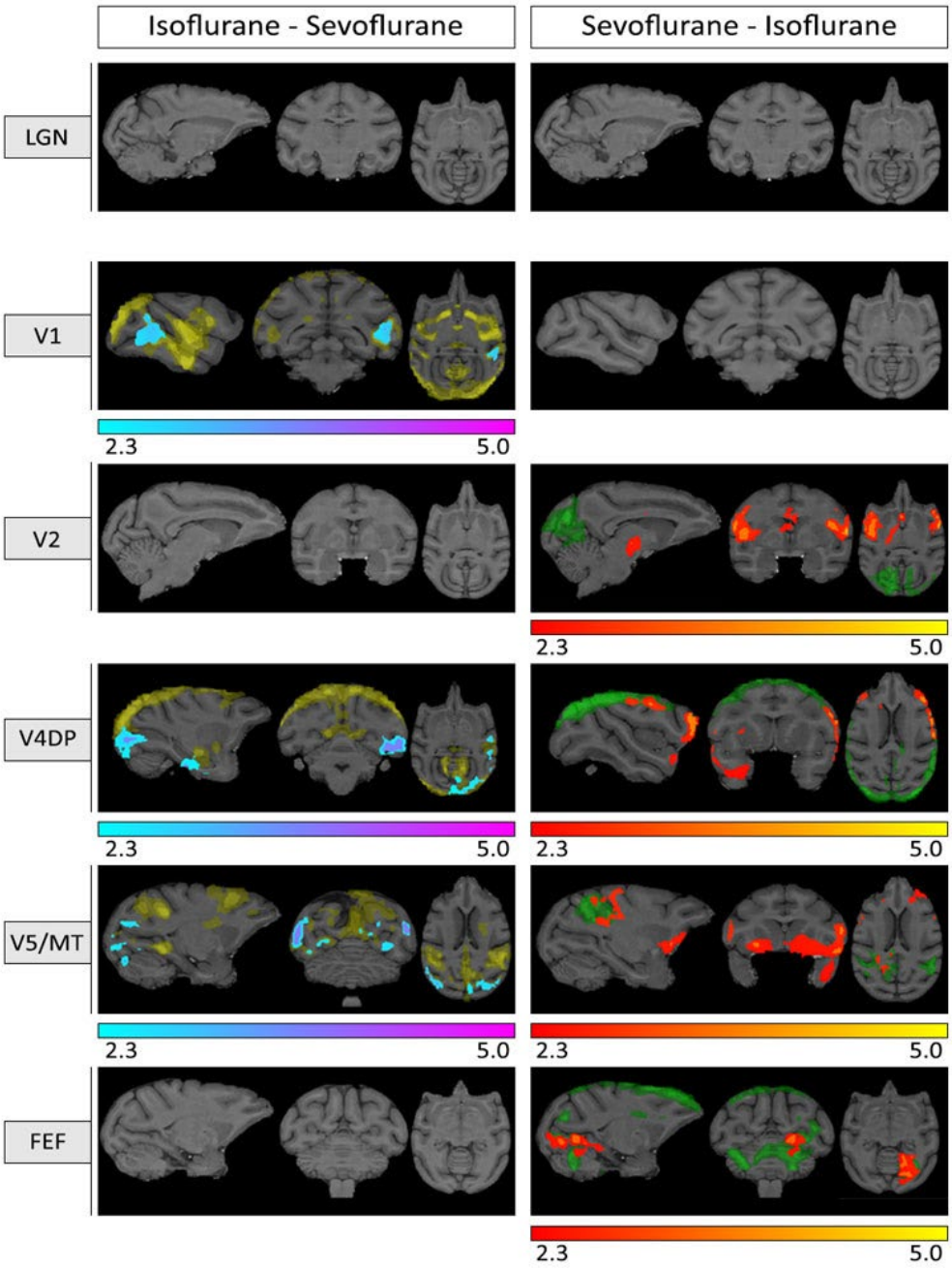


Figure 4.10 SBCA Reveals Localized Differences Between the Visual Functional Connectivity Under Sevoflurane and Isoflurane

The isoflurane and sevoflurane functional networks for the seed of interest (geniculate nuclei (LGN), the primary visual area (V1) and the secondary visual area (V2), the visual area 4 (V4DP), the middle temporal visual area (V5/MT), and the Frontal Eye Field FEF) are statistically compared.
For each seed, results of the test against H_0: There is no difference between the mean isoflurane group effect and the mean sevoflurane group effect are represented by a z-statistic map. For each seed, the first column shows the result obtained with contrast Isoflurane-Sevoflurane. To put the result in context, the functional isoflurane network (see Figure 4.4 to Figure 4.9) of the seed currently under scrutiny, thresholded at z≥2.3, is displayed in yellow. The second line presents the result obtained with contrast Sevoflurane-Isoflurane. The level of statistical significance for both tests was (z≥2.3or α=0.01). Here the seed's sevoflurane network at z≥2.3 (see Figures Figure 4.4 to Figure 4.9) is displayed in green.
All presented maps are corrected for multiple comparisons. When significant differences have been found Colourbars are employed to show the range of z-values from significance threshold to an arbitrary upper threshold of z=5.

4.4 Discussion

In this chapter, we describe the functional connectivity of the visual system under isoflurane and sevoflurane, using SBCA with bilateral seeds in LGN, V1, V2, V4DP, V5/MT, and FEF. isoflurane is often the preferred anaesthetic agent for macaques. Studies using sevoflurane are, by comparison, rarer.

A trend, similar to that observed in the results of ICA (see Chapter 3), seems evident, when comparing each RSN under isoflurane and sevoflurane. Sevoflurane RSNs generally appear smaller and include fewer areas than their equivalent isoflurane RSNs. When compared rigorously, however, only a handful of local differences were statistically significant and substantively meaningful (see Table 4.2). Both aspects of this result are undoubtedly important information. On the grand scale, if there is no substantively important difference, then researchers interested in the general effect across the brain can chose the more readily available (in terms of stock, cost, etc.) anaesthetic. Studies interested in examinations of specific relationships where a meaningful differential effect of isoflurane and sevoflurane exists (see Table 4.2) will now be in a position to make an informed decision, selecting the agent that functions in the manner more beneficial to their particular inquiry.

It could be argued that, precisely by virtue of being localized, however, the aforementioned differences between anaesthetic agents could be considered to be “low impact”, compared with the overall influence of anaesthesia. Thus, taking the results of the last two chapters together, there is ample evidence to suggest that, in the majority of cases, isoflurane and sevoflurane are functionally equivalent anaesthetic agents, for use in a study of functional connectivity.

It should be noted that this chapter introduced a substantial methodological deviation compared to past literature regarding visual system functional connectivity in the use of a noticeably more

comprehensive, and thus realistic, model. This is, among other things, due to the inclusion of an extensive list of controls (or nuisance regressors), including animal age, the delay between anaesthesia induction and data acquisition, the subject's median blood pressure, heart rate (HR), and individual MAC value, in the GLME. Each of these parameters is theorized to influence the BOLD signal. As such, their exclusion from any such model invites obvious criticism regarding the potential for omitted variable bias. Functionally, such an omission could lead to inflated effects/differences, or even incorrectly attributing effects/differences to variables that were included, which were in fact due to omitted variables. Despite this, these variables are inexplicably rarely included in such models. Statistical modelling is, of course, a balancing act between explanatory power and parsimony. There are clear benefits to employing simpler models (ease of computation, interpretation, and presentation to say the least) but they are far overshadowed by the substantive benefits inherent in the use of more realistic models, which may in turn provide more realistic, actionable information.

Indeed, we obtained a result that is, *prima facie*, confounding: the absence of significant correlations between the LGN and the V1 functional network, under either anaesthetic condition. V1 correlations in the LGN network are marginal (only observed in the calcarine), and even then only present under isoflurane. This is perplexing, because we know that the majority of afferents to V1 originate in the LGN (Hendrickson et al., 1978; Hubel & Wiesel, 1972) and the LGN also receives feedback projections from V1 (Briggs & Usrey, 2007). Past studies in awake humans have shown significant correlations between the LGN and V1 (Beckmann et al., 2005; Genç et al., 2016). As a result, we expected to find evidence of a large reciprocal correlation cluster between V1 and LGN. Indeed, not finding these clusters could be interpreted as the result of some flaw in our methodology. The most likely candidate would be that the LGN and V1 seeds were poorly aligned to the functional image and are, in reality, located over some other brain area(s). The location of

the LGN and V1 seeds in each animal's functional space was diligently checked (and re-examined in light of these results).

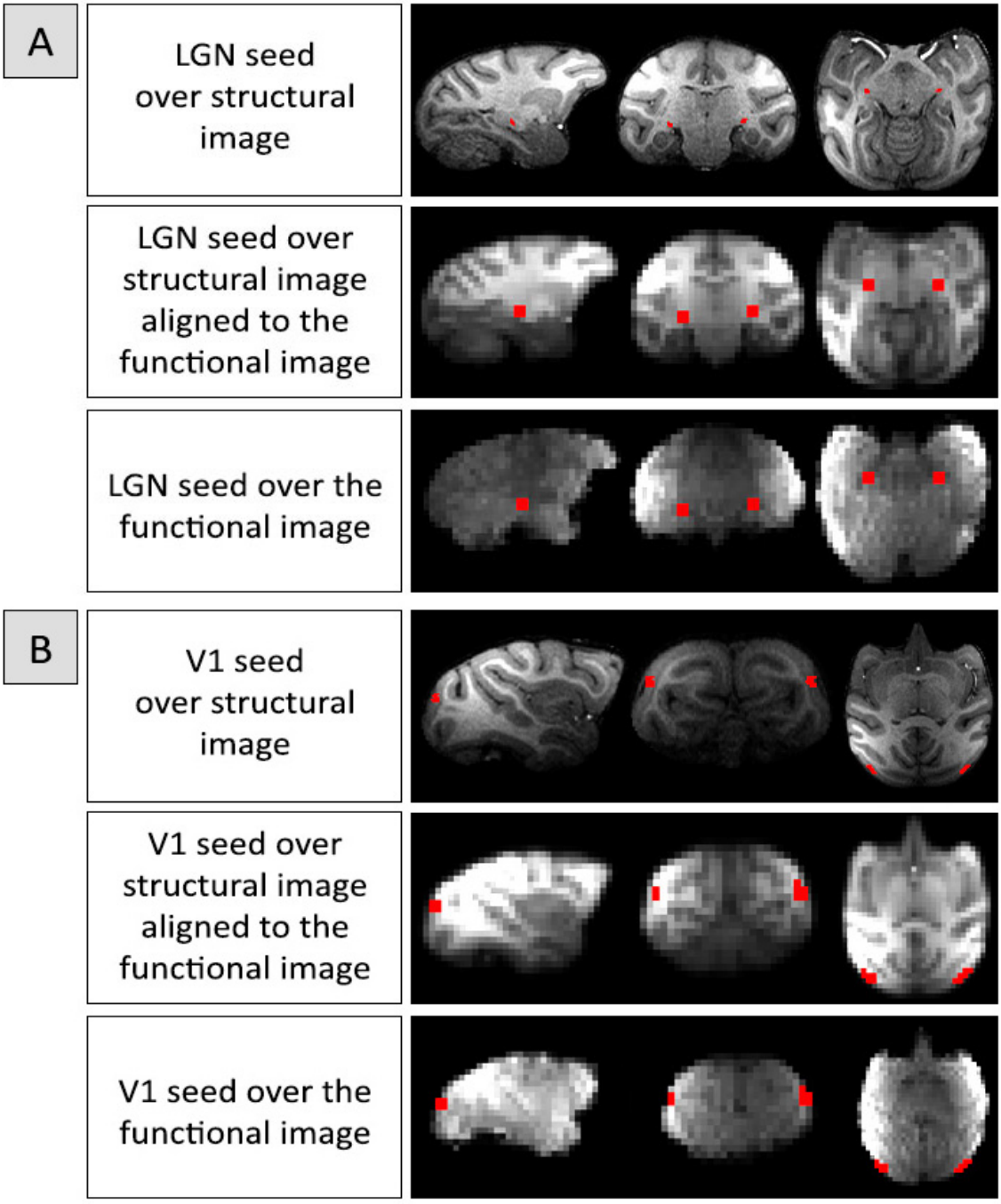


Figure 4.11 Example of LGN Seed Placement in one Animal

LGN (A) and V1(B) seeds in Monkey Orc. The first ligne of each panel shows the location of each seed in Monkey Orc structural image. Seed placements were controlled using the Atlas "A Combined MRI and Histology atlas of the Rhesus Monkey Brain in Stereotaxic Coordinates 2nd edition" (Saleem & Logothetis, 2006) and the D99 atlas v2.0 (Saleem et al., 2021). Each panel's third line shows the placement of the seeds aligned from the structural space to the functional space. Because of the poor resolution of the functional image, we also show the seed's location on Monkey Orc's structural image registered to functional space (second line).

Figure 4.11 is presented as an example of the locations of the LGN and V1 seeds in one of the animals of the isoflurane group (Monkey Orc). Seed locations were checked against "A Combined MRI and Histology atlas of the Rhesus Monkey Brain in Stereotaxic Coordinates 2nd edition" (Saleem & Logothetis, 2006) and the D99 atlas v2.0 (Saleem et al., 2021) and deemed within reasonable margins[9]. We are also comforted by the functional networks obtained with the other visual seeds tested, as they echo existing studies of both functional connectivity (Beckmann et al., 2005; Damoiseaux et al., 2006; Vincent et al., 2007) and histology (Gattass et al., 1997; Perkel et al., 1986; Ungerleider et al., 2008). It could be argued that both the V4DP isoflurane and sevoflurane networks, which appear to be superficial, may be the result of vascular artifacts. We do not believe this to be the case. Vascular artifacts are indeed often mainly involve the midline (Beckmann et al., 2005), and/or are comprised of discreet activation clusters following the path of a vein or artery (Dagli et al., 1999; Hluštík et al., 1998). We did not find either to be the case, here. Additionally, we regressed out the CSF signal, which also mitigates the risk of pulsations/blood flow artifacts.

There is, furthermore, at least one important distinction between our study and the majority of human studies used as a reference for the functional connectivity of the visual system: the manner in which data are collected. Human studies usually employ awake subjects, who are instructed to keep their eyes open; our animals were anesthetized with their eyelids shut. Agcaoglu et al. (2019) show that, in awake humans, the functional connectivity of the visual network is decreased when subjects' eyes are kept closed. Cotumero et al. (2020) also found that keeping eyes open or closed particularly modulates the functional connectivity of V1.

[9] Seed locations were, of course, checked across all monkeys in the sample(s). Presentation of those images is eschewed, since they provide little in the way of further substantive information.

Possibly more essentially, the LGN is a thalamic nucleus. The activity of the thalamus is greatly affected by anaesthesia (Mashour & Alkire, 2013; McFarland & Haber, 2002; Suzuki & Larkum, 2020). Of course, visually driven activity is still present in the LGN under anaesthesia but its neurons respond to visual stimuli with lower firing rates (Alitto et al., 2011). A follow up study using awake macaques with open eye-lids, while potentially practically challenging, could provide critical insight on the interaction (or possibly more aptly "interference") of anaesthesia and the existence of significant functional connectivity between V1 and the LGN.

5 An Examination of Functional Connectivity in Macaque Visual Cortex Following Anatomical Damage Arising During Natural Developmental Processes

5.1 Introduction

This chapter examines the case of two adults rhesus macaques, Monkey S and Monkey Y, with extensive lesions in their primary visual cortex –specifically corresponding to large portions of their calcarine cortex (see Figure 5.1). The lesions were discovered during routine MRI scans. Prior to the scans, there was no reason to believe that such lesions existed.

Naturally occurring lesions in V1 are exceedingly rare. Evidence from previous studies, however, has indicated that lesions in V1, whether accidental (Holmes, 1918; Kleiser et al., 2001) or intentionally imposed for scientific purpose (Moore et al., 1995), correspond to a loss of normal aware vision. Counterintuitively, the monkeys examined in this study showed no overt markers of severe sight disability. Indeed, as we will discuss below, they were deemed sufficiently sighted to participate in perceptual studies and, as such, they were not specifically examined for sight-related deficiencies.

In initial testing, both lesion monkeys performed within comparable margins to all the other (healthy) monkeys they were grouped with. The case of macaque Monkey S has previously been described by Bridge et al. (2019), who concluded that the remaining visual system in Monkey S appeared largely unaltered with regard to structure and function. The authors also observed significant activation in response to visual stimulation in LGN and the pulvinar as well as preserved V5/MT functional network. The discovery of lesions in Monkey Y provided an opportunity to revisit Monkey S's case, shifting our focus on resting functional connectivity.

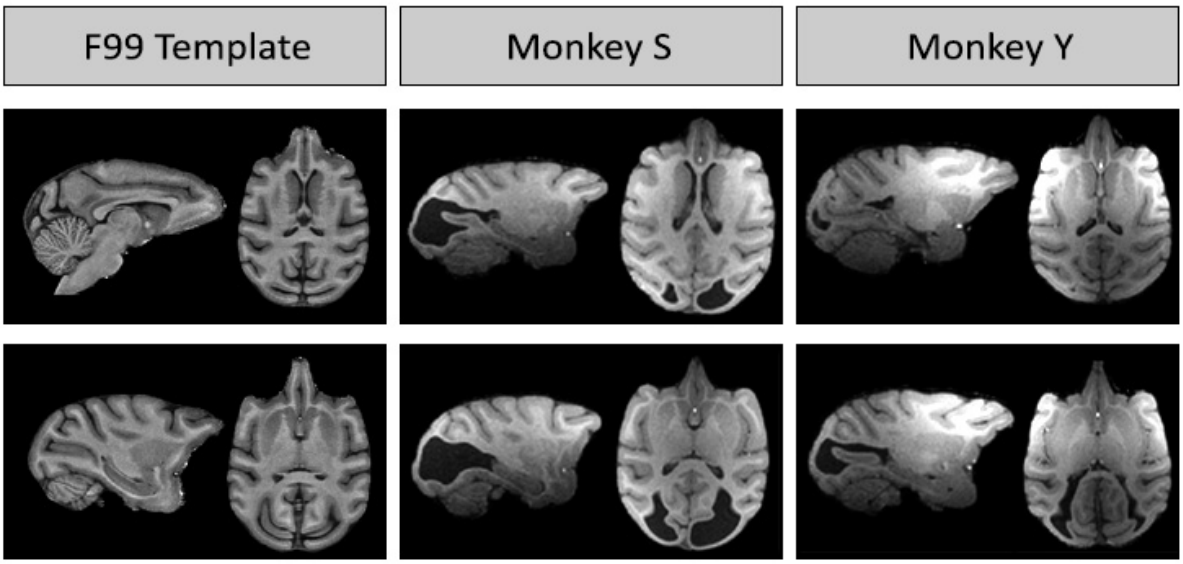


Figure 5.1 Structural Scan of the Lesion Animals Compared to the F99 Template

The first column presents a sagittal and frontal view of two different slices of the of the F99 template (top: [95 71], bottom: [101 65]). The centre column shows the corresponding slices in Monkey S's structural scan (3T, T1 weighted) and the right column shows these same slices in Monkey Y's structural scan (3T, T1 weighted). The lesion animals' structural scans are displayed in the subject's space.

5.1.1 The Central Role of V1 in Visual Processing

The primary visual cortex (V1), located in the occipital cortex, is a hub of visual afferents and efferences essential for precise visual processing. In primates, V1 receives the overwhelming majority of the LGN axons, while LGN receives most of the retinal output. V1 is the starting point of both visual processing pathways, the ventral pathway (responsible for processing shape, colour, size, brightness) and the dorsal pathway (responsible for processing motion, object localization, visually guided actions) (Mishkin et al., 1983 but see also Freud et al.(2016) for a more nuanced review). As a consequence, all extrastriate visual areas (e.g., V2, V3, V4, V5/MT) receive either direct or indirect afferents from V1.

The role of V1 in visual processing has been among the best understood of the various visual areas (see, e.g. Hubel & Wiesel, 1962, 1974). Primate V1 neurons are the first to be selective for object characteristics such as orientation (Hubel & Wiesel, 1959), colour (Lennie et al.,

1990; Wachtler et al., 2003), motion direction (Gur & Snodderly, 2007; Livingstone & Hubel, 1987) and binocular disparity (Barlow et al., 1967; Parker et al., 2016). Taking both left and right visual cortex together, V1 neurons contain the full representation of the visual field. This representation mirrors the retinal representation. So, neighbouring points in the visual field are represented in neighbouring cortical location on the surface of V1. This representation is continuous from the foveal (i.e., the centre of the visual field) representation in operculum to the periphery representation in the upper and lower calcarine banks (Dougherty et al., 2003; Van Essen et al., 1984). Visual field representation is also subject to cortical magnification. Cortical magnification is characterized by what is referred to as the magnification factor: "the linear extent of visual striate cortex to which each degree of the retina projects" (Cowey & Rolls, 1974). Thus, the greater the magnification factor, the more neurons are involved in processing a stimulus of a given size. Among all visual areas, V1 has the largest magnification factor. The magnification factor decreases across V1, from the foveal representation to the peripheral representation (R. B. Tootell et al., 1988; Van Essen et al., 1984). As a result of this, V1 is able to achieve the processing of visual stimuli at a higher spatial resolution than any other cortical visual area.

5.1.2 Lesions of V1 and Loss of Aware Vision

When V1 is lesioned, normal aware vision is generally lost in corresponding regions of the visual field. This vision loss is not, however, always absolute (Holmes, 1918; Kleiser et al., 2001; Moore et al., 1995). Humphrey (1974) reported the famous case of macaque Monkey Helen, that had undergone a bilateral removal of V1. With training she was able to navigate her surroundings and "look" at an experimenter holding a treat before trying to reach for it,

although her vision was still described as abnormal. Riddoch (1917) reported several cases of patients who suffered bullet wounds in the occipital cortex resulting in partial loss of sight, that also were able to perceive high contrast transient stimuli presented within the blind portion of the visual field. Pöppel et al. (1973) found that some patients were able to make saccades towards a still visual target (a tungsten light) displayed in the blind area, albeit with a poor accuracy. In both studies, none of the patients were able to consciously perceive the visual stimuli presented to them. This ability, referred to as "blindsight" (Weiskrantz et al., 1974), puts in question the necessity of V1 for visual processing.

Based on current understanding of visual processing, outlined above, the coexistence of the absence of a large portion the primary visual cortex and the seeming retention of sight is, in and of itself, motive enough to warrant special examination. Based on the work of Moore et al. (1996), who found that macaques who received a V1 lesion recovered more residual vision when it was inflicted in infancy than adulthood, we hypothesize the lesion occurred extremely early in the animal's lives (pre- or peri-natally). This, we further hypothesize, would allow them to develop compensatory mechanisms to effectively regain vision.

5.1.3 Thalamic Visual Pathways Circumventing V1

Animal models, including lesioned macaques (Humphrey, 1974; Humphrey & Weiskrantz, 1967; Rodman et al., 1989; Schmid et al., 2010), have offered insight into how any sight may be retained in the absence of some or all of V1. These studies proposed the existence a parallel/secondary visual system involving subcortical areas (see Figure 5.2) that could support blindsight and/or participate in the recovery of some conscious residual vision.

The LGN constitutes one of such areas. Sincich et al. (2004) showed that the LGN sends direct

afferents to MT, and these connections are still bilaterally found in patients presenting large unilateral lesions affecting V1 (Bridge et al., 2008). Rodman, Gross, and Albright (1989) showed that the bilateral ablation or inactivation of V1 in macaques did not abolish the neuronal response to visual stimuli in MT. In humans, the capacity to detected moving stimuli presented in the blind visual field has been repeatedly described in hemianopia patients (Barbur et al., 1993; Bridge et al., 2019; Goebel et al., 2001; S. Zeki & Ffytche, 1998). This ability is only observed in patients who have an intact geniculo-hMT+ connections (Ajina, Pestilli, et al., 2015). Some have adaptations of the geniculo-hMT+ pathway following a lesion in V1. In 2001, Kleiser et al. (2001) studied the case of 3 patients with unilateral lesions including V1, who experienced some residual conscious vision. Interestingly, one of these patients had a lighter visual deficit than when they were first involved in a scientific study 14 to 21 years prior (see Barbur et al., 1980; Stoerig, 1987). The patient's defect evolved from absolute blindness in the portion of the visual field affected by his lesion to progressively recovering partial vision. In a later study, Bridge et al. (2008) found in the same patient, evidence of the development of a pathway from the LGN, contralateral to the lesion, to the ipsilateral MT+/V5, that is usually absent in healthy controls. In patients with a unilateral lesion of V1, Ajina, Kennard, et al. (2015; see also Ajina, Rees, et al., 2015) also report that the BOLD response to visual stimuli (moving dots and Gabor), of the ispsilateral MT+ becomes closer to the BOLD response of V1. One potential explanation would be that MT+ responses are exclusively driven by geniculate connection what would make it closer to the connectivity of V1.

The pulvinar (another thalamic nucleus), may also be involved in vision recovery and blindsight (see Kaas and Lyon, 2007 for review). Despite the LGN receiving most of the retinal output, a small portion of the ganglion cells project to the pulvinar (Itaya & Van Hoesen, 1983;

O'Brien et al., 2001). The lateral pulvinar projects to V1, V2, and caudal V4 (Casagrande & Kaas, 1994). This relationship could help explain the findings of Schmid et al. (2009), who observed activations in the portions of V2 and V3 corresponding to a lesioned section of V1, in response to a visual stimulus. The pulvinar also connects to MT both directly, through the inferior pulvinar, and indirectly, through V1 and V2 (Cusick et al., 1993; Lin & Kaas, 1980). Kinoshita et al. (2019) also found that inactivating the pulvinar in unilaterally V1 lesioned macaques, affects their ability to perform a visually guided saccade task, despite the animals being able to perform the task until the pulvinar was inactivated.

Kinoshita et al. (2019) also raise the importance of the superior colliculus (SC) – pulvinar pathway. SC receives inputs from the retina (Vanderah & Gould, 2016) and projects to both the LGN and pulvinar (Harting et al., 1991). SC is also connected to MT via a relay in the pulvinar (Lyon et al., 2010). SC seem to be necessary to blindsight as its ablation (Rodman et al., 1990) or inactivation (Kato et al., 2011) or the inactivation of the SC-pulvinar pathway (Kinoshita et al., 2019) dramatically decreases the ability to "unconsciously see" in V1 lesioned macaques. Additionally, Leh, Johansen-Berg and Ptito (2006) found a novel pathway from the SC in the hemisphere opposite to the lesion, to the remaining hemisphere's visual association areas and primary visual areas. This pathway was present in patients who suffered an hemispherectomy of the occipital lobe (but who were experiencing blindsight), which was absent in the non-lesioned controls and in lesioned patients who did not experience blindsight. Although these results can be tempered by the study by Ajina, Pestilli, et al. (2015) who shows that an intact pathway between hMT+ and the ipsilateral to the lesion SC, can be found in blindsight negative V1 lesioned patients.

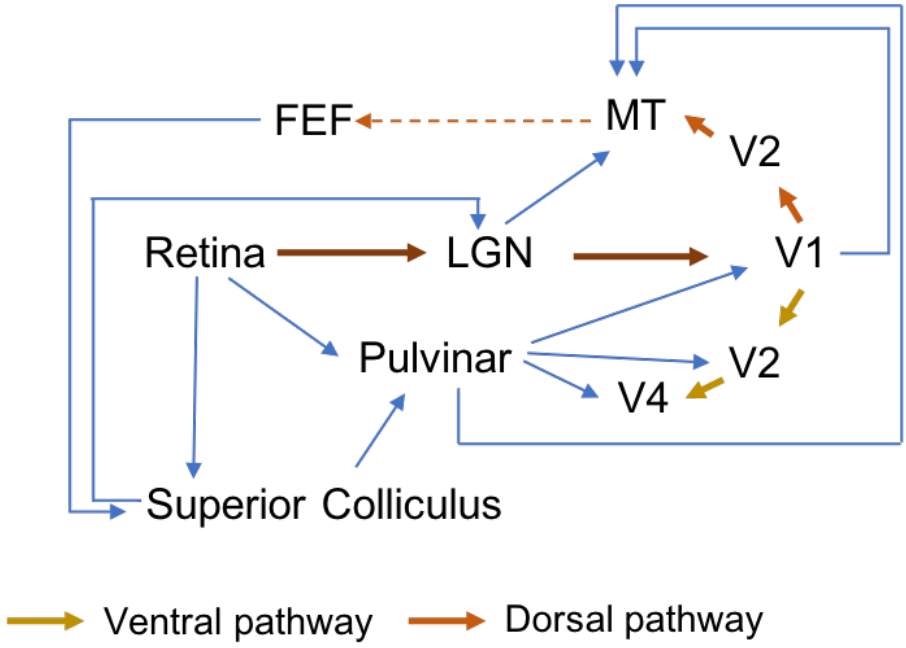


Figure 5.2 Summary of Possible Alternative Visual Processing Pathways

Adapted from Sincich et al. (2004), O'Brien et al. (2001), Casagrande and Kaas (1994), Harting et al. (1991 b), Segraves & Goldberg (1987) and Vanderah & Gould (2016). Arrows coloured in shades of brown represent the classically accepted visual processing pathway. Blue represent known anatomic connections that could be involved in alternative processing pathways if V1 is damaged.

We examine each of these alternative explanations in our lesion monkeys. We begin by examining the existence of two possible thalamic compensatory visual processing pathways involving subcortical areas, such as the LGN, pulvinar and superior coliculus (SC). We also examine pathways that are potentially compensatory, developed through the strengthening of connections between the extrastriate cortex and the remaining portion of V1. Fundamentally, we argue that, as otherwise functional areas of the somatosensory cortex are "freed up" by the loss of input in amputees (Makin et al., 2020), portions of the extrastriate cortex could theoretically be "freed up" by the partial absence of V1. During the first few months of life, the primate visual system is still fairly plastic; V1's layers and synaptic connections are still being refined and reorganized (Barone et al., 1995; Coogan & Van Essen, 1996; Garey, 1984; Huttenlocher & de Courten, 1987; Mundinano et al., 2015). As the lesions

most likely occurred during the few months preceding or following birth, the loss of the calcarine may have driven the part of extrastriate cortex normally connected with the calcarine, to develop abnormal connections with other portions of V1.

5.1.4 Resting State Functional Connectivity as a Tool to Study the Impact of a Natural Lesion of V1

In the preceding chapters of this study, we established the use of resting state functional connectivity as tool to study and compare brain networks. We also showed that SBCA provides a sound methodological platform to create and compare RSN between groups. New inquiries, however, require the discussion and description of the new partitioning of our animals into lesion and control groupings, their treatment within the study, the collection of our data, and the location and characteristics of the seeds we will examine. Of course, rigorous examinations require formal statistical tests. The results of these tests will then be presented visually, in the form of connectivity heatmaps corresponding to connectivity strength in various regions of interest across the brain for the lesion and control animals.

Any such examination must be preceded by a considered examination of the specific lesions prompting the inquiry. Following their description, we examine the lesions' focal impact on the resting state functional connectivity of the visual system. Logic dictates that the absence of extensive portions of the primary visual cortex should deeply impact the visual functional network. In the lesion animals, we also expect to observe increase in connectivity strength between ROI of interest involved in a compensatory pathway.

We first examine the functional connections between intact extrastriate visual areas and a subset of subcortical areas that could be involved in thalamic compensatory pathways (i.e.,

the LGN-MT-FEF and the Pulvinar-V2-V4 pathways as well as the SC).

We then examine the hypothesis that residual sight may be maintained through the establishment of new connection from the operculum to portions of visual areas "freed up" by the loss of the calcarine. Indeed, functional connectivity often follows anatomy. Genç et al.(2016) show that the functional connectivity of V1 follows retinotopy, in humans: portions of V2, containing the representation of the periphery of the visual field are more strongly temporally correlated with the portions of V1 that also represent the periphery, and foveal V1 is more strongly correlated with foveal V2. The authors found this result persisted for correlations between V1 and V3 as well as between V2 and V3. In macaques, the representation of the peripheral visual field is contained within the calcarine (Daniel & Whitteridge, 1961) –the portion of V1 largely missing in the lesion animals.

To test the hypothesis that residual sight persists through the establishment of new connections from the operculum to areas previously connected to the calcarine, we attempt to identify ROI satisfying each of the following criteria:

1. The ROIs have significantly higher correlations with the operculum than in lesion animals than in the control animals, and
2. The ROI is more strongly correlated with the calcarine than with the operculum in the control animals, and may thus be anatomically connected to the calcarine.

We theorise that if a ROI does satisfy these criteria, the increase in connectivity strength with V1 observed in the lesion animals could be explained by the establishment of new connections between the remainder of V1 and a visual area "freed up" (Makin et al., 2020) by the lesion.

5.2 Methods

As previously noted, the analytical methodology employed in this chapter is relatively complex and requires a fair amount of foundational knowledge to be meaningful. Below we present a description of the lesion and control animals, their anaesthesia, and the means by which data were acquired. We describe the means by which we measure the lesions in the two affected monkeys and the location, size, and intrinsic interest of the seeds placed within each subject's brain, both within and without the primary visual cortex. We outline the necessity for and the means by which individual correlation maps are created for each subject, in the process of visualizing the functional network. We present the process we follow in high-level group analysis, including the specific hypotheses we will examine. We discuss and present the necessity for a meaningful comparison of the functional connectivity of the calcarine against the V1 operculum. We present the benefits, interpretation, and construction of connectivity heatmaps, and the use of differential maps in the comparison of the functional connectivity of seeds within the primary visual cortex.

5.2.1 Animals

Discussion of the case histories of this study's subjects is necessarily divided into three parts. One part is reserved for each of the two lesion monkeys which, while similar with regard to the location of their lesions, are fundamentally unique with regard to their size and specific placement. The description of the first monkey (Monkey S) is based on the account provided in Bridge et al. (2019), whereas that of the second lesion monkey (Monkey Y) is from our own observation and assessment. The third part describes the group of control subjects, who are characterized by healthy brains and have been selected based on a series of other communal characteristics described below.

5.2.1.1 Monkey S (Lesion Monkey 1)

Bridge et al. (2019) describe the case of Monkey S, a female rhesus macaque (7 years old; 6.25kg), that was purchased by the Centre for Macaques (Porton Down, UK). We attempt to summarize this case history below. Monkey S initially showed the same fitness for training as her cagemates and gave no evidence of difficulty developing interactions with carer. Training to enter a transport box and a primate chair (Mason et al., 2019, as cited in Bridge et al., 2019) from the home cage was completed in a similar time frame as her cagemates. She was then involved in an experimental protocol involving a visual task, originally intended for a decision-making study. Monkey S was trained on this task for 5 days a week, over a period of 18 months.

Training began by encouraging Monkey S to enter a transport box from the homecage, with no other guidance than key words (e.g., "over", "down", "good girl") and visual cues (e.g., opening transport box door). No learning difficulties were observed until she was brought to a touchscreen, where she would be rewarded (with pellets) for touching anywhere on the screen during the presentation of a range of "colourful typographical characters" (Bridge et al., 2019, p. 3). Monkey S was able to do 10 trials in 3min within the first week of training. Based on these satisfactory results, Bridge et al. (2019) report that she was moved to the next training phase. The new task required targeted touching, in response to a single, colourful typographical character, displayed in random locations on the screen. She reached 40–50 trials, in increments of 10 trials, in a 30–91min-per-session timeframe. This performance was particularly poor compared to the other monkeys involved in the study and did not meet criteria required to increase task complexity. According to Bridge et al. (2019), Monkey S was never able to improve her performance and was maintained on the lowest-complexity-of-visual-presentation version of the task. After more than six weeks of training, the transport box was replaced by a primate chair (seated, but without head clamp or eye movement

control) and the reward was switched from pellets to juice. Monkey S only did 40 rewarded trials in 33min in this task, over several weeks of training sessions. The other monkeys participating in the task were expected to be "closer to 100 rewarded trials in 18–25 min" (Bridge et al., 2019, p. 3). Indeed, if the number of trials or the complexity of the task was increased, monkey S would typically stop engaging with the task.

In an attempt to improve task learning, Monkey S was trained to hold a lever and release it for reward, instead of using a touchscreen. Although she successfully learned to use the lever, Bridge et al. (2019) note that she was not able to learn to release it in response to a visual cue. On a task where she was asked to use the lever to react to a change in target colour on the screen, she typically completed no more than 10-20 trials per session, by the end of six months of training –and then, only when encouraged by the presence of the trainer in the training room. Rudimentary checks of her visual ability were performed during this period. It was determined that monkey S could detect where the reward location was and turn toward objects held up in front of her or moved around in her visual field.

In a final attempt to increase her performance, the primate chair was once again swapped for the transport box and she was again tested with the targeted touching version of the task but using high-value banana pellets as a reward. According to Bridge et al. (2019), this training continued for 6 more weeks, at which point she would complete, on average, 40 trials per session (including failed attempts) in 41–103mins, making 23–51 errors (i.e., touching the touchscreen anywhere else other than the alphanumeric character).

Bridge et al. (2019) note that a behavioural assessment of Monkey S, conducted in the homecage by a clinical neurologist and two neuroscientists, failed to detect any substantially atypical patterns of movement and visual orienting toward the other monkeys and observers. There was some

evidence that her eye fixation patterns might be abnormal, although Bridge et al. (2019) report no quantitative analysis was carried out in this respect. When Monkey S was offered treats, however, she would run past them and pick them up while running (Bridge et al., 2019). Typically, monkeys will move forward towards a treat, fixate on the treat continuously, and then reach for it more deliberately. Monkey S showed none of these typical behaviours.

Based on the obvious differences between Monkey S's performance and that of her cagemates, Bridge et al. (2019) conducted a brain scan. This structural MRI scan revealed two large lesions with a complete loss of V1 (see Chapter 5.3.1). There is no record of an injury or history that might account for these lesions, indicating that they were likely the result of a congenital or perinatal disease.

5.2.1.2 Monkey Y (Lesion Monkey 2)

Monkey Y, a male rhesus macaque (6 years old, 11.3 kg at the time of MRI scan), was purchased along with 3 other males born in the same year, from the same breeding centre as Monkey S. All four monkeys were housed together. No behavioural difference was noted between Monkey Y and the other animals. Monkey Y had no issues interacting with human carers. He was able to both follow a treat with his eyes and reach for it while remaining still. And he did particularly well at every training stage (i.e., in cage and during task). Indeed, Monkey Y's trainer described him as being the best monkey of his group, both in terms of motivation and performance.

After a few weeks during which the animals were left to acclimatize, Monkey Y's training to enter a primate chair (Mason et al., 2019) began. Monkey Y completed this training phase, involving moving across the homecage on cue, entering the primate chair by himself and accepting restriction by a neckplate, in a time frame similar to his cagemates.

Once Monkey Y was comfortable coming to the chair, he was presented with a simple task on a touchscreen: a stationary dot was displayed on the screen and the animal was rewarded for touching it. The dot size was adapted to Monkey Y's progress on the task (from an initial radius of 25 to an eventual 2 degrees). Following two weeks of refusal to engage with the task, Monkey Y improved his performance, completing 500 trials in 15 minutes. From that point, the task evolved. The dot's location was moved to a new position within the bottom half of the screen (for easy reach) at each new trial. Monkey Y performed very well on this task, completing 500 trials in 20min. Based on his satisfactory performance on this task, Monkey Y's was moved to an "Odd One Out" task.

The Odd One Out task was initiated by touching a central dot (2 degrees radius, x y coordinates: [0, -15]), located in the bottom half of the screen for easy access. Four circular patches of moving dots, or *random dot motion stimuli* (Britten et al., 1996) are then displayed around the central dot's location. A *random dot motion stimuli* is circular patch, within which a portion of the dots (% coherence) moves uniformly in a given direction while the background dots all move in random directions (Britten et al., 1996). Here coherence was kept at 100%. One of the stimuli (specifically, the target stimulus) dots' have a higher contrast to the background (mid-grey) than the other 3 stimuli. The animal was rewarded when he touched the higher contrast stimulus. After every successful trial, the four stimuli locations were randomly rotated around the central dot's location, while retaining a consistent distance from the centre dot. The contrast of the 3 distractor stimuli was gradually increased (from 0.1 to 0.7) to become closer to the contrast of the target stimulus (contrast of 1). In general, we consider an animal to have learned a behavioural task when it is able to perform said task with an accuracy of 80%. Monkey Y's performance at on this task are presented in Figure 5.2. He performed the task successfully (average accuracy: 94.97%) for 5 months. The training session lasted 24 minutes on average, averaging 332 trials.

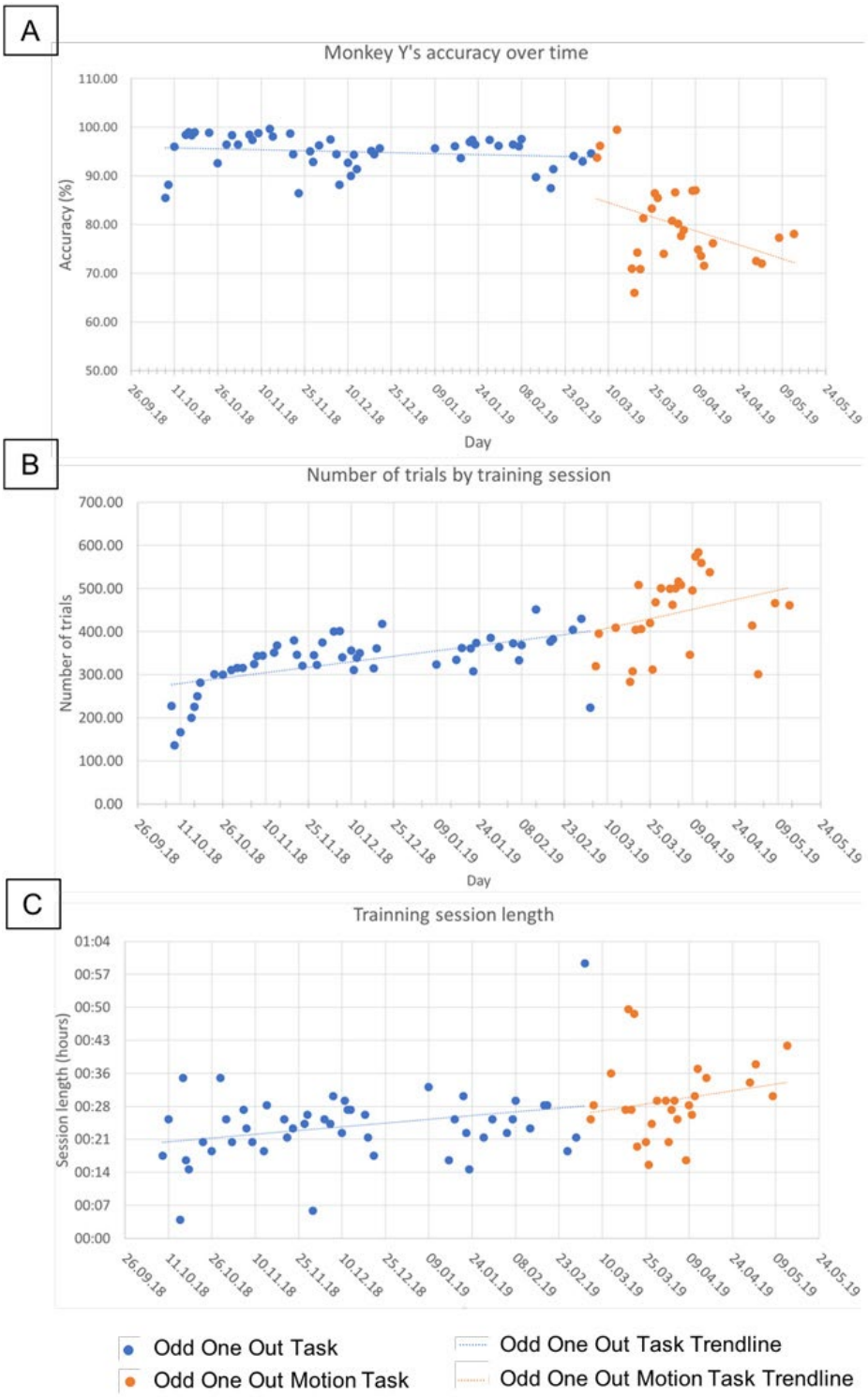


Figure 5.3 Monkey Y's Performance Over Time on Odd One Out tasks

Monkey Y was trained on two versions of the Odd One Out task. The initial version (blue) asked the animal to make the distinction between 3 stimuli with the same contrast to the background, and a fourth, more contrasting stimulus. In the second task, the Odd One Out motion task (orange), Monkey Y had to discriminate which of the 4 stimuli presented had a different motion to the other 3.

A. *Percentage of correct trials (accuracy) per training session. As a frame of reference, typical animals are expected to perfom at an accuracy of 80% or higher.*

B. *Total number of trial s per training session.* ***C.*** *Training session length*

The last recorded version of the task, the "odd one out motion" task, was initiated by touching a central dot (2 degrees radius, x y coordinates: [0, -15]). 4 random dot motion stimuli (coherence:100%, dot density: 0.7, dot speed: 45 degrees/s, dot size: 0.2 degrees) (Britten et al., 1996) were then displayed. With the exception of the three first sessions, where the target stimulus patch was slightly whiter than the background (shade: 0.4 (for reference: 0= white, 0.5= midgrey background, 1 = black)), all stimuli had the same contrast to the background. Dot direction movement in the target stimulus differed compared to the other three stimuli. The animal was rewarded for touching the target stimulus. Monkey Y was trained on this task for approximately a month and half and, excluding the three first training sessions, averaged 451.44 trials for 30min of training and an accuracy of 77.80%.

This performance was not quite optimal but was deemed close enough to prepare the animal for electrophysiological data recording. Structural MRI scans were acquired in this context, resulting in the discovery of Monkey Y's lesions. Again, no record of an event explaining an accidental acquisition of the lesion exists, so it is assumed the lesions are also congenital or perinatal.

Unfortunately, a few weeks after discovering the lesions, Monkey Y suffered a critical injury in the home cage and had to be put down. As a result, no additional behavioural data were collected.

5.2.1.3 Control Group Monkeys

In addition to Monkeys S and Y, 14 healthy rhesus macaques (*Macaca mulatta*) (3 females and 11 males), also purchased from the Centre for Macaques (Porton Down, UK), were involved in the present study. These 14 control animals took part in the research reported in Chapters 3 and 4. Since Monkeys S and Y were scanned while anesthetized under isoflurane, only the control animals that underwent data collection under isoflurane (median expired: 0.62 – 1.23

MAC) were selected from those discussed in previous chapters. All pertinent sessions that were accessible at the time of analysis were included.

As discussed in the previous chapters, all of the animals involved in the study were housed in groups of 2 to 6 animals. They lived in temperature regulated enclosure and were submitted to a 12/12-hour day/night cycle. Housing, Husbandry and carried procedures complied with Home Office (UK) regulations and European Union guidelines (EU directive 86/609/EEC; EU Directive 2010/63/EU).

5.2.2 Anaesthesia

Sedation was induced for all animals with a ketamine (7.5 mg/kg), xylazine (0.125-0.25 mg/kg) and Midazolam (0.1 mg/kg) injection. Animals were intubated and the anaesthesia was maintained with isoflurane (median expired Monkey S: 1.3% (1.0 MAC), Monkey Y: 3.36% (1.46 MAC), Controls: (0.8 – 1.6 % (0.62 – 1.23 MAC)). Monkeys also received fluid (Hartmann's solution, 2 ml/kg/hr) though an intravenous cannula. Systolic blood pressure (Monkey S: 88, Monkey Y: 90, Control: 62-129.5), rectal temperature (Monkey S: 36.7°C, Monkey Y: 37.8°C, Control: 34.45-38.15 °C), heart rate (Monkey S: 117.5, Monkey Y: 90.5, Control: 94-130) and end-expired pCO_2 (Monkey S: 35.5, Monkey Y: 35, Control: 28-43 mmHg) were continuously monitored. Monkeys were ventilated throughout the session (O_2-isoflurane). Their limbs were also regularly massaged to assist with blood flow, and 'viscotears' were applied to their corneas to prevent eye dryness.

5.2.3 Data Acquisition

A T1-weighted structural scan and a resting state functional scan were acquired on a Siemens 3T scanner for each animal involved in the study. Functional scans for the controls and Monkey Y were acquired using an ep2d sequence (TR = 2s, TE = 19mm, resolution 2mm, flip angle = 90°)

(see Chapter 2). Monkey S functional data were acquired with a gradient-echo T2* echo planar (EPI) sequence (TR = 2.00 s, TE = 29 ms, resolution 1.5 mm, flip angle = 78). Functional images contain 1600 volumes for the lesion monkeys and either 800 or 1600 volumes for the control animals. Structural scans were acquired using an MPRAGE sequence (resolution 0.5mm, TE = 4.04ms; TR = 2.5ms; flip angle = 8°, 128 slices) (see Chapter 2.1). Data pre-processing followed the protocol described in Chapter 2.2, before employing FSL FEAT to run a Seed-Based Correlation Analysis.

5.2.4 Lesion Volume Calculation in the Lesion Animals

Mask of the lesions of Monkey S and Monkey Y were drawn on each animal's structural image, using FSLeyes. Another mask of each of the lesion monkeys' brains, including the totality of the brain, was created from a previously brain extracted image (muscle and bones were removed using *BET* (Smith, 2002), using *fslmaths* (Woolrich et al. 2004) to make it binary. The volume of each mask was obtained with *fslstats* (Woolrich et al. 2004). The calculations excluded zero voxels. Finally, the volume of the lesion was divided by the volume of the brain.

5.2.5 Seed Based Correlation Analysis (SBCA)

In order to undertake the examinations outlined at the beginning of this chapter, several regions of interest were selected. We differentiate two groups of seed placement:

- one group outside the primary visual cortex to study the impact of the lesion over the functional connectivity of SC and two potentially compensatory thalamic pathways (LGN-MT-FEF) and (pulvinar-V2-V4).
- one group within the primary visual cortex to first study the impact of the lesion over

the functional connectivity of the remnants of V1. In the control group, we also will compare the functional connectivity of the calcarine against the functional connectivity of the operculum. We aim to find out if any of the test regions interest described in the first group, correlate more strongly with the calcarine than the operculum, and therefore are more likely to have anatomic connections with the calcarine.

These groups are presented and described below.

5.2.5.1 Seeds Outside the Visual Cortex

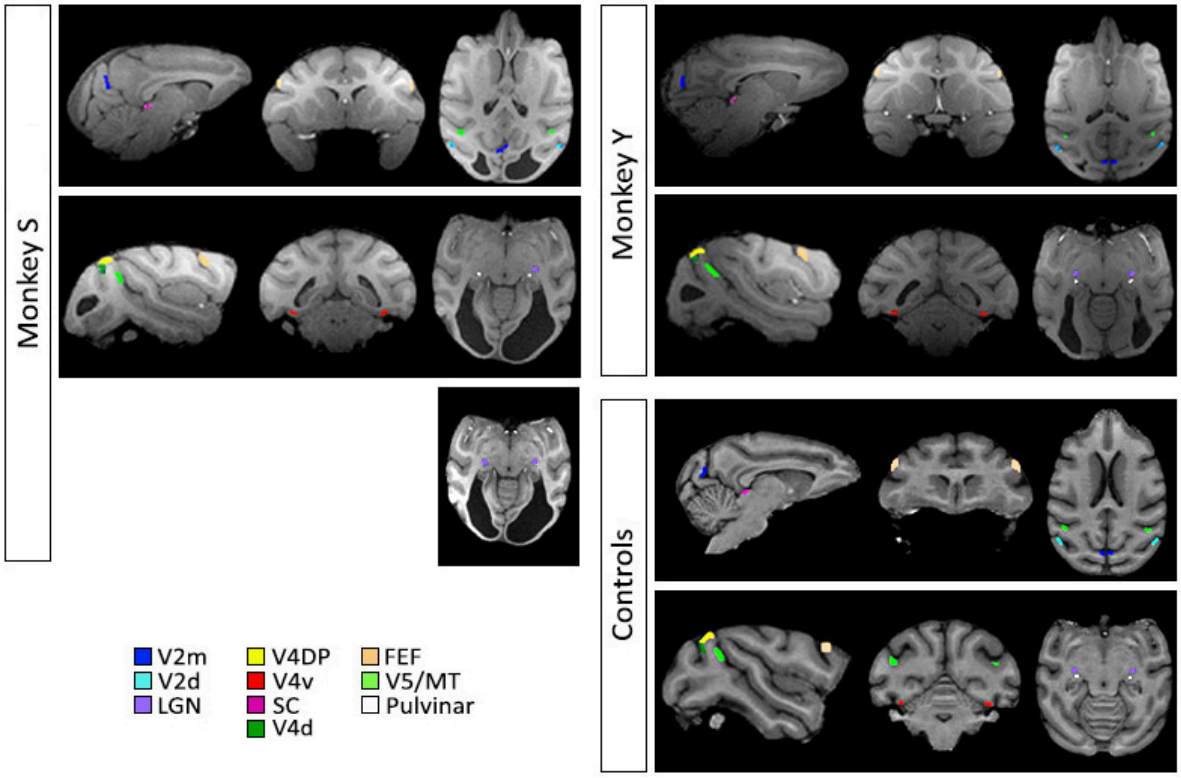


Figure 5.4 Visual Seed Locations Outside the Primary Visual Cortex

Seeds are bilateral regions of interest.
V2m: secondary visual area in the midline, V2d: dorsal secondary visual area (5x5x5 voxels/15.6 mm^3), V4DP: Visual area 4 (5x5x5 voxels/15.6 mm^3), V4d: Visual area 4 (dorsal) (5x5x5 voxels/15.6 mm^3) V4v: ventral visual area 4 (5x5x5 voxels/15.6 mm^3), FEF: Frontal Eye Field (5x5x5 voxels/15.6 mm^3), MT: Middle temporal visual area/V5 (5x5x5 voxels/15.6 mm^3), LGN: lateral geniculate nucleus (3x3x3 voxels/3.4 mm^3), pulvinar (3x3x3 voxels/3.4 mm^3), SC: superior colliculus (5x5x5 voxels/15.6 mm^3)
The seed have been drawn and are displayed on two slides of the F99 (Slice [77 130 74] and Slice [113 86 49]) template for the control and on each lesion monkey structural image.

In order to study how the functional connectivity of the visual cortex and subcortical nuclei (LGN, pulvinar, SC) could play a role in blindsight, a seed was placed in each of the relevant areas (see Table 5.1). Seeds were first drawn on the F99 template, then realigned and eventually corrected following the protocol described in Chapter 2.4.1.

Table 5.1 Seed locations outside the primary visual cortex

	Brain Area	*F99 Coordinates*	*Seed Size (voxels/mm³)*	*Seed interest*
			Visual System	
1.	**V2m**	[75 34 74; 67 35 74]	5x5x5/15.6 mm³	- First relay of the visual information after V1
2.	**V2d**	[117 46 75; 23 46 75]	5x5x5/15.6 mm³	- Connections to MT and V4 - Receives inputs from the pulvinar
3.	**V4DP**	[111 50 90; 31 46 90]	5x5x5/15.6 mm³	- Start of the ventral pathway
4.	**V4d**	[115 48 80; 25 48 80]	5x5x5/15.6 mm³	- Receives inputs from V2 and the pulvinar
5.	**V4v**	[105 62 41; 36 61 40]	5x5x5/15.6 mm³	
6.	**MT**	[112 58 76; 30 56 77]	5x5x5/15.6 mm³	- Start of the dorsal pathway - Receives inputs from V2, V4 and the LGN - Preserved in Monkey S (Bridge et al., 2019)
			Visual Association Areas	
7.	**FEF**	[111 128 84; 29 130 82]	5x5x5/15.6 mm³	- Connections with MT and SC
			Subcortical areas	
8.	**LGN**	[96 88 48; 45 88 47]	3x3x3/3.4 mm³	- Receives most retinal inputs - Sends most afferences to V1 - Other afferences are sent to MT (Sincich et al., 2004) - Preserved in Monkey S (Bridge et al., 2019)
9.	**pulvinar**	[94 78 52; 94 78 52]	3x3x3/3.4 mm³	- Receives retinal inputs - Sends afferences to V1,V2 and V4 - Sends afferences to MT - Seeds overlaps with both the inferior and the lateral pulvinar.
10.	**SC**	[76 71 56; 66 71 56]	5x5x5/15.6 mm³	- Receives retinal input - Sends afferences to the pulvinar, LGN and MT
			For noise regression	
11.	**White matter**	[89 60 71; 54 60 71]	6x6x6/27 mm³	- Necessary for noise removal
12.	**CSF**	[88 72 65; 52 72 65]	4x4x4/8 mm³	

Figure 5.4 illustrates the seed locations on the F99 template. All seeds are bilateral, with a size of 5x5x5 voxels (15.6 mm^3), except for the LGN and pulvinar. Because of these areas' small size, maintaining a size of 5x5x5 voxels would have included other structures. To avoid this, the seed size was reduced to 3x3x3 voxels (3.4 mm^3) in these areas. A 6x6x6 voxels (27 mm^3) seed was placed in the white matter and a 4x4x4 voxels (8 mm^3) seed was placed in the ventricles to later regress out signal from the white matter and CSF.

5.2.5.2 Seeds Within V1

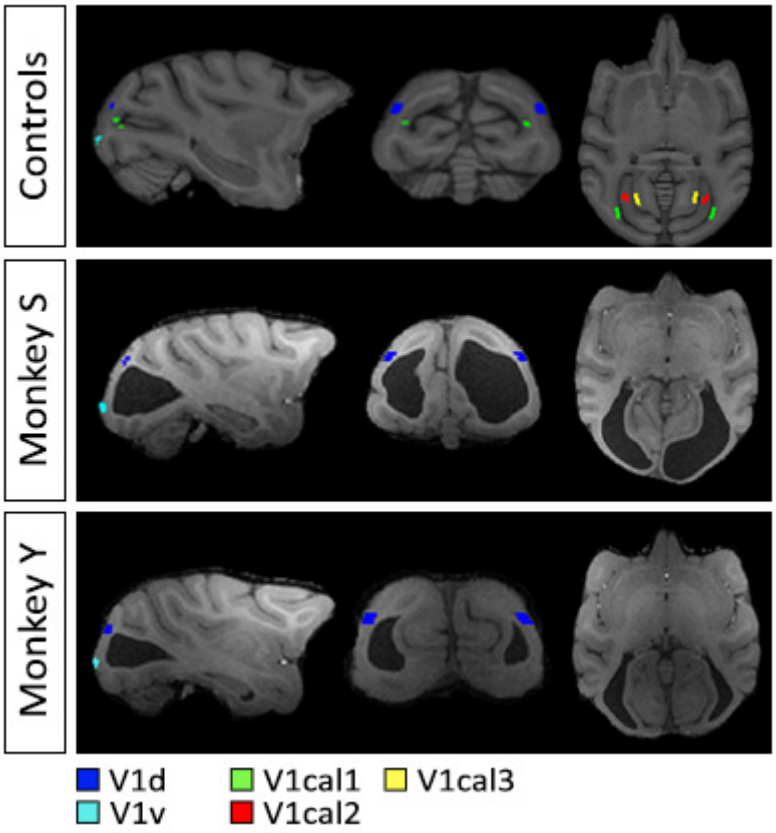


Figure 5.5 Location of the Primary Visual Cortex Seeds

5x5x5/15.6 mm^3 voxels seeds in V1
Seed are displayed on the F99 template (slice [103 24 62]) for the control animals and on equivalent slice of the structural scan of each lesion animal.

In both Monkey S and Monkey Y, the lesions overlap with the calcarine portion of V1 (for

further details see Chapter 5.3.1 and Figure 5.8). To better understand how the loss of this area impacts visual processing we must the study the functional connectivity of the operculum, still present in the lesion animals, and how/if the lesion changes it. We also want to compare it to the functional connectivity of calcarine cortex compared to the remainder of V1, in healthy controls. This comparison could help us locate regions of interest in the visual system with likely structural connections to calcarine. Therefore, two 5x5x5 (15.6 mm^3) voxels seeds were placed in the V1 operculum and three 5x5x5 voxels seeds were placed in the calcarine cortex.

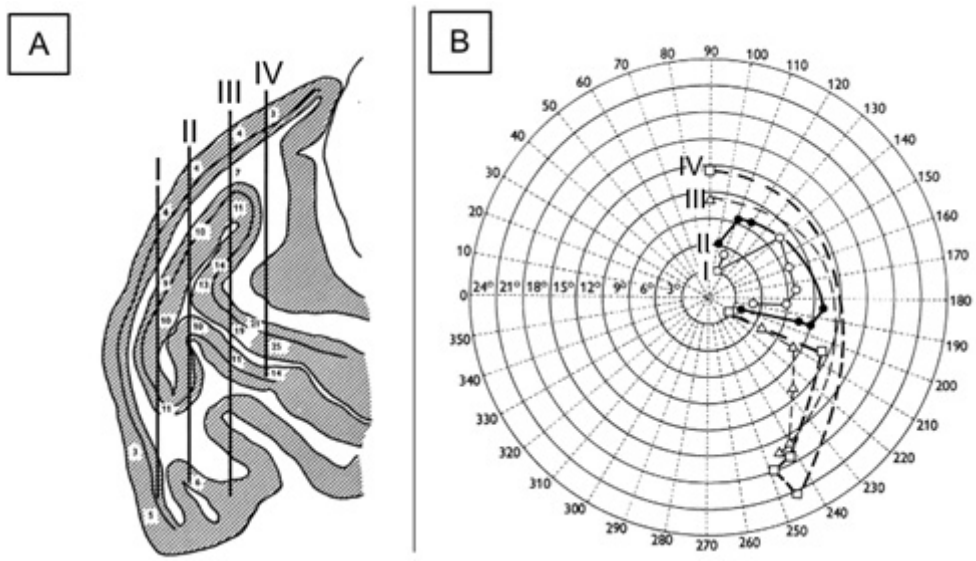


Figure 5.6 Visual Field Representation in V1

Copied from Daniel and Whitteridge (1969)
The authors drove 4 electrodes in 22 anesthetised monkeys' (Macaca mulatta, Chlorocebus pygerythrus, Macaca fascicularis) and baboon's (unknown species) primary visual cortex. They recorded the points where they obtained a signal in response to a visual stimulus.

A. *Crossection of a baboon's primary visual cortex. I, II, III and IV indicate the electrodes tracks. The numbers beside the tracks refer to the stimulus radial distance (also called eccentricity) from the fixation point in degrees when a signal was obtained.*
B. *Corresponding points in the visual field*

Figure 5.5 presents the primary visual cortex seeds' (i.e., V1d, V1v, V1cal1, V1cal2, and V1cal3) locations on the F99 template. V1d (F99 coordinates: [106 25 73; 34 25 72]) is the same seed as

the V1 seed employed in Chapter 4. It is located in the operculum of V1, which is still present in the lesion animals. This area codes for low (0-5 degrees) eccentricity points in the inferior portion of the visual field (see Figure 5.6; see also (Wandell et al., 2007)). V1v ([98 13 53; 42 13 53] is in the ventral operculum of V1, also present in the lesion animals. V1v is closer to the midline than the V1d seed. This position in the cortex represents small (although probably larger than the V1d) eccentricity points in the higher portion of the visual field. The V1d and V1v seeds are of interest in both the controls and the lesion animals as they allow the study of the functional connectivity of the remaining portion of V1 and the effect of the lesion over it

The calcarine seeds are only employed in the control animals in order to make a comparison of the functional connectivity of the portion of V1 that affected by the lesion in Monkey S and Monkey Y against the portion that is spared. V1cal1 ([104 28 63; 38 28 63]) is located in the ventral part of the roof of the calcarine cortex, which represents medium eccentricities (around 9 to 13 degrees). V1cal2 ([100 43 63; 42 41 60]) is placed in the ventral bank of the calcarine stem, while V1cal3 ([91 41 62; 50 41 62]) in the dorsal bank. The calcarine stem is the portion of V1 that represents the most peripheral part of the visual field. Following the procedure outlined in Chapter 2.4, all seeds were initially drawn using the F99 template, realigned, and then corrected, if necessary.

5.2.5.3 Individual Correlation Maps

In order to visualise the state of the functional network in the lesion monkeys, SBCA was run at the individual level. Individual correlation maps were obtained for the lesion and control animals (see Chapter 2.4.3). The average time-series at the seed location on the subject's functional scan was extracted for each seed and subject. For a given seed in each subject, the pre-processed (see

Chapter 2.2) functional scan, the timeseries from the seed, and the WM and CSF seeds were entered into FSL FEAT (first-level analysis) (Woolrich et al., 2004). The seed's timeseries was used in a GLM, as regressor of main interest. The model also used a timeseries from seeds placed in the WM and CSF as noise regressors (see above), in order to exclude the signal from the white matter and the CSF.

5.2.5.4 Higher Level Analysis in the Control Group

In order to obtain group average functional connectivity maps for each seed, the higher-level analysis step was run on the control animals. Lesion animals were examined exclusively at the individual level. Group analysis relies on good alignment between brain structure across subjects. The lesions of the two animals were judged to be too dissimilar to be joined in a group. Indeed, it is possible that pressure resulting from CSF in the lesions may have resulted in a displacement of the cortex surrounding them, potentially rendering any guarantees of good alignment moot.

A noteworthy difference exists in the structure of the models employed in the present higher-level analysis, compared to the previous two chapters: the omission of nuisance regressors in the high-level analysis. This was done to facilitate comparisons between group and individual lesion animal maps. The latter maps are the result of first level analysis. This is an important distinction, as nuisance regressors were only previously employed in high-level analysis (see Chapter 2.4 and Chapter 4.2.2), anyway. Indeed, despite the substantive value that accompanies more comprehensive models, in this case constructed through the inclusion of characteristics known to influence the BOLD signal, this was a necessary omission. To make the results of the higher-level analysis in the control group are comparable with the individual maps obtained in each lesion animal, the physiological regressor of interest would have to be

included in the model during the first level analysis. Nevertheless, doing so would have required that the acquisition of physiological data, which previously functioned as nuisance regressors, be synchronized with the BOLD acquisition, and that one data point per volume be recorded. This was not the case.

Consequently, the higher-level analysis design matrix includes only one contrast:

1. **Correlation average**: *The correlation with the seed is, on average, greater than zero*. ($H_0: \left[\left(\overline{z_{i,j}}\right)\right]_{V1cal3} = 0;\ H_a: \left[\left(\overline{z_{i,j}}\right)\right]_{V1cal3} > 0$)

The higher-level analysis was run using Multi-Level Modelling for Group Analysis (FLAME 1).

5.2.5.5 A Comparison of the functional connectivity of the calcarine vs the V1 operculum

A comparison was made using mixed effects Multi-Level Modelling for Group Analysis (FLAME 1, see also Chapter 4.2.2) to test for differences between the functional connectivity of the calcarine seed and the functional connectivity of the operculum seeds. The timeseries of each seed was used as a regressor of interest. No nuisance regressors were included. Only the control animals were involved. The contrasts employed are presented in Table 5.2. The test was run twice: once using V1d as the first operculum seed and once using V1v. To reduce the likelihood of false positives and make sure all the difference clusters satisfied the Matching Network criteria, contrast masking[10] was applied. C1, C3, C5 and C7 were masked by C9. C2 was masked by C10, C4 by C11 and C8 by C13.

[10] For more information about contrast masking see Figure 8.7 in Appendix 8.8.

Table 5.2 Contrasts Employed in the MLM Group Analysis for Differences Between the Functional Connectivity of the Calcarine Seed and the Operculum Seeds.

Contrast	*Contrast Description*
$V1_{Op1}$-$V1_{Op2}$	*The first operculum seed (*$V1_{Op1}$*) group effect is, on average, greater than the second operculum seed (*$V1_{Op2}$*) group effect* ($H_0: \left[\left(\overline{z_{i,j}}\right)\right]_{Cau1} = \left[\left(\overline{z_{i,j}}\right)\right]_{Cau2}$; $H_a: \left[\left(\overline{z_{i,j}}\right)\right]_{Cau1} > \left[\left(\overline{z_{i,j}}\right)\right]_{Cau2}$)
$V1_{Op2}$- $V1_{Op1}$	*The second operculum seed group effect is, on average, greater than the first operculum seed group effect* (($H_0: \left[\left(\overline{z_{i,j}}\right)\right]_{Cau2} = \left[\left(\overline{z_{i,j}}\right)\right]_{Cau1}$; $H_a: \left[\left(\overline{z_{i,j}}\right)\right]_{Cau2} > \left[\left(\overline{z_{i,j}}\right)\right]_{Cau1}$).
$V1_{Op1}$-V1Cal1	*The first operculum seed group effect is, on average, greater than the V1cal1 group effect* (t ($H_0: \left[\left(\overline{z_{i,j}}\right)\right]_{Cau1} = \left[\left(\overline{z_{i,j}}\right)\right]_{V1cal1}$; $H_a: \left[\left(\overline{z_{i,j}}\right)\right]_{Cau1} > \left[\left(\overline{z_{i,j}}\right)\right]_{V1cal1}$).
V1Cal1- $V1_{Op1}$	*The V1cal1 group effect is, on average, greater than the first operculum seed group effect* ($H_0: \left[\left(\overline{z_{i,j}}\right)\right]_{V1cal1} = \left[\left(\overline{z_{i,j}}\right)\right]_{Cau1}$; $H_a: \left[\left(\overline{z_{i,j}}\right)\right]_{V1cal1} > \left[\left(\overline{z_{i,j}}\right)\right]_{Cau1}$).).
$V1_{Op1}$-V1Cal2	*The first operculum seed group effect is, on average, greater than the V1cal2 group effect* ($H_0: \left[\left(\overline{z_{i,j}}\right)\right]_{Cau1} = \left[\left(\overline{z_{i,j}}\right)\right]_{V1cal2}$; $H_a: \left[\left(\overline{z_{i,j}}\right)\right]_{Cau1} > \left[\left(\overline{z_{i,j}}\right)\right]_{V1cal2}$).
V1Cal2- $V1_{Op1}$	*The V1cal2 group effect is, on average, greater than the first operculum seed group effect* ($H_0: \left[\left(\overline{z_{i,j}}\right)\right]_{V1cal2} = \left[\left(\overline{z_{i,j}}\right)\right]_{Cau1}$; $H_a: \left[\left(\overline{z_{i,j}}\right)\right]_{V1cal2} > \left[\left(\overline{z_{i,j}}\right)\right]_{Cau1}$).
$V1_{Op1}$-V1Cal3	*The V1cal3 group effect is, on average, greater than the first operculum seed group effect* ($H_0: \left[\left(\overline{z_{i,j}}\right)\right]_{V1cal3} = \left[\left(\overline{z_{i,j}}\right)\right]_{Cau1}$; $H_a: \left[\left(\overline{z_{i,j}}\right)\right]_{V1cal3} > \left[\left(\overline{z_{i,j}}\right)\right]_{Cau1}$).
V1Cal3- $V1_{Op1}$	*The first operculum seed group effect is, on average, greater than the V1cal3 group effect* ($H_0: \left[\left(\overline{z_{i,j}}\right)\right]_{Cau1} = \left[\left(\overline{z_{i,j}}\right)\right]_{V1cal3}$; $H_a: \left[\left(\overline{z_{i,j}}\right)\right]_{Cau1} > \left[\left(\overline{z_{i,j}}\right)\right]_{V1cal3}$).

5.2.6 Connectivity Heatmaps

Connectivity heatmaps are visual representations of connectivity strength across a given set of ROI. Regions are depicted in a graphical representation of a correlation matrix, with varying colours across a spectrum representing different correlation strengths between two ROI. This ordered depiction allows quick and easy comparisons of connectivity between sets of ROI (examining any singular cell) or, for example, of the connectivity of one ROI with all of the other ROI (scanning across a row or column).

Figure 5.7 illustrates the method used to obtain the heatmaps presented in this chapter.

Seven visual seeds outside of V1, three subcortical seeds thought to be related to blindsight (see Table 5.1 and Figure 5.4), and two seeds in the primary visual cortex operculum (see

Figure 5.5) were selected for the SBCA. This allowed us to examine how strongly each seed's timeseries correlates with the timeseries of the other seeds (here regions of interest, or ROI), in the controls compared to each of the lesion animals. Thus, for example, when examining V1v, our ROIs would include the LGN, V2m, V2d, V4DP, V4d, V4v, MT, the pulvinar, SC and, FEF seeds.

The timeseries at the location of each extrastriate and subcortical seed, as well as in the V1d and V1v seeds, was extracted in all animals using *fslmeants*. For each subject, each seed's timeseries was then imported into MATLAB (The Math Works, Inc. 2017). The Pearson correlation coefficient[11] between each seed timeseries and the other seed's is then calculated using MATLAB's *corrcoef* function.

In the control group, correlation coefficients between a given seed and ROI are averaged across all control animals. There is, of course, no guarantee that the V1 lesions affect each lesion animal's functional connectivity in the same way. Thus, the correlation coefficient values calculated in each lesion animal were retained and employed without averaging, resulting in the construction of three connectivity heatmaps, in total: one for each lesion animal and one for the control groups.

[11] The z-scores presented in the individual correlations maps (see 5.2.5.3) are the result of a Fisher transformation of Pearson correlations

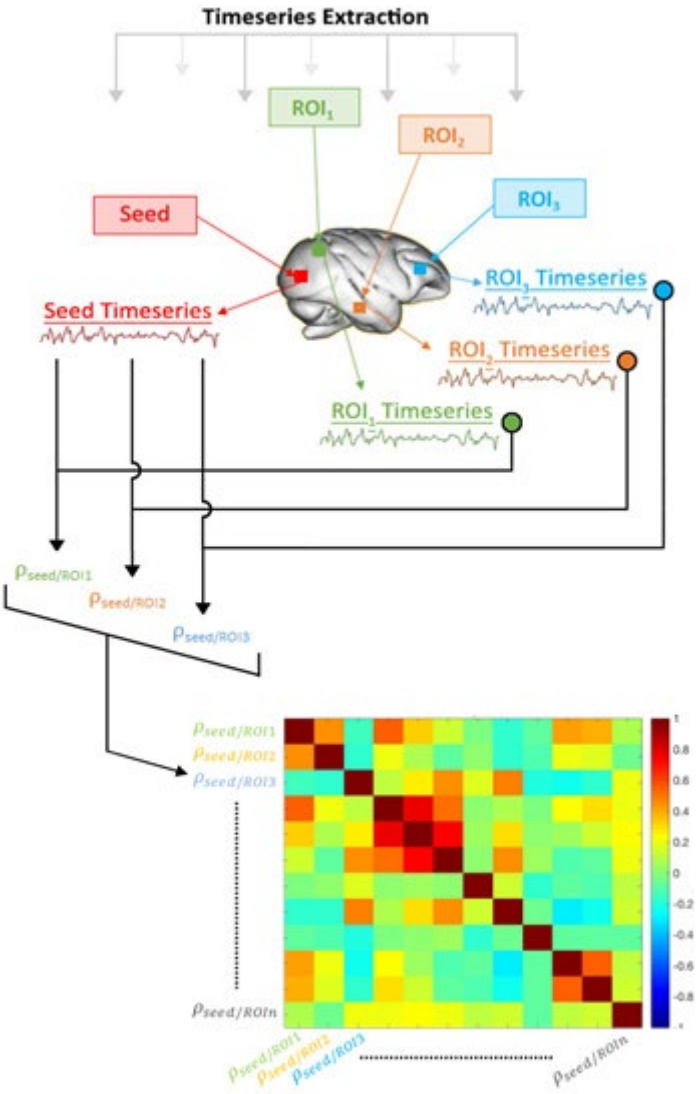


Figure 5.7 Obtaining Connectivity Heatmaps

The timeseries from 12 ROI (V1d,V1v, LGN, V2m, V2d, V4DP,V4d, V4v, MT, the pulvinar, SC and, FEF) were extracted. Then the Person correlations ($\rho_{seed/ROI}$) between each of the timeseries are calculated in MATLAB. Finally, the values are plotted in a heatmap, a graphical representation where each plot is attributed a colour across a spectrum of correlation values (-1 to 1) representing different correlation strengths between two ROI

Heatmaps were constructed using the MATLAB function *imagesc*. Correlation strength is represented on a colour spectrum from dark blue, corresponding to a correlation of -1, to green, corresponding to a correlation of 0, to dark red, corresponding to a correlation of +1 (see Figure 5.18). Differences between the average correlation value across the control group and correlation observed within each lesion monkeys were examined using independent

samples t-tests. The significance level was set to $\alpha = \left(\frac{0.05}{No.of\ ROI - 1}\right) = \left(\frac{0.05}{12-1}\right) = \left(\frac{0.05}{11}\right) = 0.0045$[12]. It should be noted that this is equivalent to setting the level of statistical significance to $\alpha = \left(\frac{0.05}{No.of\ concurrent\ comparisons\ made}\right)$ and is done to correct for the bias inherent to multiple comparisons. The error margin for the control group average was set to three standard errors, for the same reason.

5.2.7 Comparison of Primary Visual Cortex Seed Connectivity Strength

In the healthy controls, we compared the connectivity strength of each of the primary visual cortex seeds (2 operculum seeds: V1d, V1v; 3 calcarine seeds: V1cal1, V1cal2, V1cal3) with the ROI used in the heatmaps, in order to establish whether any of them has a stronger functional relationship with either the calcarine or the operculum. In a similar fashion to the heatmaps, timeseries for each of the primary visual cortex seeds and ROIs were extracted in each of the control animals using *fslmeants*. Timeseries were imported into MATLAB (The Math Works, Inc. 2017) and the correlation coefficient between each of the 5 V1 seeds and each ROI were calculated for each control monkey using the *corrcoef* function. The averaged results for each of the ROI we plotted on a bar plot.

For each of the ROI, a one-way ANOVA was run to test for differences in correlation strength between the ROI and each of the V1 seeds with the *anova1* function. The ANOVA was followed by a post-hoc Bonferroni test, using the *multcompare* function.

[12] The denominator of this fraction employs $(No.of\ ROI - 1)$ because we disregard the ROI with which we are examining the strength of the relationship.

5.3 Results

Like the presentation of the methodology employed in this chapter, the presentation of their results is also a relatively complex undertaking, comprised of multiple self-contained but interconnected parts. We provide a description of the volume and location of the lesions in Monkeys S and Y and a brief discussion of their theorized impact. We follow this with an examination of the actual focal impact of these lesions on the functional connectivity of the visual system, examining the remaining portions of V1 in the lesion monkeys, and each of three proposed compensatory visual processing pathways for them (i.e., LGN-MT-FEF, Pulvinar-V2-V4, and SC). We then present the results of a comparison between the functional connectivity of the calcarine and V1 operculum in the control group monkeys, in an attempt to derive substantial and substantive insight regarding connections between the remaining portions of V1 in the lesion monkeys and the rest of the traditional visual processing pathway. This, in turn, provides a more meaningful context within which we can process and discuss findings regarding the aforementioned compensatory pathways.

5.3.1 Lesion Description

Structural scans for both lesion animals were visually inspected and compared to *A combined MRI and Histology Atlas of the Rhesus Monkey brain in Stereotaxic coordinates* (Saleem & Logothetis, 2006).

Despite the overall similar appearance of the lesions in Monkey S and Monkey Y (see Figure 5.8), the lesions differ in size. Monkey S's lesion, which covers 7.0% of its brain's volume, is larger than Monkey Y's lesion, which corresponds to only 1.69 % of his total brain volume. Monkey S's lesion is also larger in the left hemisphere, while Monkey Y's lesion is larger in the right hemisphere.

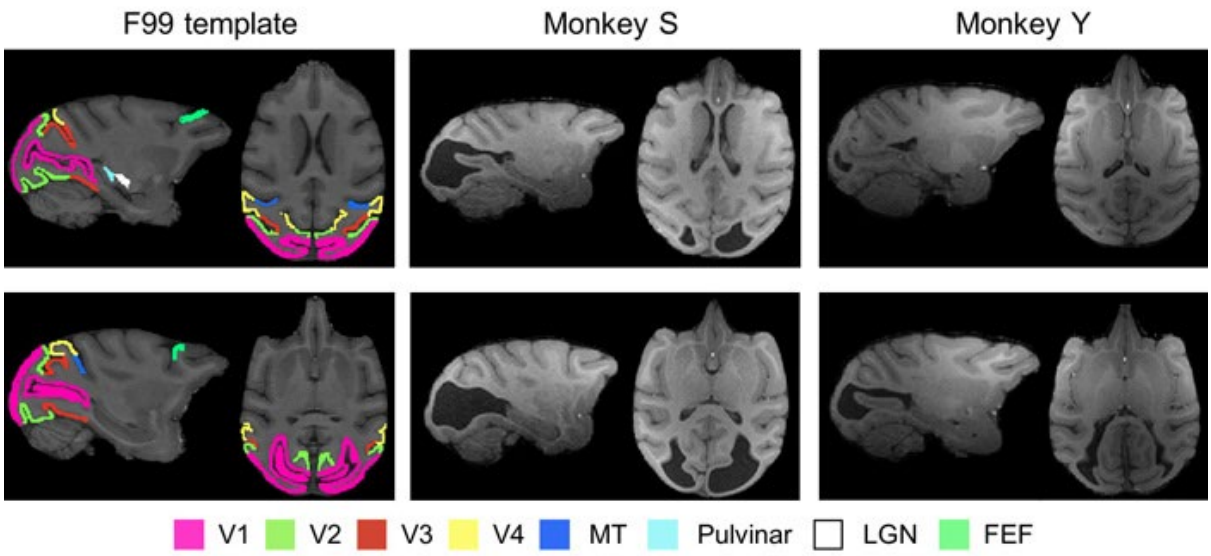


Figure 5.8 Structural Scan of Monkey S and Monkey Y, Compared to the F99 Template

Structural scans of Monkey S and Monkey Y were acquired (Siemens, 3T, 2mm).
The sagittal and frontal view at two different locations are presented for the F99 template (top: [95 75], bottom: [101 65]) on the left, Monkey S's structural scan (centre) and Monkey Y's structural scan (right) in the subject's space.
To better highlight the brain area affected in Monkey S and Monkey Y's lesion, several brain areas relevant to visual processing were drawn on the F99 template: the primary visual area (V1), the second visual area (V2), the third visual area (V3), the visual area 4 (V4), the middle temporal area (MT), the pulvinar, the lateral geniculate nucleus (LGN) and the frontal eye field (FEF).

Both animals lost cortex in the calcarine sulcus. The calcarine sulcus is home to V1 and, more precisely, the area responsible for processing inputs from the periphery of the visual field (Daniel & Whitteridge, 1961). The calcarine cortex is better preserved in Monkey Y, though.

Other early visual areas do not seem to overlap with the lesion. Both lesion animals' scans show indications that the CSF contained in the enlarged ventricles may put pressure on the surrounding cortex.

Patients who suffer a lesion of V1 sometimes develop a lesion in the LGN by retrograde degeneration (Kleiser et al., 2001; Van Buren, 1963). Bridge et al. (2019) found no degradation of the LGN in Monkey S. No evidence of degeneration of the LGN or any areas, other than those previously mentioned, is evident from the structural scans of Monkey Y, either. A

proper histological study, however, has yet to be done in either monkey to confirm the absence of degradations in both animals with certainty.

5.3.2 Focal Impact of V1 Lesions over the Visual System Functional Connectivity

5.3.2.1 Introduction

In order to understand the mechanisms supporting blindsight, SBCA was used to uncover potential strenghtened relationships between visual areas and the rest of the brain in the lesion animals. The z-score correlation maps obtained for each of the lesion animals were visually inspected and compared to the high-level analysis maps for the control group. It may seem reasonable to expect that lesions as large as the ones present in Monkey S and Monkey Y would substantially impact the functional connectivity of the visual system. As we discuss below, however, the lesions do not appear to dramatically affect the functional connectivity of the tested areas.

We begin by describing the functional connectivity of the portion of V1 which is unaffected by the lesions, in comparison to the equivalent sections of V1 in the control group. To do so, we employ two seeds: one in the dorsal portion of V1 (V1d) and one in the ventral portion (V1v). This is, in a sense, a coarse examination of the functional connectivity of the visual systems of the lesion and control animals. It is also agnostic, in that we examine the existence of differences between lesions and controls without *a priori* expectation of the existence of a specific compensatory visual pathway or even whether one exists, at all.

From this point onward, our examinations are explicitly founded on the basis of hypotheses. We assume and examine the existence of three specific compensatory visual processing pathways:

i. The LGN-MT-FEF pathway,

ii. The Pulvinar-V2-V4 pathway, and

iii. The SC pathway.

Examination of the LGN-MT-FEF pathway allows us to evaluate the projections of the primary thalamic relay nucleus to secondary visual areas. The Pulvinar-V2-V4 pathway allows us to examine the potential compensatory role of secondary thalamic relay nuclei in supporting adjustment to loss of primary cortical areas. Like the LGN, the SC also receives direct inputs from the retina and the SC pathway is connected to the starting points of the previous two pathways. Thus, examination of the SC pathway is, in one sense, an examination of extended versions of the other two pathways. It is also, however, an examination of the role of a midbrain nucleus in compensatory sight mechanisms.

There are comparably strong arguments for each of the three subcortical pathways supporting the existence of blindsight and/or residual vision in the presence of a V1 lesion. The LGN, pulvinar and SC are each connected, directly or indirectly, to at least one area of the visual system (see Figure 5.2). V1 receives direct projections from the LGN (Perkel et al., 1986) and the pulvinar (from the lateral ventro-lateral and inferior centro-lateral nuclei) (Casagrande & Kaas, 1994; Kaas & Lyon, 2007). SC projects to the LGN and the pulvinar (Harting et al., 1991). The subcortical seeds are also (directly or indirectly) connected to the remainder of the visual system. V2 and V4 receive direct afference from the pulvinar and indirect connections from the LGN through V1. The LGN sends direct efferences to MT (Nassi et al., 2006; Sincich et al., 2004). MT has reciprocal connections with the FEF, a frontal area involved in the control of visual attention and eye movements (Sharpe, 2014; Stanton et al., 1995). FEF is particularly interesting since, in some ways, it could be considered the end point of the dorsal pathway. MT also receives direct inputs from the inferior pulvinar and indirect pulvinar afferences through V1 and V2 (Cusick et al., 1993; Lin & Kaas, 1980). SC receives direct inputs from the retina and projects to the LGN and the pulvinar (Harting et al.,

1991), providing it with an indirect connection to the visual system. Additionally, evidence from research on patients who suffered a lesion in V1 and animals where V1 was either inactivated of lesioned has shown that the inactivation of the LGN (Schmid et al., 2010), the pulvinar (Kinoshita et al., 2019) or SC (Kato et al., 2011) disable the subject's residual's vision.

5.3.2.2 Functional Connectivity of the Surviving Portion of V1 in Controls and Lesion Animals

Sight, as we understand it, is dependent on the existence and function of the primary visual cortex. Lesions in V1 or of the axons *coming and going to and from the area,* and other functional deficiencies involving V1 directly impact subjects' ability to process visual information. The persistence of any degree of sight in subjects with extensive V1 lesions is inherently intriguing. The ability to retain or adapt functionality in surviving portions of V1 may provide substantive insight into an enhanced understanding of the function of V1 in the visual processing pathway, of other brain areas whose role is normally masked by V1, and of the various means by which the brain may adapt to the loss of what is (by all accounts) a vital component of one of its sensory information processing systems.

We begin below by describing the functional connectivity of the surviving portions of V1 (i.e., those unaffected by the lesions) in our lesion animals, compared to the equivalent sections of V1 in the control group. We present the results of an agnostic (i.e., without prejudice with regard to the existence specific compensatory pathways) examination of the functional connectivity of the dorsal V1 operculum, represented by the V1d seed, and the ventral V1 operculum, represented by the V1v seed (see Chapter 5.2.5.2).

5.3.2.2.1 Functional Connectivity of the Dorsal V1 Operculum

The V1d seed (see Figure 5.9), located in the dorsal primary visual cortex operculum, appears to be particularly well connected to the other visual areas of interest in the control group but also in the lesion animals.

The control group average correlations map shows several ventral pathway areas are significantly ($z \geq 2.3$) correlated with the seed's timeseries. Correlation with V2, V4, and the visual association areas in the inferior temporal cortex, as well as TE and TEO, are present in both hemispheres. The dorsal pathway is also represented through significant correlations in the left MT and left FST. There were no significant correlations between V1d and the LGN, pulvinar or SC.

Correlations in areas of the V3A-AIP-F5 (Ventral premotor cortex) pathway are also evident in the z-score maps. This pathway is parallel to the dorsal pathway, and involved in object recognition for visually guided grasping behaviour (Theys et al., 2015). In the control group average maps, there are significant correlations present in V3A, the ventral premotor area, and in the ventral premotor cortex (including F5).

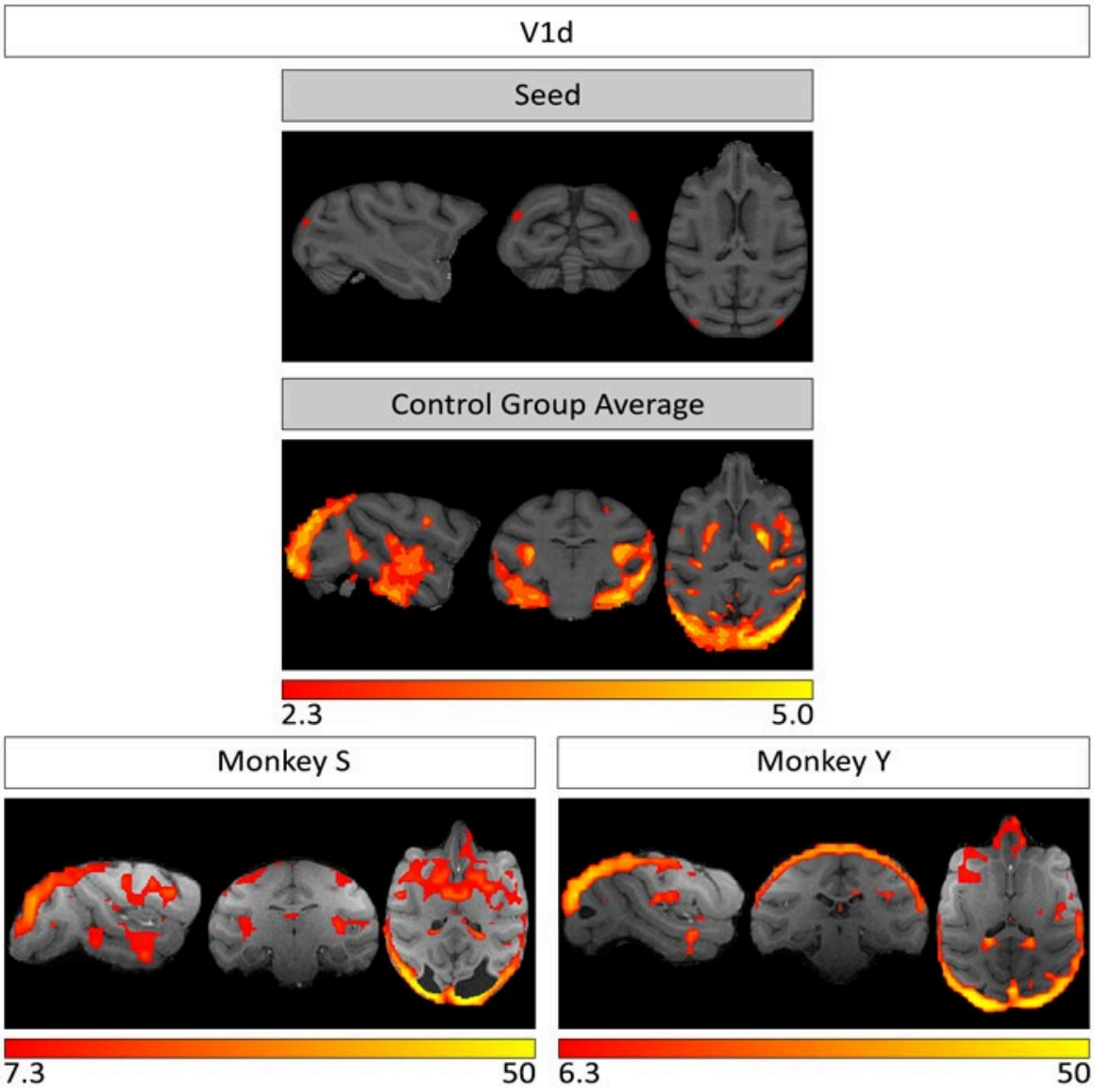


Figure 5.9 Comparison Between the Functional Connectivity of the V1d Seed in the Lesion Animals Versus the Control Average

First line: V1d (15.62 mm^3) bilateral seed location
Second Line: Average correlation map for V1d across the control animal group. The map is displayed on the F99 template at the z≥2.3 significance level.
The third line presents the z-score maps obtained with the same seed, placed in the same location, in Monkey S and Monkey Y (titled respectively). The results obtained in the lesion animals are presented at increased thresholds (Monkey S z=7.3, Monkey Y z=6.3) to facilitate comparison with the control group for the reader. To examine these results at the z≥ 2.3 significance level, see Appendix 8.9. A mask was applied to eliminate any correlations inside the lesions.
Colour bars represent the range of positive z-scores from the lower threshold in each case. To help with direct comparison across the different figures presented in this chapter, voxels over z=5 in the controls and z=50 in the lesion animals are presented under the colour at the upper end of the gradient (yellow).

In many ways, V1d functional connectivity for the lesion animals is similar to the V1d control

average (see Figure 5.9).

In the ventral pathway, both lesion animals and the control group average show significant (z≥2.3) correlations in V2, V4 and TE and TEO. Although, In the controls, the V2 and V4 correlations include both areas' ventral parts, only local significant correlations in ventral V2 are evident in Monkey Y (in addition of the dorsal V2 and V4 correlations). In Monkey S, a small significant cluster is bilaterally present in ventral V2 but correlations in V4 are exclusively dorsal.

The lesion animals show similar connections with the V1d seed, relative to the dorsal pathway. There is a cluster of significant voxels centred on the left FST, including a handful of voxels in MT, which are also evident in Monkey S. A small cluster of voxels is also present in Monkey Y's left FST. Notably, however, while Monkey Y showed evidence of significant correlations in the right hemisphere FEF, none were present in either the control group average or Monkey S.

No significant correlations were found between V1d and the LGN, the pulvinar or SC in the lesion or control animals.

5.3.2.2.2 Functional Connectivity of the Ventral V1 Operculum

The control average network for V1v (see Figure 5.10), a seed place in the ventral operculum, varies little on average from the functional connectivity associated with its sister seed, V1d, across the control groups. All visual and visual associated areas included in the V1d network (Figure 5.9) are also included in the V1v network.

There are, however, some noteworthy differences between the V1v and V1d networks. In the control group, significant clusters located in ventral areas are larger in the V1v network. Both lesion and control group average V1v networks include significant correlations both in dorsal V4 and ventral V4 (V4d and V4v, respectively), the ventral V4 cluster includes more voxels in the V1v map.

A similar trend is evident for the clusters in TE and TEO. In addition, the V1v network includes a small unilateral cluster in the left LIP and a bilateral cluster in FEF, which are not apparent in the V1d map.

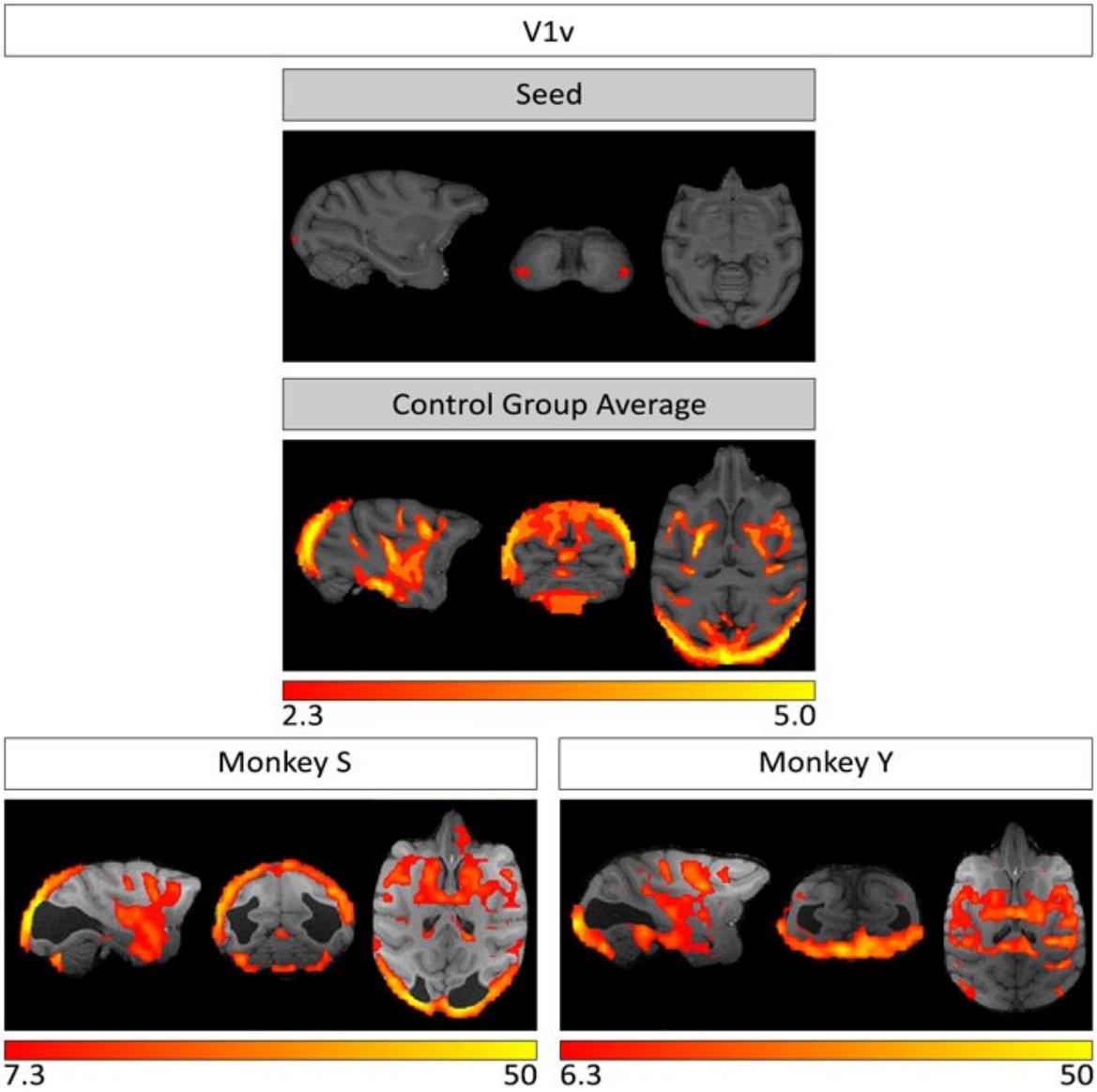


Figure 5.10 Comparison Between the Functional Connectivity of the V1v Seed in the Lesion Animals Versus the Control Average

First line: V1v (15.62 mm^3) bilateral seed location
Second Line Mean correlation map for V1v among control animals. The map is displayed on the F99 template at the z≥ 2.3significance level.
The third line presents the z-score maps obtained with the same seed, placed in the same location, in Monkey S and Monkey Y (titled respectively). The results obtained in the lesion animals are presented at increased thresholds (Monkey S z=7.3, Monkey Y z=6.3) to facilitate comparison with the control group for the reader. To examine these lesion animals' results at the z≥ 2.3significance level, see Appendix 8.9. A mask was applied to eliminate any correlations inside the lesions.
Colour bars represent the range of positive z-scores from the lower threshold in each case. To help with direct comparison across the different figures presented in this chapter, voxels over z=5 in the controls and z=50 in the lesion animals are presented under the colour at the upper end of the gradient (yellow).

Comparably to the control group average, Monkey S's V1v presents larger ventral clusters than in V1d –most notably in TE. Significant correlations with V1v are present in the dorsal and ventral parts of both V4 and V2. In the temporal cortex, Monkey S presents bilateral correlations with FST. In the frontal cortex she presents bilateral correlations with FEF. Bilateral correlations clusters are present in F5 and AIP but not in V3A.

Monkey Y's V1v map is the most divergent from the control group average and, by extension, its V1d equivalent. The control group average network includes dorsal clusters in V2, the left MT, and FST. No large dorsal cluster is present in Monkey Y's map. A small dorsal cluster in V2, a bilateral cluster (larger than in the control group average) in MT, and significant correlations with FST are evident in Monkey Y. Significant correlations with areas which are not involved in the control network are present in the LGN, LIP (bilaterally), and the left V3d. Commensurate with the control group average, however, large ventral cortex clusters are present in TEO, ventral V4, and V3v.

In short, the lesion monkeys' operculum functional connectivity appears fundamentally similar to that of the control group average. In other words, damage to (or, really, loss of) the calcarine does not appear to have impacted the functional connectivity of the primary visual cortex in the lesion animals.

5.3.2.3 Functional Connectivity of the LGN-MT-FEF Pathway

The LGN receives the majority of the retinal input. It is the primary thalamic relay of visual information and the final step in the visual processing pathway before the primary visual cortex. Indeed, in healthy mammals, the overwhelming majority of projections from LGN go to V1. Presumably, therefore, damage to V1 should mean the loss of a great deal of information, which is to say substantial detriment to, if not complete loss of, sight. Thus, if sight persists, we must first

look to the LGN for compensatory mechanisms, in an attempt to discern where it has redirected its projections. Indeed, examination of the LGN-MT-FEF pathway provides a singular opportunity to evaluate the projections of the primary thalamic relay nucleus to secondary visual areas.

MT receives afferences from several visual areas, including direct projections from the LGN. In healthy subjects, V1 and MT share a feedback loop. MT is also indirectly linked to V1 through V2, from which MT receives the majority of its afferences. MT also receives afferences from V4. MT also shares a feedback loop with FEF (the frontal end of the dorsal pathway). MT is a key area in the dorsal pathway, which processes movement, whose processing is (typically) spared in blindsight (Riddoch, 1917; Weiskrantz, 2009).

Previous examinations of Monkey S by Bridge et al (2019) found that LGN activity and MT functional network are preserved in Monkey S. The following section examines the functional connectivity of the LGN, MT, and FEF in both lesion monkeys and the control group.

5.3.2.3.1 LGN

There is only evidence for very small number of correlations between the LGN and the visual areas in the control group average and all of these are unilateral (see Figure 5.11). In the controls group average no significant correlations are evident between the LGN and V1 operculum. Monkey Y shows evidence of a bilateral correlation cluster in operculum V1. Both lesion animals also presented significant correlations with V1 around the midline, an area with a dense vascular activity.

The LGN control map, also includes unilateral significant visual correlations are present in the left ventral part of V2 and a few significant voxels are found in the left dorsal V2. The lesion animals show significant correlations between LGN and V2, albeit not at the same location.

Monkey S's V2 cluster is located in medial V2 (V2m), while Monkey Y's are dorsal and ventral.

In the control group a small significant correlations cluster is present in the left ventral V4. Ventral V4 correlation, but bilateral, are also evident in In Monkey Y. No significant correlation with V4 was found in Monkey S. Monkey Y also presents significant correlations in the left TEO and left TE. No correlations with TEO are present in the LGN network for the control group.

Regarding LGN's connectivity with MT, in the control group, no significant correlations with MT were found with the LGN seed. Significant correlations between the LGN and MT are however evident in both lesion animals, although they only are present in the left hemisphere for Monkey S[13]. The lesion monkeys, also show significant correlation in dorsal pathway-associated areas, such as MST, LIP and FEF.

Outside the visual system we note that in all animal groups' LGN maps, significant bilateral clusters are present in the insula, the somatosensory cortex, and in areas that have been described as relevant to visuomotor processing (i.e., the AIP, motor cortex, and ventral premotor cortex). The LGN is also functionally connected with other nuclei in the thalamus, notably on the context of the current discussion, the LGN is functionally connected to the pulvinar in the control average map. Both lesion monkeys show evidence of significant correlations clusters

[13] Bridge et al. (2019), in their previous examination of Monkey S found significant activation LGN in response to visual stimuli. They also found that Monkey S V5/MT's functional connectivity was similar to the control animals. Diffusion imaging results between MT and the LGN, however, concluded that it is unlikely that any residual vision in monkey S was due to a strengthening of the connections between MT and the LGN.

in the pulvinar.

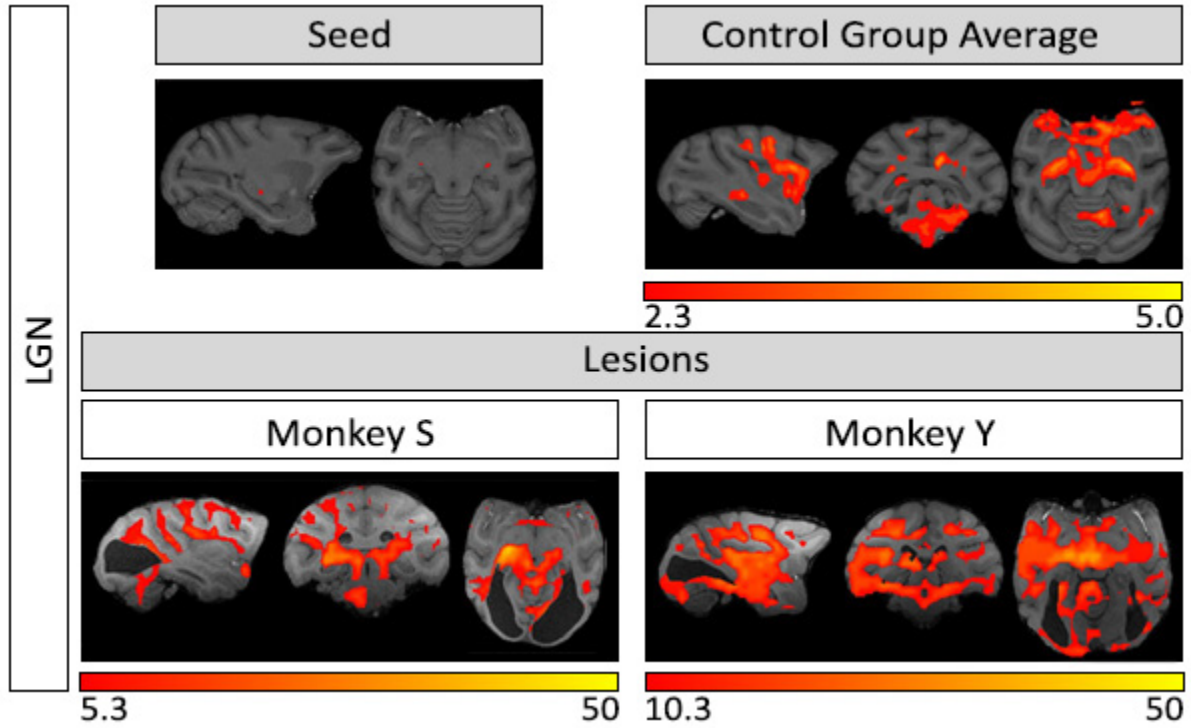


Figure 5.11 Comparison Between the Functional Connectivity of the LGN in the Lesion Animals Versus the Control Average

First line: LGN (3.4 mm^3) bilateral seed location
Second Line: Mean correlation map for the LGN among control animals. The map is displayed on the F99 template at the z≥2.3significance level.
The third line presents the z-score maps obtained with the same seed, placed in the same location, in Monkey S and Monkey Y (titled respectively). The results obtained in the lesion animals are presented on their structural image, at increased threshold (Monkey S z=5.3 Monkey Y z=10.3) facilitate comparison with the control group for the reader. To examine these results at the z≥2.3 significance level, see Appendix 8.9. A mask was applied to eliminate any correlations inside the lesions.
Colour bars represent the range of positive z-scores from the lower threshold in each case. To help with direct comparison across the different figures presented in this chapter, voxels over z=5 in the controls and z=50 in the lesion animals are presented under the colour at the upper end of the gradient (yellow).

5.3.2.3.2 MT and FEF

In line with previous findings by Bridge et al. (2019), MT's functional connectivity with the visual system in the lesion animals is close to that of the controls. Most of the cortical visual processing areas are found in the MT functional connectivity network, across all animals (see Figure 5.12).

One noteworthy difference may be located at the subcortical level. Significant correlations between MT and the LGN are only observed in the left hemispheres of Monkeys Y and S, when no correlation between MT and LGN are evident in the control group average. Of course, the veracity of the existence of any LGN cluster could be a point of contention, as it is only a few voxels wide in both lesion animals. No significant correlations with the pulvinar were evident for all animals/groups.

In the FEF control group average map (see Figure 5.12) there is no evidence of significant clusters in the LGN or the pulvinar. Monkey S shows evidence of a cluster of significant voxels partially overlapping the pulvinar and the LGN. No pulvinar clusters are evident in Monkey Y.

In the cortex, significant correlations between the MT seed and V1 are present in the both the control average group and the lesion animals. In the control group average map, the V1 cluster is exclusively located in the calcarine. In the lesion animals, significant correlations with V1 are evident in both the ventral operculum and the remnants of the calcarine. In Monkey Y, however, the right calcarine cluster is only a few voxels wide and noticeably smaller than its left hemisphere equivalent. In the right hemisphere of the FEF control group average map, significant correlations are also evident in the calcarine portion of V1. The lesion animals show evidence of significant correlations in V1, in both the operculum and the residual calcarine.

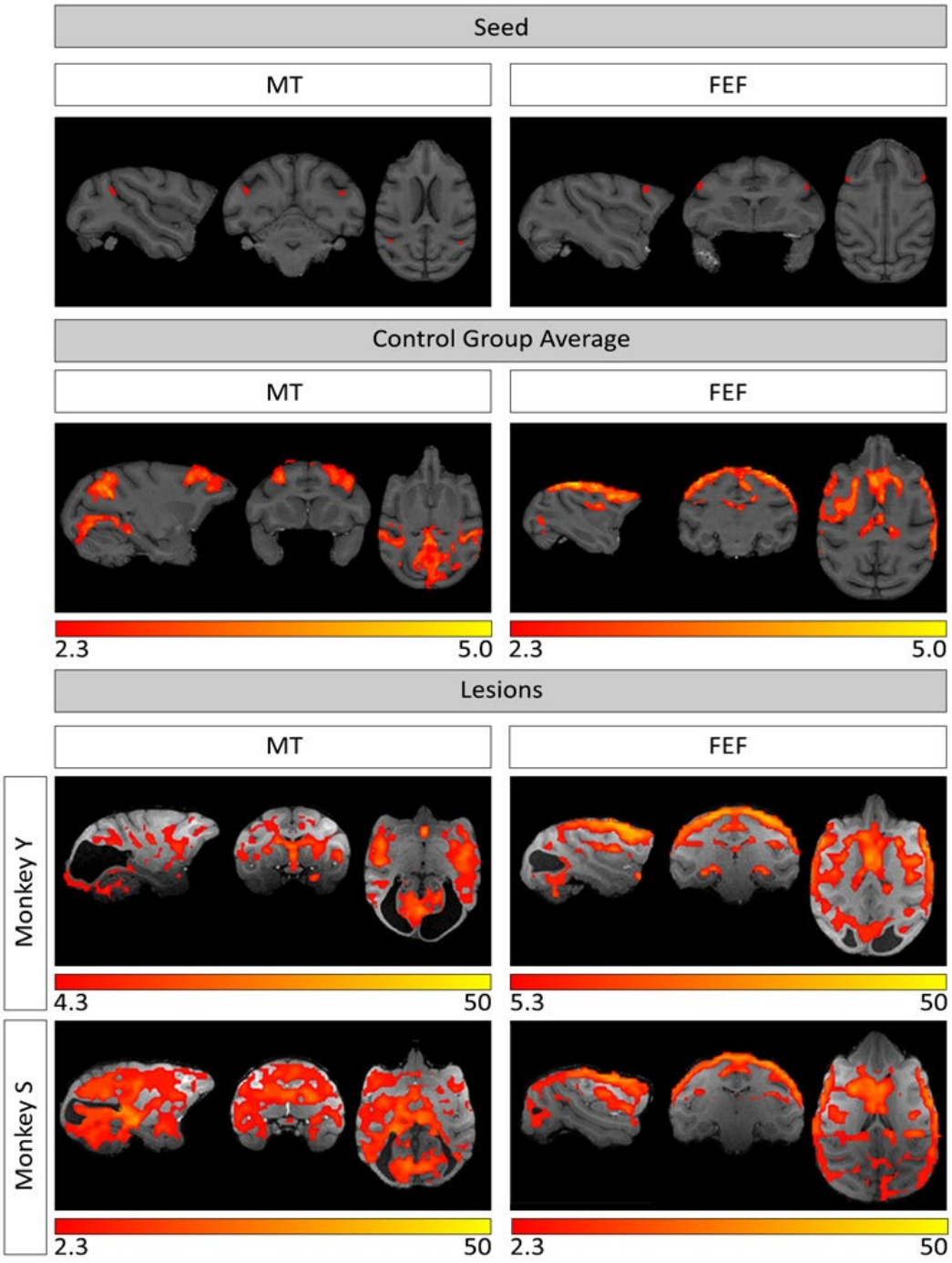


Figure 5.12 Comparison Between the Functional Connectivity of the MT and FEF Seeds in the Lesion Animals Versus the Control Average

First line: FEF and MT (15.62 mm$^{3)}$ bilateral seed location
Second Line Mean correlation map for the MT and FEF among control animals. The map is displayed on the F99 template at the z≥2.3 significance level
The third line presents the z-score maps obtained with the same seed, placed in the same location, in Monkey S and Monkey Y (titled respectively). The results obtained in the lesion animals are presented on their structural image. Monkey Y results are presents at an increased threshold of z=4.3 for MT and z=5.3 for FEF to help direct comparison with the control group and Monkey S. Monkey Y results at the z≥2.3 significance level are presented in Appendix 8.9. A mask was applied to eliminate any correlations inside the lesions.
Colour bars represent the range of positive z-scores from the lower threshold in each case. To help with direct comparison across the different figures presented in this chapter, voxels over z=5 in the controls and z=50 in the lesion animals are presented under the colour at the upper end of the gradient (yellow).

The MT control group average connectivity map includes a large portion of V2. Bilateral clusters of significant voxels are evident in the dorsal V2. The MT map also presents a significant correlation in the right ventral V2, which is also evident in the control FEF map. No other significant correlation in V2 is found in the FEF control average map. Significant bilateral correlations are also present in dorsal and ventral V2, in both Monkey S and Monkey Y's MT maps. Significant clusters are evident in the dorsal (V2d) and medial (V2m) parts of V2, in both lesion animals FEF map, and in ventral V2 (V2v) in Monkey Y.

Significant correlations are evident in V3v for the control group average, bilaterally in MT and unilaterally in the right hemisphere in FEF. In the MT map, additional clusters are found in V3d and V3A. The lesion animals present significant correlations in V3d, in both maps. In the lesion animals MT maps, significant correlations are also evident in V3d and one cluster is present in V3A, in Monkey Y. Monkey S's FEF map also exhibits correlations with V3A.

The ventral pathway is where the most obvious differences between the control average and the lesion animals' MT maps become apparent. The control group average map presents significant correlations with both the ventral and dorsal parts of V4. Dorsal correlations are absent from Monkey Y. All animals/groups have significant correlation clusters in ventral V4. Significant correlations with MT were evident in TEO in all animals/groups. Significant correlations with TE are only present in the lesion animals.

The FEF control group average network includes significant bilateral, localized, temporal correlations in dorsal V4. Both Monkey Y and Monkey S present significant bilateral correlations in dorsal V4. No significant ventral V4 clusters were found in the lesion animals. In the controls, the correlation cluster present in V3v extends past the V3v/V4v border to include some voxels in V4v

In the MT network, all animals/groups show significant correlations with areas that are either motion sensitive or involved in eye movements. The control group average includes significant correlations in FST and MST. These are also evident in the lesion animals, although the FST cluster is only present in the left hemisphere in Monkey S. Correlations are also present in MIP in all animal groups, FEF bilaterally for the control group average and Monkey Y, and in the right hemisphere for Monkey S.

Both MT and the FEF have reciprocal connections with LIP (Saalmann et al., 2007; Stanton et al., 1995). Significant bilateral correlations with LIP are evident in the MT network of the control group average and Monkey Y. Bilateral correlations in LIP are also evident in the FEF control network and in each lesion animal, although in Monkey S the cluster is more centred on area 7 Opt.

As noted above, MT projects into FEF. The control group average and each of the lesion animal show bilateral correlations with FEF, in the MT maps. In Monkey Y, the FEF cluster is larger in the right hemisphere. In the FEF map, no significant correlations were found in MT in either the control group average map or Monkey Y, though. A significant bilateral cluster is present in MT for Monkey S.

It is worth mentioning that in monkeys, the FEF receives the majority of its neural inputs from other cortical eye fields –most notably the supplementary eye field (SEF), posterior eye field (PEF) and principal sulcus area (Schall et al., 1993; Tian & Lynch, 1996). FEF projects to several areas of the frontal cortex (Stanton et al., 1995). In all animals/groups the FEF connectivity network involves more fronto-parietal than visual areas (see Figure 5.12). Indeed, large clusters are present the insula, somatosensory cortex area 1-2, motor cortex (F1), premotor cortex, dorsolateral prefrontal cortex and ventrolateral prefrontal cortex. Frontal and parietal

clusters are also evident in the MT networks. Significant correlations with the seed are evident in the dorsolateral prefrontal area (controls 9d, 8Bd, 46d; Monkey S: 8Bd, 9d, 46d, right 46v; Monkey Y: 8bd 46d left 46v), in all animals/groups. Monkey S also presents a significant bilateral correlation cluster in the dorsomedial prefrontal area 9m.

Significant somatosensory correlations are present in the somatosensory area 1-2 in midline region, in the control group average. In Monkeys S and Y no somatosensory clusters are found in area 1-2, although significant correlations with somatosensory areas 3a/b and secondary somatosensory cortex are observed. Motor clusters are also evident in the MT maps. Both the control group average and lesion monkeys present significant correlations between the MT and the premotor cortex (control average: F7, F2, F5; Monkey S: F2, F5, F4, F7; Monkey Y: right F2, F4, F5, F7). No significant cluster in the motor cortex is evident in the control group average, while such clusters are present in both lesion animals.

In summary, the lesion animals and controls have relatively similar MT and FEF correlation maps. The lesion animals' LGN connectivity maps share many of the areas included in the control group average. More often than not, however, the lesion Monkeys' significant correlation clusters are bilateral, while they are unilateral in the controls. We note the presence of significant correlations between MT and LGN in the Lesion animals, which are evident in both LGN and MT Maps.

5.3.2.4 Functional Connectivity of the Pulvinar-V2-V4 Pathway

Bridge et al. (2019) report that the pulvinar was activated by moving dots stimuli in Monkey S which suggests its function is preserved in this animal. The pulvinar is the second thalamic nucleus connected to the visual system. The pulvinar receives direct and indirect retinal inputs

(through SC) and, in healthy subjects, is directly connected to V1, V2, and V4. In other words, it receives retinal input and filters it into the visual processing system. In the presence of a damaged V1, it is important to examine the potential compensatory role played by the secondary thalamic relay nucleus in residual sight and blindsight.

5.3.2.4.1 Pulvinar

Most of the areas present in the control group average pulvinar maps are also present in the lesion animals (see Figure 5.13).

At first glance, the pulvinar functional network is mainly a fronto-parietal network. Nevertheless, it also involves some key visual areas. No significant correlations with the pulvinar are evident in the V1's operculum in the control group average but small clusters of significant correlations are present in the calcarine. This is also the case in the lesion animals, where significant correlations with V1 can also be found in the calcarine remnant. Both lesion animals and the control group also display significant correlations in both ventral V3 and V3A. Correlations in the dorsal V3 are also present in the lesion animals.

In the control group average, the significant correlation cluster centred in ventral V3 partially includes ventral V2. No other significant correlations with V2 are evident. In the lesion animals, the network includes a much larger portion of V2. Significant correlations with V2m are present in both lesion monkeys. Additional V2 correlations are also found in dorsal V2 in Monkey Y, although not at the same location as the V2d ROI.

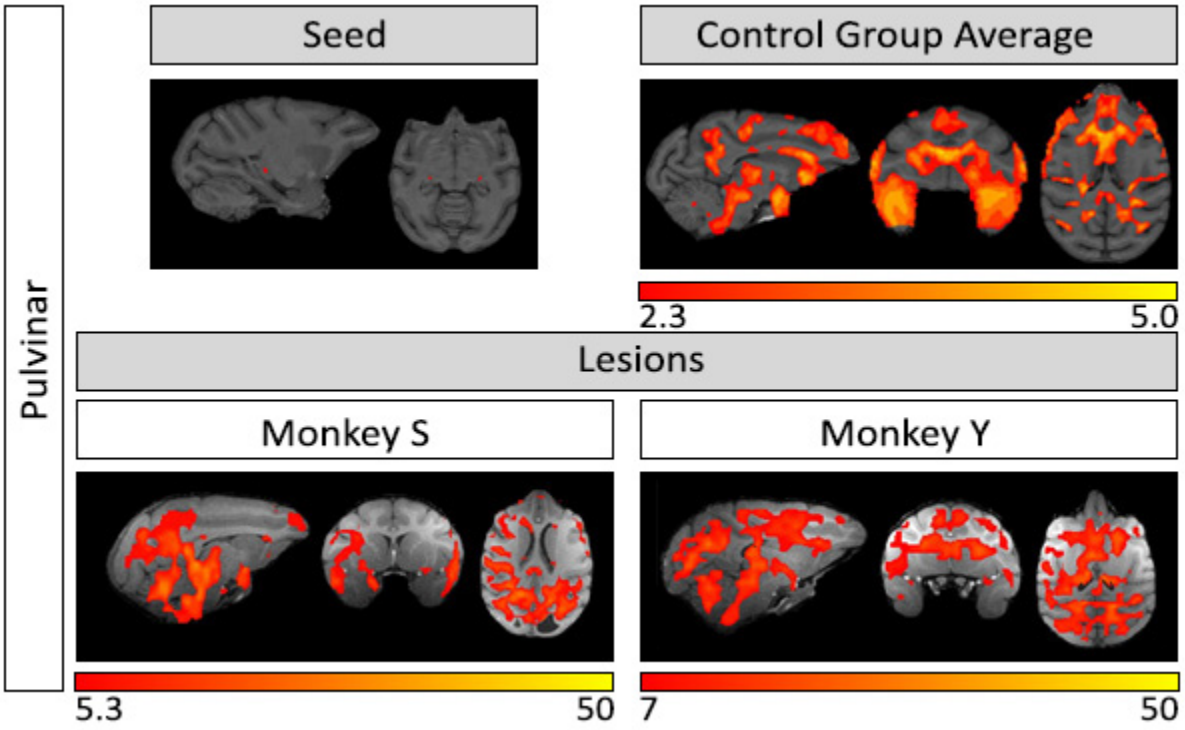


Figure 5.13 Comparison Between the Functional Connectivity of the Pulvinar in the Lesion Animals Versus the Control Average

First line: pulvinar (3.4 mm^3) bilateral seed location
Second Line: Significant (z≥ 2.3) correlation map for the pulvinar among control animals. The map is displayed on the F99 template.
The third line presents the z-score maps obtained with the same seed, placed in the same location, in Monkey S and Monkey Y (titled respectively). The results obtained in the lesion animals are presented on their structural image, at increased thresholds and with an upper threshold of z=50 to facilitate comparison with the control group for the reader. To examine these results at the z≥ 2.3 significance level, see Appendix 8.9. A mask was applied to eliminate any correlations inside the lesions.
Colour bars represent the range of positive z-scores from the lower threshold in each case. To help with direct comparison across the different figures presented in this chapter, voxels over z=5 in the controls and z=50 in the lesion animals are presented under the colour at the upper end of the gradient (yellow).

The lesion animals show no evidence of significant bilateral correlations with the ventral part of V4 (V4v) but significant clusters absent from the control average map are present in area TE. The lesion animals also present significant correlations in MT, which is not the case in the control group average. Significant correlation clusters are evident in FEF (unilateral left in Monkey S) and MST in all animal groups, though. The midbrain correlations did not include SC in the control average but both lesion animals have significant correlations in this area.

5.3.2.4.2 V2m and V2d

V2m's connectivity (Figure 5.14) seems relatively unaffected by the existence of V1 lesions. Significant correlations with V2m are equally evident in many areas, including both the ventral and dorsal parts of V3, V3A, dorsal V4, MT, MST, MIP, and FEF, for both lesion monkeys and the control group average. The control group average and lesion monkeys also present bilateral correlations in the STS, in both the fundus and the dorsal bank areas. Significant correlations are also evident in V1 for both the control group average and the lesion animals. While the control group does show evidence of V1 correlations located in both the operculum and the calcarine, however, V1 clusters are only located in the residual calcarine cortex in the lesion animals.

Other areas are also significantly correlated to the V2m seed, albeit with a handful of noteworthy variations between the control group and the lesion animals. In the control group, bilateral clusters are present in TEO. Only one small, unilateral cluster is present in Monkey Y's right hemisphere; none are evident in Monkey S. In FST, both the control group and Monkey S present bilateral correlations; no correlations in FST are evident in Monkey Y.

Some areas present exclusively in the lesion animals. Significant correlations are evident in the lesion animals' pulvinar. This is not the case in the control group average. When control animals were examined separately, only one monkey showed evidence of a single unilateral correlation between V2m and the pulvinar. The lesion animals' pulvinar clusters are of particular interest, as they mirror the novel correlations observed in the V2 in the pulvinar correlation maps (see Figure 5.14). Monkey S's pulvinar cluster also extends for a few voxels into the LGN.

The V2d seed control group average functional network (Figure 5.14) is smaller than its sister seed's (V2m) in the medial line. The control group average network includes bilateral

correlations in several dorsal areas. Significant correlation clusters are present in the dorsal part of V4 and in V3d. The cluster in V4d is also evident in the lesion animals but no correlations with V3d are evident in either Monkeys Y or S (see Figure 5.14). In the control group average, significant bilateral correlations are also evident in V1. This cluster is mainly dorsal and includes both the operculum and the left calcarine. In Monkey Y, correlations with V1 are only present in the dorsal V1 operculum and the left calcarine. In Monkey S, only a small cluster is evident in the V1 operculum, next to the midline (i.e., a different location than the V1d and V1v ROIs) and in the remainder of the right calcarine. In the parietal cortex, bilateral correlations are found in MIP in the control group average, but not in the lesion animals. Nevertheless, a significant unilateral correlation cluster is present in the left LIP in Monkey Y.

The control group average V2d network also includes unilateral correlations in the left hemisphere. Significant correlations were evident in the left TEO and left TE. In the lesion animals, significant correlations with the seeds are also evident in TE, although here they are bilateral. A bilateral cluster is also found in TEO in Monkey S; no TEO cluster is present in Monkey Y. Significant correlations are also present in the left V3a, and the left V3v. In Monkey S, a cluster is evident in the right V3a. No significant correlations with V3v are evident in the lesion animals. In the occipital cortex, significant correlations are present in the left MT in the control group. A significant cluster in the right MT is present in Monkey S but no significant correlations with MT are present in Monkey Y. In the left STS, the control group average map also includes significant clusters in the FST and the IPA. A similar cluster is evident in Monkey S's right STS. A frontal cluster partially overlapping with FEF is present in the right hemisphere in the control group average map. A similar cluster is present bilaterally in Monkey S and a small cluster is evident in Monkey Y's FEF. No pulvinar, LGN or SC correlations are evident in either lesion animal or the group average.

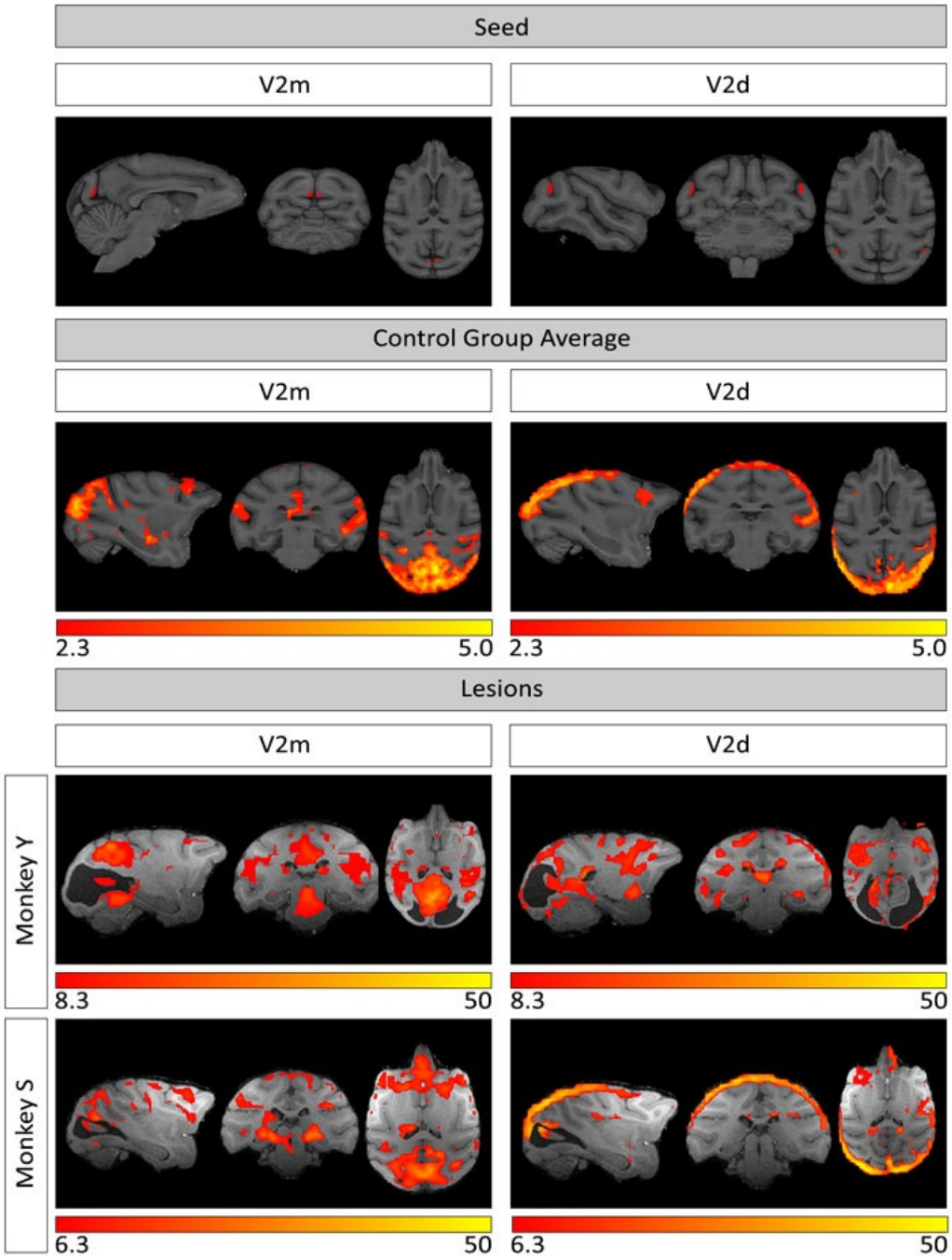


Figure 5.14 Comparison Between the Functional Connectivity of the V2m and V2d Seeds in the Lesion Animals Versus the Control Average

Seed: V2m and V2d (15.62 mm$^{3)}$ seed location.
Control Average Group: Average correlation with dorsal visual area 4 seeds (either V4DP or V4d) across the control animal group. Each map is displayed on the F99 template at the z≥2.3 significance level
Lesions: z-score maps obtained with the V2m or V2d seed in Monkey S and Monkey Y (titled respectively). The results obtained in the lesion animals are presented at increased thresholds to facilitate comparison with the control group for the reader. To examine these results at significance level (z≥2.3), see Appendix 8.9. A mask was applied to eliminate any correlations inside the lesions.
Colour bars represent the range of positive z-scores from the lower threshold in each case. To help with direct comparison across the different figures presented in this chapter, voxels over z=5 in the controls and z=50 in the lesion animals are presented under the colour at the upper end of the gradient (yellow).

5.3.2.4.3 V4DP and V4d

The V4DP and V4d seeds are located in the dorsal visual area 4 (see Figure 5.4). They are also closely situated spatially and have similar functional networks (see Figure 5.15). The V4DP and V4d seeds are well connected to other dorsal visual areas. In the control group average as well as the two lesion animals, significant correlations are present with both V2 and V1. In the control group, V1 correlations are mainly present in the dorsal portion for both seeds. Correlation clusters in V1 expand within the cortex in the calcarine sulcus in the controls, the area most affected by the lesions. In the lesion animals, no activity can be found in what remains of Monkey S's calcarine sulcus but a significant cluster was present in the corresponding region for Monkey Y. The cluster is mostly located in the left hemisphere, but a few significant voxels are present in the right calcarine.

In the control group, most V2 correlations with either seed are in the dorsal or medial part, although some local correlations are also evident in ventral V2, in the V4DP network. In Monkey Y ventral correlations with V2 are present in both V4DP and V4d networks. Ventral correlations with V2 are absent in Monkey S, however.

The V4 dorsal seeds are also functionally connected to TE and TEO, two areas belonging to the ventral pathway. In the controls, however, significant V4DP correlations in TE can only be found in the left hemisphere. Correlations with TE in the V4d network are also unilateral but in the right hemisphere. In the lesion animals, V4DP-TE correlations are present in the right hemisphere in Monkey S and bilaterally in Monkey Y.

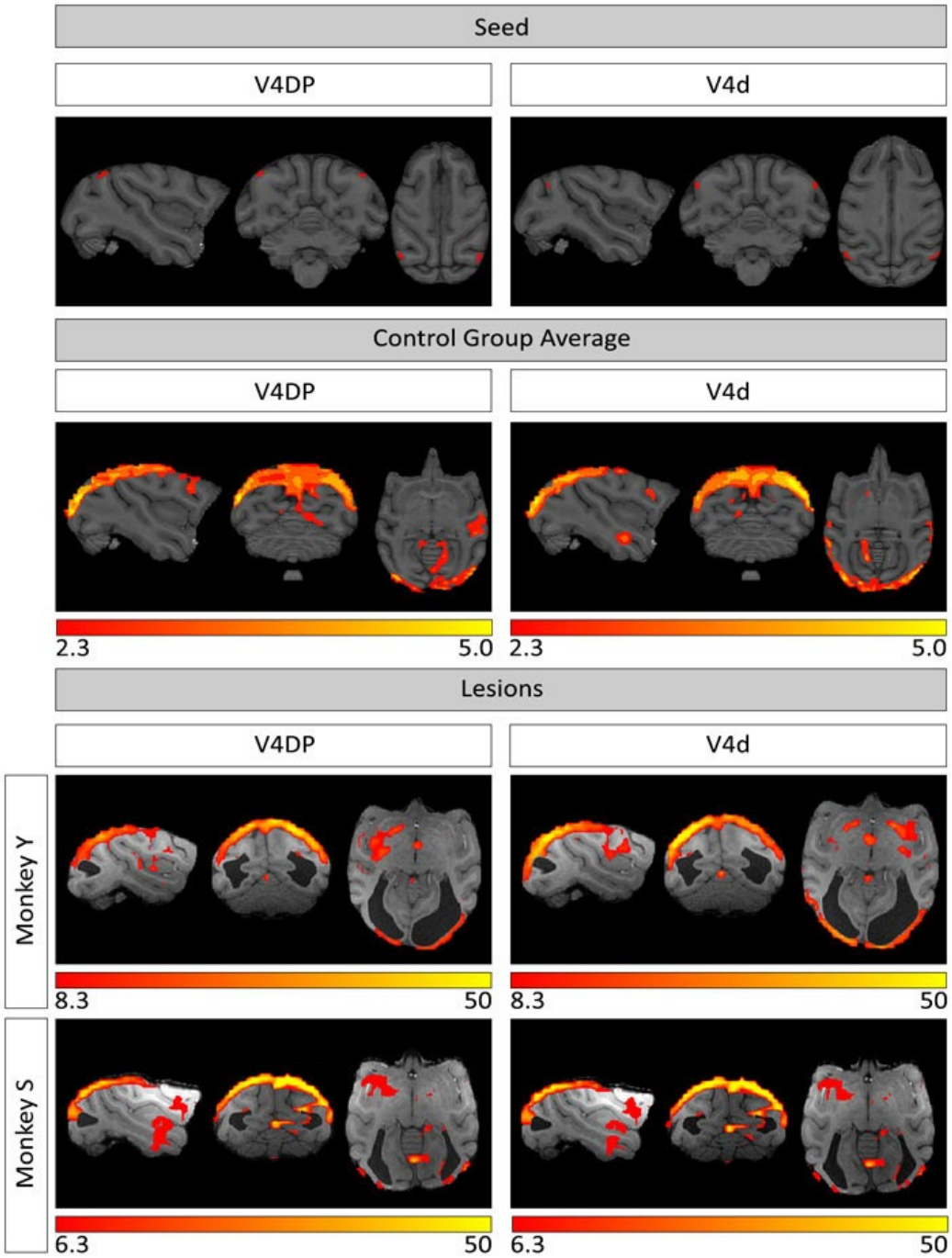


Figure 5.15 Comparison Between the Functional Connectivity of the V4DP and V4d Seeds in the Lesion Animals Versus the Control Average

Seed: V4DP and V4d (15.62 mm^3) seed location.
Control Average Group: Average correlation with dorsal visual area 4 seeds (either V4DP or V4d) across the control animal group. Each map is displayed on the F99 template at significance level ($z \geq 2.3$).
Lesions: z-score maps obtained with the V4DP or V4d seed in Monkey S and Monkey Y (titled respectively). The results obtained in the lesion animals are presented at increased thresholds to facilitate comparison with the control group for the reader. To examine these results at significance level ($z \geq 2.3$)., see Appendix 8.9. A mask was applied to eliminate any correlations inside the lesions.
Colour bars represent the range of positive z-scores from the lower threshold in each case. To help with direct comparison across the different figures presented in this chapter, voxels over z=5 in the controls and z=50 in the lesion animals are presented under the colour at the upper end of the gradient (yellow).

5.3.2.4.4 V4v

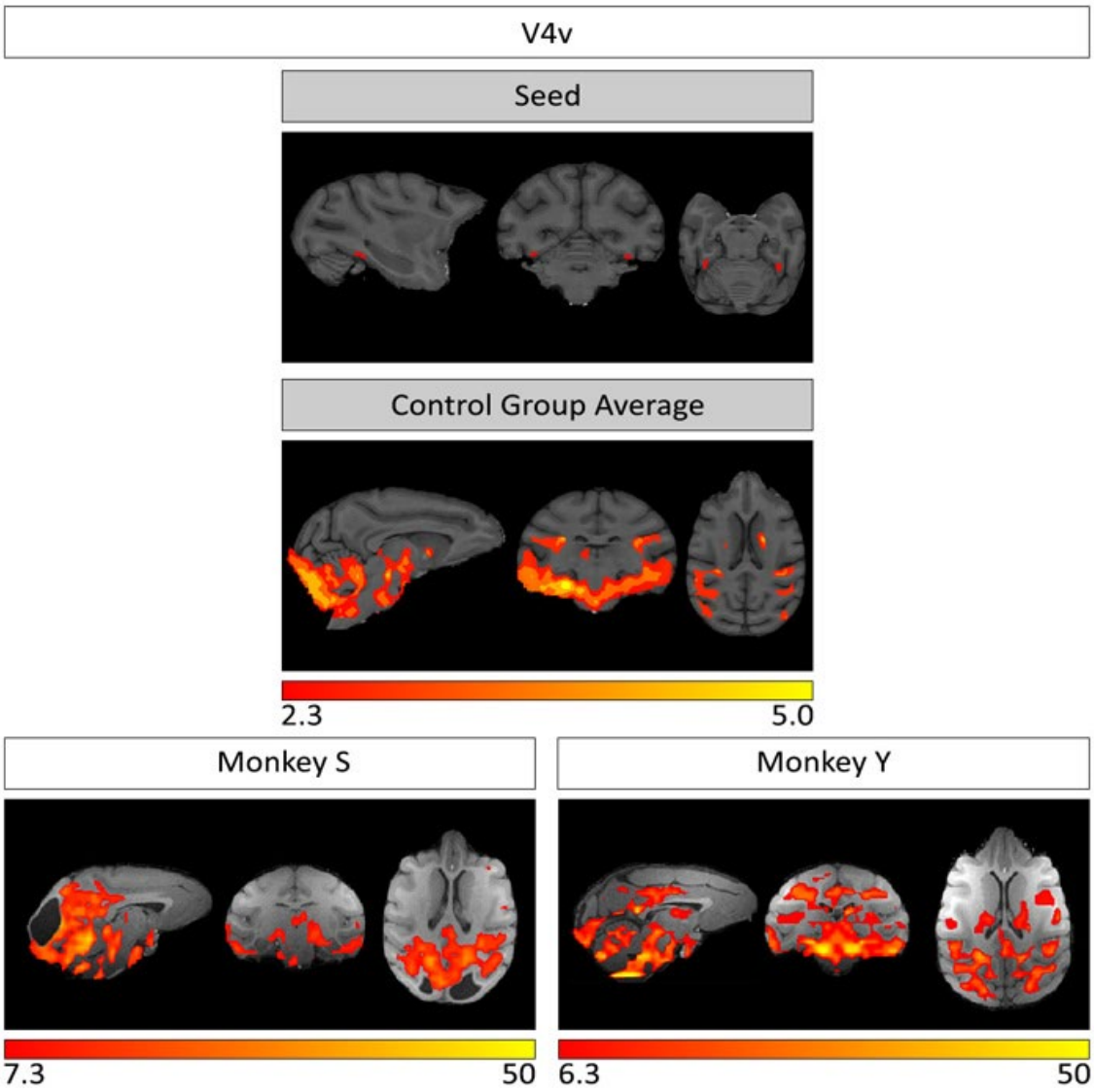


Figure 5.16 Comparison Between the Functional Connectivity of the V4v Seed in the Lesion Animals Versus the Control Average

First line: V4v (15.62 mm$^{3)}$ bilateral seed location
Second Line Mean correlation map for V4v among control animals. The map is displayed on the F99 template at significance level (z≥2.3).
The third line presents the z-score maps obtained with the same seed, placed in the same location, in Monkey S and Monkey Y (titled respectively). The results obtained in the lesion animals are presented at increased thresholds to facilitate comparison with the control group for the reader. To examine these results at the significance level (z≥2.3), see Appendix 8.9. A mask was applied to eliminate any correlations inside the lesions. Colour bars represent the range of positive z-scores from the lower threshold in each case. To help with direct comparison across the different figures presented in this chapter, voxels over z=5 in the controls and z=50 in the lesion animals are presented under the colour at the upper end of the gradient (yellow).

The V4v seed is located in the ventral part of V4. It is, therefore, fairly unsurprising that its

functional network is more centred on the ventral part of the brain (see Figure 5.16). In both the control group and the lesion animals, significant correlations with the ventral parts of V1, V2 and V3 are present. The V4v connectivity network also includes area TE and TEO in all animals/groups. The TEO cluster is unilateral (left) in Monkey S.

Some dorsal clusters are also included. In the control group average, small bilateral correlation clusters are present in dorsal V2 (but not in the medial part) and V3d. In addition, significant correlation with seed activity over time exist in the occipital cortex in MT and in the temporal cortex in MST, across all groups. In the lesion animals, significant correlations are present in LIP. The lesion animals' V4v networks also include bilateral significant correlations with the pulvinar, SC and LGN. In the control group average, there is only one small correlation cluster present in the right LGN.

To summarise, we do not observe extreme differences in the functional connectivity of the second thalamic pathway. We nevertheless notice correlations clusters between the pulvinar and V2 in the lesion animals we do not find in the control group. The lesion animals also presented significant correlations in MT in the pulvinar correlation maps. In the lesion animals' in the pulvinar, both V2 and the dorsal V4 maps, we observe the existence of significant correlations in the remnants of V1 (most times they also are present in the control average).

5.3.2.5 Functional Connectivity of the SC-FEF Pathway

SC is a midbrain nucleus whose traditional role in the literature is to modulate sensory inputs into motor output (e.g. eye movements towards or away from a stimulus) (Gandhi & Katnani, 2011). It receives retinal inputs. As a matter of fact it is the second richest target of retinal projections after the LGN in primates (Perry & Cowey, 1984). The pulvinar sends direct

projections to both LGN and the pulvinar (Harting et al., 1991; Lyon et al., 2010) and therefore could act as a gateway to both thalamic pathways. In macaques, SC receives some visual feedback through direct projections from FEF (Pouget et al., 2009; Segraves & Goldberg, 1987), although they do not involve many axons and are unlikely to be observed using fMRI. It has also been shown that the lesion of SC abolishes both the residual response observed in MT (Rodman et al., 1990) and the residual vision observed after a lesion of the striate cortex (Kato et al., 2011; Kinoshita et al., 2019; Tamietto et al., 2010).

In the following section we compare the functional connectivity of SC in the lesion animals to the controls.

5.3.2.5.1 SC

SC is of particular interest in the search for compensatory mechanisms supporting blindsight and residual vision. This is partially due to its established anatomic connections with the pulvinar, LGN, themselves connected to MT. In the SC correlation map (see Figure 5.17). LGN and pulvinar significant correlation clusters are present across all animals/groups. Unilateral correlations in MT are present in the control group average and in Monkey S. Bilateral significant correlations in MT are present in Monkey Y.

The SC functional connectivity map includes many other visual areas. All animals/groups present significant correlations with V1. In the control group average, a bilateral V1 cluster is present in the calcarine. In the lesion animals, significant correlations with V1 are bilaterally found in the ventral operculum and the calcarine remnants. Significant clusters in V3d, V3v and V3A are also present in all animals/groups. Significant correlations are present in the control group average in the right ventral V2 and right dorsal V2. Bilateral clusters of significant voxels are also present in these areas

in the lesion animals. Both lesion animals also present significant correlations with medial V2.

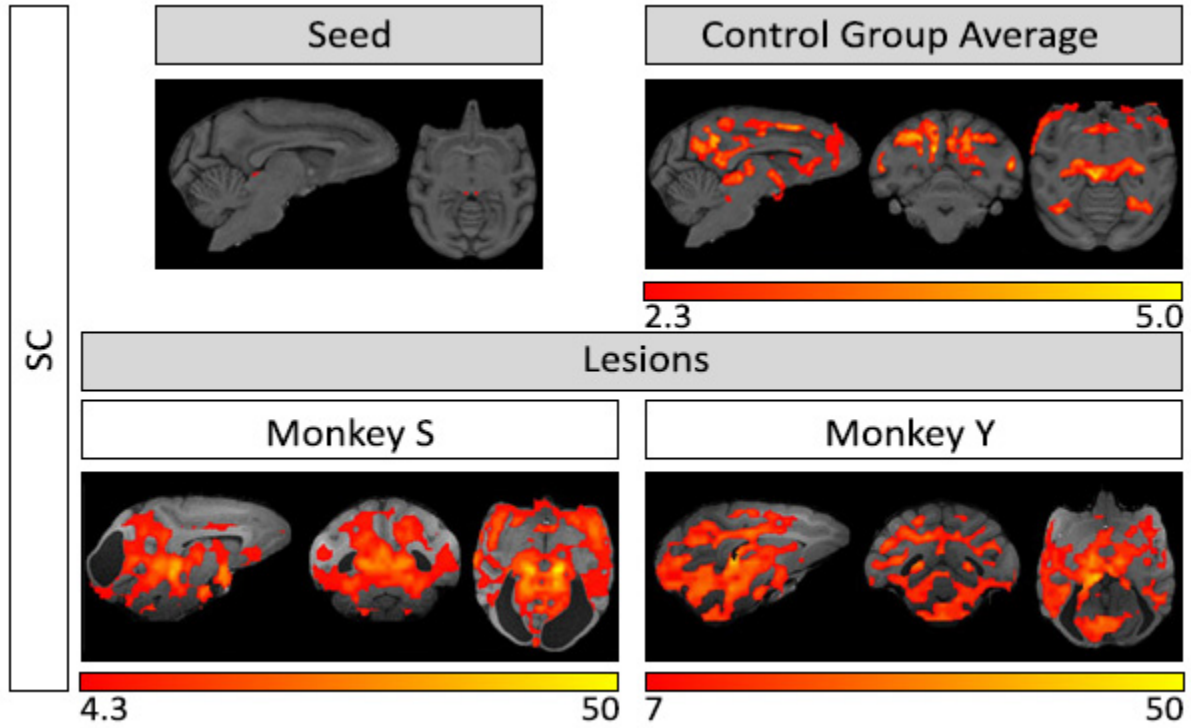


Figure 5.17 Comparison Between the Functional Connectivity of the Superior Collliculus in the Lesion Animals Versus the Control Average

First line: SC (15.6 mm^3) bilateral seed location
Second Line: Mean correlation map for SC among control animals. The map is displayed on the F99 template at the significance level ($z \geq 2.3$).
The third line presents the z-score maps obtained with the same seed, placed in the same location, in Monkey S and Monkey Y (titled respectively). The results obtained in the lesion animals are presented on their structural image, at increased thresholds to facilitate comparison with the control group for the reader. To examine these results at the significance level ($z \geq 2.3$), see Appendix 8.9. A mask was applied to eliminate any correlations inside the lesions.
Colour bars represent the range of positive z-scores from the lower threshold in each case. To help with direct comparison across the different figures presented in this chapter, voxels over z=5 in the controls and z=50 in the lesion animals are presented under the colour at the upper end of the gradient (yellow).

The ventral pathway is well represented in the lesion animals' SC functional network. Significant correlations with SC are present in ventral V4v and areas TEO and TE. There are also significant clusters in V3d and V3A which (may) extend a few voxels into dorsal V4. Despite this, we cannot conclude that significant correlations with dorsal V4 exist in the lesion animals. No significant correlations with V4 are evident in the control group average, barring

a few voxels in the right dorsal V4. A unilateral cluster in the right TE is also present in the control group average connectivity map for SC. No evidence of significant correlations with the FEF are present in the control group or Monkey S. Monkey Y, however, presents a significant FEF cluster in the right hemisphere.

The SC functional network also involves several visual associated areas. In the temporal sulcus a cluster in MST is evident for all animals/ groups. Unilateral clusters are evident in FST in the left hemisphere for Monkey S and in the right hemisphere in Monkey Y. No significant correlations in FST are evident in the control group. All animals/groups present significant correlations in the parietal cortex with the VIP, PIP, LIP, superior parietal area, and the caudal inferior parietal lobule area. A cluster in the lateral occipital parietal area (LOP) is evident bilaterally in the control average and Monkey S and in the right hemisphere in Monkey Y.

Significant correlations with SC were also observed in several of the previously described functional connectivity maps. In the LGN maps, both lesion monkeys show evidence of significant correlations clusters in SC (seed Figure 5.11). No significant correlations with SC were found for the control group average. Significant correlations with SC are present in Monkey Y's MT map (but not in the control group average) (see Figure 5.12). No significant correlations between SC and the V2m seed (see Figure 5.14) are apparent in the controls. Nevertheless, significant bilateral correlations are evident in SC in Monkey S and a colliculus cluster extending into SC is evident in Monkey Y.The lesion animals' V4v networks (see Figure 5.16) also include bilateral significant correlations SC, not observed in the control group average.

However, no animals showed evidence of a significant correlation between FEF and SC in the FEF maps (see Figure 5.12) or between the pulvinar and SC in the pulvinar map (see Figure 5.13).

In short, we find little differences in the functional connectivity of SC in the lesion animals and the controls. Significant correlations with several visual areas are present in all animals/groups. Notably, both controls and lesion animals present significant correlations with V1 and MT. Significant correlations with LGN and the pulvinar are also evident.

Significant correlations with SC were observed in several previously described functional connectivity maps. In the lesion animals' significant correlations with SC were also observed in LGN maps, MT maps, and V4v maps. This was not the case in their control group average equivalent.

5.3.2.6 Focal Impact of the V1 Lesion Over Connectivity Strength

Functional connectivity is quantifiable using measures of statistical dependence, such as correlation, between brain areas' timeseries. These dependencies can be illustrated in functional connectivity heatmaps where each plot represents the connectivity between two areas of interest and the colour the strength of this connectivity (Fornito et al., 2016). Each brain area has a unique pattern of connectivity dictated by the correlation strength between this area and the remainder of the brain (Passingham et al., 2002). Changes in correlation strength could be the result of deep structural changes. Therefore, we take interest in how the loss of the calcarine affects the functional connectivity strength of V1, SC and each of the areas involved in the two previously studied thalamic pathways.

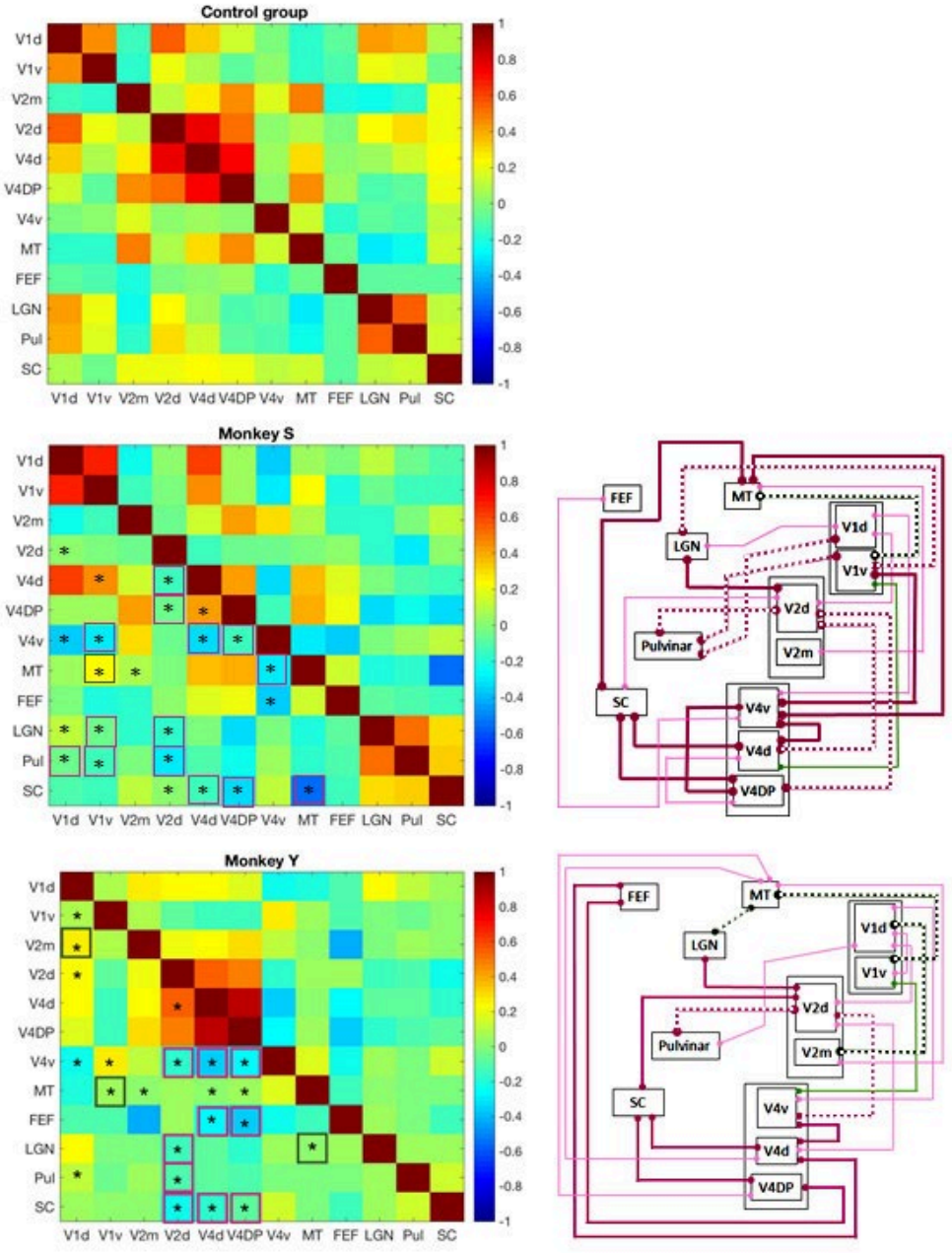


Figure 5.18 Difference in Connectivity Strength Between the Control Group and the Lesion Animals

Left column : Connectivity heatmaps are a visual representation of the connectivity strength of each ROI (8 visual seed (V1d, V1v, V2m, V2d, V4DP, V4d, V4v, MT), 1 visual association seed (FEF), 3 subcortical seed (LGN, pulvinar (Pul), Superior colliculus (SC)) with the remainder of the ROI. The Pearson correlations between the timeseries of each ROI were calculated. Colours represent the range of correlation values from -1 to 1 (inclusive). In the lesion animals (Monkey S and Monkey Y), an independent samples t-tests was conducted to examine differences in correlation with the control group. Significant (α=0.0045 –the adjusted level, to correct for multiple comparisons) difference in correlation strength, compared to the control group average are indicated by "". Magenta frames represent the shift from positive correlation in the control group to negative correlation in the lesion animal. Dark green frames illustrate the inverse (negative in the controls but positive in the lesion animals). Right : schematic summary of significantly different correlation between the control group and Monkey S (2nd line) or Monkey Y (3rd line). Pink lines represent lower than the controls correlations. Green lines represent higher than the controls correlations. Larger magenta line represent a shift from positive correlation in the control group to negative correlation in the lesion animal and larger dark green lines a shift from a negative correlations to a positive correlation. Doted lines correspond to know anatomic connectivity which could support blindsight.*

Correlation strength with both operculum seeds and V4v is also lower than the controls in both Lesion Animals. Additionally, the correlation coefficient between the V1 operculum seeds and the LGNs and, the V1 operculum seeds are lower than the controls in Monkey S. This is also the case in the pulvinar. Monkey S correlation coefficient value for the V1d/pulvinar, V1v/ LGN, V1v/pulvinar couples are negative while being positive in the control group. A significantly weaker correlation between the pulvinar and V1d is also present in Monkey Y.

Several significant differences in the strength of the correlations with the V1 operculum seeds timeseries are found between the controls and the lesion animal (see Figure 5.18). Compared the controls, significantly higher correlations are observed between in several ROI couples, in Monkey Y. An increased value is present in the V1v/V4v couple. Higher than the controls correlations are present between V1v and V4d in Monkey S. More intriguingly the relationship between V1d and V2m, and V1v and MT increased from a negative value in the controls (ρ=-0.180) to a positive value in Monkey Y (ρ=0.052). A negative to positive correlation switch is also observed in V1v/MT in Monkey S (ρ=0.247). Lower than the controls correlations coefficient between V1d and V2d are present in both Monkey S and Monkey Y.

Regarding the connectivity strength of the first thalamic pathway**,** the correlation between the LGN and MT is greater than it is for the control group in Monkey Y, being negative (ρ=-0.290) in the group average and positive in the lesion monkey (ρ=0.026). However, no significant difference with the control average in correlation strength between MT/LGN was found in Monkey S. Similarly, no significant difference in correlation strength between MT and FEF are evident between the control group average and the lesion animals. Outside of the previously mentioned difference with the control group in correlation strength between the LGN and the operculum V1 ROIs observed in Monkey S, only one other significant difference exists. Both lesion animals show

negative correlations between LGN and V2d (Monkey S: ρ= -0.181, Monkey Y: ρ= -0.126) while the control group present a positive correlation (ρ=0.242).

In addition, both Monkey S and Monkey Y present weaker correlations between the MT seed and the V2m ROI than the controls, although all three correlations were positive, in this case. No significant differences with the controls were found between the MT seed and the V2d ROI. Both MT and FEF show lower correlations with V4v than in the control group average in Monkey S. The correlations between MT and V4v are another case where positive correlations are observed in the control group average (ρ=0.135) but negative correlations were found in Monkey S (ρ=-0.294). Weaker correlations than in the control group average were also found between both the MT and FEF seeds and the dorsal V4 ROIs in Monkey Y. Theses correlations with FEF are negative in Monkey Y (V4d: ρ=-0.268, V4DP: ρ=-0.369) while being positive in the controls (V4d: ρ=0.006, V4DP: ρ= 0.056)

In the second Thalamic pathway, we observe significant differences with the control average in the connectivity strength between the pulvinar and the V2d ROI. Both lesion animals show a significantly weaker correlation. Indeed, the correlation switched from a positive correlation in the controls (ρ=0.305) to a negative correlation in the lesion animals (Monkey S: ρ= -0.298, Monkey Y: ρ= -0.115). There is no evidence of significant differences in the relationship between the pulvinar with V2m or the V4 ROIs. We also do not find differences between the control group average and either lesion animal exists with regard to connectivity strength between MT and pulvinar.

No significant difference in connectivity strength between SC, the pulvinar and the LGN was found between the controls and the lesion animals. Nevertheless, significant differences in the correlations with the visual system exists. Correlations between SC and the seed in dorsal V4 (V4d and V4DP) in the lesion animals are negative (Monkey S: V4d ρ=-0.138, V4DP: ρ= -0.314; Monkey

Y: V4d ρ=-0.168, V4DP ρ=-0.093), while a positive relationship exists in the control group (V4d: ρ=0.243; V4DP: ρ=0.215). Weaker than the controls correlations are also found between SC and V2d. In Monkey Y this correlation also switches from a positive correlation in the controls (ρ=0.216) to a negative correlation ρ=-0.240). Finally, the correlation between MT and SC is negative and of average strength in Monkey S and weak and positive in the control group average (Monkey S: -0.557 Control: 0.140) (see Figure 5.18).

In short, significant differences with the control average in connectivity strength exist across the entire visual system. Most show a decrease in the connectivity strength in the lesion animal. They often involve a switch from a positive correlation in the controls to a negative correlation in the lesion animals. We also find a handful of areas where the connectivity strength is increased in the lesion animals compared to the controls. Both lesion animals have higher correlation strength between V1v and V4 (V4d for Monkey S and V4v for Monkey Y). Other pairs show positive correlations in the lesion animals where there was a negative correlation in the controls. This is the case for V1 and MT in both animals as well as LGN and MT and V1d and V2m for Monkey Y.

5.3.3 Functional Connectivity of the Calcarine vs the Operculum in Control Animals

Analysis of functional connectivity strength shows an increase in connectivity strength between V1 and several visual areas (which, here, represent ROI). As discussed in the introduction to this chapter (see Chapter 5.1.4), this increase in functional connectivity could be the result of the development of new connections between the surviving portion of V1 and portions of visual areas normally anatomically connected to the calcarine. In conjunction with Genç et al.(2016)'s finding, that the functional connectivity of V1 follows retinotopy, in humans, it is possible that, in macaques:

- The functional connectivity of different areas within the V1 operculum and calcarine varies across different portions of other visual areas
- The portions of the subcortical and visual areas selected as seeds may be more strongly connected with the calcarine than the operculum (or *vice versa*).

In the following sections, the functional connectivity of three calcarine seeds (V1cal1, V1cal2, and V1cal3) is compared with each of two seeds in the V1 operculum (V1d and V1v)[14]. We chose to employ three calcarine seeds instead of one in order to sample a larger portion of the calcarine than a one seed alone could (for more information on the calcarine seeds, see Chapter 5.2.5.2). The functional connectivity of each of the calcarine seeds is compared to the operculum seed's (see Figure 5.21).

5.3.3.1 Differences in Functional Connectivity Between the Calcarine and the Operculum

We initially compare the functional connectivity of the operculum against that of the calcarine, to illustrate the existence of a difference in functional connectivity between these two portions of V1. This examination was conducted agnostically, which is to say, without prejudicial assumption regarding the location of eventual significant difference clusters may be located. To this end, we employed two operculum seeds (V1v and V1d) and three calcarine seeds (V1cal1, V1cal2, V1cal3) and consecutively ran one SBCA per seed was, in each of the 14 control animals. The three calcarine functional connectivity maps were then compared twice: first to the V1d seed's functional connectivity maps and then to the V1v seed's functional connectivity maps.

[14] For more details about seed's locations see 5.2.5.2.

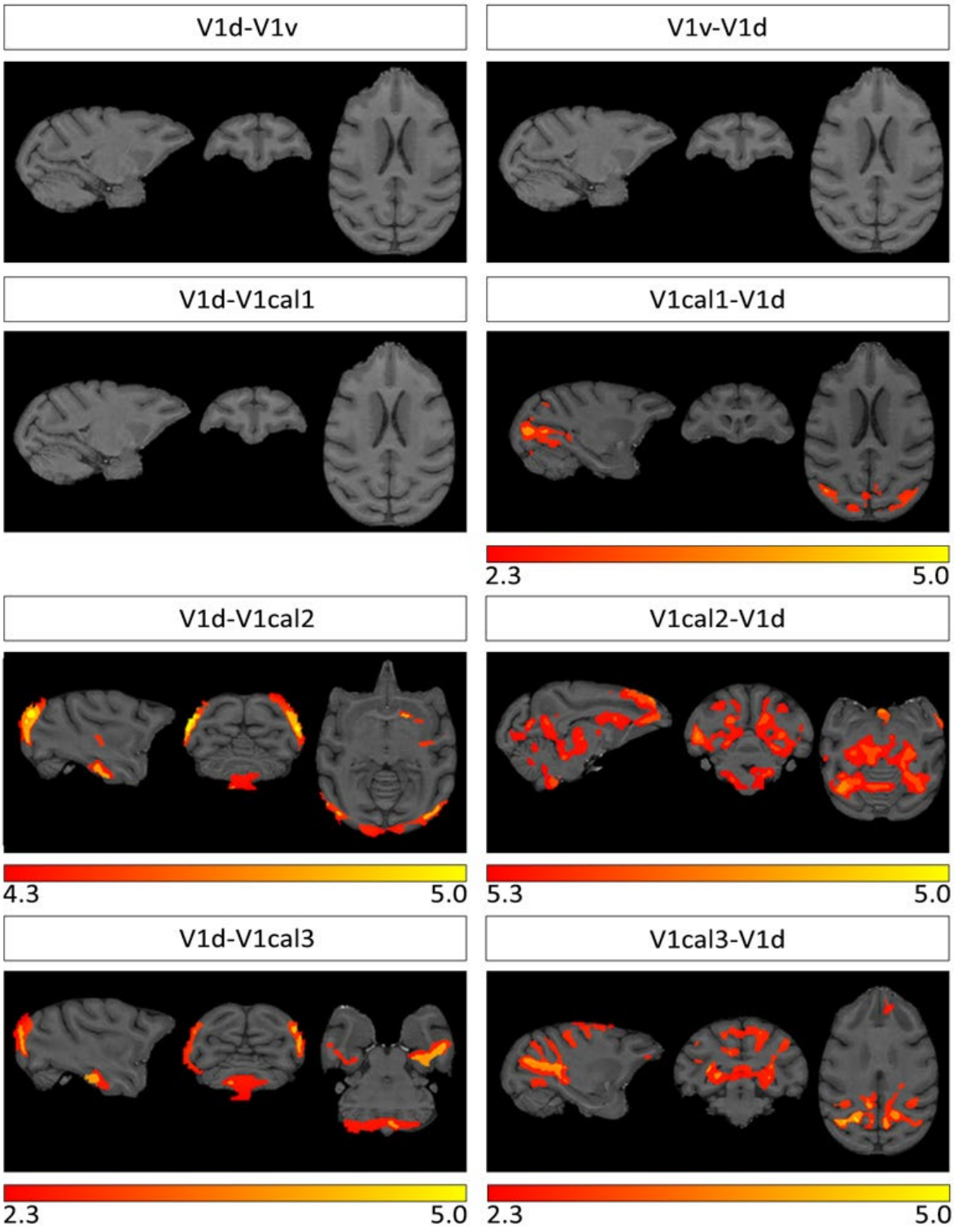


Figure 5.19 Functional Connectivity Differences Between Calcarine Seeds and V1d

Results of the differences tests between the functional connectivity network of the calcarine bilateral seeds V1cal1, V1cal2, V1cal3, the bilateral ventral operculum seed V1v, and one of the bilateral dorsal operculum seed V1d

Difference maps are displayed at the z≥2.3 significance level. Voxels over z=5 are shown under the same gradient's colour (yellow). Results are displayed on the F99 template. Display slices were selected to represent as many clusters as possible. All maps are corrected for multiple comparisons.

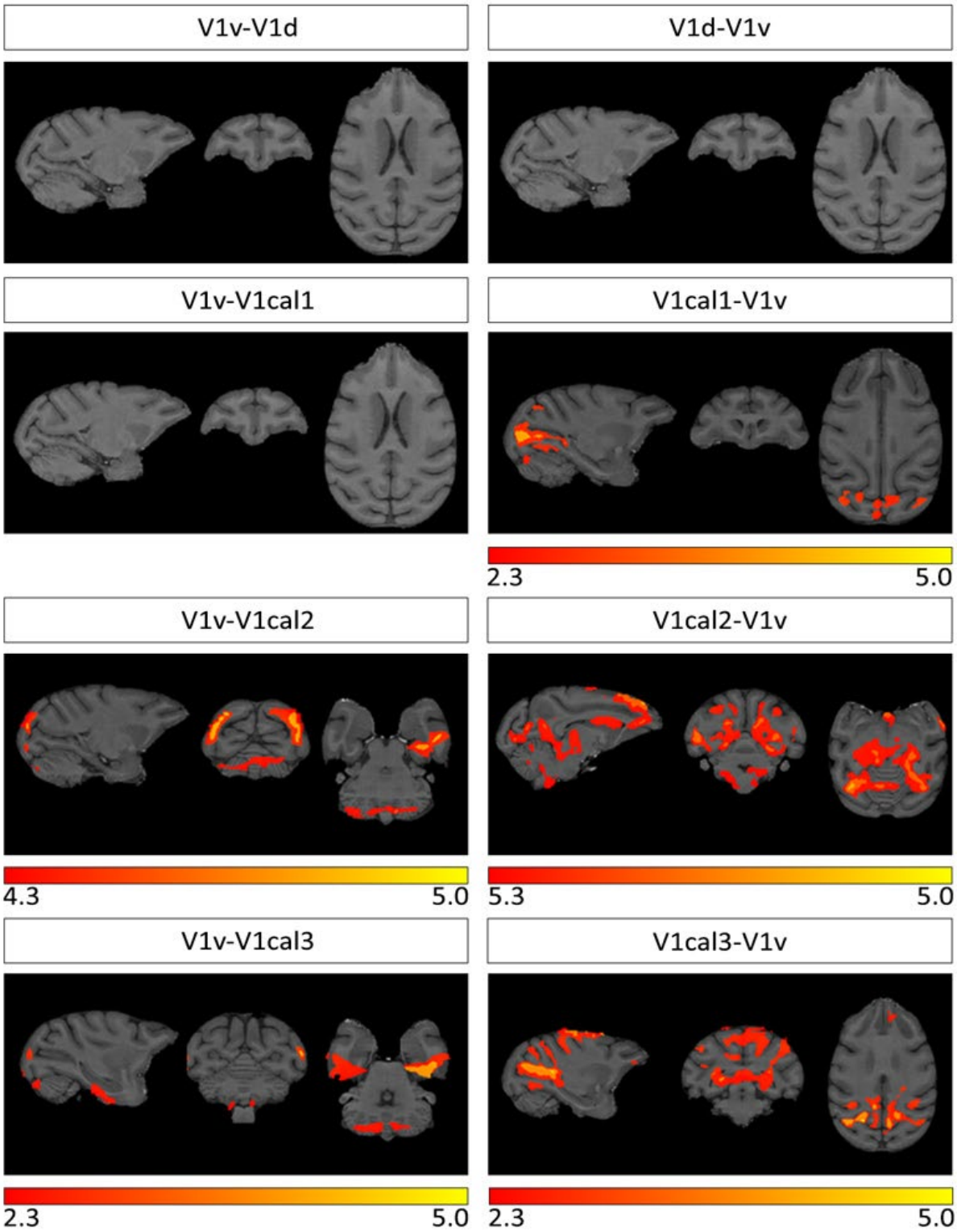


Figure 5.20 Functional Connectivity Differences Between Calcarine Seeds and V1v

Result of the differences test between the functional connectivity network of
bilateral calcarine seeds V1cal1, V1cal2, V1cal3, the dorsal operculum bilateral seed V1d and that of the dorsal operculum bilateral primary visual seed V1d
Difference maps are displayed at the z≥2.3 significance level. Voxels over z=5 are shown under the same gradient's colour (yellow). Results are displayed on the F99 template. Display slices were selected to represent as many clusters as possible. All maps are corrected for multiple comparisons.

In both cases, no significant ($z \geq 2.3$) differences were found between the V1d and V1v connectivity maps (see Figure 5.19 and Figure 5.20). It is, thus, perhaps no surprise that the difference maps between each operculum seed and the calcarine seeds appear quite similar.

No brain areas are more highly correlated with either V1d or V1v than with V1cal1 (see Figure 5.19 and Figure 5.20). V1cal1, however, presents stronger correlations than either operculum seed. V1cal1 correlations were higher across V2. Clusters of significant differences are found in the dorsal, medial and ventral part of V2. V2 dorsal and medial correlations include but are not limited to the V2d and V2m seeds. Differences are also evident in V3v, the right V3a and right V3d and the left parieto-occipital area, in both comparisons. An additional difference cluster in favour of V1cal1 is found in the difference map between V1d and V1cal1 in the right ventral V4 (see Figure 5.19).

Clusters of significant differences are also found between the operculum seed and V1cal2. V1d (see Figure 5.19) and V1v (see Figure 5.20) are more strongly correlated with the left ventral V2 and left TE than they are with V1cal2. Outside the visual system, a cluster of significant differences is also located in the left parahippocampal cortex. The V1d network also presents higher correlations in the right dorsal V4 and the left putamen than the V1cal2 network (see Figure 5.19).

V1cal2 correlations surpass V1d's in several visual areas (see Figure 5.20). Significant clusters are present in V1 (calcarine), dorsal V2, V3A, V3v, V3d, dorsal V4, V4v, MT and the left LGN. Stronger V1cal2 correlations are also found in areas associated with the visual system, such as TE, the right TEO, left TPO, left FEF temporal pole, along the STS sulcus (MST, FST and PGa), and the intraparietal cortex (LIP, MIP and VIP).

Differences in favour of V1cal2 also exist in deeper structures such as the thalamus (notably in the left pulvinar) but also in the parahippocampal cortex, and the putamen and caudate nuclei. A cluster of significant differences is also apparent in the colliculus, although it primarily involves the inferior

colliculus. In the fronto-parietal areas, V2cal2 shows stronger correlations than V1d with the dorsal premotor cortex (F2), the prefrontal area, and dorsolateral prefrontal areas. The V1cal2-V1v maps (see Figure 5.20) include the same areas as the V1cal2-V1d maps, with the exception of the right TEO. A cluster of significant differences is, however, present in the left motor cortex. The V1cal3 functional network presents stronger correlations than V1d and V1v in TE, the parahippocampal cortex, and the left ventral V2 (see Figure 5.19 and Figure 5.20). Correlations with V1v are stronger than with V1Cal3 in left perirhinal cortex, in the right ventral V4.

In short, in healthy controls, there is no significant difference in the operculum seed functional network. We find significant differences between the functional connectivity of the operculum and the calcarine seeds. V1cal1 and V1cal2 correlations were higher across V2. V1cal2 also has higher correlations in portions of dorsal V4 and MT. V1Cal3 has higher correlations than the operculum seeds in portions of V2 and V4, although the clusters are unilateral. These portions of higher visual areas may therefore correspond to areas containing the representation of the peripheral visual field.

5.3.3.2 Relationship Between the Calcarine and the Extrastriate Visual Cortex

We now want to make a more specific observation in the controls of how strongly each of the visual and subcortical ROI we employed in the previous sections correlate with the operculum and the calcarine. Indeed, the calcarine contains the peripheral representation of the visual field in V1 (Daniel & Whitteridge, 1961) and the functional connectivity of V1 has been shown to follow retinotopy in humans (Genç et al., 2016). So if a visual/subcortical ROI is found to have higher correlations with the calcarine seeds than the operculum seeds, it is more likely to be located in an area containing the peripheral visual field representation.

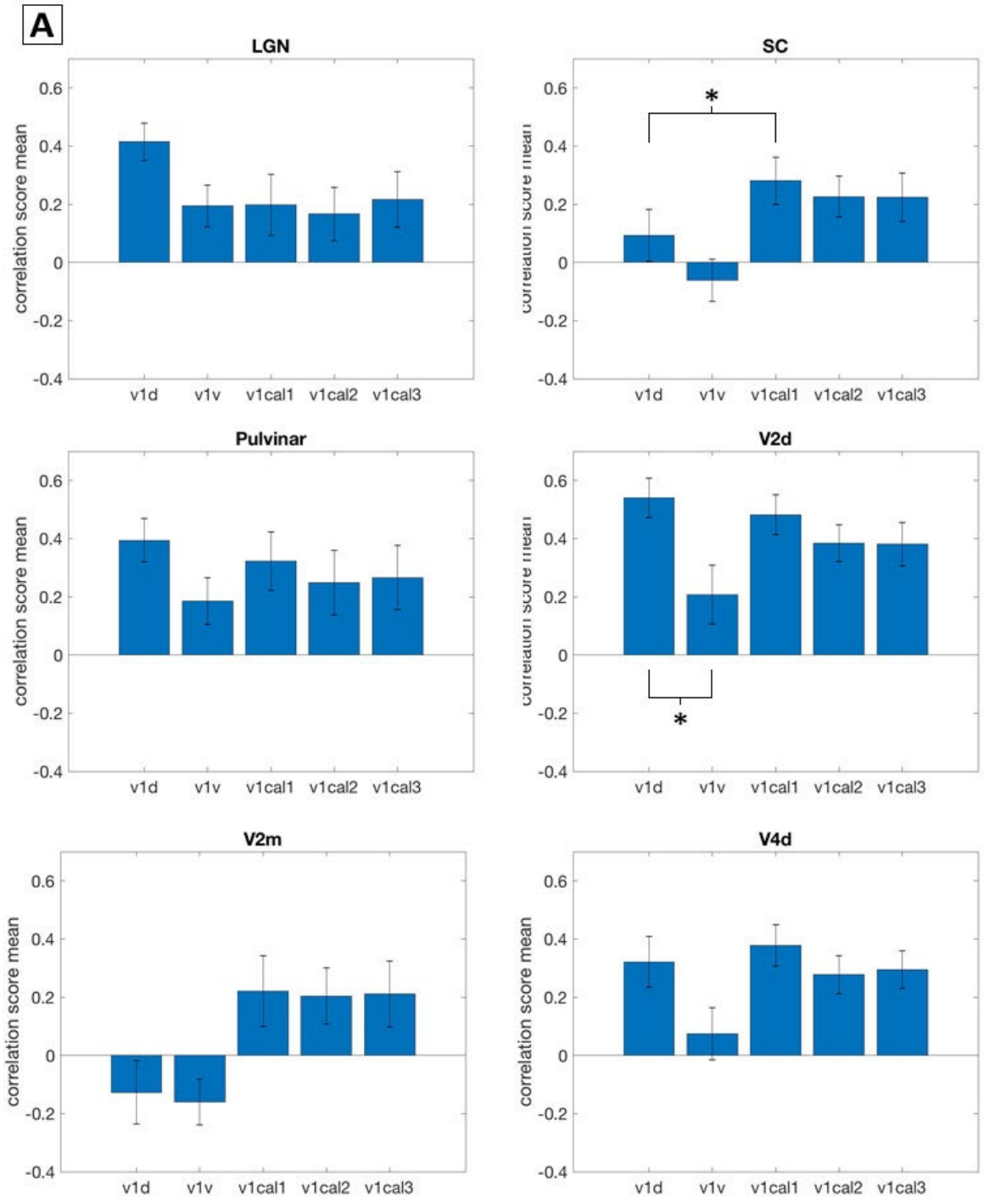
The average correlation scores between each of the primary cortex seeds and each of the regions interest was plotted on a bar graph (see Figure 5.21). The results of the examination of these figures seemed to indicate the existence of several significant differences. A more rigorous examination, in the form of an F-test to compare the multiple average correlations, seems to support this position, *prima facie* (see Table 5.3). However, the results of F-tests (and ANOVA in general) do not provide information on *where* differences exists, only whether they exist or not.

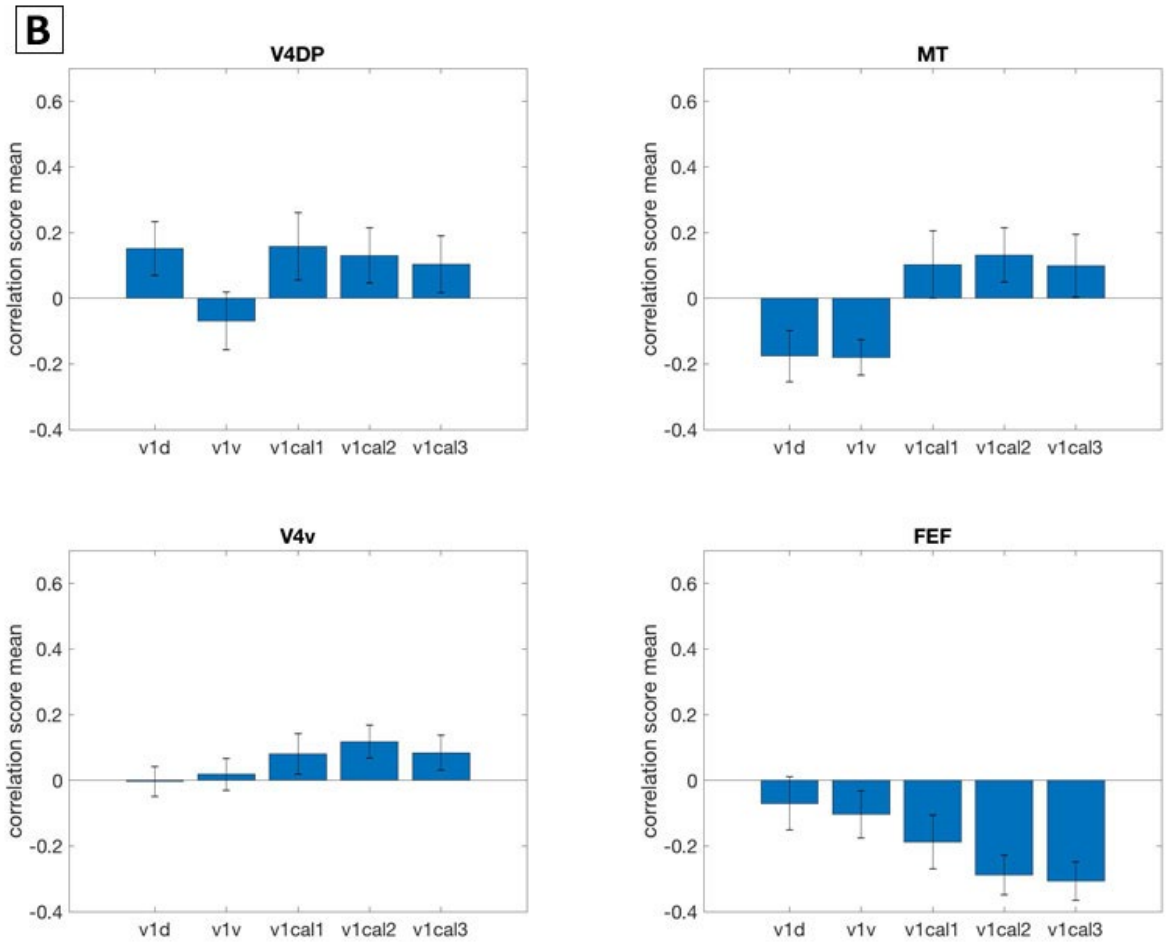
Table 5.3 AN.O.VA of Correlation Between Primary Visual Cortex and Visual and Subcortical Seeds

	ROI	*LGN*	*Pulvinar*	*SC*	*V2d*	*V2m*	*V4d*	*V4DP*	*V4v*	*MT*	*FEF*
ANOVA											
F		1.3364	0.6695	2.9946	2.7593	3.4655	2.2890	1.1286	0.9427	3.5526	2.1986
Prob > F		0.2659	0.6155	**0.0248**	**0.0350**	**0.0125**	0.0692	0.3508	0.4450	**0.0111**	0.0788
F - Test											
Group1	**Group2**	Sig.									
V1d	*V1v*	0.7762	1.0000	1.0000	**0.0297**	1.0000	0.2518	0.8268	1.0000	1.0000	1.0000
V1d	*V1cal1*	0.8259	1.0000	1.0000	1.0000	0.2196	1.0000	1.0000	1.0000	0.2255	1.0000
V1d	*V1cal2*	0.4715	1.0000	1.0000	1.0000	0.2894	1.0000	1.0000	1.0000	0.1199	0.3518
V1d	*V1cal3*	1.0000	1.0000	1.0000	1.0000	0.2607	1.0000	1.0000	1.0000	0.2436	0.2266
V1v	*V1cal1*	1.0000	1.0000	**0.0349**	0.1314	0.1245	0.0645	0.7457	1.0000	0.2081	1.0000
V1v	*V1cal2*	1.0000	1.0000	0.1326	1.0000	0.1668	0.6456	1.0000	1.0000	0.1101	0.7255
V1v	*V1cal3*	1.0000	1.0000	0.1389	1.0000	0.1493	0.4489	1.0000	1.0000	0.2250	0.4873
V1cal1	*V1cal2*	1.0000	1.0000	1.0000	1.0000	1.0000	1.0000	1.0000	1.0000	1.0000	1.0000
V1cal1	*V1cal3*	1.0000	1.0000	1.0000	1.0000	1.0000	1.0000	1.0000	1.0000	1.0000	1.0000
V1cal2	*V1cal3*	1.0000	1.0000	1.0000	1.0000	1.0000	1.0000	1.0000	1.0000	1.0000	1.0000

Figure 5.21 Comparison of the Operculum Seed Connectivity Strength Versus the Calcarine Seed

In each of the control animal the correlation coefficient between each of the five primary visual cortex seed (operculum: V1d, V1v; Calcarine: V1cal1 V1cal2 V1cal3) and the other visual and subcortical seed was calculated. Correlation coefficients were averaged across the control group. An ANOVA followed by a Bonferoni test were used to test for difference in connectivity strength between a visual/subcortical seed and each of the primary visual seed. Significant differences (p<0.05) are marked by "".*
For legibility, the figure has been cut in two parts. A. part 1. B. part 2





Indeed, our test indicated that differences between the primary visual cortex and visual and subcortical seeds existed in SC, V2d, V2m, and MT. To discern precisely where these differences existed, the initial F-test was necessarily followed up by a Bonferroni post-hoc test. Based on the results of the post-hoc test, significant differences ($p \leq 0.05$) in correlation strength between the operculum seed V1d and the calcarine seeds V1cal1 could be only found for SC (see Figure 5.21). (V1cal1 > V1d; p= 0.035). Significant difference in correlation strength also exist with V2d but only among the operculum seed. V1d is more strongly correlated withV2d than V1v (p= 0.030).

Interestingly, Figure 5.21 also shows a clear trend for both V2m and MT, with negative correlations with the operculum seeds but positive correlations with the calcarine seeds.

In short, with the exception of SC, we cannot establish that the ROI we employed are more

likely to be anatomically connected to the calcarine than the operculum. It is unlikely however that SC is involved in compensatory mechanisms involving the remnants of V1, in the lesion animals. Indeed, no difference in connectivity strength compared to the controls was observed between the operculum and SC ROI Figure 5.18.

5.4 Discussion

Intuition, when observing the presence of lesions in the primary visual cortex as large at those apparent in Monkey S and Monkey Y, would be that the visual functional connectivity must be greatly impacted (Droby et al., 2016; Gillebert & Mantini, 2013; Guggisberg et al., 2008). We, however, found no drastic differences between the control group average functional connectivity maps and the lesion animals, for any of the 12 seeds tested.

It worth mentioning that we did not find significant correlations between the LGN and V1 in the control group. As discussed in Chapter 4, which involved the same isoflurane animals as our control group, this is likely due to the use of anaesthetics (see Chapter 4.4). We also note that the Functional connectivity maps appear to include a great deal of white matter in both controls and lesion animals. This is likely a result of poor spatial smoothing as we regressed the white matter signal during the first level analysis

Perhaps the most interesting results can be found in the observed differences in connectivity strength between the control groups and each of the lesion animals. Both lesion animals show increased correlation strength between ventral V1 and V4 (V4d for Monkey S and V4v for Monkey Y). Several areas presenting negative correlations in the control group average but positive correlations in the lesion monkeys. This was the case for V1v and MT in both lesion animals and LGN and MT, and V1d and V2m in Monkey Y. Comparing connectivity strength

between the primary visual cortex seeds with V2m and MT highlighted a trend where the calcarine seeds correlated more strongly with either ROI than the operculum seeds did. The fact that in this precise case the results of the ANOVA indicated the existence of a significant difference but the post hoc test did not may suggest a lack of statistical power. In conjunction with the visual evidence offered by the bar plots, this may mean that equivalent testing in a study including a larger sample would result in significant results. As a matter of fact, the calcarine - operculum difference maps showed clusters of significant differences in V2m in favour of V1cal1 and V1cal3 (although the latter was unilateral). Additionally, V1cal2 presented a cluster of significant differences in its difference map, indicating stronger correlations with MT than the operculum seeds.

Studies combining DTI and resting state functional connectivity (Honey et al., 2009; Skudlarski et al., 2008) show that while not all positive correlations have a structural counterpart, positive correlations *are* good predictors of anatomy. Thus, new positive functional connectivity could be the result of the development of new structural connections between the remnants of V1 and two areas that were perhaps most prominently connected with the calcarine, in the lesion animals. It is also interesting to observe novel positive functional connectivity (i.e., negative in the control but positive in Monkey Y) between in LGN and MT in Monkey Y but not in Monkey S. Indeed, the LGN-MT pathway is proposed as a possible alternative pathway supporting blindsight (Schmid et al., 2010). Bridge et al. (2019), however, rejected the LGN-MT as a candidate to explain residual vision in Monkey S as the results of DTI did not indicate the development of new axons between the two areas. It is, nevertheless, possible that Monkey Y did develop additional connections between LGN and MT.

This last statement could be surprising if only the results presented in the functional connectivity

maps were taken into account. We indeed found a significant unilateral cluster in MT in Monkey S's LGN functional network while no significant correlations in MT were present in the controls' LGN network. This result could lead the reader to wrongly assume that the correlation between the LGN and MT is higher in Monkey S than in the controls. Indeed, we are comparing an individual map (Monkey S), result of the first level analysis where no correction was applied, to a group map, result of a higher-level analysis (Controls) where we corrected for multiple comparison. Group maps are consequently more selective than individual maps. Correlations in Individual maps, particularly when they are unilateral, are more likely to be false positive. It is consequently important to consider both the results of the functional connectivity maps and the connectivity strength comparison, as it is a more rigorous approach. Another example is the presence of significant correlations in MT in the pulvinar functional map in the lesion animals but not in the controls, suggesting an enhanced pulvinar-MT connection in the lesion animals. Both pulvinar and MT neurons are motion selective and are activated by the moving dot stimulus (Bridge et al., 2019; Britten et al., 1996; Shadlen & Newsome, 1996; Villeneuve et al., 2005). Bridge et al. (2019), however, found that, in Monkey S, moving dots activated the pulvinar but not MT, which contradicts the hypothesis of an enhanced pulvinar-MT connection. Nevertheless, we also find no significant difference in correlation strength between the lesion animals and the controls. Bridge et al. (2019) also found that MT's functional network in Monkey S is similar to the controls', which coincides with the results of our correlation strength comparison. The significant correlations between the pulvinar seed and MT are likely to be false positive. Similar reasoning can also be applied to the significant correlations observed in the pulvinar, SC and LGN in the lesion animals' V4v functional maps, but not in the controls

In most cases where a difference in connectivity strength between the control group and the lesion monkeys was observed, however, the correlations score is lower in Monkey S and Monkey

Y than in the controls. Most interestingly, in both lesion animals, when a decrease is reported, in more than half of the cases (Monkey S: 68 %; Monkey Y: 54 %), the decrease corresponded to a switch from a positive value in the Control group to a negative correlation in the lesion monkeys. This result is particularly striking as it involves area pairs which would have been good candidates for alternative visual pathways supporting blindsight (e.g., the LGN and V2d, the pulvinar and V2d, SC and V4d, SC and V4DP).

Mathematically speaking, the meaning of negative correlations is intuitive. Two variables that are negatively temporally correlated change in opposition to one-another across time (i.e., as the values of one increase, over time, the values of the other decrease, and vice-versa). In the context of functional connectivity, however, their origin and physiological meaning is highly debated. Negative functional connectivity, also called anticorrelation, has been reported from the early onset of functional connectivity research (B. Biswal et al., 1995). It has been interpreted as an artefact of the global signal regression during the pre-processing stage (Giove et al., 2009; Murphy et al., 2009; Weissenbacher et al., 2009). As a result, several studies excluded negative functional connectivity, altogether (Buckner et al., 2009; Meunier et al., 2009). Nevertheless, negative functional connectivity presents characteristics (e.g., spatial distribution and cross-subject consistency) that can only be attributed to a biological basis (Fox et al., 2009). Skuldlarski et al. (2008) make direct comparisons between resting state functional connectivity and anatomical connectivity data using combined resting state fMRI and DTI. They conclude that negative correlations frequently fail to accurately depict anatomical connectivity. The sign of the correlation coefficient is more informative than its absolute value when it comes to evaluating if the observed functional connection is real. When the correlation score is negative, more often than not, no structural connections can be found.

In a computational study in humans, Chen et al. (2011) argue that functional connectivity does not only result from direct structural connections. Synchronised oscillatory activity between two areas can also result from indirect connection involving several nodes in the network. They present the example of the connectivity between the amygdala and the L-dlPFC, two areas with no established direct anatomical connection (Amaral & Insausti, 1992; Ghashghaei & Barbas, 2002; Siegle et al., 2007) and between which strong negative functional connectivity has been consistently reported (G. Chen et al., 2011; Roy et al., 2009). Negative functional connectivity between these areas is decreased in disorders such as schizophrenia (Satterthwaite et al., 2010), Bipolar (Chepenik et al., 2010), and heroin addiction (Ma et al., 2010). Chen et al. (2011) show that the strength of negative functional connectivity correlates with the shortest path length between two nodes of the network. Thus, a decrease in functional connectivity could be the result of structural changes. In the same light, the fact that the lesion animals present negative correlation coefficients where positive coefficient where expected could be due to structural changes, such a decrease in structural connections between the areas discussed above or an increase in the shortest path length. Such suppositions, as well as those put forward in the previous paragraph, cannot be proven with the data we currently possess but could be reinforced (or refuted) by future research using DTI. DTI would also be useful to distinguish between feedforward and feedback connections. Indeed, functional connectivity does not provide any information about connection direction (Ramnani et al., 2004).

It is also entirely possible that the effects of lesions (e.g., *the extent to which* and, indeed, even *which*, connections were severed) may differ between the two hemispheres. As a result, it is also possible that adaptation mechanisms can develop unevenly in one or the other hemisphere (Bridge et al., 2008). As such, future research should arguably include the use of unilateral seeds

when employing SBCA, in order to study potential asymmetrical lesion effects.

There is also an argument to be made that the conclusion of this chapter could have been strengthened by the inclusion of a non-visual seed as a control. The extent, however, to which a lesion in the calcarine fissure affects the functional connectivity of non-visual areas is unknown. From the lesion animals' structural scan, we could surmise that frontal areas are unlikely to be affected by the lesion. Past literature, however, contains reports of connections between the visual system and frontal areas. In rhesus macaques, the ventral pathway projects to both the Dorsal Prefrontal Cortex and the lOFC (Macko et al., 1982). The ACC receives visual inputs in mice (Huda et al., 2020) and ACC neurons fire in response to a visual stimulus in monkeys (Konoike et al., 2020). The parietal cortex also receives visual inputs.

We previously established the existence of a functional relationship between several visual areas and the somatosensory cortex (see Chapter 4). Transcranial Magnetic Stimulation (TMS) of the somatosensory cortex increases the regional cerebral blood flow (rCBF) in visual areas in early blind subjects (Wittenberg et al., 2004). The premotor cortex is also functionally connected to MT and FEF (see Chapter 4.3 and Hutchison and Everling, 2012). Deeper structures can also receive visual input. The amygdala receives inputs from the inferior temporal cortex (Price, 2003), which is part of the ventral pathway. Some authors also argue that the hippocampus could have a visual role, contributing to scene perception in a manner different to simple memory retrieval (A. C. H. Lee et al., 2005). In short, selecting a brain area devoid of visual influence to employ as a control is a difficult proposition, under the best of circumstances.

It could also be argued that there would be merit in the removal of the lesion artefacts. Unfortunately, there is no general consensus regarding how to analyse data acquired in brains with lesions. Often, as was done here, the presence of a lesion is addressed by regressing the

signal coming from the CSF (Ainsworth et al., 2018; O'Reilly et al., 2013). This, however, was insufficient to prevent significant correlations inside the lesion. Yourganov et al. (2018) propose an alternative, in which MELODIC is used to isolate the source of variance in the resting-state fMRI data that is driven by the lesion in each animal. The lesion driven component would then be excluded from the resting state data before running the SBCA. Failing consensus, or at the very least, strong evidence in favour of one approach or the other, it could be argued that the two are equally valid (or, in any case, neither is substantially more problematic than the other).

It is ultimately the aim of this study and others of its kind to identify new therapeutic targets to treat blindness in humans. It is, therefore, reasonable to compare this study with previous research measuring functional connectivity maps in blind humans. This is particularly true with regard to manner in which the visual experience shapes the functional connectivity between visual areas. Retinal and eye defects are a more common cause of blindness than lesions (Flaxman et al., 2017). As in the case of the Lesion animals, there was an expectation that blindness due to this kind of defect would have a deep impact on the resting state functional connectivity, particularly in the case of congenital blindness. Indeed, Wiese and Hubel (1963, and 1965) established that the physiological maturation process and the resulting characteristics of the primary and early visual areas rely on the presence of visual input during a critical period of early life. Additionally, full visual deprivation can cause reorganisation(s) within the visual areas, allowing them to process other sensory input, including touch and auditory (Merabet & Pascual-Leone, 2010).

The present study found that perinatal lesions of the calcarine had little impact on the resting state functional connectivity of the visual system. This is not unheard of, as Striem-Amit et al.

(2015) found the absence of visual experience in the congenitally blind minimally impacted the retinotopic organisation of the visual functional connectivity network. Nevertheless, Striem-Amit et al. (2015) found that functional connectivity between the visual system and non-visual brain areas in the blind differed profoundly compared to the sighted. Central V1 was more connected to language areas, while peripheral V1 was more strongly connected to spatial attention and control networks. We did not study the connectivity between the visual system and non-visual areas in our lesion animals, but do not exclude it as a potential subject for future research.

Butt et al. (2015) examined the impact of the visual experience on the connectivity between homotopic visual areas (e.g., between left dorsal V2 & left ventral V2) and/or hierarchical areas (e.g., V1 & V2). They found that correlation increased between hierarchical areas but decreases between homotopic areas in blind subjects. To some extent, this too coincides with our findings. Both lesion monkeys present decreased correlations between V4d and V4v. And all of the correlation increases we observed in the lesion animals were between hierarchical areas. Nevertheless, the comparison between Butt et al.'s (2015) study and ours is necessarily limited as they employed unilateral seeds. This allowed them to demonstrate that the relative amplitude of fine-scale correlations between hierarchical areas is higher in congenitally blind subjects. They proposed that this increase could be due to the development of broader between-visual-area axonal arborization. We believe that a similar phenomenon, occurring between the remnant of V1 and the visual areas receiving direct connections form V1, could also explain why the lesion animals retained at least partial sight.

Finally, it is worth noting that, while the cause of the lesions observed in Monkey S and Monkey Y is arguably beyond the scope of the present study/chapter, it nonetheless remains

an interesting consideration. At the time of the study, we were only aware of one other case: Monkey B, a male born in the same centre as Monkeys S and Y, the Centre for Macaques, in Porton Down (UK). Genetic testing between Monkey S and Monkey B (unpublished) concluded the animals were unrelated. Monkey Y was not tested for any relationship to either Monkey (likely owing to the fact that his lesion was uncovered much later).

6 Summary, Conclusions, Limitations, and Recommendations

6.1 Summary

This study was primarily concerned with the examination of three questions:

1. Is there a difference in the effects of isoflurane and sevoflurane on the Functional Connectivity of the whole brain?
2. Is there a difference in the effects of isoflurane and sevoflurane on the Functional Connectivity of the visual system, specifically?
3. What compensation mechanisms explain residual vision after substantial natural lesions in the primary visual cortex?

6.1.1 Method Summary

The data necessary to answer the questions asked by the study required a substantial amount of cleaning, preprocessing, and sundry preliminary work. The data employed in this thesis, collected from observations on 2 rhesus macaque monkeys with lesions in V1, and 23 healthy (i.e., lesion free) Rhesus macaque Monkeys, was not originally composed for the express purpose of examining these questions. Indeed, it was acquired for use in this study in its raw format and required extensive preprocessing. This included a visual quality check, preprocessing using FSL (Fischl et al., 1999; Jenkinson et al., 2012; Reuter et al., 2012), comprising the removal of non-brain structures from the raw structural and MRI data, high-pass filtering using fslmaths, and extensive first level analysis using FSL FEAT (see Chapter 2.2). After preprocessing, Independent Component Analysis (see Chapter 2.3) was employed to examine the existence of whole-brain level differences in the effect of isoflurane and sevoflurane (see Chapter 3), while Seed-Based Correlation Analysis (see Chapter 2.4) was

employed to examine these differences on the functional connectivity of the visual system (see Chapter 4) and the existence of compensatory mechanisms explaining residual vision from V1 lesions arising during the animal's natural developmental processes (see Chapter 5).

6.1.2 Comparison of Isoflurane and Sevoflurane Effects on the Whole Brain Functional Connectivity

The ICA, run on functional resting-state brain data, identified 22 ICs, which correspond to our understanding of the anatomy of the visual system, somatomotor networks, visual search associated attention, and auditory activity. This allowed us a reasonably comprehensive collection of brain areas to examine the existence of differential anaesthetic effects of isoflurane and sevoflurane over the RSN as a whole. There are numerous similarities between the two agents (see Chapter 3.1), both agents being fluorinated ethers binding with $GABA_A$ receptors (Jurd et al., 2003). There are also several differences (see Chapter 3.4), including the way each agent interacts with potassium channels (Hudson et al., 2013; Pandit & Buckler, 2009). Thus, while common sense might indicate that the two are functionally interchangeable, there is also reason to expect differentiation. Indeed, based on a preliminary visual examination of the results of the ICA, one might intuitively conclude that the two anaesthetics function in markedly different manners. And formal testing confirms the existence significant and meaningful (i.e. positive) differential effect of sevoflurane and isoflurane in one frontal IC, on frontal sevoflurane IC and one sevoflurane visual IC. But, from a substantive standpoint, the significant difference clusters were small and unilateral. Most authors seem to agree that isoflurane and sevoflurane affect brain activity in similar ways (Hutchison et al., 2014; Muta et al., 2022; Peltier et al., 2005), albeit without presenting

rigorous evidence to this effect. Our results, however, show that this may not be the case, when focusing on the functional connectivity of specific brain regions. Consequently, we shifted to a more focused examination of the visual system.

6.1.3 Comparison of Isoflurane and Sevoflurane Effects on the Visual System Functional Connectivity

The SBCA, carried out to more closely examine the functional connectivity of the visual system, returned functional networks largely supported by existing studies of both functional connectivity (e.g., Genç et al., 2016; Hutchison et al., 2012; Vincent et al., 2007; Wardak et al., 2006) and anatomy (e.g., Briggs & Usrey, 2007; Distler et al., 1993; Mashour & Alkire, 2013; McFarland & Haber, 2002; Perkel et al., 1986; Ungerleider et al., 2008). The results of the SBCA naturally retained similarities to the results of the ICA. To some extent, this is to be expected; more refined and/or targeted methods rarely overturn coarser examinations –nor should they. Indeed, as was previously the case, RSNs generally appear to be smaller under sevoflurane than under isoflurane. Like the ICA, the SBCA also indicated that some differential impact of the two agents over the functional connectivity of the visual system does, in fact, exist (see Table 4.2).

6.1.4 Exploring Changes in Functional Connectivity of the Visual System in Macaques with Natural Lesions of V1

Examinations of the functional connectivity of the visual network are extensive in the literature. It is a particular function of the brain that is intriguing to scientific researchers and one which substantially and substantively impacts a great proportion of the world's

population. The World Health Organization (*World Report on Vision*, n.d.) estimates that at least 2.2 Billion people have some form of visual impairment, representing a global financial burden of approximately $4.11 Billion (or £3.4B, at the current exchange rate) (*Causes of Blindness and Vision Impairment in 2020 and Trends over 30 Years, and Prevalence of Avoidable Blindness in Relation to VISION 2020: The Right to Sight: An Analysis for the Global Burden of Disease Study - PubMed*, n.d.). This loss represents not only a functional deficit for society but also (and one might argue more substantively) a substantial Quality of Life deficit for nearly a quarter of the world's population[15]. In this light, the benefits inherent in any progress made toward furthering our understanding of the workings of the visual system must surely require no further justification.

Subjects possessing lesions in the primary visual cortex, particularly those that show evidence of a continued ability to see, are therefore particularly interesting. They represent a deviation from the normative state of the brain. Any deviation in their brains' function(s), whether evident in their behaviour, or even solely upon closer and more focused examination, inherently provides us with greater understanding of not only the effect of such deviations but also (indirectly) of the normative state itself.

Evidence supports the hypothesis that both of the lesion Monkeys possessed some degree of residual aware vision or at least what Weiskrantz (2009)[16] termed "blindsight". Thus, we

[15] This estimate is based on a world population of 8,009,598,620 (*World Population Clock: 8 Billion People (LIVE, 2023) - Worldometer*, n.d.).

[16] We say "presumably" because extenuating circumstances, discussed below, prevented formal testing to examine whether or not their visual processing occurred exclusively "below the level of visual awareness" (Girkin & Miller, 2001, p. 383), but also bolstered by the somewhat less stringent definition given by Leopold (2012).

extended our inquiries further into the cases of the Monkey S and Monkey Y, with natural lesions of V1, in hopes of gaining a better understanding of the means by which their brains may have attempted to compensate for these deviations from the normative state.

The size and location of the lesions apparent in Monkeys S and Y resulted in expectations of substantial impact on visual functional connectivity (Droby et al., 2016; Gillebert & Mantini, 2013; Guggisberg et al., 2008). Intriguingly, however, functional connectivity in the visual system in general did not appear to be greatly impacted (see Chapter 5.3). What does change between the two, however, is the strength of the functional connectivity between specific areas of the visual system.

We identified several areas in each lesion monkey where connectivity was increased, compared to the control group. In lay terms, these stronger connections between areas may represent the development of more connections between areas. This, in turn, facilitated the examination of the veracity of existing claims regarding compensatory mechanisms for visual processing. It also allowed us to make informed hypotheses regarding the potential establishment of novel compensatory visual processing mechanisms.

Of course, while we lack perfect understanding of the function of the brain, we are far from ignorant of it. As such, our enquiries into these compensatory mechanisms are neither random, nor uninformed. They are, rather, investigations of educated suggestions, based on our knowledge of the interconnected nature of various areas of the brain. Thus, we believe that residual vision could be supported by one of two main phenomena or a combination of them. The first phenomenon is the development of new connections between the remnants of V1 and the balance of the visual system; the second phenomenon is the reinforcement of thalamic pathways. Two distinct thalamic pathways exist in parallel to the traditional visual

processing pathway (Mishkin et al., 1983), which both circumvent V1, while delivering retinal input to the visual system.

We reviewed the LGN-MT pathway (Lund, 1988) based on the understanding that the LGN, the main thalamic relay of retinal inputs, projects directly into MT (Nassi et al., 2006; Sincich et al., 2004). Much like Bridge et al. (2019), however, our findings did not support the existence of an LGN-MT pathway in Monkey S. Evidence from Monkey Y suggests that the LGN-MT pathway is not a compensatory mechanism for visual processing in this animal. We cannot rigorously rule out the possibility, however, since we did not have the opportunity to conduct DTI (the primary mechanism in disregarding the LGN-MT pathway in Monkey S) on him.

The secondary thalamic pathway involves the pulvinar. The pulvinar pathway receives a minimal amount of direct retinal input (Itaya & Van Hoesen, 1983; Nakagawa & Tanaka, 1984), as well as indirect retinal input through SC (Benevento & Fallon, 1975). The pulvinar is also connected to several visual areas and sends afferences to V2, V4 and MT (Kaas & Lyon, 2007). SC, in turn, projects to the LGN (Harting et al., 1991) and its projections to the pulvinar are relayed to MT (Kaas & Lyon, 2007).

6.2 Conclusions

6.2.1 The Practical Equivalence of Isoflurane and Sevoflurane in the Study of Functional Connectivity

As is often the case, the answer to whether isoflurane and sevoflurane function in the same way is not as straightforward a proposition as one might hope. Indeed, the answer appears to depend on how focused the one's research interest is. In broad strokes and, thus, for most applications (or, in lay terms, at the whole-brain level and disregarding subtler mechanisms),

it seems safe to say that the two anaesthetics are functionally equivalent, making the choice of one or the other a question of convenience, availability, and cost. If, however, one's interest is, for example, focused on the functional connectivity of the visual system, specifically and, even more so, if they are particularly interested in any of the relationships which satisfy both the Matching Network and Significance criteria (see Chapter 4.3.7 and Table 4.1), for example between MT and V1. In this case, the differences are not only numerous but also fairly varied, among the various RSNs examined in this study. In focused research of this nature, the selection of one of the other anaesthetics is no longer a question of convenience but one of consequence.

6.2.2 Compensatory Pathways in V1 Lesioned Monkeys May Involve Strengthened Connections with the Remnants

In a more focused examination of the visual network, particularly of the impact of a natural lesion of the calcarine V1, we found interesting, if somewhat varied, results. The lesions did not appear drastically impact the functional connectivity network of the remaining portions of V1 or any of the tested visual areas. This finding held true at the level of the pathways under examination, as well. There were no substantive variations in the functional connectivity of each of the thalamic pathways and SC between the control average and the lesion animals. Having said that, several statistically significant differences in connectivity strength are evident when comparing the lesion monkeys to the control group. Connectivity strength between V1 and V4 is increased in the lesion animals. Both lesion animals had positive correlations between V1v and MT, where negative correlations were found in the controls. This was also the case between V1d and V2m, in Monkey Y.

We compared the strength of the correlations of both V2m and MT to with the V1 operculum and calcarine, in the control group. This provided compelling (if not statistically significant) evidence supporting anatomical connections between the portions of V2m and MT where the ROIs are and the calcarine, in healthy macaques.

Positive functional connectivity is a good predictor of anatomy (Honey et al., 2009; Skudlarski et al., 2008). An increase in the connectivity between operculum V1 and several areas of the visual system in the lesion animals may be the result of an increase in the number of synapses of exiting connections. Such increases may also be the result of the development of new connections from the operculum to portions of visual areas that would normally be connected to the calcarine. We also observed a switch from a negative correlation in the controls to a positive correlation between LGN and MT, in Monkey Y, which may indicate a strengthening of the first thalamic pathway in Monkey Y.

6.3 Limitations

It is unlikely in the extreme that any study of this magnitude would be without substantial limitations. The acknowledgement of such limitations is not only necessary but desirable, since they highlight the realities of practical research and inform the results of the study, by couching their interpretation in a realistic framework.

6.3.1 Limitations in Understanding the Impact of Lesions in V1 in Absence of Behavioural Data

A number of limitations in understanding the impact of V1 were discussed earlier in this study (see the latter sections of Chapter 5.4). One necessary limitation of all neuroscientific examinations that we have no touched on yet, however, is that our knowledge of the finer

workings of the brain remains imperfect. This imperfection persists, despite our knowledgebase being substantially greater than it was even a few short years ago and growing at an exponential rate, through the implementation of newer, more sophisticated, focused, and granular techniques. Indeed, the more specific the question we wish to answer, the more pronounced the imperfect nature of our understanding becomes. Salient to our particular study, the imperfect nature of our understanding of the functional mechanisms of the brain has a *de facto* knock-on effect on our understanding of deviations from the normative state, whether these are imposed by abnormalities or other external factors.

One such deviation from the norm, which could be a cause for some debate, is the location of the lesions within the primary visual cortex. In both monkeys, the lesions were located in a section of V1 that is traditionally understood to code for peripheral vision (Daniel & Whitteridge, 1961; Van Essen et al., 1984). As a result, it is possible that their foveal vision was still quite good. We say possible because, while Monkey Y performed on par if not better than his cage-mates in most tasks (see Chapter 5.2.1.2), we have informal but substantial behavioural markers that indicate that Monkey S's foveal vision was substantially impacted – most notably in the particular mannerisms she employed in the retrieval of treats (see Chapter 5.2.1.1). Additionally, Bridge et al (2019) conducted a more in depth anatomic study in Monkey S than we were able to conduct on Monkey Y. The authors found that the V1 operculum cortex was thinner in Monkey S than in the controls. They also found no activations in V1, in response to visual stimuli. These results led them to discard V1 as a normally functioning area in Monkey S. Nevertheless, it is worth remembering that Monkey S's lesions covered more than 4 times the brain volume of Monkey Y's lesions and presented inverted hemisphere prominence, so it is possible the that the impact of the lesion on V1 was different in Monkey Y. This ties into one previously noted concern and is indicative of another. Since

we do not perfectly understand the function of V1, we cannot perfectly predict the impact of abnormalities in V1. Since we cannot perfectly predict the impact of a given abnormality in V1, we are also unable to perfectly grasp the potential differences resulting from *different* abnormalities in V1. Unless, however, we obtain perfect knowledge of the functioning of V1, there seems to be no way to address this issue, other than extensive and repeated research of such lesions, coupled with rigorous documentation and meta-analysis.

As noted above, (initially) non-targeted observation of the lesion monkeys indicated varying degrees of visual field deficit. The unfortunate abrupt and unexpected need to sacrifice both animals, soon after the discovery of their lesions, meant that we were unable to conduct behavioural tests to formally and rigorously evaluate their visual field deficits. And, we note, these observations came from just two lesion monkeys. Granted, this is a generally acceptable sample size for animal trials of this nature. As sample sizes go, however, it creates marked uncertainty with regard to inference. It is also symptomatic of an arguably more substantial consideration: individual variability. Since it is, practically speaking, impossible to monitor all aspects of a given subject, from the birth until such time as they are inducted into a given study, it is also impossible to guarantee direct comparability between any two (or more) subjects. We cannot, for example, know that their lesions developed at the same time, in the same way(s) or even for the same reasons. Indeed, the same could be said for such compensatory mechanisms as each subject appears to have developed, as well.

Overall, the lack of behavioural data designed to precisely test for blind spots in the visual field leaves us with unavoidably unresolved questions. If we accept that the lesion animals' peripheral vision is affected by the lesion but their central vision is persevered, do they retain the ability to experience sight (almost) normally? Our intuition, informed by past studies with

human patients is that this is likely the case. Pöppel, Held and Frost (1973) describe the case of four patients with lesions in the visual cortex, resulting in a scotoma either in the right upper quadrants, the left upper quadrants, the right lower quadrants or the left lower quadrants (with considerable involvement of the left upper quadrants) but who presented "intact foveal vision".

A second relevant (but not directly answerable) question deal with whether the existence of intact central vision precludes the development of peripheral blindsight. Again, our only recourse is to turn to studies involving human subjects. All four patients in the aforementioned study were able to move their eyes toward visual stimuli presented within their scotoma. Azzopardi and Cowey (2001) describe the case of three patients whose scotoma partially overlaps with their central vision. All three patients were able to detect the presence of a moving stimulus presented within the blind region of their visual field. Barton and Sharp (1997) examined patients presenting varying degrees of central vision impairment in the same manner but none of their patients were able to detect the stimulus. It appears, therefore, that the integrity (or not) of central vision plays no part in patients' development of blindsight.

It is, therefore, incumbent upon us to question whether the lesion monkeys were even experiencing blindsight. Indeed, Blindsight is a rare phenomenon - not all patients with a lesion in V1 are able to perform it and, even then, its discovery and verification requires rigorous testing in humans (see reviews by Ajina & Bridge, 2017; Stoerig & Cowey, 1997). It is established that monkeys *can* experience blindsight (Cowey & Stoerig, 1995). Indeed, the case of Monkey Helen (Humphrey, 1974), who underwent a total bilateral ablation of V1, yet was able to navigate her surroundings and "look" at an experimenter holding a treat before reaching for it, gives us reason to believe that macaque sight is relatively resilient to the loss

of V1. It is consequently possible that the lesion monkeys experienced some kind of residual peripheral vision. Lacking behavioural data, however, it is impossible to know if this was the case but also, if this was the case, if it was unconscious (i.e., blindsight) or not.

6.3.2 Functional Connectivity Only Allows Limited Conclusions on Anatomy

The limited sample size also results in a lack of statistical power, which prevented us from making firmer conclusions regarding the potential development of new connections between the remnants of V1 and the rest of the visual system, in the lesion animals. The inclusion and examination of a larger number of healthy controls would, for example, provide us more and more substantial evidence when concluding whether the V2d and MT ROI did, indeed, have stronger functional connections with the calcarine than with the operculum.

It is also worth remembering that, while positive functional connectivity often corresponds to established anatomic connections (Honey et al., 2009; Wang et al., 2013), it does not always translate into anatomical connectivity. Functional connectivity also gives no information on the direction of theses connections (i.e., feedforward or feedback). A rigorous examination of the existence of anatomical connections corresponding to the functional connections observed in this study necessitates the application of analytical approaches beyond than those employed herein. These include, though are not necessarily limited to, DTI and retrograde tracers.

At least one of our study's limitations is not inherent to the study or its design but is, rather, the result of an ongoing debate which arguably has the potential to affect any study of functional connectivity: that of the substantive interpretation of negative functional connectivity (G. Chen et al., 2011; Giove et al., 2009; Murphy et al., 2009; Weissenbacher et al., 2009). Negative

functional connectivity is (at least for the time being) harder to interpret than positive functional connectivity. We observed a general increase in negative functional connectivity in the lesion animals compared to the control group. It may be the case that negative correlations in the lesion monkeys, where positive correlations are present in the control group, are the result of structural changes. Rigorous answers to this question, however, regardless of which conclusion they support, also require further and other types of analysis (e.g., DTI, Histology, etc.).

6.3.3 The Challenges of Consistent and Reproducible Functional Connectivity Research Using Non-Human Primates

The nature of resting state research itself imposes a limitation on any relevant studies. The aim of most neuroscience studies using animal models, such as macaques, is to describe mechanisms in these animals that also hold true in humans, in order to increase our understanding of the human brain. This necessitates that data acquisition and analysis in non-human-primates be conducted in a manner that is not only reproducible across various studies using the same model but also that is comparable to Human studies. MRI researchers studying non-human-primates are slowly moving towards a standardized approach (Autio et al., 2021), acquiring uniform structural and functional MRI data –within a given field of research, at least. Obtaining data, much less consistent results, however, remains challenging. Beyond the aforementioned (frequently) necessary use of anaesthetics, animal models are accompanied by technological and methodological challenges. Most available MRI scanners and hardware are calibrated for the adult human brain. Macaques brains (100 cm^3) are thirteen times smaller than Human's (1300 cm^3) (Herculano-Houzel, 2009). This size disparity creates resolution issues and increases the signal-to-noise ratio (Autio et al., 2021), driving research teams to develop

species-specific scanning sequences, coils, and protocols. The absence of universal preprocessing pipelines, specific to non-human primates, can often force research groups to develop their own preprocessing tools. This introduces an additional layer of variability not only between Human and non-Human-primate studies but also between studies of non-Human-primates –even between studies of the *same* non-Human-primates (Botvinik-Nezer et al., 2020; Carp, 2012). We attempted to limit variability due to pre-processing by using FSL (Jenkinson et al., 2012), a publicly available and widely employed toolbox. Of course, this only guarantees comparability (with regard to preprocessing) to other studies that have employed FSL as well. Short of the establishment of a universal protocol across the field, perfect comparability remains, sadly, beyond both our reach and our ability to control for.

Moreover, while resting state functional connectivity is a valuable tool to describe brain networks, it has low sensitivity and specificity. This inherently complicates procuring perfectly reproducible results (Autio et al., 2021). It is worth noting, however, that the functional visual system network may be less sensitive to variability, as it is often close to its equivalent task network (Glasser et al., 2018).

This should not be taken to construe that comparisons of non-human-primate resting state functional connectivity to Human resting state functional connectivity are meaningless. Far from it. While not perfect matches, the resting state networks reported by each of the many resting state studies present many homologies among members of the same species (Beckmann et al., 2005; Damoiseaux et al., 2006; Vincent et al., 2007; Yacoub et al., 2020). Macaque functional connectivity is, moreover, qualitatively similar to human functional connectivity, even with anesthetized animals (Hutchison et al., 2013; Hutchison & Everling, 2012; Miranda-Dominguez et al., 2014). Some functional networks obtained in humans even

echo structural networks obtained in macaques using histology (Margulies et al., 2009; Miranda-Dominguez et al., 2014). And macaque resting state functional connectivity has been found to match anatomic networks obtained with DTI in humans (Mars et al., 2011). It is, however, true that, for a given functional network in humans, macaques tend to present weaker correlations between the areas involved (Hutchison et al., 2013; Miranda-Dominguez et al., 2014) –possibly due to the aforementioned, necessary, use of anaesthetics.

6.4 Recommendations

Both our conclusions and our limitations indicate the strong need for targeted future research on subjects with lesions in the primary visual cortex. This is, of course, a difficult proposition, for many reasons. The existence of lesions which occurred in the primary visual cortex without intervention is, to the best of our knowledge, a rare occurrence. Thus, the likelihood of finding suitable subjects for such research is inherently difficult. This is compounded by the fact that we are effectively limited, for both ethical and practical reasons, to the population of subjects generally available to us for study. This population is comprised of those subjects (ideally rhesus macaques, for reasons discussed in previous chapters), that are either currently in or can be procured to laboratory environments. Naturally, this population comprises only a small portion of the world's overall rhesus macaque population, making subjects with lesions a rare sub-group of an already severely limited population.

It is also important to expand our search to include human subjects with lesions in the primary visual cortex. While we recognize that it is inherently more difficult to conduct human trials, the rarity of the phenomenon is such that the inclusion of human subjects may prove to be necessary, in the long run. Regardless of the potential short-term necessity, however, the

long-term goal of such research is, of course, the better understanding of the *human* brain. As a result, human trials are ultimately unavoidable, if we hope to ensure that such understanding as we gain from animal trials translates to humans, thus guiding potential future clinical applications.

The expansion of the body of research in the particular field will also contribute to the establishment of a framework of lesion characteristics and their commensurate visual field impacts. There is an argument to be made for the benefits of such stockpiling of knowledge being both direct and indirect. Directly, we would increase our understanding of the function of the brain in general and V1 in particular. Indirectly, better understanding of the function of V1, paired with a more expansive knowledgebase of brain abnormalities and their impact(s) on brain function, would allow us to make better predictions regarding the effect of any given deviations from the norm on the functional mechanisms of the brain. This would, in turn, inform more and more-targeted research, while also allowing us to both better identify clinical targets and the most appropriate interventions in each.

The inherently limited population of any study examining lesions in the primary visual cortex, however, means that we must be open to the possibility that we will be incapable of finding a truly appropriate, naturally occurring sample for such research. It is, however, possible to expand our population synthetically. This could be achieved in at least two ways. We could create lesions in V1, by excising some or all of an otherwise healthy monkey's calcarine. It is also possible, if more methodologically challenging, to use reversible methods, such as TMS (Maniglia et al., 2019) or Focused Ultrasound Stimulation (FUS) (Yang et al., 2022) (in conjunction with MRI), to temporarily negate the function of a particular region of the brain (here, again, the calcarine). These approaches also have the substantial benefit of allowing us

to obtain data from both pre- and post-lesion conditions in our subjects. By virtue of being reversible and non-invasive, TMS also circumvents many of the ethical considerations that would render invasive techniques (such as excision) prohibitive in humans[17].

It is also theoretically possible to employ micro-stimulation in V1, while performing real-time electrophysiological recordings on healthy subjects, in an attempt to understand how complex precepts are formed. Such an undertaking could contribute to the development of finer processes for more localized stimulation, as well as the stimulation of patterns more representative of the manner in which visual information is encoded in the primary visual cortex.

It could, in any case, be argued that to understand the brain is to understand the human being. Understanding the details of the function of the human brain is, therefore, among the great undertakings of human society. Thus, understanding of the human brain in general and of any given component thereof specifically has far-reaching consequences, spreading to almost every aspect of daily life; education, recreation, and occupation, to name but a few. Even if we were to limit ourselves to understanding the function of the visual system and then, again, to increasing our understanding of the function of the primary visual cortex, we will have taken a step toward improving the quality of life of nearly one quarter of the world's population. For this and all the reasons delineated above, it is incumbent upon us to conduct this further, more targeted research, and to expand our studies' populations, whether by means of dogged persistence or ingenuous synthesis.

[17] Logic would indicate that this could also be the case for FUS. It is, however, a newer technique and, as such, not as well tried and tested, making ethical approval for its use a more complicated endeavor.

7 References

Abe, H., Tani, T., Mashiko, H., Kitamura, N., Hayami, T., Watanabe, S., Sakai, K., Suzuki, W., Mizukami, H., Watakabe, A., Yamamori, T., & Ichinohe, N. (2018). Axonal Projections From the Middle Temporal Area in the Common Marmoset. *Frontiers in Neuroanatomy*, *12*. https://www.frontiersin.org/article/10.3389/fnana.2018.00089

Abou Elseoud, A., Littow, H., Remes, J., Starck, T., Nikkinen, J., Nissilä, J., Timonen, M., Tervonen, O., & Kiviniemi, V. (2011). Group-ICA Model Order Highlights Patterns of Functional Brain Connectivity. *Frontiers in Systems Neuroscience*, *5*, 37–37. PubMed. https://doi.org/10.3389/fnsys.2011.00037

Aertsen, A. M., Gerstein, G. L., Habib, M. K., & Palm, G. (1989). Dynamics of neuronal firing correlation: Modulation of "effective connectivity." *Journal of Neurophysiology*, *61*(5), Article 5. https://doi.org/10.1152/jn.1989.61.5.900

Agcaoglu, O., Wilson, T. W., Wang, Y.-P., Stephen, J., & Calhoun, V. D. (2019). Resting state connectivity differences in eyes open versus eyes closed conditions. *Human Brain Mapping*, *40*(8), 2488–2498. https://doi.org/10.1002/hbm.24539

Ainsworth, M., Browncross, H., Mitchell, D. J., Mitchell, A. S., Passingham, R. E., Buckley, M. J., Duncan, J., & Bell, A. H. (2018). Functional reorganisation and recovery following cortical lesions: A preliminary study in macaque monkeys. *Neuropsychologia*, *119*, 382–391. https://doi.org/10.1016/j.neuropsychologia.2018.08.024

Ajina, S., & Bridge, H. (2017). Blindsight and Unconscious Vision: What They Teach Us about the Human Visual System. *The Neuroscientist : A Review Journal Bringing Neurobiology, Neurology and Psychiatry*, *23*(5), 529–541. https://doi.org/10.1177/1073858416673817

Ajina, S., Kennard, C., Rees, G., & Bridge, H. (2015). Motion area V5/MT+ response to global motion in the absence of V1 resembles early visual cortex. *Brain*, *138*(1), 164–178. https://doi.org/10.1093/brain/awu328

Ajina, S., Pestilli, F., Rokem, A., Kennard, C., & Bridge, H. (2015). Human blindsight is mediated by an intact geniculo-extrastriate pathway. *ELife*, *4*, e08935. https://doi.org/10.7554/eLife.08935

Ajina, S., Rees, G., Kennard, C., & Bridge, H. (2015). Abnormal Contrast Responses in the Extrastriate Cortex of Blindsight Patients. *Journal of Neuroscience*, *35*(21), 8201–8213. https://doi.org/10.1523/JNEUROSCI.3075-14.2015

Aksenov, D. P., Li, L., Miller, M. J., Iordanescu, G., & Wyrwicz, A. M. (2015). Effects of anesthesia on BOLD signal and neuronal activity in the somatosensory cortex. *Journal of Cerebral Blood Flow & Metabolism*, *35*(11), 1819–1826. https://doi.org/10.1038/jcbfm.2015.130

Aksenov, D. P., Miller, M. J., Dixon, C. J., & Wyrwicz, A. M. (2019). The effect of sevoflurane and isoflurane anesthesia on single unit and local field potentials. *Experimental Brain Research*, *237*(6), Article 6. https://doi.org/10.1007/s00221-019-05528-9

Alexander, A. L., Lee, J. E., Lazar, M., & Field, A. S. (2007). Diffusion tensor imaging of the brain. *Neurotherapeutics*, *4*(3), 316–329. https://doi.org/10.1016/j.nurt.2007.05.011

Alitto, H. J., Moore, B. D., Rathbun, D. L., & Usrey, W. M. (2011). A comparison of visual responses in the lateral geniculate nucleus of alert and anaesthetized macaque monkeys. *The Journal of Physiology*, *589*(Pt 1), Article Pt 1. https://doi.org/10.1113/jphysiol.2010.190538

Alkire, M. T., Asher, C. D., Franciscus, A. M., & Hahn, E. L. (2009). Thalamic microinfusion of antibody to a voltage-gated potassium channel restores consciousness during

anesthesia. *Anesthesiology*, *110*(4), Article 4. https://doi.org/10.1097/aln.0b013e31819c461c

Allen, G., Barnard, H., McColl, R., Hester, A. L., Fields, J. A., Weiner, M. F., Ringe, W. K., Lipton, A. M., Brooker, M., McDonald, E., Rubin, C. D., & Cullum, C. M. (2007). Reduced Hippocampal Functional Connectivity in Alzheimer Disease. *Archives of Neurology*, *64*(10), 1482–1487. https://doi.org/10.1001/archneur.64.10.1482

Allman, J. M., & Kass, J. H. (1975). The dorsomedial cortical visual area: A third tier area in the occipital lobe of the owl monkey (aotus trivirgatus). *Brain Research*, *100*(3), Article 3. https://doi.org/10.1016/0006-8993(75)90153-5

Amaral, D. G., & Insausti, R. (1992). Retrograde transport of D-[3H]-aspartate injected into the monkey amygdaloid complex. *Experimental Brain Research*, *88*(2), 375–388. https://doi.org/10.1007/BF02259113

Amzica, F. (2015). What does burst suppression really mean? *Epilepsy & Behavior*, *49*, 234–237. https://doi.org/10.1016/j.yebeh.2015.06.012

Anand, A., Li, Y., Wang, Y., Lowe, M. J., & Dzemidzic, M. (2009a). Resting state corticolimbic connectivity abnormalities in unmedicated bipolar disorder and unipolar depression. *Psychiatry Research: Neuroimaging*, *171*(3), 189–198. https://doi.org/10.1016/j.pscychresns.2008.03.012

Anderson, J. C., & Martin, K. A. C. (2002). Connection from cortical area V2 to MT in macaque monkey. *Journal of Comparative Neurology*, *443*(1), 56–70. https://doi.org/10.1002/cne.10100

Anzai, A., Peng, X., & Van Essen, D. C. (2007). Neurons in monkey visual area V2 encode combinations of orientations. *Nature Neuroscience*, *10*(10), Article 10. https://doi.org/10.1038/nn1975

Arsenault, J. T., Caspari, N., Vandenberghe, R., & Vanduffel, W. (2018). Attention Shifts Recruit the Monkey Default Mode Network. *Journal of Neuroscience*, *38*(5), Article 5. https://doi.org/10.1523/JNEUROSCI.1111-17.2017

Autio, J. A., Zhu, Q., Li, X., Glasser, M. F., Schwiedrzik, C. M., Fair, D. A., Zimmermann, J., Yacoub, E., Menon, R. S., Van Essen, D. C., Hayashi, T., Russ, B., & Vanduffel, W. (2021). Minimal specifications for non-human primate MRI: Challenges in standardizing and harmonizing data collection. *NeuroImage*, *236*, 118082. https://doi.org/10.1016/j.neuroimage.2021.118082

Azzopardi, P., & Cowey, A. (2001). Motion discrimination in cortically blind patients. *Brain: A Journal of Neurology*, *124*(Pt 1), 30–46. https://doi.org/10.1093/brain/124.1.30

Baizer, J. S. (1982). Receptive field properties of V3 neurons in monkey. *Investigative Ophthalmology & Visual Science*, *23*(1), 87–95.

Baizer, J. S., Ungerleider, L. G., & Desimone, R. (1991). Organization of visual inputs to the inferior temporal and posterior parietal cortex in macaques. *The Journal of Neuroscience: The Official Journal of the Society for Neuroscience*, *11*(1), 168–190. https://doi.org/10.1523/JNEUROSCI.11-01-00168.1991

Bak, M., Girvin, J. P., Hambrecht, F. T., Kufta, C. V., Loeb, G. E., & Schmidt, E. M. (1990). Visual sensations produced by intracortical microstimulation of the human occipital cortex. *Medical and Biological Engineering and Computing*, *28*(3), 257–259. https://doi.org/10.1007/BF02442682

Barbur, J. L., Ruddock, K. H., & Waterfield, V. A. (1980). Human visual responses in the absence of the geniculo-calcarine projection. *Brain: A Journal of Neurology*, *103*(4), 905–928. https://doi.org/10.1093/brain/103.4.905

Barbur, J. L., Watson, J. D. G., Frackowiak, R. S. J., & Zeki, S. (1993). Conscious visual perception

without VI. *Brain*, *116*(6), 1293–1302. https://doi.org/10.1093/brain/116.6.1293

Barlow, H. B., Blakemore, C., & Pettigrew, J. D. (1967). The neural mechanism of binocular depth discrimination. *The Journal of Physiology*, *193*(2), 327–342.

Barone, P., Dehay, C., Berland, M., Bullier, J., & Kennedy, H. (1995). Developmental remodeling of primate visual cortical pathways. *Cerebral Cortex (New York, N.Y.: 1991)*, *5*(1), 22–38. https://doi.org/10.1093/cercor/5.1.22

Bartlett, J., & Doty, R. (1980). *An exploration of the ability of macaques to detect microstimulation of striate cortex*. *40*, 713–728.

Barton, J. J. S., & Sharpe, J. A. (1997). Motion direction discrimination in blind hemifields. *Annals of Neurology*, *41*(2), 255–264. https://doi.org/10.1002/ana.410410217

Barttfeld, P., Uhrig, L., Sitt, J. D., Sigman, M., Jarraya, B., & Dehaene, S. (2015). Signature of consciousness in the dynamics of resting-state brain activity. *Proceedings of the National Academy of Sciences*, *112*(3), Article 3.

Basser, P. J., Pajevic, S., Pierpaoli, C., Duda, J., & Aldroubi, A. (2000). In vivo fiber tractography using DT-MRI data. *Magnetic Resonance in Medicine*, *44*(4), 625–632. https://doi.org/10.1002/1522-2594(200010)44:4<625::AID-MRM17>3.0.CO;2-O

Beckmann, C. F., DeLuca, M., Devlin, J. T., & Smith, S. M. (2005). Investigations into resting-state connectivity using independent component analysis. *Philosophical Transactions of the Royal Society of London. Series B, Biological Sciences*, *360*(1457), 1001–1013. PubMed. https://doi.org/10.1098/rstb.2005.1634

Beckmann, C. F., Mackay, C. E., Filippini, N., & Smith, S. M. (2009). *Group comparison of resting-state FMRI data using multi-subject ICA and dual regression*.

Beckmann, C. F., & Smith, S. M. (2004). Probabilistic independent component analysis for functional magnetic resonance imaging. *IEEE Transactions on Medical Imaging*, *23*(2),

137–152. https://doi.org/10.1109/TMI.2003.822821

Benevento, L. A., & Fallon, J. H. (1975). The ascending projections of the superior colliculus in the rhesus monkey (Macaca mulatta). *Journal of Comparative Neurology*, *160*(3), 339–361. https://doi.org/10.1002/cne.901600306

Ben-Haim, M. S., Dal Monte, O., Fagan, N. A., Dunham, Y., Hassin, R. R., Chang, S. W. C., & Santos, L. R. (2021). Disentangling perceptual awareness from nonconscious processing in rhesus monkeys (Macaca mulatta). *Proceedings of the National Academy of Sciences*, *118*(15), e2017543118. https://doi.org/10.1073/pnas.2017543118

Bentivoglio, M., Kuypers, H. G. J. M., Catsman-Berrevoets, C. E., Loewe, H., & Dann, O. (1980). Two new fluorescent retrograde neuronal tracers which are transported over long distances. *Neuroscience Letters*, *18*(1), 25–30. https://doi.org/10.1016/0304-3940(80)90208-6

Berken, J. A., Chai, X., Chen, J.-K., Gracco, V. L., & Klein, D. (2016). Effects of Early and Late Bilingualism on Resting-State Functional Connectivity. *Journal of Neuroscience*, *36*(4), 1165–1172. https://doi.org/10.1523/JNEUROSCI.1960-15.2016

Bertrand, H. G. M. J., Springer, S., Burnside, W., Sandersen, C., & Flecknell, P. A. (2017). Comparison of emergence times and quality between isoflurane and sevoflurane in rhesus macaque (Macaca mulatta) undergoing neurosurgical procedure. *Laboratory Animals*, *51*(5), 518–525. https://doi.org/10.1177/0023677217692371

Biswal, B. B. (2012). Resting state fMRI: A personal history. *NeuroImage*, *62*(2), 938–944. https://doi.org/10.1016/j.neuroimage.2012.01.090

Biswal, B., Yetkin, F. Z., Haughton, V. M., & Hyde, J. S. (1995). Functional connectivity in the motor cortex of resting human brain using echo-planar MRI. *Magnetic Resonance in Medicine*, *34*(4), 537–541. https://doi.org/10.1002/mrm.1910340409

Bluhm, R. L., Williamson, P. C., Osuch, E. A., Frewen, P. A., Stevens, T. K., Boksman, K., Neufeld, R. W. J., Théberge, J., & Lanius, R. A. (2009). Alterations in default network connectivity in posttraumatic stress disorder related to early-life trauma. *Journal of Psychiatry & Neuroscience : JPN*, *34*(3), Article 3.

Born, R. T., & Bradley, D. C. (2005). Structure and Function of Visual Area MT. *Annual Review of Neuroscience*, *28*(1), 157–189. https://doi.org/10.1146/annurev.neuro.26.041002.131052

Bosco, A., Breveglieri, R., Chinellato, E., Galletti, C., & Fattori, P. (2010). Reaching Activity in the Medial Posterior Parietal Cortex of Monkeys Is Modulated by Visual Feedback. *Journal of Neuroscience*, *30*(44), 14773–14785. https://doi.org/10.1523/JNEUROSCI.2313-10.2010

Bosking, W. H., Sun, P., Ozker, M., Pei, X., Foster, B. L., Beauchamp, M. S., & Yoshor, D. (2017). Saturation in Phosphene Size with Increasing Current Levels Delivered to Human Visual Cortex. *The Journal of Neuroscience: The Official Journal of the Society for Neuroscience*, *37*(30), 7188–7197. https://doi.org/10.1523/JNEUROSCI.2896-16.2017

Botvinik-Nezer, R., Holzmeister, F., Camerer, C. F., Dreber, A., Huber, J., Johannesson, M., Kirchler, M., Iwanir, R., Mumford, J. A., Adcock, R. A., Avesani, P., Baczkowski, B. M., Bajracharya, A., Bakst, L., Ball, S., Barilari, M., Bault, N., Beaton, D., Beitner, J., … Schonberg, T. (2020). Variability in the analysis of a single neuroimaging dataset by many teams. *Nature*, *582*(7810), 84–88. https://doi.org/10.1038/s41586-020-2314-9

Bourne, R. R. A., Adelson, J., Flaxman, S., Briant, P., Bottone, M., Vos, T., Naidoo, K., Braithwaite, T., Cicinelli, M., Jonas, J., Limburg, H., Resnikoff, S., Silvester, A., Nangia, V., & Taylor, H. R. (2020). Global Prevalence of Blindness and Distance and Near Vision Impairment in 2020: Progress towards the Vision 2020 targets and what the future

holds. *Investigative Ophthalmology & Visual Science*, *61*(7), 2317.

Bremmer, F., Distler, C., & Hoffmann, K.-P. (1997). Eye Position Effects in Monkey Cortex. II. Pursuit- and Fixation-Related Activity in Posterior Parietal Areas LIP and 7A. *Journal of Neurophysiology*, *77*(2), 962–977. https://doi.org/10.1152/jn.1997.77.2.962

Brewer, A. A., Press, W. A., Logothetis, N. K., & Wandell, B. A. (2002). Visual areas in macaque cortex measured using functional magnetic resonance imaging. *The Journal of Neuroscience: The Official Journal of the Society for Neuroscience*, *22*(23), Article 23.

Bridge, H., Bell, A. H., Ainsworth, M., Sallet, J., Premereur, E., Ahmed, B., Mitchell, A. S., Schüffelgen, U., Buckley, M., Tendler, B. C., Miller, K. L., Mars, R. B., Parker, A. J., & Krug, K. (2019). Preserved extrastriate visual network in a monkey with substantial, naturally occurring damage to primary visual cortex. *ELife*, *8*, e42325. https://doi.org/10.7554/eLife.42325

Bridge, H., Thomas, O., Jbabdi, S., & Cowey, A. (2008). Changes in connectivity after visual cortical brain damage underlie altered visual function. *Brain: A Journal of Neurology*, *131*(Pt 6), 1433–1444. https://doi.org/10.1093/brain/awn063

Briggs, F., & Usrey, W. M. (2007). A fast, reciprocal pathway between the lateral geniculate nucleus and visual cortex in the macaque monkey. *The Journal of Neuroscience : The Official Journal of the Society for Neuroscience*, *27*(20), Article 20. PubMed. https://doi.org/10.1523/JNEUROSCI.1035-07.2007

Brindley, G. S., & Lewin, W. S. (1968). The sensations produced by electrical stimulation of the visual cortex. *The Journal of Physiology*, *196*(2), 479–493. https://doi.org/10.1113/jphysiol.1968.sp008519

Britten, K. H., Newsome, W. T., Shadlen, M. N., Celebrini, S., & Movshon, J. A. (1996). A relationship between behavioral choice and the visual responses of neurons in

macaque MT. *Visual Neuroscience*, *13*(1), 87–100. https://doi.org/10.1017/S095252380000715X

Buckner, R. L., Sepulcre, J., Talukdar, T., Krienen, F. M., Liu, H., Hedden, T., Andrews-Hanna, J. R., Sperling, R. A., & Johnson, K. A. (2009). Cortical Hubs Revealed by Intrinsic Functional Connectivity: Mapping, Assessment of Stability, and Relation to Alzheimer's Disease. *Journal of Neuroscience*, *29*(6), 1860–1873. https://doi.org/10.1523/JNEUROSCI.5062-08.2009

Bukhari, Q., Schroeter, A., Cole, D. M., & Rudin, M. (2017). Resting State fMRI in Mice Reveals Anesthesia Specific Signatures of Brain Functional Networks and Their Interactions. *Frontiers in Neural Circuits*, *11*, 5. https://doi.org/10.3389/fncir.2017.00005

Burkhalter, A., & Van Essen, D. C. (1986). Processing of color, form and disparity information in visual areas VP and V2 of ventral extrastriate cortex in the macaque monkey. *The Journal of Neuroscience: The Official Journal of the Society for Neuroscience*, *6*(8), Article 8.

Butt, O. H., Benson, N. C., Datta, R., & Aguirre, G. K. (2015). Hierarchical and homotopic correlations of spontaneous neural activity within the visual cortex of the sighted and blind. *Frontiers in Human Neuroscience*, *9*, 25. https://doi.org/10.3389/fnhum.2015.00025

Cardoso, J.-F. (1998). Blind signal separation: Statistical principles. *Proceedings of the IEEE*, *86*(10), 2009–2025. https://doi.org/10.1109/5.720250

Carp, J. (2012). On the Plurality of (Methodological) Worlds: Estimating the Analytic Flexibility of fMRI Experiments. *Frontiers in Neuroscience*, *6*, 149. https://doi.org/10.3389/fnins.2012.00149

Casagrande, V. A., & Kaas, J. H. (1994). The Afferent, Intrinsic, and Efferent Connections of

Primary Visual Cortex in Primates. In A. Peters & K. S. Rockland (Eds.), *Primary Visual Cortex in Primates* (Vol. 10, pp. 201–259). Springer US. https://doi.org/10.1007/978-1-4757-9628-5_5

Castoldi, V., d'Isa, R., Marenna, S., Comi, G., & Leocani, L. (2021). Non-invasive visual evoked potentials under sevoflurane versus ketamine-xylazine in rats. *Heliyon*, *7*(11), Article 11. https://doi.org/10.1016/j.heliyon.2021.e08360

Cauda, F., Sacco, K., Duca, S., Cocito, D., D'Agata, F., Geminiani, G. C., & Canavero, S. (2009). Altered Resting State in Diabetic Neuropathic Pain. *PLOS ONE*, *4*(2), e4542. https://doi.org/10.1371/journal.pone.0004542

Causes of blindness and vision impairment in 2020 and trends over 30 years, and prevalence of avoidable blindness in relation to VISION 2020: The Right to Sight: An analysis for the Global Burden of Disease Study—PubMed. (n.d.). Retrieved January 7, 2023, from https://pubmed.ncbi.nlm.nih.gov/33275949/

Celesia, G. G., & DeMarco, P. J. J. (1994). Anatomy and Physiology of the Visual System. *Journal of Clinical Neurophysiology*, *11*(5), Article 5.

Chen, G., Chen, G., Xie, C., & Li, S.-J. (2011). Negative Functional Connectivity and Its Dependence on the Shortest Path Length of Positive Network in the Resting-State Human Brain. *Brain Connectivity*, *1*(3), 195–206. https://doi.org/10.1089/brain.2011.0025

Chen, S., Ross, T. J., Zhan, W., Myers, C. S., Chuang, K.-S., Heishman, S. J., Stein, E. A., & Yang, Y. (2008). Group independent component analysis reveals consistent resting-state networks across multiple sessions. *Brain Research*, *1239*, 141–151. https://doi.org/10.1016/j.brainres.2008.08.028

Chen, X., Wang, F., Fernandez, E., & Roelfsema, P. R. (2020). Shape perception via a high-

channel-count neuroprosthesis in monkey visual cortex. *Science (New York, N.Y.)*, *370*(6521), 1191–1196. https://doi.org/10.1126/science.abd7435

Chepenik, L. G., Raffo, M., Hampson, M., Lacadie, C., Wang, F., Jones, M. M., Pittman, B., Skudlarski, P., & Blumberg, H. P. (2010). Functional connectivity between ventral prefrontal cortex and amygdala at low frequency in the resting state in bipolar disorder. *Psychiatry Research*, *182*(3), 207–210. https://doi.org/10.1016/j.pscychresns.2010.04.002

Cherry, E. C. (1953). Some Experiments on the Recognition of Speech, with One and with Two Ears. *Acoustical Society of America Journal*, *25*, 975. https://doi.org/10.1121/1.1907229

Cicmil, N., & Krug, K. (2015). Playing the electric light orchestra—How electrical stimulation of visual cortex elucidates the neural basis of perception. *Philosophical Transactions of the Royal Society B: Biological Sciences*, *370*(1677). https://doi.org/10.1098/rstb.2014.0206

Conley, M., & Fitzpatrick, D. (1989). Morphology of retinogeniculate axons in the macaque. *Visual Neuroscience*, *2*(3), 287–296. https://doi.org/10.1017/s0952523800001206

Coogan, T. A., & Van Essen, D. C. (1996). Development of connections within and between areas V1 and V2 of macaque monkeys. *The Journal of Comparative Neurology*, *372*(3), 327–342. https://doi.org/10.1002/(SICI)1096-9861(19960826)372:3<327::AID-CNE1>3.0.CO;2-4

Costumero, V., Bueichekú, E., Adrián-Ventura, J., & Ávila, C. (2020). Opening or closing eyes at rest modulates the functional connectivity of V1 with default and salience networks. *Scientific Reports*, *10*(1), Article 1. https://doi.org/10.1038/s41598-020-66100-y

Cowey, A., & Rolls, E. T. (1974). Human cortical magnification factor and its relation to visual

acuity. *Experimental Brain Research*, *21*(5), 447–454. https://doi.org/10.1007/BF00237163

Cowey, A., & Stoerig, P. (1995). Blindsight in monkeys. *Nature*, *373*(6511), Article 6511. https://doi.org/10.1038/373247a0

Cumming, B. G., & DeAngelis, G. C. (2001). The Physiology of Stereopsis. *Annual Review of Neuroscience*, *24*(1), 203–238. https://doi.org/10.1146/annurev.neuro.24.1.203

Curtis, C. E., & D'Esposito, M. (2003). Persistent activity in the prefrontal cortex during working memory. *Trends in Cognitive Sciences*, *7*(9), 415–423. https://doi.org/10.1016/s1364-6613(03)00197-9

Cusick, C. G., Scripter, J. L., Darensbourg, J. G., & Weber, J. T. (1993). Chemoarchitectonic subdivisions of the visual pulvinar in monkeys and their connectional relations with the middle temporal and rostral dorsolateral visual areas, MT and DLr. *Journal of Comparative Neurology*, *336*(1), 1–30. https://doi.org/10.1002/cne.903360102

Dagli, M. S., Ingeholm, J. E., & Haxby, J. V. (1999). Localization of Cardiac-Induced Signal Change in fMRI. *NeuroImage*, *9*(4), 407–415. https://doi.org/10.1006/nimg.1998.0424

Damoiseaux, J. S., & Greicius, M. D. (2009). Greater than the sum of its parts: A review of studies combining structural connectivity and resting-state functional connectivity. *Brain Structure and Function*, *213*(6), Article 6. https://doi.org/10.1007/s00429-009-0208-6

Damoiseaux, J. S., Rombouts, S. A. R. B., Barkhof, F., Scheltens, P., Stam, C. J., Smith, S. M., & Beckmann, C. F. (2006a). Consistent resting-state networks across healthy subjects. *Proceedings of the National Academy of Sciences*, *103*(37), Article 37. https://doi.org/10.1073/pnas.0601417103

Daniel, P. M., & Whitteridge, D. (1961). The representation of the visual field on the cerebral cortex in monkeys. *The Journal of Physiology*, *159*(2), 203. https://doi.org/10.1113/jphysiol.1961.sp006803

DeAngelis, G. C., Cumming, B. G., & Newsome, W. T. (1998). Cortical area MT and the perception of stereoscopic depth. *Nature*, *394*(6694), 677–680. https://doi.org/10.1038/29299

Deco, G., Jirsa, V. K., & McIntosh, A. R. (2013). Resting brains never rest: Computational insights into potential cognitive architectures. *Trends in Neurosciences*, *36*(5), Article 5. https://doi.org/10.1016/j.tins.2013.03.001

Deloitte Economics. (2021). *Impact of COVID-19 on sight loss and blindness in the UK | Deloitte Australia | Economics*. https://www2.deloitte.com/au/en/pages/economics/articles/impact-covid-19-sight-loss-blindness-uk.html

Denomme, N., Hull, J. M., & Mashour, G. A. (2019). Role of Voltage-Gated Sodium Channels in the Mechanism of Ether-Induced Unconsciousness. *Pharmacological Reviews*, *71*(4), 450. https://doi.org/10.1124/pr.118.016592

Deshpande, G., Kerssens, C., Sebel, P. S., & Hu, X. (2010). Altered local coherence in the default mode network due to sevoflurane anesthesia. *Brain Research*, *1318*, 110–121. https://doi.org/10.1016/j.brainres.2009.12.075

Distler, C., Boussaoud, D., Desimone, R., & Ungerleider, L. G. (1993). Cortical connections of inferior temporal area TEO in macaque monkeys. *Journal of Comparative Neurology*, *334*(1), Article 1. https://doi.org/10.1002/cne.903340111

Dobelle, W. H. (2000). Artificial vision for the blind by connecting a television camera to the visual cortex. *ASAIO Journal (American Society for Artificial Internal Organs: 1992)*,

46(1), 3–9. https://doi.org/10.1097/00002480-200001000-00002

Dobelle, W. H., Mladejovsky, M. G., Evans, J. R., Roberts, T. S., & Girvin, J. P. (1976). "Braille" reading by a blind volunteer by visual cortex stimulation. *Nature*, *259*(5539), 111–112.

Dougherty, R. F., Koch, V. M., Brewer, A. A., Fischer, B., Modersitzki, J., & Wandell, B. A. (2003). Visual field representations and locations of visual areas V1/2/3 in human visual cortex. *Journal of Vision*, *3*(10), 1–1. https://doi.org/10.1167/3.10.1

Droby, A., Yuen, K. S. L., Muthuraman, M., Reitz, S.-C., Fleischer, V., Klein, J., Gracien, R.-M., Ziemann, U., Deichmann, R., Zipp, F., & Groppa, S. (2016). Changes in brain functional connectivity patterns are driven by an individual lesion in MS: A resting-state fMRI study. *Brain Imaging and Behavior*, *10*(4), 1117–1126. https://doi.org/10.1007/s11682-015-9476-3

Dubner, R., & Zeki, S. M. (1971). Response properties and receptive fields of cells in an anatomically defined region of the superior temporal sulcus in the monkey. *Brain Research*, *35*(2), 528–532. https://doi.org/10.1016/0006-8993(71)90494-X

Dueck, M. H., Petzke, F., Gerbershagen, H. J., Paul, M., Heßelmann, V., Girnus, R., Krug, B., Sorger, B., Goebel, R., Lehrke, R., Sturm, V., & Boerner, U. (2005). Propofol attenuates responses of the auditory cortex to acoustic stimulation in a dose-dependent manner: A FMRI study. *Acta Anaesthesiologica Scandinavica*, *49*(6), 784–791. https://doi.org/10.1111/j.1399-6576.2005.00703.x

Ecker, A. S., Berens, P., Cotton, R. J., Subramaniyan, M., Denfield, G. H., Cadwell, C. R., Smirnakis, S. M., Bethge, M., & Tolias, A. S. (2014). State Dependence of Noise Correlations in Macaque Primary Visual Cortex. *Neuron*, *82*(1), Article 1. https://doi.org/10.1016/j.neuron.2014.02.006

Eger, E. I. (1981). Isoflurane: A Review. *Anesthesiology*, *55*(5), Article 5.

https://doi.org/10.1097/00000542-198111000-00014

Eickhoff, S. B., Jbabdi, S., Caspers, S., Laird, A. R., Fox, P. T., Zilles, K., & Behrens, T. E. J. (2010). Anatomical and Functional Connectivity of Cytoarchitectonic Areas within the Human Parietal Operculum. *Journal of Neuroscience*, *30*(18), 6409–6421. https://doi.org/10.1523/JNEUROSCI.5664-09.2010

Etkin, A., Prater, K. E., Schatzberg, A. F., Menon, V., & Greicius, M. D. (2009). Disrupted Amygdalar Subregion Functional Connectivity and Evidence of a Compensatory Network in Generalized Anxiety Disorder. *Archives of General Psychiatry*, *66*(12), Article 12. https://doi.org/10.1001/archgenpsychiatry.2009.104

European Union. (2010). DIRECTIVE 2010/63/EU on the protection of animals used for scientific purposes. *EU Official Journal*, *L276*, 19–28.

Fattori, P., Breveglieri, R., Bosco, A., Gamberini, M., & Galletti, C. (2017). Vision for Prehension in the Medial Parietal Cortex. *Cerebral Cortex*, *27*(2), 1149–1163. https://doi.org/10.1093/cercor/bhv302

Felleman, D. J. (2009). Extrastriate Visual Cortex. In M. D. Binder, N. Hirokawa, & U. Windhorst (Eds.), *Encyclopedia of Neuroscience* (pp. 1526–1532). Springer. https://doi.org/10.1007/978-3-540-29678-2_3247

Felleman, D. J., Burkhalter, A., & Van Essen, D. C. (1997). Cortical connections of areas V3 and VP of macaque monkey extrastriate visual cortex. *Journal of Comparative Neurology*, *379*(1), 21–47. https://doi.org/10.1002/(SICI)1096-9861(19970303)379:1<21::AID-CNE3>3.0.CO;2-K

Felleman, D. J., & Essen, D. C. V. (1987). Receptive field properties of neurons in area V3 of macaque monkey extrastriate cortex. *Journal of Neurophysiology*. https://doi.org/10.1152/jn.1987.57.4.889

Felleman, D. J., & Van Essen, D. C. (1991). Distributed hierarchical processing in the primate cerebral cortex. *Cerebral Cortex (New York, N.Y.: 1991)*, *1*(1), 1–47. https://doi.org/10.1093/cercor/1.1.1-a

Ffytche, D. H., Blom, J. D., & Catani, M. (2010). Disorders of visual perception. *Journal of Neurology, Neurosurgery & Psychiatry*, *81*(11), Article 11. https://doi.org/10.1136/jnnp.2008.171348

Figueroa-Jimenez, M. D., Cañete-Massé, C., Carbó-Carreté, M., Zarabozo-Hurtado, D., Peró-Cebollero, M., Salazar-Estrada, J. G., & Guàrdia-Olmos, J. (2021). Resting-state default mode network connectivity in young individuals with Down syndrome. *Brain and Behavior*, *11*(1), e01905. https://doi.org/10.1002/brb3.1905

Fischl, B., Sereno, M. I., & Dale, A. M. (1999). Cortical Surface-Based Analysis: II: Inflation, Flattening, and a Surface-Based Coordinate System. *NeuroImage*, *9*(2), 195–207. https://doi.org/10.1006/nimg.1998.0396

Fitzpatrick, D., Usrey, W. M., Schofield, B. R., & Einstein, G. (1994). The sublaminar organization of corticogeniculate neurons in layer 6 of macaque striate cortex. *Visual Neuroscience*, *11*(2), Article 2. https://doi.org/10.1017/s0952523800001656

Flaxman, S. R., Bourne, R. R. A., Resnikoff, S., Ackland, P., Braithwaite, T., Cicinelli, M. V., Das, A., Jonas, J. B., Keeffe, J., Kempen, J. H., Leasher, J., Limburg, H., Naidoo, K., Pesudovs, K., Silvester, A., Stevens, G. A., Tahhan, N., Wong, T. Y., Taylor, H. R., … Zheng, Y. (2017). Global causes of blindness and distance vision impairment 1990–2020: A systematic review and meta-analysis. *The Lancet Global Health*, *5*(12), e1221–e1234. https://doi.org/10.1016/S2214-109X(17)30393-5

Foerster, O. (1929). *Breitrage zur pathophysiologie der sehbabahn und der sphesphare*. *39*, 435–463.

Folloni, D., Verhagen, L., Mars, R. B., Fouragnan, E., Constans, C., Aubry, J.-F., Rushworth, M. F. S., & Sallet, J. (2019). Manipulation of Subcortical and Deep Cortical Activity in the Primate Brain Using Transcranial Focused Ultrasound Stimulation. *Neuron*, *101*(6), 1109-1116.e5. https://doi.org/10.1016/j.neuron.2019.01.019

Fornito, A., Zalesky, A., & Bullmore, E. T. (Eds.). (2016). Chapter 3—Connectivity Matrices and Brain Graphs. In *Fundamentals of Brain Network Analysis* (pp. 89–113). Academic Press. https://doi.org/10.1016/B978-0-12-407908-3.00003-0

Fox, M. D., Corbetta, M., Snyder, A. Z., Vincent, J. L., & Raichle, M. E. (2006). Spontaneous neuronal activity distinguishes human dorsal and ventral attention systems. *Proceedings of the National Academy of Sciences of the United States of America*, *103*(26), 10046–10051. PubMed. https://doi.org/10.1073/pnas.0604187103

Fox, M. D., & Raichle, M. E. (2007). Spontaneous fluctuations in brain activity observed with functional magnetic resonance imaging. *Nature Reviews Neuroscience*, *8*(9), Article 9. https://doi.org/10.1038/nrn2201

Fox, M. D., Zhang, D., Snyder, A. Z., & Raichle, M. E. (2009). The Global Signal and Observed Anticorrelated Resting State Brain Networks. *Journal of Neurophysiology*, *101*(6), 3270–3283. https://doi.org/10.1152/jn.90777.2008

Freud, E., Plaut, D. C., & Behrmann, M. (2016). 'What' Is Happening in the Dorsal Visual Pathway. *Trends in Cognitive Sciences*, *20*(10), 773–784. https://doi.org/10.1016/j.tics.2016.08.003

Frink, E. J., Malan, P. T., Atlas, M., Dominguez, L. M., DiNardo, J. A., & Brown, B. R. (1992). Clinical Comparison of Sevoflurane and Isoflurane in Healthy Patients. *Anesthesia & Analgesia*, *74*(2), Article 2. https://journals.lww.com/anesthesia-analgesia/Fulltext/1992/02000/Clinical_Comparison_of_Sevoflurane_and_Isoflurane

.12.aspx

Friston, K. J., Frith, C. D., Liddle, P. F., & Frackowiak, R. S. J. (1993). Functional Connectivity: The Principal-Component Analysis of Large (PET) Data Sets. *Journal of Cerebral Blood Flow & Metabolism*, *13*(1), Article 1. https://doi.org/10.1038/jcbfm.1993.4

Gandhi, N. J., & Katnani, H. A. (2011). Motor Functions of the Superior Colliculus. *Annual Review of Neuroscience*, *34*, 205–231. https://doi.org/10.1146/annurev-neuro-061010-113728

Garey, L. J. (1984). Structural development of the visual system of man. *Human Neurobiology*, *3*(2), 75–80.

Gattass, R., Sousa, A., & Gross, C. (1988). Visuotopic organization and extent of V3 and V4 of the macaque. *The Journal of Neuroscience*, *8*(6), 1831–1845. https://doi.org/10.1523/JNEUROSCI.08-06-01831.1988

Gattass, R., Sousa, A. P., Mishkin, M., & Ungerleider, L. G. (1997). Cortical projections of area V2 in the macaque. *Cerebral Cortex (New York, N.Y.: 1991)*, *7*(2), 110–129. https://doi.org/10.1093/cercor/7.2.110

Gaudy, J.-H., Sicard, J.-F., Maneglia, R., & Quignon, M. (1993). Effets de l'halothane sur les gaz du sang et l'équilibre acido-basique artériels chez le rat intact et chez le rat chémodénervé. *Canadian Journal of Anaesthesia*, *40*(9), 883–890. https://doi.org/10.1007/BF03009263

Gegenfurtner, K. R., Kiper, D. C., & Levitt, J. B. (1997). Functional Properties of Neurons in Macaque Area V3. *Journal of Neurophysiology*, *77*(4), 1906–1923. https://doi.org/10.1152/jn.1997.77.4.1906

Genç, E., Schölvinck, M. L., Bergmann, J., Singer, W., & Kohler, A. (2016). Functional Connectivity Patterns of Visual Cortex Reflect its Anatomical Organization. *Cerebral*

Cortex, *26*(9), Article 9. https://doi.org/10.1093/cercor/bhv175

Geuter, S., Qi, G., Welsh, R. C., Wager, T. D., & Lindquist, M. A. (2018). *Effect Size and Power in fMRI Group Analysis* (p. 295048). bioRxiv. https://doi.org/10.1101/295048

Ghashghaei, H. T., & Barbas, H. (2002). Pathways for emotion: Interactions of prefrontal and anterior temporal pathways in the amygdala of the rhesus monkey. *Neuroscience*, *115*(4), 1261–1279. https://doi.org/10.1016/s0306-4522(02)00446-3

Giacometti, C., Dureux, A., Autran-Clavagnier, D., Wilson, C. R. E., Sallet, J., Dirheimer, M., Procyk, E., Hadj-Bouziane, F., & Amiez, C. (2021). Frontal Cortical Functional Connectivity Is Impacted by Anaesthesia in Macaques. *Cerebral Cortex (New York, N.Y.: 1991)*, bhab465. https://doi.org/10.1093/cercor/bhab465

Giaschi, D., Jan, J. E., Bjornson, B., Au, S., MSc, M. T., Lyons, C. J., & Kh, P. (2003). Conscious visual abilities in a patient with early bilateral occipital damage. *Developmental Medicine & Child Neurology*, *45*(11), 772–781. https://doi.org/10.1111/j.1469-8749.2003.tb00888.x

Gilbert, C. D., & Li, W. (2013). Top-down influences on visual processing. *Nature Reviews Neuroscience*, *14*(5), Article 5. https://doi.org/10.1038/nrn3476

Gillebert, C. R., & Mantini, D. (2013). Functional Connectivity in the Normal and Injured Brain. *The Neuroscientist*, *19*(5), 509–522. https://doi.org/10.1177/1073858412463168

Giove, F., Gili, T., Iacovella, V., Macaluso, E., & Maraviglia, B. (2009). Images-based suppression of unwanted global signals in resting-state functional connectivity studies. *Magnetic Resonance Imaging*, *27*(8), 1058–1064. https://doi.org/10.1016/j.mri.2009.06.004

Girard, G., Caminiti, R., Battaglia-Mayer, A., St-Onge, E., Ambrosen, K. S., Eskildsen, S. F., Krug, K., Dyrby, T. B., Descoteaux, M., Thiran, J.-P., & Innocenti, G. M. (2020). On the cortical

connectivity in the macaque brain: A comparison of diffusion tractography and histological tracing data. *NeuroImage*, *221*, 117201. https://doi.org/10.1016/j.neuroimage.2020.117201

Girkin, C. A., & Miller, N. R. (2001a). Central disorders of vision in humans. *Survey of Ophthalmology*, *45*(5), 379–405. https://doi.org/10.1016/s0039-6257(00)00208-3

Glasser, M. F., Coalson, T. S., Bijsterbosch, J. D., Harrison, S. J., Harms, M. P., Anticevic, A., Van Essen, D. C., & Smith, S. M. (2018). Using temporal ICA to selectively remove global noise while preserving global signal in functional MRI data. *NeuroImage*, *181*, 692–717. https://doi.org/10.1016/j.neuroimage.2018.04.076

Goebel, R., Muckli, L., Zanella, F. E., Singer, W., & Stoerig, P. (2001). Sustained extrastriate cortical activation without visual awareness revealed by fMRI studies of hemianopic patients. *Vision Research*, *41*(10), 1459–1474. https://doi.org/10.1016/S0042-6989(01)00069-4

Goodale, M. A., & Milner, A. D. (1992). Separate visual pathways for perception and action. *Trends in Neurosciences*, *15*(1), 20–25. https://doi.org/10.1016/0166-2236(92)90344-8

Greve, D. N., & Fischl, B. (2009). Accurate and robust brain image alignment using boundary-based registration. *NeuroImage*, *48*(1), 63–72. https://doi.org/10.1016/j.neuroimage.2009.06.060

Griffanti, L. (2019, September 7). *MELODIC - FslWiki*. FSLwiki - MELODIC. https://fsl.fmrib.ox.ac.uk/fsl/fslwiki/MELODIC

Griffanti, L., Douaud, G., Bijsterbosch, J., Evangelisti, S., Alfaro-Almagro, F., Glasser, M. F., Duff, E. P., Fitzgibbon, S., Westphal, R., Carone, D., Beckmann, C. F., & Smith, S. M. (2017). Hand classification of fMRI ICA noise components. *Cleaning up the FMRI Time*

Series: Mitigating Noise with Advanced Acquisition and Correction Strategies, *154*, 188–205. https://doi.org/10.1016/j.neuroimage.2016.12.036

Grill-Spector, K., Kourtzi, Z., & Kanwisher, N. (2001). The lateral occipital complex and its role in object recognition. *Vision Research*, *41*(10), 1409–1422. https://doi.org/10.1016/S0042-6989(01)00073-6

Guggisberg, A. G., Honma, S. M., Findlay, A. M., Dalal, S. S., Kirsch, H. E., Berger, M. S., & Nagarajan, S. S. (2008). Mapping functional connectivity in patients with brain lesions. *Annals of Neurology*, *63*(2), 193–203. https://doi.org/10.1002/ana.21224

Gur, M., & Snodderly, D. M. (2007). Direction selectivity in V1 of alert monkeys: Evidence for parallel pathways for motion processing. *The Journal of Physiology*, *585*(Pt 2), Article Pt 2. https://doi.org/10.1113/jphysiol.2007.143040

Harting, J. K., Huerta, M. F., Hashikawa, T., & van Lieshout, D. P. (1991). Projection of the mammalian superior colliculus upon the dorsal lateral geniculate nucleus: Organization of tectogeniculate pathways in nineteen species. *The Journal of Comparative Neurology*, *304*(2), 275–306. https://doi.org/10.1002/cne.903040210

Hendrickson, A. E., Wilson, J. R., & Ogren, M. P. (1978). The neuroanatomical organization of pathways between the dorsal lateral geniculate nucleus and visual cortex in Old World and New World primates. *The Journal of Comparative Neurology*, *182*(1), 123–136. https://doi.org/10.1002/cne.901820108

Hendry, S. H., Huntsman, M. M., Vinuela, A., Mohler, H., Blas, A. de, & Jones, E. G. (1994). GABAA receptor subunit immunoreactivity in primate visual cortex: Distribution in macaques and humans and regulation by visual input in adulthood. *Journal of Neuroscience*, *14*(4), 2383–2401. https://doi.org/10.1523/JNEUROSCI.14-04-02383.1994

Herculano-Houzel, S. (2009). The Human Brain in Numbers: A Linearly Scaled-up Primate Brain. *Frontiers in Human Neuroscience*, *3*, 31. https://doi.org/10.3389/neuro.09.031.2009

Hluštík, P., Noll, D. C., & Small, S. L. (1998). Suppression of Vascular Artifacts in Functional Magnetic Resonance Images Using MR Angiograms. *NeuroImage*, *7*(3), 224–231. https://doi.org/10.1006/nimg.1998.0320

H.M.S.C. (1986). *Animals (Scientific Procedures) Act 1986*. https://www.animallaw.info/sites/default/files/Animals%20%28Scientific%20Procedures%29%20Act%201986.pdf

Holmes, G. (1918). Disturbances of vision by cerebral lesions. *The British Journal of Ophthalmology*, *2*(7), 353–384.

Honey, C. J., Sporns, O., Cammoun, L., Gigandet, X., Thiran, J. P., Meuli, R., & Hagmann, P. (2009). Predicting human resting-state functional connectivity from structural connectivity. *Proceedings of the National Academy of Sciences of the United States of America*, *106*(6), 2035–2040. https://doi.org/10.1073/pnas.0811168106

Hori, Y., Schaeffer, D. J., Gilbert, K. M., Hayrynen, L. K., Cléry, J. C., Gati, J. S., Menon, R. S., & Everling, S. (2020). Altered Resting-State Functional Connectivity Between Awake and Isoflurane Anesthetized Marmosets. *Cerebral Cortex*, *30*(11), Article 11. https://doi.org/10.1093/cercor/bhaa168

Horwitz, G. D., & Hass, C. A. (2012). Nonlinear analysis of macaque V1 color tuning reveals cardinal directions for cortical color processing. *Nature Neuroscience*, *15*(6), Article 6. https://doi.org/10.1038/nn.3105

Howells, H., Simone, L., Borra, E., Fornia, L., Cerri, G., & Luppino, G. (2020). Reproducing macaque lateral grasping and oculomotor networks using resting state functional

connectivity and diffusion tractography. *Brain Structure and Function*, *225*(8), Article 8. https://doi.org/10.1007/s00429-020-02142-2

Hu, L., Zhang, L., Chen, R., Yu, H., Li, H., & Mouraux, A. (2015). The primary somatosensory cortex and the insula contribute differently to the processing of transient and sustained nociceptive and non-nociceptive somatosensory inputs. *Human Brain Mapping*, *36*(11), Article 11. https://doi.org/10.1002/hbm.22922

Hubel, D. H., & Wiesel, T. N. (1959). Receptive fields of single neurones in the cat's striate cortex. *The Journal of Physiology*, *148*(3), Article 3.

Hubel, D. H., & Wiesel, T. N. (1962). Receptive fields, binocular interaction and functional architecture in the cat's visual cortex. *The Journal of Physiology*, *160*(1), 106-154.2.

Hubel, D. H., & Wiesel, T. N. (1972). Laminar and columnar distribution of geniculo-cortical fibers in the macaque monkey. *The Journal of Comparative Neurology*, *146*(4), 421–450. https://doi.org/10.1002/cne.901460402

Hubel, D. H., & Wiesel, T. N. (1974). Uniformity of monkey striate cortex: A parallel relationship between field size, scatter, and magnification factor. *The Journal of Comparative Neurology*, *158*(3), Article 3. https://doi.org/10.1002/cne.901580305

Hubel, D. H., Wiesel, T. N., & Stryker, M. P. (1977). Orientation columns in macaque monkey visual cortex demonstrated by the 2-deoxyglucose autoradiographic technique. *Nature*, *269*(5626), Article 5626. https://doi.org/10.1038/269328a0

Huda, R., Sipe, G. O., Breton-Provencher, V., Cruz, K. G., Pho, G. N., Adam, E., Gunter, L. M., Sullins, A., Wickersham, I. R., & Sur, M. (2020). Distinct prefrontal top-down circuits differentially modulate sensorimotor behavior. *Nature Communications*, *11*(1), Article 1. https://doi.org/10.1038/s41467-020-19772-z

Hudetz, A. G. (2012). General anesthesia and human brain connectivity. *Brain Connectivity*,

2(6), 291–302. PubMed. https://doi.org/10.1089/brain.2012.0107

Hudson, A. E., Herold, K. F., & Hemmings, H. C. (2013). Pharmacology of Inhaled Anesthetics. In *Pharmacology of Inhaled Anesthetics*. Elsevier. https://doi.org/10.1016/B978-1-4377-1679-5.00010-7

Huerta, M. F., Krubitzer, L. A., & Kaas, J. H. (1986). Frontal eye field as defined by intracortical microstimulation in squirrel monkeys, owl monkeys, and macaque monkeys: I. Subcortical connections. *Journal of Comparative Neurology*, *253*(4), Article 4. https://doi.org/10.1002/cne.902530402

Huff, T., Mahabadi, N., & Tadi, P. (2022). Neuroanatomy, Visual Cortex. In *StatPearls*. StatPearls Publishing. http://www.ncbi.nlm.nih.gov/books/NBK482504/

Humayun S., Weiland James D., Fujiia Gildo Y, Greenberg Robert, Williamson Richard, Little Jim, Mech Brian, Cimmarusti Valerie, Van Boemel Gretchen, Dagnelie Gislin, & de Juan Eugene Jr. (2003). Visual perception in a blind subject with a chronic microelectronic retinal prosthesis. *Vision Research*, *43*, 2573–2581.

Humphrey, N. K. (1974). Vision in a monkey without striate cortex: A case study. *Perception*, *3*(3), 241–255. https://doi.org/10.1068/p030241

Humphrey, N. K., & Weiskrantz, L. (1967). Vision in Monkeys after Removal of the Striate Cortex. *Nature*, *215*(5101), Article 5101. https://doi.org/10.1038/215595a0

Hutchison, R. M., & Everling, S. (2012). Monkey in the middle: Why non-human primates are needed to bridge the gap in resting-state investigations. *Frontiers in Neuroanatomy*, *0*. https://doi.org/10.3389/fnana.2012.00029

Hutchison, R. M., Gallivan, J. P., Culham, J. C., Gati, J. S., Menon, R. S., & Everling, S. (2012). Functional connectivity of the frontal eye fields in humans and macaque monkeys investigated with resting-state fMRI. *Journal of Neurophysiology*, *107*(9), Article 9.

https://doi.org/10.1152/jn.00891.2011

Hutchison, R. M., Hutchison, M., Manning, K. Y., Menon, R. S., & Everling, S. (2014). Isoflurane induces dose-dependent alterations in the cortical connectivity profiles and dynamic properties of the brain's functional architecture. *Human Brain Mapping*, *35*(12), 5754–5775. https://doi.org/10.1002/hbm.22583

Hutchison, R. M., Womelsdorf, T., Gati, J. S., Everling, S., & Menon, R. S. (2013). Resting-State Networks Show Dynamic Functional Connectivity in Awake Humans and Anesthetized Macaques. *Human Brain Mapping*, *34*, 2154–2177.

Huttenlocher, P. R., & de Courten, C. (1987). The development of synapses in striate cortex of man. *Human Neurobiology*, *6*(1), 1–9.

Hyvärinen, A., & Oja, E. (2000). Independent component analysis: Algorithms and applications. *Neural Networks : The Official Journal of the International Neural Network Society*, *13*(4–5), 411–430. https://doi.org/10.1016/s0893-6080(00)00026-5

IBM SPSS Statistics for Windows (Version 27.0). (2020). [Computer software]. IBM Corp.

Itaya, S. K., & Van Hoesen, G. W. (1983). Retinal projections to the inferior and medial pulvinar nuclei in the old-world monkey. *Brain Research*, *269*(2), 223–230. https://doi.org/10.1016/0006-8993(83)90131-2

Jacobs, G. H. (1996). Primate photopigments and primate color vision. *Proceedings of the National Academy of Sciences*, *93*(2), 577–581. https://doi.org/10.1073/pnas.93.2.577

Jafri, M. J., Pearlson, G. D., Stevens, M., & Calhoun, V. D. (2008). A method for functional network connectivity among spatially independent resting-state components in schizophrenia. *NeuroImage*, *39*(4), Article 4. https://doi.org/10.1016/j.neuroimage.2007.11.001

Jeffs, J., Federer, F., Ichida, J. M., & Angelucci, A. (2013). High-resolution mapping of anatomical connections in marmoset extrastriate cortex reveals a complete representation of the visual field bordering dorsal V2. *Cerebral Cortex (New York, N.Y.: 1991)*, *23*(5), Article 5. https://doi.org/10.1093/cercor/bhs088

Jenkins, A., Franks, N. P., & Lieb, W. R. (1999). Effects of temperature and volatile anesthetics on GABA(A) receptors. *Anesthesiology*, *90*(2), Article 2. https://doi.org/10.1097/00000542-199902000-00024

Jenkinson, M., Bannister, P., Brady, M., & Smith, S. (2002). Improved optimization for the robust and accurate linear registration and motion correction of brain images. *NeuroImage*, *17*(2), 825–841. https://doi.org/10.1016/s1053-8119(02)91132-8

Jenkinson, M., Beckmann, C. F., Behrens, T. E. J., Woolrich, M. W., & Smith, S. M. (2012). FSL. *NeuroImage*, *62*(2), 782–790. https://doi.org/10.1016/j.neuroimage.2011.09.015

Jenkinson, M., & Smith, S. (2001). A global optimisation method for robust affine registration of brain images. *Medical Image Analysis*, *5*(2), 143–156. https://doi.org/10.1016/s1361-8415(01)00036-6

Jonckers, E., Delgado y Palacios, R., Shah, D., Guglielmetti, C., Verhoye, M., & Van der Linden, A. (2014). Different anesthesia regimes modulate the functional connectivity outcome in mice. *Magnetic Resonance in Medicine*, *72*(4), Article 4. https://doi.org/10.1002/mrm.24990

Jones, D. K., Simmons, A., Williams, S. C. R., & Horsfield, M. A. (1999). Non-invasive assessment of axonal fiber connectivity in the human brain via diffusion tensor MRI. *Magnetic Resonance in Medicine*, *42*(1), 37–41. https://doi.org/10.1002/(SICI)1522-2594(199907)42:1<37::AID-MRM7>3.0.CO;2-O

Jurd, R., Arras, M., Lambert, S., Drexler, B., Siegwart, R., Crestani, F., Zaugg, M., Vogt, K. E.,

Ledermann, B., Antkowiak, B., & Rudolph, U. (2003). General anesthetic actions in vivo strongly attenuated by a point mutation in the GABA(A) receptor beta3 subunit. *FASEB Journal : Official Publication of the Federation of American Societies for Experimental Biology*, *17*(2), 250–252. https://doi.org/10.1096/fj.02-0611fje

Kaas, J. H., & Lyon, D. C. (2007). Pulvinar contributions to the dorsal and ventral streams of visual processing in primates. *Brain Research Reviews*, *55*(2), 285–296. https://doi.org/10.1016/j.brainresrev.2007.02.008

Kato, R., Takaura, K., Ikeda, T., Yoshida, M., & Isa, T. (2011). Contribution of the retino-tectal pathway to visually guided saccades after lesion of the primary visual cortex in monkeys. *European Journal of Neuroscience*, *33*(11), 1952–1960. https://doi.org/10.1111/j.1460-9568.2011.07729.x

Kaushal, M., Oni-Orisan, A., Chen, G., Li, W., Leschke, J., Ward, D., Kalinosky, B., Budde, M., Schmit, B., Li, S.-J., Muqeet, V., & Kurpad, S. (2017). Large-Scale Network Analysis of Whole-Brain Resting-State Functional Connectivity in Spinal Cord Injury: A Comparative Study. *Brain Connectivity*, *7*(7), 413–423. https://doi.org/10.1089/brain.2016.0468

Kinoshita, M., Kato, R., Isa, K., Kobayashi, K., Kobayashi, K., Onoe, H., & Isa, T. (2019). Dissecting the circuit for blindsight to reveal the critical role of pulvinar and superior colliculus. *Nature Communications*, *10*(1), Article 1. https://doi.org/10.1038/s41467-018-08058-0

Kleiser, R., Wittsack, J., Niedeggen, M., Goebel, R., & Stoerig, P. (2001). Is V1 Necessary for Conscious Vision in Areas of Relative Cortical Blindness? *NeuroImage*, *13*(4), 654–661. https://doi.org/10.1006/nimg.2000.0720

Knill, R. L., Kieraszewicz, H. T., Dodgson, B. G., & Clement, J. L. (1983). Chemical regulation of

ventilation during isoflurane sedation and anaesthesia in humans. *Canadian Anaesthetists' Society Journal*, *30*(6), 607–614. https://doi.org/10.1007/BF03015231

Konoike, N., Iwaoki, H., & Nakamura, K. (2020). Potent and Quick Responses to Conspecific Faces and Snakes in the Anterior Cingulate Cortex of Monkeys. *Frontiers in Behavioral Neuroscience*, *14*, 156. https://doi.org/10.3389/fnbeh.2020.00156

Kristensson, K., & Olsson, Y. (1971). Retrograde axonal transport of protein. *Brain Research*, *29*(2), 363–365. https://doi.org/10.1016/0006-8993(71)90044-8

Krubitzer, L. A., & Kass, J. H. (1990). Cortical connections of MT in four species of primates: Areal, modular, and retinotopic patterns. *Visual Neuroscience*, *5*(2), 165–204. Cambridge Core. https://doi.org/10.1017/S0952523800000213

Künzle, H., & Akert, K. (1977). Efferent connections of cortical, area 8 (frontal eye field) in Macaca fascicularis. A reinvestigation using the autoradiographic technique. *Journal of Comparative Neurology*, *173*(1), Article 1. https://doi.org/10.1002/cne.901730108

Le Bihan, D., & Breton, E. (1985). Imagerie de diffusion in-vivo par résonance magnétique nucléaire. *Comptes-Rendus de l'Académie Des Sciences*, *93*(5), 27–34.

Lee, A. C. H., Bussey, T. J., Murray, E. A., Saksida, L. M., Epstein, R. A., Kapur, N., Hodges, J. R., & Graham, K. S. (2005). Perceptual deficits in amnesia: Challenging the medial temporal lobe 'mnemonic' view. *Neuropsychologia*, *43*(1), 1–11. https://doi.org/10.1016/j.neuropsychologia.2004.07.017

Lee, U., & Mashour, G. A. (2018). Role of Network Science in the Study of Anesthetic State Transitions. *Anesthesiology*, *129*(5), Article 5. https://doi.org/10.1097/ALN.0000000000002228

Leh, S. E., Johansen-Berg, H., & Ptito, A. (2006). Unconscious vision: New insights into the neuronal correlate of blindsight using diffusion tractography. *Brain*, *129*(7), 1822–

1832. https://doi.org/10.1093/brain/awl111

Leichnetz, G. R., Spencer, R. F., Hardy, S. G. P., & Astruc, J. (1981). The prefrontal corticotectal projection in the monkey; An anterograde and retrograde horseradish peroxidase study. *Neuroscience*, *6*(6), Article 6. https://doi.org/10.1016/0306-4522(81)90068-3

Lennie, P., Krauskopf, J., & Sclar, G. (1990). Chromatic mechanisms in striate cortex of macaque. *The Journal of Neuroscience*, *10*(2), 649–669. https://doi.org/10.1523/JNEUROSCI.10-02-00649.1990

Leopold, D. A. (2012). Primary visual cortex, awareness and blindsight. *Annual Review of Neuroscience*, *35*, 91–109. https://doi.org/10.1146/annurev-neuro-062111-150356

Lin, C.-S., & Kaas, J. H. (1980). Projections from the medial nucleus of the inferior pulvinar complex to the middle temporal area of the visual cortex. *Neuroscience*, *5*(12), 2219–2228. https://doi.org/10.1016/0306-4522(80)90138-4

Liu, R., Ueda, M., Okazaki, N., & Ishibe, Y. (2001). Role of Potassium Channels in Isoflurane- and Sevoflurane-induced Attenuation of Hypoxic Pulmonary Vasoconstriction in Isolated Perfused Rabbit Lungs. *Anesthesiology*, *95*(4), Article 4. https://doi.org/10.1097/00000542-200110000-00024

Liu, Y., Yu, C., Liang, M., Li, J., Tian, L., Zhou, Y., Qin, W., Li, K., & Jiang, T. (2007). Whole brain functional connectivity in the early blind. *Brain*, *130*(8), Article 8. https://doi.org/10.1093/brain/awm121

Livingstone, M., & Hubel, D. H. (1987). Psychophysical evidence for separate channels for the perception of form, color, movement, and depth. *The Journal of Neuroscience*, *7*(11), Article 11. https://doi.org/10.1523/JNEUROSCI.07-11-03416.1987

Lobo, S. A., Ojeda, J., Dua, A., Singh, K., & Lopez, J. (2022). Minimum Alveolar Concentration. In *StatPearls*. StatPearls Publishing.

https://www.ncbi.nlm.nih.gov/books/NBK532974/

Logothetis, N. K., Pauls, J., Augath, M., Trinath, T., & Oeltermann, A. (2001). Neurophysiological investigation of the basis of the fMRI signal. *Nature*, *412*, 150–157.

Lopez-Barneo, J., Pardal, R., & Ortega-Saenz, P. (2001). Cellular Mechanisms of Oxygen Sensing. *Annual Review of Physiology*, *63*, 259.

Lowe, M. J., Phillips, M. D., Lurito, J. T., Mattson, D., Dzemidzic, M., & Mathews, V. P. (2002). Multiple Sclerosis: Low-Frequency Temporal Blood Oxygen Level–Dependent Fluctuations Indicate Reduced Functional Connectivity—Initial Results. *Radiology*, *224*(1), Article 1. https://doi.org/10.1148/radiol.2241011005

Lund, J. S. (1973). Organization of neurons in the visual cortex, area 17, of the monkey (Macaca mulatta). *Journal of Comparative Neurology*, *147*(4), 455–495. https://doi.org/10.1002/cne.901470404

Lund, J. S. (1988). Anatomical organization of macaque monkey striate visual cortex. *Annual Review of Neuroscience*, *11*, 253–288. https://doi.org/10.1146/annurev.ne.11.030188.001345

Lund, J. S., Lund, R. D., Hendrickson, A. E., Bunt, A. H., & Fuchs, A. F. (1975). The origin of efferent pathways from the primary visual cortex, area 17, of the macaque monkey as shown by retrograde transport of horseradish peroxidase. *The Journal of Comparative Neurology*, *164*(3), Article 3. https://doi.org/10.1002/cne.901640303

Lv, P., Xiao, Y., Liu, B., Wang, Y., Zhang, X., Sun, H., Li, F., Yao, L., Zhang, W., Liu, L., Gao, X., Wu, M., Tang, Y., Chen, Q., Gong, Q., & Lui, S. (2016). Dose-dependent effects of isoflurane on regional activity and neural network function: A resting-state fMRI study of 14 rhesus monkeys: An observational study. *Neuroscience Letters*, *611*, 116–122. https://doi.org/10.1016/j.neulet.2015.11.037

Lynch, J. C., Hoover, J. E., & Strick, P. L. (1994). Input to the primate frontal eye field from the substantia nigra, superior colliculus, and dentate nucleus demonstrated by transneuronal transport. *Experimental Brain Research*, *100*(1), Article 1. https://doi.org/10.1007/BF00227293

Lynch, J. C., & Tian, J.-R. (2006). Cortico-cortical networks and cortico-subcortical loops for the higher control of eye movements. *Progress in Brain Research*, *151*, 461–501. https://doi.org/10.1016/S0079-6123(05)51015-X

Lyon, D. C., & Connolly, J. D. (2012). The case for primate V3. *Proceedings of the Royal Society B: Biological Sciences*, *279*(1729), Article 1729. https://doi.org/10.1098/rspb.2011.2048

Lyon, D. C., & Kaas, J. H. (2001). Connectional and Architectonic Evidence for Dorsal and Ventral V3, and Dorsomedial Area in Marmoset Monkeys. *Journal of Neuroscience*, *21*(1), Article 1. https://doi.org/10.1523/JNEUROSCI.21-01-00249.2001

Lyon, D. C., Nassi, J. J., & Callaway, E. M. (2010). A disynaptic relay from superior colliculus to dorsal stream visual cortex in macaque monkey. *Neuron*, *65*(2), 270–279. https://doi.org/10.1016/j.neuron.2010.01.003

Ma, N., Liu, Y., Li, N., Wang, C.-X., Zhang, H., Jiang, X.-F., Xu, H.-S., Fu, X.-M., Hu, X., & Zhang, D.-R. (2010). Addiction related alteration in resting-state brain connectivity. *NeuroImage*, *49*(1), 738–744. https://doi.org/10.1016/j.neuroimage.2009.08.037

Macko, K. A., Jarvis, C. D., Kennedy, C., Miyaoka, M., Shinohara, M., Sololoff, L., & Mishkin, M. (1982). Mapping the Primate Visual System with [2-14C]Deoxyglucose. *Science*, *218*(4570), 394–397. https://doi.org/10.1126/science.7123241

Makin, T., Amoruso, E., Arribas, M., Buehler, S., Dowdall, L., Kieliba, P., Kop, B., Thomas Kollamkulam, M., Schone, H., Kromm, M., Maimon-Mor, R., Sanchez, M., Muret, D.,

Ozdemir, I., & Root, V. (2020). *Phantom limbs and brain plasticity in amputees*. https://doi.org/10.1093/acrefore/9780190264086.013.50

Maniglia, M., Trotter, Y., & Aedo-Jury, F. (2019). TMS reveals inhibitory extrastriate cortico-cortical feedback modulation of V1 activity in humans. *Brain Structure and Function*, *224*(9), 3399–3408. https://doi.org/10.1007/s00429-019-01964-z

Mantini, D., Gerits, A., Nelissen, K., Durand, J.-B., Joly, O., Simone, L., Sawamura, H., Wardak, C., Orban, G. A., Buckner, R. L., & Vanduffel, W. (2011). *Default Mode of Brain Function in Monkeys* (36). *31*(36), Article 36.

Marcus, D. S., & Van Essen, D. C. (2002). Scene segmentation and attention in primate cortical areas V1 and V2. *Journal of Neurophysiology*, *88*(5), Article 5. https://doi.org/10.1152/jn.00916.2001

Margulies, D. S., Vincent, J. L., Kelly, C., Lohmann, G., Uddin, L. Q., Biswal, B. B., Villringer, A., Castellanos, F. X., Milham, M. P., & Petrides, M. (2009). Precuneus shares intrinsic functional architecture in humans and monkeys. *Proceedings of the National Academy of Sciences*, *106*(47), 20069. https://doi.org/10.1073/pnas.0905314106

Mars, R. B., Jbabdi, S., Sallet, J., O'Reilly, J. X., Croxson, P. L., Olivier, E., Noonan, M. P., Bergmann, C., Mitchell, A. S., Baxter, M. G., Behrens, T. E. J., Johansen-Berg, H., Tomassini, V., Miller, K. L., & Rushworth, M. F. S. (2011). Diffusion-Weighted Imaging Tractography-Based Parcellation of the Human Parietal Cortex and Comparison with Human and Macaque Resting-State Functional Connectivity. *The Journal of Neuroscience*, *31*(11), 4087. https://doi.org/10.1523/JNEUROSCI.5102-10.2011

Martuzzi, R., Ramani, R., Qiu, M., Rajeevan, N., & Constable, R. T. (2010a). Functional connectivity and alterations in baseline brain state in humans. *NeuroImage*, *49*(1), Article 1. https://doi.org/10.1016/j.neuroimage.2009.07.028

Mashour, G. A., & Alkire, M. T. (2013). Consciousness, Anesthesia, and the Thalamocortical System. *Anesthesiology*, *118*(1), Article 1. https://doi.org/10.1097/ALN.0b013e318277a9c6

Masland, R. H. (2012). The neuronal organization of the retina. *Neuron*, *76*(2), 266–280. PubMed. https://doi.org/10.1016/j.neuron.2012.10.002

Mason, S., Premereur, E., Pelekanos, V., Emberton, A., Honess, P., & Mitchell, A. S. (2019). Effective chair training methods for neuroscience research involving rhesus macaques (Macaca mulatta). *Journal of Neuroscience Methods*, *317*, 82–93. https://doi.org/10.1016/j.jneumeth.2019.02.001

MATLAB (Version 2017b). (2017). [Computer software]. The Math Works, Inc.

Matute, C., & Ransom, B. R. (2012). Roles of white matter in central nervous system pathophysiologies. *ASN NEURO*, *4*(2), e00079. https://doi.org/10.1042/AN20110060

Maunsell, J. H., & Newsome, W. T. (1987). Visual processing in monkey extrastriate cortex. *Annual Review of Neuroscience*, *10*, 363–401. https://doi.org/10.1146/annurev.ne.10.030187.002051

Maunsell, J. H., & Van Essen, D. C. (1983). Functional properties of neurons in middle temporal visual area of the macaque monkey. I. Selectivity for stimulus direction, speed, and orientation. *Journal of Neurophysiology*, *49*(5), 1127–1147. https://doi.org/10.1152/jn.1983.49.5.1127

May, J. G., & Andersen, R. A. (1986). Different patterns of corticopontine projections from separate cortical fields within the inferior parietal lobule and dorsal prelunate gyrus of the macaque. *Experimental Brain Research*, *63*(2), 265–278. https://doi.org/10.1007/BF00236844

McFarland, N. R., & Haber, S. N. (2002). Thalamic relay nuclei of the basal ganglia form both

reciprocal and nonreciprocal cortical connections, linking multiple frontal cortical areas. *The Journal of Neuroscience: The Official Journal of the Society for Neuroscience*, *22*(18), Article 18.

McKeown, M. J., Makeig, S., Brown, G. G., Jung, T. P., Kindermann, S. S., Bell, A. J., & Sejnowski, T. J. (1998). Analysis of fMRI data by blind separation into independent spatial components. *Human Brain Mapping*, *6*(3), 160–188. https://doi.org/10.1002/(SICI)1097-0193(1998)6:3<160::AID-HBM5>3.0.CO;2-1

Merabet, L. B., & Pascual-Leone, A. (2010). Neural reorganization following sensory loss: The opportunity of change. *Nature Reviews Neuroscience*, *11*(1), Article 1. https://doi.org/10.1038/nrn2758

Meunier, D., Achard, S., Morcom, A., & Bullmore, E. (2009). Age-related changes in modular organization of human brain functional networks. *NeuroImage*, *44*(3), 715–723. https://doi.org/10.1016/j.neuroimage.2008.09.062

Mhuircheartaigh, R. N., Rosenorn-Lanng, D., Wise, R., Jbabdi, S., Rogers, R., & Tracey, I. (2010). Cortical and Subcortical Connectivity Changes during Decreasing Levels of Consciousness in Humans: A Functional Magnetic Resonance Imaging Study using Propofol. *The Journal of Neuroscience*, *30*(27), 9095–9102. https://doi.org/10.1523/JNEUROSCI.5516-09.2010

Miller, R. D., Eriksson, L., Fleisher, L., Wiener-Kronish, J., Cohen, N., & Young, N. (2015). *Anesthesia. 8th Edition* (Philadelphia, PA : Elsevier/Saunders).

Mion, G., & Villevieille, T. (2013). Ketamine Pharmacology: An Update (Pharmacodynamics and Molecular Aspects, Recent Findings). *CNS Neuroscience & Therapeutics*, *19*(6), Article 6. https://doi.org/10.1111/cns.12099

Miranda-Dominguez, O., Mills, B. D., Grayson, D., Woodall, A., Grant, K. A., Kroenke, C. D., & Fair, D. A. (2014). Bridging the Gap between the Human and Macaque Connectome: A Quantitative Comparison of Global Interspecies Structure-Function Relationships and Network Topology. *The Journal of Neuroscience*, *34*(16), 5552–5563. https://doi.org/10.1523/JNEUROSCI.4229-13.2014

Mishkin, M., Ungerleider, L. G., & Macko, K. A. (1983). Object vision and spatial vision: Two cortical pathways. *Trends in Neurosciences*, *6*, 414–417. https://doi.org/10.1016/0166-2236(83)90190-X

Moeller, S., Nallasamy, N., Tsao, D. Y., & Freiwald, W. A. (2009). Functional connectivity of the macaque brain across stimulus and arousal states. *The Journal of Neuroscience : The Official Journal of the Society for Neuroscience*, *29*(18), Article 18. PubMed. https://doi.org/10.1523/JNEUROSCI.0220-09.2009

Mohammadi, B., Kollewe, K., Samii, A., Krampfl, K., Dengler, R., & Münte, T. F. (2009). Changes of resting state brain networks in amyotrophic lateral sclerosis. *Experimental Neurology*, *217*(1), Article 1. https://doi.org/10.1016/j.expneurol.2009.01.025

Monk, C. S., Peltier, S. J., Wiggins, J. L., Weng, S.-J., Carrasco, M., Risi, S., & Lord, C. (2009). Abnormalities of intrinsic functional connectivity in autism spectrum disorders,. *NeuroImage*, *47*(2), Article 2. https://doi.org/10.1016/j.neuroimage.2009.04.069

Moore, T., Rodman, H. R., Repp, A. B., & Gross, C. G. (1995). Localization of visual stimuli after striate cortex damage in monkeys: Parallels with human blindsight. *Proceedings of the National Academy of Sciences*, *92*(18), 8215–8218. https://doi.org/10.1073/pnas.92.18.8215

Movshon, J. A., Thompson, I. D., & Tolhurst, D. J. (1978). Spatial and temporal contrast sensitivity of neurones in areas 17 and 18 of the cat's visual cortex. *The Journal of*

Physiology, *283*, 101–120. https://doi.org/10.1113/jphysiol.1978.sp012490

Mundinano, I.-C., Kwan, W. C., & Bourne, J. A. (2015). Mapping the mosaic sequence of primate visual cortical development. *Frontiers in Neuroanatomy*, *9*, 132. https://doi.org/10.3389/fnana.2015.00132

Murphy, K., Birn, R. M., Handwerker, D. A., Jones, T. B., & Bandettini, P. A. (2009). The impact of global signal regression on resting state correlations: Are anti-correlated networks introduced? *NeuroImage*, *44*(3), 893–905. https://doi.org/10.1016/j.neuroimage.2008.09.036

Muta, K., Hata, J., Kawaguchi, N., Haga, Y., Yoshimaru, D., Hagiya, K., Kaneko, T., Miyabe-Nishiwaki, T., Komaki, Y., Seki, F., Okano, H. J., & Okano, H. (2022). Effect of sedatives or anesthetics on the measurement of resting brain function in common marmosets. *Cerebral Cortex*, bhac406. https://doi.org/10.1093/cercor/bhac406

Nakagawa, S., & Tanaka, S. (1984). Retinal projections to the pulvinar nucleus of the macaque monkey: A re-investigation using autoradiography. *Experimental Brain Research*, *57*(1), 151–157. https://doi.org/10.1007/BF00231141

Nallasamy, N., & Tsao, D. Y. (2011). Functional Connectivity in the Brain: Effects of Anesthesia. *The Neuroscientist*, *17*(1), 94–106. https://doi.org/10.1177/1073858410374126

Nassi, J. J., Lyon, D. C., & Callaway, E. M. (2006). The parvocellular LGN provides a robust disynaptic input to the visual motion area MT. *Neuron*, *50*(2), 319–327. https://doi.org/10.1016/j.neuron.2006.03.019

Nelissen, K., Borra, E., Gerbella, M., Rozzi, S., Luppino, G., Vanduffel, W., Rizzolatti, G., & Orban, G. A. (2011). Action Observation Circuits in the Macaque Monkey Cortex. *Journal of Neuroscience*, *31*(10), Article 10. https://doi.org/10.1523/JNEUROSCI.4803-10.2011

Nichols, T. E., & Holmes, A. P. (2001). Nonparametric permutation tests for functional neuroimaging: A primer with examples. *Human Brain Mapping*, *15*(1), 1–25. https://doi.org/10.1002/hbm.1058

Nickerson, L. D., Smith, S. M., Ongur, D., & Beckmann, C. F. (2017). Using Dual Regression to Investigate Network Shape and Amplitude in Functional Connectivity Analyses. *Frontiers in Neuroscience*, *11*, 115. https://doi.org/10.3389/fnins.2017.00115

Niu, B., Xiao, J., Fang, Y., Zhou, B., Li, J., Cao, F., Tian, Y., & Mei, W. (2017). Sevoflurane-induced isoelectric EEG and burst suppression: Differential and antagonistic effect of added nitrous oxide. *Anaesthesia*, *72*. https://doi.org/10.1111/anae.13843

Noble, S., Scheinost, D., & Constable, R. T. (2020). Cluster failure or power failure? Evaluating sensitivity in cluster-level inference. *NeuroImage*, *209*, 116468. https://doi.org/10.1016/j.neuroimage.2019.116468

Nyquist, J. B., Lappin, J. S., Zhang, R., & Tadin, D. (2016). Perceptual training yields rapid improvements in visually impaired youth. *Scientific Reports*, *6*(1), Article 1. https://doi.org/10.1038/srep37431

O'Brien, B. J., Abel, P. L., & Olavarria, J. F. (2001). The retinal input to calbindin-D28k-defined subdivisions in macaque inferior pulvinar. *Neuroscience Letters*, *312*(3), 145–148. https://doi.org/10.1016/s0304-3940(01)02220-0

O'Reilly, J. X., Croxson, P. L., Jbabdi, S., Sallet, J., Noonan, M. P., Mars, R. B., Browning, P. G. F., Wilson, C. R. E., Mitchell, A. S., Miller, K. L., Rushworth, M. F. S., & Baxter, M. G. (2013). Causal effect of disconnection lesions on interhemispheric functional connectivity in rhesus monkeys. *Proceedings of the National Academy of Sciences of the United States of America*, *110*(34), 13982–13987. https://doi.org/10.1073/pnas.1305062110

Paasonen, J., Stenroos, P., Salo, R. A., Kiviniemi, V., & Gröhn, O. (2018). Functional connectivity under six anesthesia protocols and the awake condition in rat brain. *NeuroImage*, *172*, 9–20. https://doi.org/10.1016/j.neuroimage.2018.01.014

Pandit, J. J., & Buckler, K. J. (2009). Differential effects of halothane and sevoflurane on hypoxia-induced intracellular calcium transients of neonatal rat carotid body type I cells†. *British Journal of Anaesthesia*, *103*(5), 701–710. https://doi.org/10.1093/bja/aep223

Pandit, J. J., Winter, V., Bayliss, R., & Buckler, K. J. (2010). Differential Effects of Halothane and Isoflurane on Carotid Body Glomus Cell Intracellular Ca2+ and Background K+ Channel Responses to Hypoxia. In I. Homma, H. Onimaru, & Y. Fukuchi (Eds.), *New Frontiers in Respiratory Control* (pp. 205–208). Springer. https://doi.org/10.1007/978-1-4419-5692-7_41

Parker, A. J., Smith, J. E. T., & Krug, K. (2016). Neural architectures for stereo vision. *Philosophical Transactions of the Royal Society of London Series B, Biological Sciences*, *371*(1697), 20150261. https://doi.org/10.1098/rstb.2015.0261

Passingham, R. E., Stephan, K. E., & Kötter, R. (2002). The anatomical basis of functional localization in the cortex. *Nature Reviews Neuroscience*, *3*(8), Article 8. https://doi.org/10.1038/nrn893

Peltier, S. J., Kerssen, C., Hamann, S. B., Sebel, P. S., Byas-Smith, M., & Hu, X. (2005). Functional connectivity changes with concentration of sevoflurane anesthesia. *NeuroReport*, *18*(3), Article 3.

Perkel, D. J., Bullier, J., & Kennedy, H. (1986a). Topography of the afferent connectivity of area 17 in the macaque monkey: A double-labelling study. *Journal of Comparative Neurology*, *253*(3), 374–402. https://doi.org/10.1002/cne.902530307

Perry, V. H., & Cowey, A. (1984). Retinal ganglion cells that project to the superior colliculus and pretectum in the macaque monkey. *Neuroscience*, *12*(4), 1125–1137. https://doi.org/10.1016/0306-4522(84)90007-1

Pezzullo, L., Streatfeild, J., Simkiss, P., & Shickle, D. (2018). The economic impact of sight loss and blindness in the UK adult population. *BMC Health Services Research*, *18*, 63. https://doi.org/10.1186/s12913-018-2836-0

Ponte, J., & Sadler, C. L. (1989). Effect of halothane, enflurane and isoflurane on carotid body chemoreceptor activity in the rabbit and the cat. *British Journal of Anaesthesia*, *62*(1), 33–40. https://doi.org/10.1093/bja/62.1.33

Pöppel, E., Held, R., & Frost, D. (1973). Residual Visual Function after Brain Wounds involving the Central Visual Pathways in Man. *Nature*, *243*(5405), Article 5405. https://doi.org/10.1038/243295a0

Pouget, P., Stepniewska, I., Crowder, E., Leslie, M., Emeric, E., Nelson, M., & Schall, J. (2009). Visual and motor connectivity and the distribution of calcium-binding proteins in macaque frontal eye field: Implications for saccade target selection. *Frontiers in Neuroanatomy*, *3*. https://www.frontiersin.org/articles/10.3389/neuro.05.002.2009

Price, J. L. (2003). Comparative Aspects of Amygdala Connectivity. *Annals of the New York Academy of Sciences*, *985*(1), 50–58. https://doi.org/10.1111/j.1749-6632.2003.tb07070.x

Pugin, D., Hofmeister, J., Gasche, Y., Vulliemoz, S., Lövblad, K.-O., Ville, D. V. D., & Haller, S. (2020). Resting-State Brain Activity for Early Prediction Outcome in Postanoxic Patients in a Coma with Indeterminate Clinical Prognosis. *American Journal of Neuroradiology*, *41*(6), 1022–1030. https://doi.org/10.3174/ajnr.A6572

Ramnani, N., Behrens, T. E. J., Penny, W., & Matthews, P. M. (2004). New approaches for

exploring anatomical and functional connectivity in the human brain. *Biological Psychiatry*, *56*(9), 613–619. https://doi.org/10.1016/j.biopsych.2004.02.004

Randomise/UserGuide—FslWiki. (2019, April 23). https://fsl.fmrib.ox.ac.uk/fsl/fslwiki/Randomise/UserGuide

Reuter, M., Schmansky, N. J., Rosas, H. D., & Fischl, B. (2012). Within-subject template estimation for unbiased longitudinal image analysis. *NeuroImage*, *61*(4), 1402–1418. https://doi.org/10.1016/j.neuroimage.2012.02.084

Riddoch, G. (1917). Dissociation of visual perceptions due to occipital injuries, with especial reference to appreciation of movement. *Brain*, *40*(1), 15–57. https://doi.org/10.1093/brain/40.1.15

Riecanský, I. (2004). Extrastriate area V5 (MT) and its role in the processing of visual motion. *Ceskoslovenska Fysiologie*, *53*(1), 17–22.

Rodman, H. R., Gross, C. G., & Albright, T. D. (1989). Afferent basis of visual response properties in area MT of the macaque. I. Effects of striate cortex removal. *The Journal of Neuroscience : The Official Journal of the Society for Neuroscience*, *9*(6), 2033–2050. PubMed. https://doi.org/10.1523/JNEUROSCI.09-06-02033.1989

Rodman, H. R., Gross, C. G., & Albright, T. D. (1990). Afferent basis of visual response properties in area MT of the macaque. II. Effects of superior colliculus removal. *Journal of Neuroscience*, *10*(4), 1154–1164. https://doi.org/10.1523/JNEUROSCI.10-04-01154.1990

Rosa, M. G. P., Palmer, S. M., Gamberini, M., Tweedale, R., Piñon, M. C., & Bourne, J. A. (2005). Resolving the organization of the New World monkey third visual complex: The dorsal extrastriate cortex of the marmoset (Callithrix jacchus). *The Journal of Comparative Neurology*, *483*(2), Article 2. https://doi.org/10.1002/cne.20412

Roy, A. K., Shehzad, Z., Margulies, D. S., Kelly, A. M. C., Uddin, L. Q., Gotimer, K., Biswal, B. B., Castellanos, F. X., & Milham, M. P. (2009). Functional Connectivity of the Human Amygdala using Resting State fMRI. *NeuroImage*, *45*(2), 614–626. https://doi.org/10.1016/j.neuroimage.2008.11.030

Saalmann, Y. B., Pigarev, I. N., & Vidyasagar, T. R. (2007). Neural Mechanisms of Visual Attention: How Top-Down Feedback Highlights Relevant Locations. *Science*, *316*(5831), 1612–1615. https://doi.org/10.1126/science.1139140

Saleem, K. S., Avram, A. V., Glen, D., Yen, C. C.-C., Ye, F. Q., Komlosh, M., & Basser, P. J. (2021). High-resolution mapping and digital atlas of subcortical regions in the macaque monkey based on matched MAP-MRI and histology. *NeuroImage*, *245*, 118759. https://doi.org/10.1016/j.neuroimage.2021.118759

Saleem, K. S., & Logothetis, N. K. (2006). *A Combined MRI and Histology Atlas of the Rhesus Monkey Brain in Stereotaxic Coordinates 2nd Edition*. London: Academic Press.

Salimi-Khorshidi, G., Douaud, G., Beckmann, C. F., Glasser, M. F., Griffanti, L., & Smith, S. M. (2014). Automatic denoising of functional MRI data: Combining independent component analysis and hierarchical fusion of classifiers. *NeuroImage*, *90*, 449–468. PubMed. https://doi.org/10.1016/j.neuroimage.2013.11.046

Satterthwaite, T. D., Wolf, D. H., Loughead, J., Ruparel, K., Valdez, J. N., Siegel, S. J., Kohler, C. G., Gur, R. E., & Gur, R. C. (2010). Association of enhanced limbic response to threat with decreased cortical facial recognition memory response in schizophrenia. *The American Journal of Psychiatry*, *167*(4), 418. https://doi.org/10.1176/appi.ajp.2009.09060808

Sawaya, H., Johnson, K., Schmidt, M., Arana, A., Chahine, G., Atoui, M., Pincus, D., George, M. S., Panksepp, J., & Nahas, Z. (2015). Resting-State Functional Connectivity of Antero-

Medial Prefrontal Cortex Sub-Regions in Major Depression and Relationship to Emotional Intelligence. *International Journal of Neuropsychopharmacology*, *18*(6), pyu112. https://doi.org/10.1093/ijnp/pyu112

Schall, J. D. (2009). Frontal Eye Fields. In L. R. Squire (Ed.), *Encyclopedia of Neuroscience* (pp. 367–374). Academic Press. https://doi.org/10.1016/B978-008045046-9.01111-6

Schall, J. D., Hanes, D. P., Thompson, K. G., & King, D. J. (1995). Saccade target selection in frontal eye field of macaque. I. Visual and premovement activation. *Journal of Neuroscience*, *15*(10), Article 10. https://doi.org/10.1523/JNEUROSCI.15-10-06905.1995

Schall, J. D., Morel, A., & Kaas, J. H. (1993). Topography of supplementary eye field afferents to frontal eye field in macaque: Implications for mapping between saccade coordinate systems. *Visual Neuroscience*, *10*(2), 385–393. https://doi.org/10.1017/s0952523800003771

Schmid, M. C., Mrowka, S. W., Turchi, J., Saunders, R. C., Wilke, M., Peters, A. J., Ye, F. Q., & Leopold, D. A. (2010). Blindsight depends on the lateral geniculate nucleus. *Nature*, *466*(7304), 373–377. https://doi.org/10.1038/nature09179

Schmid, M. C., Panagiotaropoulos, T., Augath, M. A., Logothetis, N. K., & Smirnakis, S. M. (2009). Visually Driven Activation in Macaque Areas V2 and V3 without Input from the Primary Visual Cortex. *PLOS ONE*, *4*(5), e5527. https://doi.org/10.1371/journal.pone.0005527

Schwender, D., Daunderer, M., Klasing, S., Finsterer, U., & Peter, K. (1998). Power spectral analysis of the electroencephalogram during increasing end-expiratory concentrations of isoflurane, desflurane and sevoflurane. *Anaesthesia*, *53*(4), Article 4.

Seeley, W. W., Crawford, R. K., Zhou, J., Miller, B. L., & Greicius, M. D. (2009).

Neurodegenerative Diseases Target Large-Scale Human Brain Networks. *Neuron*, *62*(1), Article 1. https://doi.org/10.1016/j.neuron.2009.03.024

Segraves, M. A., & Goldberg, M. E. (1987). Functional properties of corticotectal neurons in the monkey's frontal eye field. *Journal of Neurophysiology*. https://doi.org/10.1152/jn.1987.58.6.1387

Sereno, M. I., & Tootell, R. B. (2005). From monkeys to humans: What do we now know about brain homologies? *Current Opinion in Neurobiology*, *15*(2), 135–144. https://doi.org/10.1016/j.conb.2005.03.014

Setogawa, T., Eldridge, M. A. G., Fomani, G. P., Saunders, R. C., & Richmond, B. J. (2021a). Contributions of the Monkey Inferior Temporal Areas TE and TEO to Visual Categorization. *Cerebral Cortex*, *31*(11), 4891–4900. https://doi.org/10.1093/cercor/bhab129

Shadlen, M. N., & Newsome, W. T. (1996). Motion perception: Seeing and deciding. *Proceedings of the National Academy of Sciences*, *93*(2), 628–633. https://doi.org/10.1073/pnas.93.2.628

Sharpe, J. A. (2014). Eye Movements; Smooth Pursuit. In M. J. Aminoff & R. B. Daroff (Eds.), *Encyclopedia of the Neurological Sciences (Second Edition)* (pp. 252–257). Academic Press. https://doi.org/10.1016/B978-0-12-385157-4.00130-5

Siegle, G. J., Thompson, W., Carter, C. S., Steinhauer, S. R., & Thase, M. E. (2007). Increased Amygdala and Decreased Dorsolateral Prefrontal BOLD Responses in Unipolar Depression: Related and Independent Features. *Biological Psychiatry*, *61*(2), 198–209. https://doi.org/10.1016/j.biopsych.2006.05.048

Sincich, L. C., Park, K. F., Wohlgemuth, M. J., & Horton, J. C. (2004). Bypassing V1: A direct geniculate input to area MT. *Nature Neuroscience*, *7*(10), 1123–1128.

https://doi.org/10.1038/nn1318

Skudlarski, P., Jagannathan, K., Calhoun, V. D., Hampson, M., Skudlarska, B. A., & Pearlson, G. (2008). Measuring Brain Connectivity: Diffusion Tensor Imaging Validates Resting State Temporal Correlations. *NeuroImage*, *43*(3), 554–561. https://doi.org/10.1016/j.neuroimage.2008.07.063

Sloan, M. H., Conard, P. F., Karsunky, P. K., & Gross, J. B. (1996). Sevoflurane Versus Isoflurane: Induction and Recovery Characteristics with Single-Breath Inhaled Inductions of Anesthesia. *Anesthesia & Analgesia*, *82*(3), Article 3. https://journals.lww.com/anesthesia-analgesia/Fulltext/1996/03000/Sevoflurane_Versus_Isoflurane__Induction_and.18.aspx

Slupe, A. M., & Kirsch, J. R. (2018). Effects of anesthesia on cerebral blood flow, metabolism, and neuroprotection. *Journal of Cerebral Blood Flow & Metabolism*, *38*(12), 2192–2208. https://doi.org/10.1177/0271678X18789273

Smith, S. M. (2002). Fast robust automated brain extraction. *Human Brain Mapping*, *17*(3), 143–155. https://doi.org/10.1002/hbm.10062

Smith, S. M., & Nichols, T. E. (2009). Threshold-free cluster enhancement: Addressing problems of smoothing, threshold dependence and localisation in cluster inference. *NeuroImage*, *44*(1), 83–98. https://doi.org/10.1016/j.neuroimage.2008.03.061

Soma, L. R., Tierney, W. J., Hogan, G. K., & Satoh, N. (1995). The Effects of Multiple Administrations of Sevoflurane to Cynomolgus Monkeys: Clinical Pathologic, Hematologic, and Pathologic Study. *Anesthesia & Analgesia*, *81*(2), Article 2. https://journals.lww.com/anesthesia-analgesia/Fulltext/1995/08000/The_Effects_of_Multiple_Administrations_of.24.aspx

Sonner, J. M., Antognini, J. F., Dutton, R. C., Flood, P., Gray, A. T., Harris, R. A., Homanics, G. E., Kendig, J., Orser, B., Raines, D. E., Trudell, J., Vissel, B., & Eger, E. I. 2nd. (2003). Inhaled anesthetics and immobility: Mechanisms, mysteries, and minimum alveolar anesthetic concentration. *Anesthesia and Analgesia*, *97*(3), Article 3. https://doi.org/10.1213/01.ANE.0000081063.76651.33

Stamatakis, E. A., Adapa, R. M., Absalom, A. R., & Menon, D. K. (2010). Changes in Resting Neural Connectivity during Propofol Sedation. *PLoS ONE*, *5*(12), e14224. https://doi.org/10.1371/journal.pone.0014224

Stanton, G. B., Bruce, C. J., & Goldberg, M. E. (1995). Topography of projections to the frontal lobe from the macaque frontal eye fields. *Journal of Comparative Neurology*, *330*(2), 286–301. https://doi.org/10.1002/cne.903300209

Steffey, E. P., Baggot, J. D., Eisele, J. H., Willits, N., Woliner, M. J., Jarvis, K. A., Elliott, A. R., & Tagawa, M. (1994). Morphine-isoflurane interaction in dogs, swine and Rhesus monkeys. *Journal of Veterinary Pharmacology and Therapeutics*, *17*(3), Article 3. https://doi.org/10.1111/j.1365-2885.1994.tb00234.x

Steffey, E. P., Mama, K. R., & Brosnan, R. J. (2015). Inhalation Anesthetics. In *Veterinary Anesthesia and Analgesia* (pp. 297–331). John Wiley & Sons, Ltd. https://doi.org/10.1002/9781119421375.ch16

Stepniewska, I., & Kaas, J. H. (1996). Topographic patterns of V2 cortical connections in macaque monkeys. *The Journal of Comparative Neurology*, *371*(1), 129–152. https://doi.org/10.1002/(SICI)1096-9861(19960715)371:1<129::AID-CNE8>3.0.CO;2-5

Stingl, K., Bartz-Schmidt, K. U., Besch, D., Braun, A., Bruckmann, A., Gekeler, F., Greppmaier, U., Hipp, S., Hörtdörfer, G., Kernstock, C., Koitschev, A., Kusnyerik, A., Sachs, H., Schatz,

A., Stingl, K. T., Peters, T., Wilhelm, B., & Zrenner, E. (2013). Artificial vision with wirelessly powered subretinal electronic implant alpha-IMS. *Proceedings. Biological Sciences*, *280*(1757), 20130077. https://doi.org/10.1098/rspb.2013.0077

Stoerig, P. (1987). Chromaticity and achromaticity. Evidence for a functional differentiation in visual field defects. *Brain: A Journal of Neurology*, *110 (Pt 4)*, 869–886. https://doi.org/10.1093/brain/110.4.869

Stoerig, P., & Cowey, A. (1997). Blindsight in man and monkey. *Brain*, *120*(3), 535–559. https://doi.org/10.1093/brain/120.3.535

Striem-Amit, E., Ovadia-Caro, S., Caramazza, A., Margulies, D. S., Villringer, A., & Amedi, A. (2015). Functional connectivity of visual cortex in the blind follows retinotopic organization principles. *Brain*, *138*(6), 1679–1695. https://doi.org/10.1093/brain/awv083

Suzuki, M., & Larkum, M. E. (2020). General Anesthesia Decouples Cortical Pyramidal Neurons. *Cell*, *180*(4), 666-676.e13. https://doi.org/10.1016/j.cell.2020.01.024

Tamietto, M., Cauda, F., Corazzini, L. L., Savazzi, S., Marzi, C. A., Goebel, R., Weiskrantz, L., & de Gelder, B. (2010). Collicular vision guides nonconscious behavior. *Journal of Cognitive Neuroscience*, *22*(5), 888–902. https://doi.org/10.1162/jocn.2009.21225

Tehovnik, E. J., & Slocum, W. M. (2007). Phosphene induction by microstimulation of macaque V1. *Brain Research Reviews*, *53*(2), 337–343. https://doi.org/10.1016/j.brainresrev.2006.11.001

Tetzlaff, J. E., O'Hara, J. F., & Walsh, M. T. (1993). Potassium and anaesthesia. *Canadian Journal of Anaesthesia = Journal Canadien D'anesthesie*, *40*(3), 227–246. https://doi.org/10.1007/BF03037035

Theys, T., Romero, M. C., van Loon, J., & Janssen, P. (2015). Shape representations in the

primate dorsal visual stream. *Frontiers in Computational Neuroscience*, *9*, 43. https://doi.org/10.3389/fncom.2015.00043

Thompson, K. G., Biscoe, K. L., & Sato, T. R. (2005). Neuronal basis of covert spatial attention in the frontal eye field. *The Journal of Neuroscience : The Official Journal of the Society for Neuroscience*, *25*(41), Article 41. PubMed. https://doi.org/10.1523/JNEUROSCI.0741-05.2005

Tian, J. R., & Lynch, J. C. (1996). Corticocortical input to the smooth and saccadic eye movement subregions of the frontal eye field in Cebus monkeys. *Journal of Neurophysiology*, *76*(4), 2754–2771. https://doi.org/10.1152/jn.1996.76.4.2754

Tippett, D. C., & Keser, Z. (2022). Clinical and neuroimaging characteristics of primary progressive aphasia. In *Handbook of Clinical Neurology* (Vol. 185, pp. 81–97). Elsevier. https://doi.org/10.1016/B978-0-12-823384-9.00016-5

Tootell, R. B. H., Tsao, D., & Vanduffel, W. (2003). Neuroimaging Weighs In: Humans Meet Macaques in "Primate" Visual Cortex. *The Journal of Neuroscience*, *23*(10), Article 10. https://doi.org/10.1523/JNEUROSCI.23-10-03981.2003

Tootell, R. B., Switkes, E., Silverman, M. S., & Hamilton, S. L. (1988). Functional anatomy of macaque striate cortex. II. Retinotopic organization. *Journal of Neuroscience*, *8*(5), 1531–1568. https://doi.org/10.1523/JNEUROSCI.08-05-01531.1988

Uhrig, L., Dehaene, S., & Jarraya, B. (2014). A Hierarchy of Responses to Auditory Regularities in the Macaque Brain. *The Journal of Neuroscience*, *34*(4), Article 4. https://doi.org/10.1523/JNEUROSCI.3165-13.2014

Uhrig, L., Sitt, J. D., Jacob, A., Tasserie, J., Barttfeld, P., Dupont, M., Dehaene, S., & Jarraya, B. (2018). Resting-state Dynamics as a Cortical Signature of Anesthesia in Monkeys. *Anesthesiology*, *129*(5), Article 5. https://doi.org/10.1097/ALN.0000000000002336

Ungerleider, L. G., & Desimone, R. (1986). Cortical connections of visual area MT in the macaque. *Journal of Comparative Neurology*, *248*(2), 190–222. https://doi.org/10.1002/cne.902480204

Ungerleider, L. G., Desimone, R., Galkin, T. W., & Mishkin, M. (1984). Subcortical projections of area MT in the macaque. *The Journal of Comparative Neurology*, *223*(3), Article 3. https://doi.org/10.1002/cne.902230304

Ungerleider, L. G., Galkin, T. W., Desimone, R., & Gattass, R. (2008). Cortical Connections of Area V4 in the Macaque. *Cerebral Cortex*, *18*(3), Article 3. https://doi.org/10.1093/cercor/bhm061

Ungerleider, L. G., & Mishkin, M. (1982a). Two cortical visual systems. In D. J. Ingle, M. A. Goodale, & R. J. W. Mansfield (Eds.), *Analysis of visual behavior* (pp. 549–586). MIT Press.

Ungerleider, L. G., & Mishkin, M. (1982b). Two cortical visual systems. In D. J. Ingle, A. G. Goodale, & R. J. W. Mansfield (Eds.), *Analysis of Visual Behavior* (pp. 549–586). MIT press. https://www.cns.nyu.edu/~tony/vns/readings/ungerleider-mishkin-1982.pdf

University of California, Irvine. (2022). *Eye-opening discovery about adult brain's ability to recover vision: The adult brain has the potential to partially recover from inherited blindness*. ScienceDaily. https://www.sciencedaily.com/releases/2022/10/221006121213.htm

Usrey, W. M., & Alitto, H. J. (2015). Visual Functions of the Thalamus. *Annual Review of Vision Science*, *1*, 351–371. https://doi.org/10.1146/annurev-vision-082114-035920

Van Buren, J. M. (1963). Trans-synaptic retrograde degeneration in the visual system of primates. *Journal of Neurology, Neurosurgery, and Psychiatry*, *26*(5), 402–409.

Van Essen, D. C. (2002). Surface-Based Atlases of Cerebellar Cortex in the Human, Macaque,

and Mouse. *Annals of the New York Academy of Sciences*, *978*(1 THE CEREBELLU), 468–479. https://doi.org/10.1111/j.1749-6632.2002.tb07588.x

Van Essen, D. C., & Maunsell, J. H. R. (1983). Hierarchical organization and functional streams in the visual cortex. *Trends in Neurosciences*, *6*, 370–375. https://doi.org/10.1016/0166-2236(83)90167-4

Van Essen, D. C., Newsome, W. T., & Maunsell, J. H. R. (1984). The visual field representation in striate cortex of the macaque monkey: Asymmetries, anisotropies, and individual variability. *Vision Research*, *24*(5), 429–448. https://doi.org/10.1016/0042-6989(84)90041-5

Van Essen, D. C., Newsome, W. T., Maunsell, J. H. R., & Bixby, J. L. (1986). The projections from striate cortex (V1) to areas V2 and V3 in the macaque monkey: Asymmetries, areal boundaries, and patchy connections. *Journal of Comparative Neurology*, *244*(4), Article 4. https://doi.org/10.1002/cne.902440405

Vanderah, T. W., & Gould, D. (2016). *Nolte's the human brain: An introduction to its functional anatomy [electronic resource]* (Seventh edition.). Elsevier. https://ezproxy-prd.bodleian.ox.ac.uk/login?url=http://ebookcentral.proquest.com/lib/oxford/detail.action?docID=2036217

Vanhaudenhuyse, A., Noirhomme, Q., Tshibanda, L. J.-F., Bruno, M.-A., Boveroux, P., Schnakers, C., Soddu, A., Perlbarg, V., Ledoux, D., Brichant, J.-F., Moonen, G., Maquet, P., Greicius, M. D., Laureys, S., & Boly, M. (2009). Default network connectivity reflects the level of consciousness in non-communicative brain-damaged patients. *Brain*, *133*(1), Article 1. https://doi.org/10.1093/brain/awp313

Vann, S. D., Aggleton, J. P., & Maguire, E. A. (2009). What does the retrosplenial cortex do? *Nature Reviews Neuroscience*, *10*(11), Article 11. https://doi.org/10.1038/nrn2733

Villeneuve, M. Y., & Casanova, C. (2003). On the use of isoflurane versus halothane in the study of visual response properties of single cells in the primary visual cortex. *Journal of Neuroscience Methods*, *129*(1), Article 1. https://doi.org/10.1016/S0165-0270(03)00198-5

Villeneuve, M. Y., Kupers, R., Gjedde, A., Ptito, M., & Casanova, C. (2005). Pattern–motion selectivity in the human pulvinar. *NeuroImage*, *28*(2), 474–480. https://doi.org/10.1016/j.neuroimage.2005.06.015

Vincent, J. L., Patel, G. H., Fox, M. D., Snyder, A. Z., Baker, J. T., Van Essen, D. C., Zempel, J. M., Snyder, L. H., Corbetta, M., & Raichle, M. E. (2007). Intrinsic functional architecture in the anaesthetized monkey brain. *Nature*, *447*(7140), 83–86. https://doi.org/10.1038/nature05758

Wachtler, T., Sejnowski, T. J., & Albright, T. D. (2003). Representation of Color Stimuli in Awake Macaque Primary Visual Cortex. *Neuron*, *37*(4), 681–691.

Wandell, B. A., Dumoulin, S. O., & Brewer, A. A. (2007). Visual Field Maps in Human Cortex. *Neuron*, *56*(2), 366–383. https://doi.org/10.1016/j.neuron.2007.10.012

Wang, Z., Chen, L. M., Négyessy, L., Friedman, R. M., Mishra, A., Gore, J. C., & Roe, A. W. (2013). The relationship of anatomical and functional connectivity to resting state connectivity in primate somatosensory cortex. *Neuron*, *78*(6), Article 6. https://doi.org/10.1016/j.neuron.2013.04.023

Wardak, C., Ibos, G., Duhamel, J.-R., & Olivier, E. (2006). Contribution of the monkey frontal eye field to covert visual attention. *The Journal of Neuroscience: The Official Journal of the Society for Neuroscience*, *26*(16), Article 16. PubMed. https://doi.org/10.1523/JNEUROSCI.3336-05.2006

Weiskrantz, L. (2009). Is blindsight just degraded normal vision? *Experimental Brain Research*,

192(3), 413–416. https://doi.org/10.1007/s00221-008-1388-7

Weiskrantz, L., Warrington, E. K., Sanders, M. D., & Marshall, J. (1974). Visual capacity in the hemianopic field following a restricted occipital ablation. *Brain: A Journal of Neurology*, *97*(4), 709–728. https://doi.org/10.1093/brain/97.1.709

Weissenbacher, A., Kasess, C., Gerstl, F., Lanzenberger, R., Moser, E., & Windischberger, C. (2009). Correlations and anticorrelations in resting-state functional connectivity MRI: A quantitative comparison of preprocessing strategies. *NeuroImage*, *47*(4), 1408–1416. https://doi.org/10.1016/j.neuroimage.2009.05.005

Welsh, Li. (2009). *Anaesthesia for veterinary nurses 2nd edition* (Wiley-Blackwell).

West, G., Heard, D. J., Caulkett, N., & Abou-Madi, N. (2014). *Zoo animal and wildlife immobilization and anesthesia*. Wiley Blackwell.

Wiesel, T. N., & Hubel, D. H. (1963). Single-cell Response in Striaste Cortex of Kittens Deproved of Vision in One Eye. *Journal of Neurophysiology*, *26*, 1003–1017. https://doi.org/10.1152/jn.1963.26.6.1003

Wiesel, T. N., & Hubel, D. H. (1965). Comparison of the effects of unilateral and bilateral eye closure on cortical unit responses in kittens. *Journal of Neurophysiology*, *28*(6), 1029–1040. https://doi.org/10.1152/jn.1965.28.6.1029

Winkler, A. M., Ridgway, G. R., Webster, M. A., Smith, S. M., & Nichols, T. E. (2014). Permutation inference for the general linear model. *NeuroImage*, *92*, 381–397. https://doi.org/10.1016/j.neuroimage.2014.01.060

Winterborn, A. N., Bates, W. A., Feng, C., & Wyatt, J. D. (2008). The efficacy of orally dosed ketamine and ketamine/medetomidine compared with intramuscular ketamine in rhesus macaques (Macaca mulatta) and the effects of dosing route on haematological stress markers. *Journal of Medical Primatology*, *37*(3), Article 3.

https://doi.org/10.1111/j.1600-0684.2007.00234.x

Wittenberg, G. F., Werhahn, K. J., Wassermann, E. M., Herscovitch, P., & Cohen, L. G. (2004). Functional connectivity between somatosensory and visual cortex in early blind humans. *European Journal of Neuroscience*, *20*(7), 1923–1927. https://doi.org/10.1111/j.1460-9568.2004.03630.x

Woo, C.-W., Krishnan, A., & Wager, T. D. (2014). Cluster-extent based thresholding in fMRI analyses: Pitfalls and recommendations. *NeuroImage*, *91*, 412–419. PubMed. https://doi.org/10.1016/j.neuroimage.2013.12.058

Woolrich, M. W., Behrens, T. E. J., Beckmann, C. F., Jenkinson, M., & Smith, S. M. (2004). Multilevel linear modelling for FMRI group analysis using Bayesian inference. *NeuroImage*, *21*(4), 1732–1747. PubMed. https://doi.org/10.1016/j.neuroimage.2003.12.023

Woolrich, M. W., Ripley, B. D., Brady, M., & Smith, S. M. (2001). Temporal Autocorrelation in Univariate Linear Modeling of FMRI Data. *NeuroImage*, *14*(6), 1370–1386. https://doi.org/10.1006/nimg.2001.0931

World Population Clock: 8 Billion People (LIVE, 2023)—Worldometer. (n.d.). Retrieved January 7, 2023, from https://www.worldometers.info/world-population/

World report on vision. (n.d.). Retrieved January 7, 2023, from https://www.who.int/publications-detail-redirect/9789241516570

Wu, T.-L., Mishra, A., Wang, F., Yang, P.-F., Gore, J. C., & Chen, L. M. (2016). Effects of isoflurane anesthesia on resting-state fMRI signals and functional connectivity within primary somatosensory cortex of monkeys. *Brain and Behavior*, *6*(12), Article 12. https://doi.org/10.1002/brb3.591

Xie, H., Chung, D. Y., Kura, S., Sugimoto, K., Aykan, S. A., Wu, Y., Sakadžić, S., Yaseen, M. A.,

Boas, D. A., & Ayata, C. (2020). Differential effects of anesthetics on resting state functional connectivity in the mouse. *Journal of Cerebral Blood Flow & Metabolism*, *40*(4), Article 4. https://doi.org/10.1177/0271678X19847123

Y. Chou, S. Roy, C. Chang, J. A. Butman, & D. L. Pham. (2018). Deep learning of resting state networks from independent component analysis. *2018 IEEE 15th International Symposium on Biomedical Imaging (ISBI 2018)*, 747–751. https://doi.org/10.1109/ISBI.2018.8363681

Yacoub, E., Grier, M. D., Auerbach, E. J., Lagore, R. L., Harel, N., Adriany, G., Zilverstand, A., Hayden, B. Y., Heilbronner, S. R., Uğurbil, K., & Zimmermann, J. (2020). Ultra-high field (10.5 T) resting state fMRI in the macaque. *NeuroImage*, *223*, 117349. https://doi.org/10.1016/j.neuroimage.2020.117349

Yang, P.-F., Phipps, M. A., Newton, A. T., Jonathan, S., Manuel, T. J., Gore, J. C., Grissom, W. A., Caskey, C. F., & Chen, L. M. (2022). Differential dose responses of transcranial focused ultrasound at brain regions indicate causal interactions. *Brain Stimulation*, *15*(6), 1552–1564. https://doi.org/10.1016/j.brs.2022.12.003

Youakim, M., Bender, D. B., & Baizer, J. S. (2001). Vertical meridian representation on the prelunate gyrus in area V4 of macaque. *Brain Research Bulletin*, *56*(2), 93–100. https://doi.org/10.1016/s0361-9230(01)00608-6

Yourganov, G., Fridriksson, J., Stark, B., & Rorden, C. (2018). Removal of artifacts from resting-state fMRI data in stroke. *NeuroImage: Clinical*, *17*, 297–305. https://doi.org/10.1016/j.nicl.2017.10.027

Zang, Y.-F., Zhu, C.-Z., Zao, Q.-J., Sui, M.-Q., Liang, L., Tian, L.-X., Jiang, T.-Z., & Wang, Y.-F. (2007). Altered baseline brain activity in children with ADHD revealed by resting-state functional MRI. *Brain and Development*, *29*(2), Article 2.

https://doi.org/10.1016/j.braindev.2006.07.002

Zeki, S., & Ffytche, D. H. (1998). The Riddoch syndrome: Insights into the neurobiology of conscious vision. *Brain*, *121*(1), 25–45. https://doi.org/10.1093/brain/121.1.25

Zeki, S. M. (1978). Uniformity and diversity of structure and function in rhesus monkey prestriate visual cortex. *The Journal of Physiology*, *277*, 273–290. https://doi.org/10.1113/jphysiol.1978.sp012272

8 Appendices

8.1 Manual Seed Corrections

This appendix is comprised of a series of 15 tables indicating the locations in which manual seed corrections were necessary.

Table 8.1 Manual Seed Corrections for V5/MT

Seed	Coordinates in F99 space	Ch.	Monkey group	Monkeys	Automatically registered	Corrected at the structural level	Corrected at the functional level
V5/MT	**[112 58 76; 30 56 77]**	**4 & 5**	Control isoflurane Anesthetized	oct			x
				orca		x	
				orv		x	
				pic		x	
				ple		x	
				pug		x	
				sad		x	
				sb		x	
				tor		x	
				tur		x	
				ulr		x	
				val		x	
				vas		x	
				woo		x	
			Control sevoflurane Anesthetized	jck		x	
				jum			x
				oly		x	
				orl		x	
				pck		x	
				pug		x	
				sea		x	
				saf		x	
				sel		x	
				swe		x	
			Lesion	Monkey S			x
				Monkey Y			x

Table 8.2 Manual Seed Corrections for FEF

Seed	Coordinates in F99 space	Ch.	Monkey group	Monkeys	Automatically registered	Corrected at the structural level	Corrected at the functional level
FEF	**[111 128 84; 29 130 82]**	**4 & 5**	Control isoflurane Anesthetized	oct		x	
				orca		x	
				orv		x	
				pic		x	
				ple			x
				pug		x	
				sad		x	
				sb			x
				tor		x	
				tur		x	
				ulr		x	
				val			x
				vas		x	
				woo		x	
			Control sevoflurane Anesthetized	jck		x	
				jum		x	
				oly		x	
				orl		x	
				pck		x	
				pug		x	
				sea		x	
				saf			x
				sel		x	
				swe		x	
			Lesion	Monkey S			x
				Monkey Y			x

Table 8.3 Manual Seed Corrections for V2m

Seed	Coordinates in F99 space	Ch.	Monkey group	Monkeys	Automatically registered	Corrected at the structural level	Corrected at the functional level
V2m	[75 34 74; 67 35 74]	4 & 5	Control isoflurane Anesthetized	oct			x
				orca		x	
				orv		x	
				pic			x
				ple			x
				pug		x	
				sad			x
				sb		x	
				tor		x	
				tur		x	
				ulr		x	
				val		x	
				vas			x
				woo		x	
			Control sevoflurane Anesthetized	jck		x	
				jum		x	
				oly		x	
				orl		x	
				pck		x	
				pug		x	
				sea		x	
				saf		x	
				sel		x	
				swe		x	
			Lesion	Monkey S			x
				Monkey Y			x

Table 8.4 Manual Seed Corrections for V2d

Seed	Coordinates in F99 space	Ch.	Monkey group	Monkeys	Automatically registered	Corrected at the structural level	Corrected at the functional level
V2d	**[117 46 75; 23 46 75]**	**5**	Control isoflurane Anesthetized	oct		x	
				orca		x	
				orv		x	
				pic			x
				ple		x	
				pug		x	
				sad			x
				sb		x	
				tor			x
				tur		x	
				ulr		x	
				val			x
				vas		x	
				woo		x	
			Control sevoflurane Anesthetized	jck			
				jum			
				oly			
				orl			
				pck			
				pug			
				sea			
				saf			
				sel			
				swe			
			Lesion	Monkey S			
				Monkey Y			

Table 8.5 Manual Seed Corrections for V1d

Seed	Coordinates in F99 space	Ch.	Monkey group	Monkeys	Automatically registered	Corrected at the structural level	Corrected at the functional level
V1d	[106 25 73; 34 25 72]1	4 & 5	Control isoflurane Anesthetized	oct		x	
				orca		x	
				orv		x	
				pic		x	
				ple		x	
				pug		x	
				sad		x	
				sb		x	
				tor		x	
				tur		x	
				ulr		x	
				val		x	
				vas		x	
				woo		x	
			Control sevoflurane Anesthetized	jck		x	
				jum		x	
				oly		x	
				orl		x	
				pck		x	
				pug		x	
				sea		x	
				saf		x	
				sel		x	
				swe		x	
			Lesion	Monkey S			x
				Monkey Y			x

Table 8.6 Manual Seed Corrections for V1v

Seed	Coordinates in F99 space	Ch.	Monkey group	Monkeys	Automatically registered	Corrected at the structural level	Corrected at the functional level
V1v	[98 13 53; 42 13 53]	4 & 5	Control isoflurane Anesthetized	oct			x
				orca			x
				orv			x
				pic			x
				ple			x
				pug			x
				sad			x
				sb			x
				tor			x
				tur			x
				ulr	x		
				val		x	
				vas		x	
				woo		x	
			Control sevoflurane Anesthetized	jck			
				jum			
				oly			
				orl			
				pck			
				pug			
				sea			
				saf			
				sel			
				swe			
			Lesion	Monkey S			x
				Monkey Y			x

Table 8.7 Manual Seed Corrections for V4DP

Seed	Coordinates in F99 space	Ch.	Monkey group	Monkeys	Automatically registered	Corrected at the structural level	Corrected at the functional level
V4DP	**[111 50 90; 31 46 90]**	**4 & 5**	Control isoflurane Anesthetized	oct			x
				orca			x
				orv			x
				pic			x
				ple			x
				pug			x
				sad			x
				sb			x
				tor			x
				tur			x
				ulr			x
				val			x
				vas			x
				woo			x
			Control sevoflurane Anesthetized	jck			x
				jum		x	
				oly		x	
				orl		x	
				pck		x	
				pug		x	
				sea		x	
				saf			x
				sel		x	
				swe		x	
			Lesion	Monkey S			x
				Monkey Y			x

Table 8.8 Manual Seed Corrections for V4d

Seed	Coordinates in F99 space	Ch.	Monkey group	Monkeys	Automatically registered	Corrected at the structural level	Corrected at the functional level
V4d	[115 48 80; 25 48 80]	5	Control isoflurane Anesthetized	oct			x
				orca		x	
				orv		x	
				pic			x
				ple		x	
				pug		x	
				sad		x	
				sb		x	
				tor			x
				tur			x
				ulr	x		
				val		x	
				vas		x	
				woo		x	
			Control sevoflurane Anesthetized	jck			
				jum			
				oly			
				orl			
				pck			
				pug			
				sea			
				saf			
				sel			
				swe			
			Lesion	Monkey S			x
				Monkey Y			x

Table 8.9 Manual Seed Corrections for V4v

Seed	Coordinates in F99 space	Ch.	Monkey group	Monkeys	Automatically registered	Corrected at the structural level	Corrected at the functional level
V4v	[105 62 41; 36 61 40]	5	Control isoflurane Anesthetized	oct			x
				orca		x	
				orv	x		
				pic	x		
				ple			x
				pug			x
				sad	x		
				sb		x	
				tor		x	
				tur			x
				ulr		x	
				val		x	
				vas		x	
				woo	x		
			Control sevoflurane Anesthetized	jck			
				jum			
				oly			
				orl			
				pck			
				pug			
				sea			
				saf			
				sel			
				swe			
			Lesion	Monkey S		x	
				Monkey Y		x	

Table 8.10 Manual Seed Corrections for LGN

Seed	Coordinates in F99 space	Ch.	Monkey group	Monkeys	Automatically registered	Corrected at the structural level	Corrected at the functional level
LGN	**[96 88 48; 45 88 47]**	**4 & 5**	Control isoflurane Anesthetized	oct			x
				orca		x	
				orv			x
				pic			x
				ple	x		
				pug		x	
				sad	x		
				sb	x		
				tor	x		
				tur		x	
				ulr	x		
				val		x	
				vas			x
				woo			x
			Control sevoflurane Anesthetized	jck			x
				jum	x		
				oly			x
				orl	x		
				pck			x
				pug	x		
				sea			x
				saf	x		
				sel		x	
				swe	x		
			Lesion	Monkey S			x
				Monkey Y	x		

Table 8.11 Manual Seed Corrections for Pulvinar

Seed	Coordinates in F99 space	Ch.	Monkey group	Monkeys	Automatically registered	Corrected at the structural level	Corrected at the functional level
Pulvinar	**[94 78 52; 94 78 52]**	**5**	Control isoflurane Anesthetized	oct	x		
				orca		x	
				orv		x	
				pic		x	
				ple		x	
				pug	x		
				sad		x	
				sb	x		
				tor		x	
				tur	x		
				ulr	x		
				val		x	
				vas	x		
				woo	x		
			Control sevoflurane Anesthetized	jck			
				jum			
				oly			
				orl			
				pck			
				pug			
				sea			
				saf			
				sel			
				swe			
			Lesion	Monkey S	x		
				Monkey Y	x		

Table 8.12 Manual Seed Corrections for SC

Seed	Coordinates in F99 space	Ch.	Monkey group	Monkeys	Automatically registered	Corrected at the structural level	Corrected at the functional level
SC	**[76 71 56; 66 71 56]**	**5**	Control isoflurane Anesthetized	oct	x		
				orca			x
				orv			x
				pic		x	
				ple			x
				pug			x
				sad			x
				sb			x
				tor			x
				tur			x
				ulr			x
				val			x
				vas			x
				woo			x
			Control sevoflurane Anesthetized	jck			
				jum			
				oly			
				orl			
				pck			
				pug			
				sea			
				saf			
				sel			
				swe			
			Lesion	Monkey S	x		
				Monkey Y	x		

Table 8.13 Manual Seed Corrections for V1Cal1

Seed	Coordinates in F99 space	Ch.	Monkey group	Monkeys	Automatically registered	Corrected at the structural level	Corrected at the functional level
V1Cal1	[104 28 63; 38 28 63])	5	Control isoflurane Anesthetized	oct		x	
				orca		x	
				orv		x	
				pic			x
				ple			x
				pug		x	
				sad		x	
				sb		x	
				tor			x
				tur		x	
				ulr		x	
				val		x	
				vas		x	
				woo		x	
			Control sevoflurane Anesthetized	jck			
				jum			
				oly			
				orl			
				pck			
				pug			
				sea			
				saf			
				sel			
				swe			
			Lesion	Monkey S			
				Monkey Y			

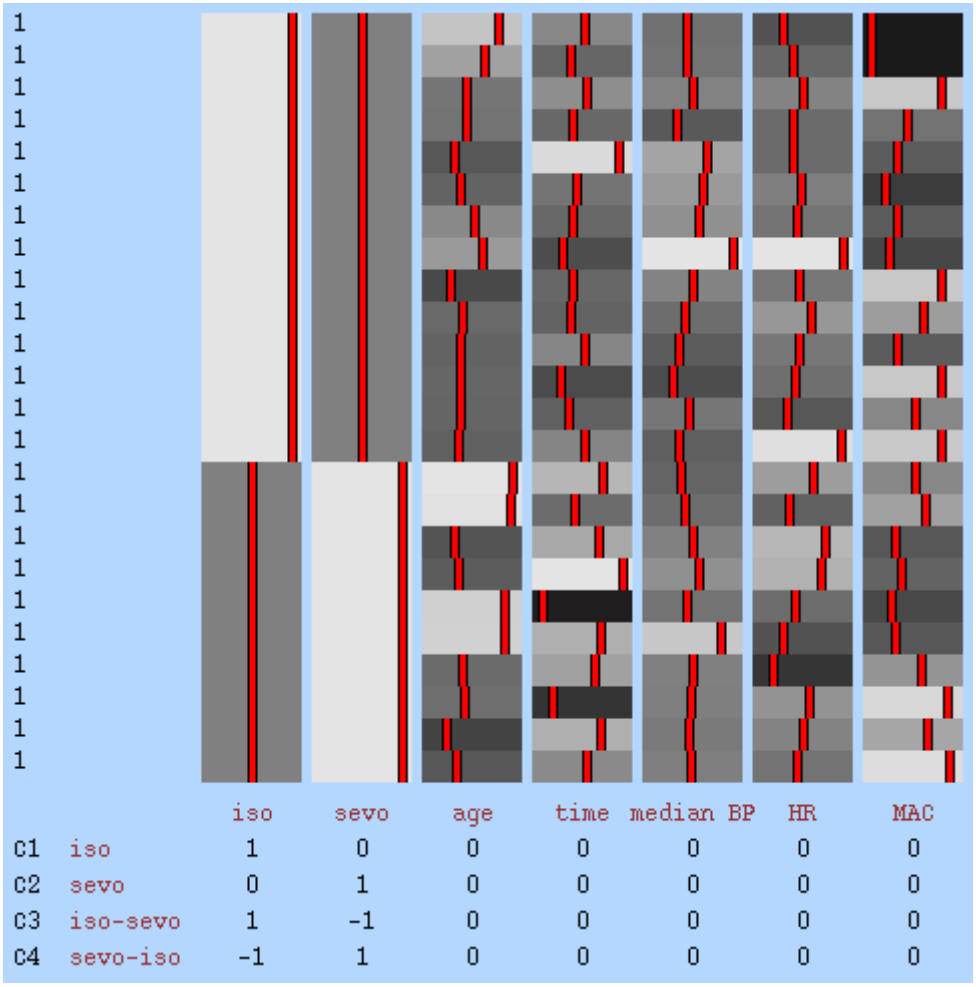
Table 8.14 Manual Seed Corrections for V1Cal2

Seed	Coordinates in F99 space	Ch.	Monkey group	Monkeys	Automatically registered	Corrected at the structural level	Corrected at the functional level
V1Cal2	[100 43 63; 42 41 60]	5	Control isoflurane Anesthetized	oct		x	
				orca		x	
				orv			x
				pic		x	
				ple			x
				pug		x	
				sad		x	
				sb		x	
				tor			x
				tur			x
				ulr		x	
				val		x	
				vas		x	
				woo		x	
			Control sevoflurane Anesthetized	jck			
				jum			
				oly			
				orl			
				pck			
				pug			
				sea			
				saf			
				sel			
				swe			
			Lesion	Monkey S			
				Monkey Y			

Table 8.15 Manual Seed Corrections for V1C

Seed	Coordinates in F99 space	Ch.	Monkey group	Monkeys	Automatically registered	Corrected at the structural level	Corrected at the functional level
V1Cal3	[91 41 62; 50 41 62]	5	Control isoflurane Anesthetized	oct			x
				orca			x
				orv		x	
				pic			x
				ple		x	
				pug			x
				sad		x	
				sb		x	
				tor			x
				tur			x
				ulr		x	
				val		x	
				vas		x	
				woo		x	
			Control sevoflurane Anesthetized	jck			
				jum			
				oly			
				orl			
				pck			
				pug			
				sea			
				saf			
				sel			
				swe			
			Lesion	Monkey S			
				Monkey Y			

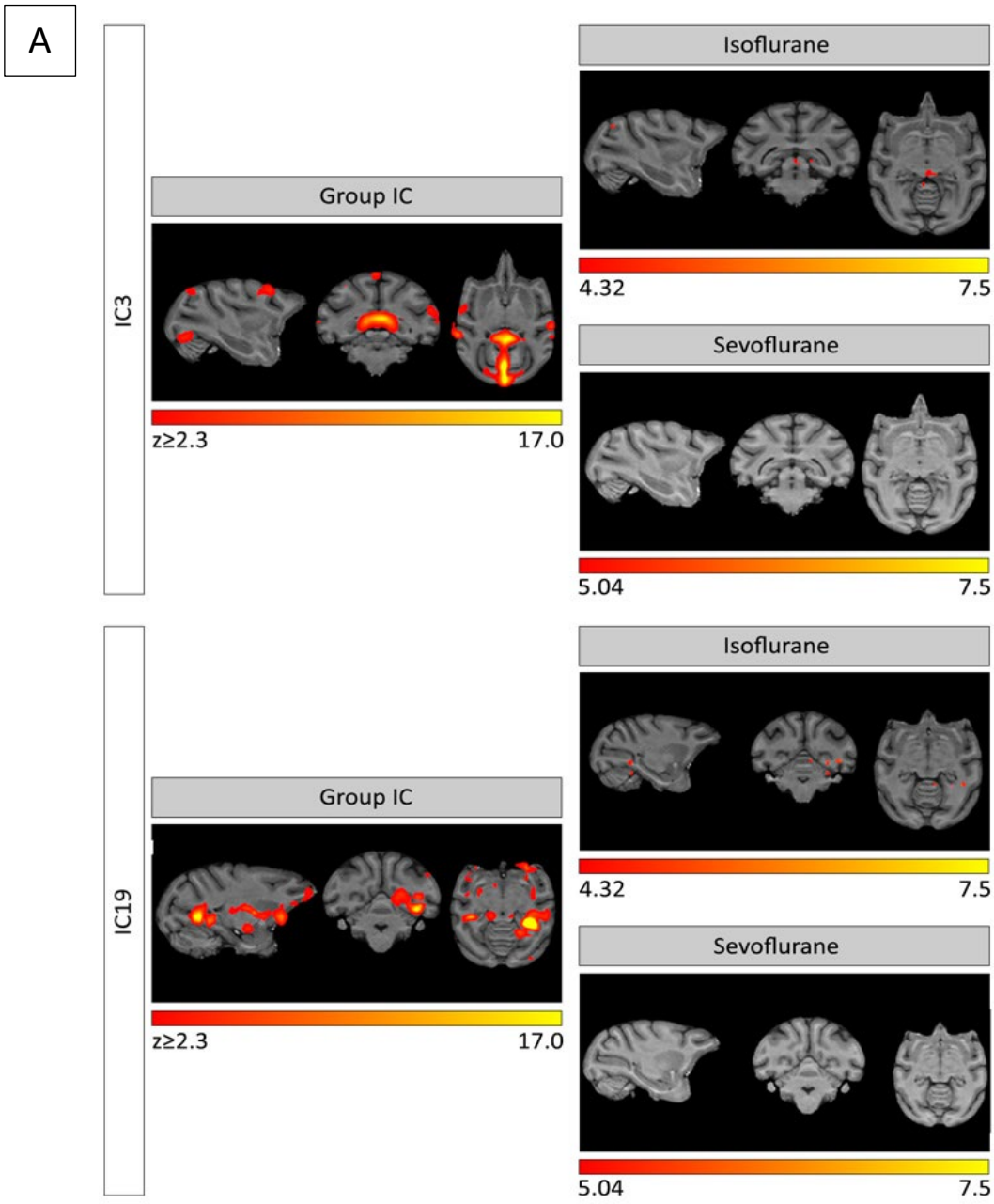
8.2 GLME Matrix Design

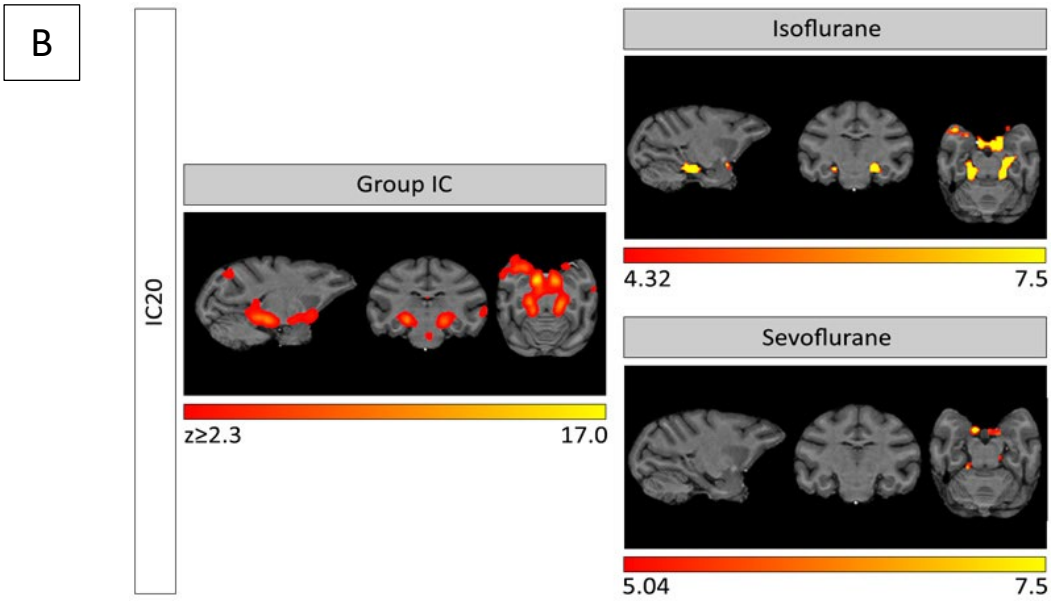

1
1
1

8.3 Noisy ICs

Figure 8.2 Noisy ICs

Noisy ICs were excluded from the results. Group IC maps are the thresholded (z ≥ 2.3) individual components, resulting from the group ICA (see Chapter 2.3). They represent a given IC for all subjects independently of the anaesthetic condition. The colour bar under the group IC represents the range of the positive z-values from the significance threshold. The isoflurane and sevoflurane IC are the result of the dual regression, representing the IC under isoflurane and sevoflurane (significance level α=0.001), respectively. The colour bar under the isoflurane and sevoflurane IC represents the range of the positive t-values from the significance threshold.





Of the 25 IC resulting from the group ICA, three (see Figure B1) were excluded from the results for the following reasons:

- IC 3 contains only the median line. It does not reflect neuronal activity but is due presumably to the strong circulatory activity present in that area, a major junction of the cerebral artery
- IC 19 has no coherent spatial pattern.
- IC20 reflects the activity of the CSF.

8.4 Group ICs

Figure 8.3 Group IC

Output of the group ICA. The group ICA isolates common spatial pattern among all individual IC across all subjects without concerns of what anaesthetic group they belong to. Colourbars represent the range of the positive values of z from the significance threshold (z=2.3) for a given IC. All maps are displayed on the F99 template.
For illustration purpuses, Appendix C was divided in 3 parts.
A. *Figure C1A* ***B.*** *Figure C1B* ***C.*** *Figure C1C - cont'd following pages.*

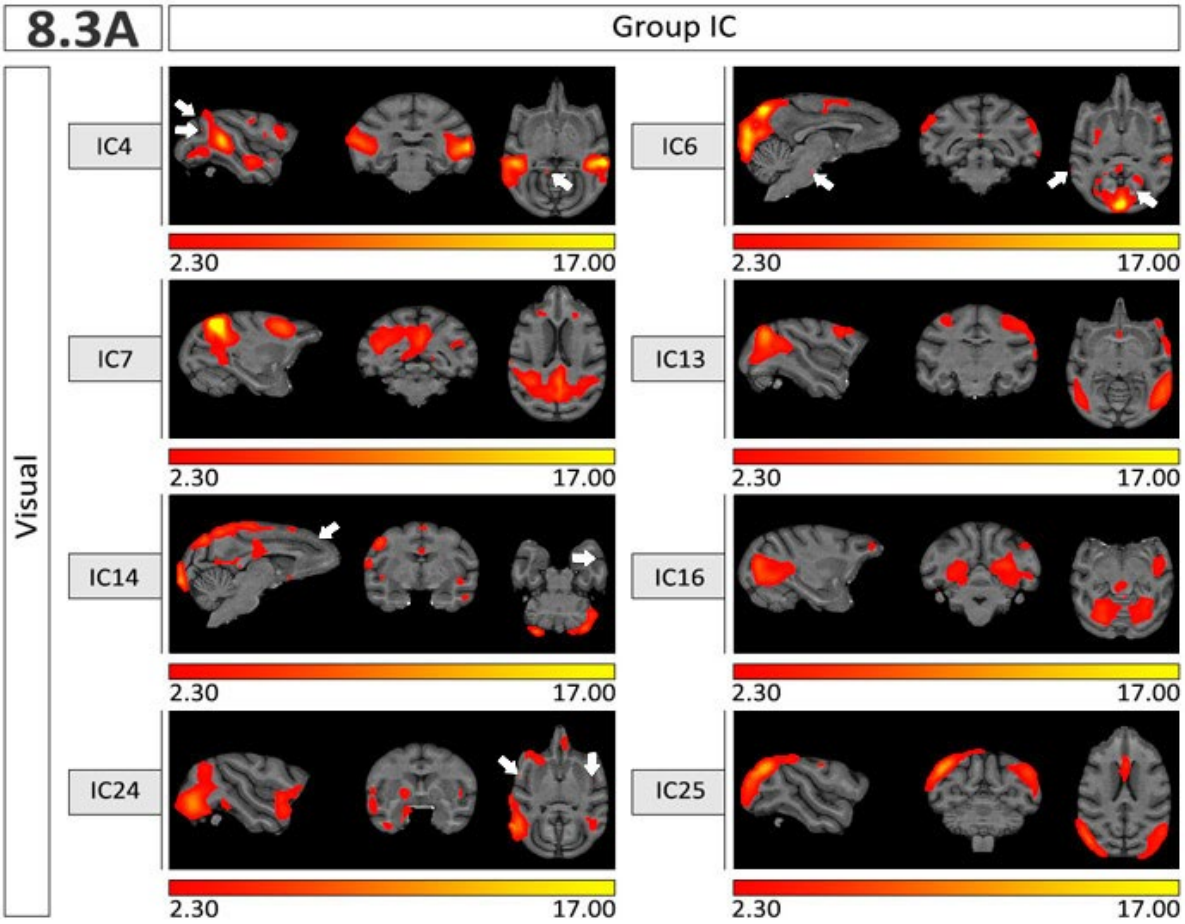


Figure 8.3 cont'd.

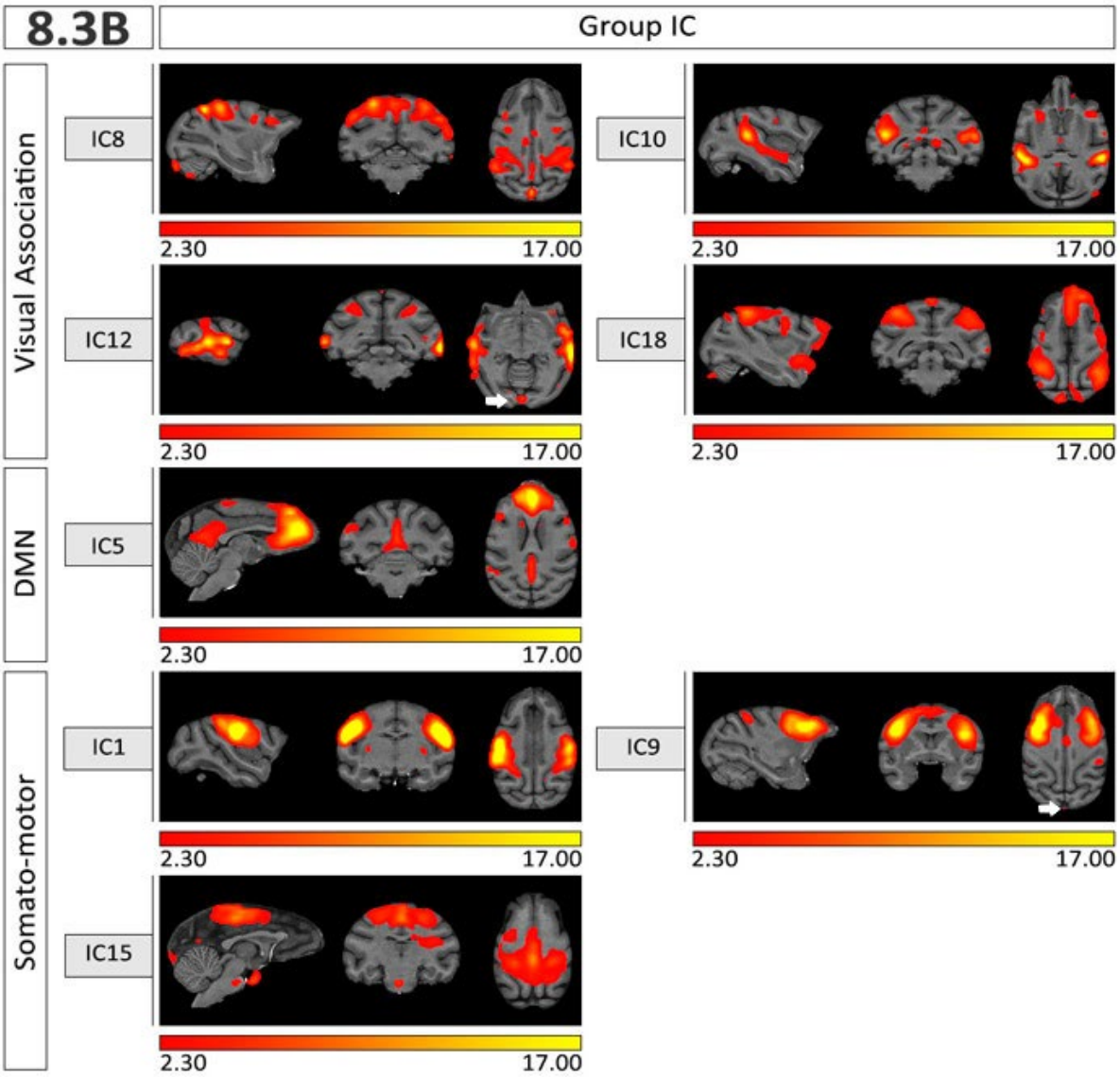
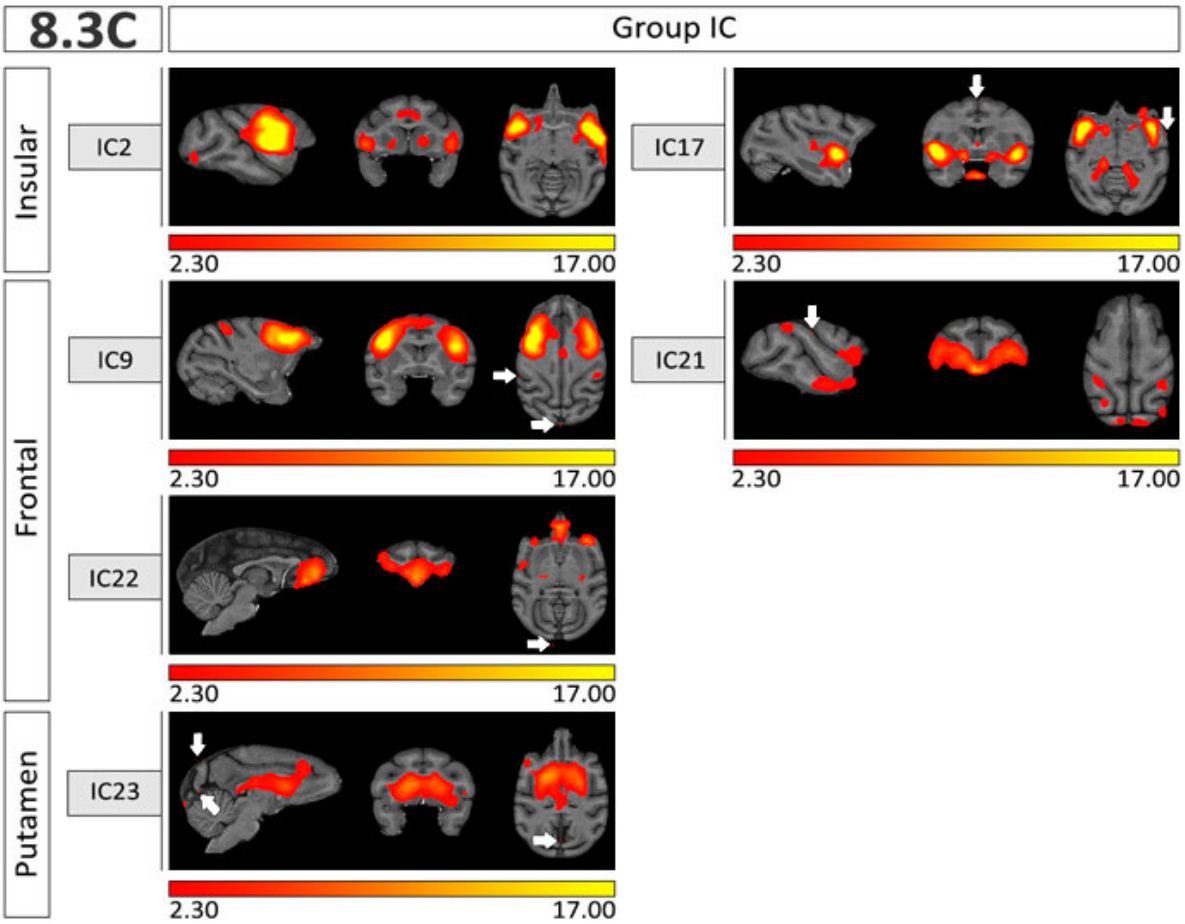
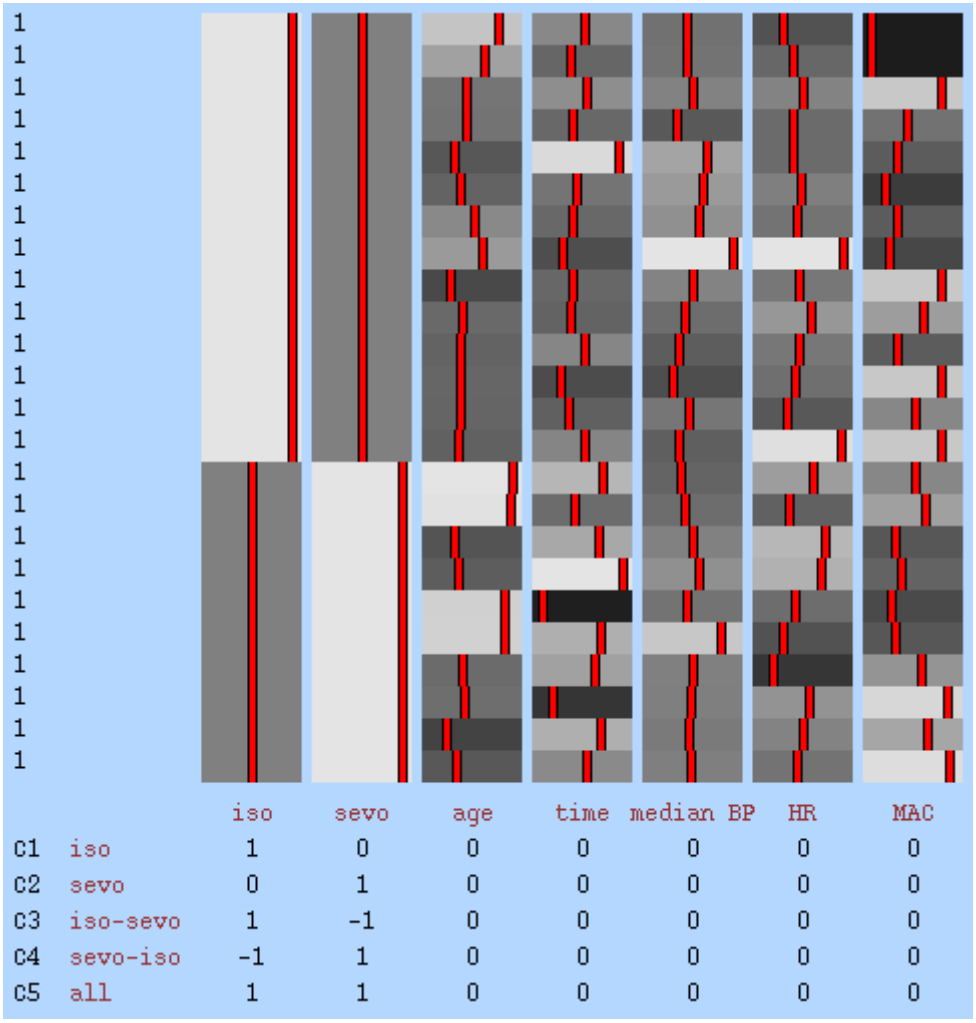


Figure 8.3 cont'd.



8.5 Group SBCA GLME Design Matrix



		iso	sevo	age	time	median BP	HR	MAC
C1	iso	1	0	0	0	0	0	0
C2	sevo	0	1	0	0	0	0	0
C3	iso-sevo	1	-1	0	0	0	0	0
C4	sevo-iso	-1	1	0	0	0	0	0
C5	all	1	1	0	0	0	0	0

Figure 8.4 GLME Design Matrix for Group SBCA

The design matrix contains two regressors of interest (subject was anaesthetized with isoflurane (iso) and subject was anaesthetized with sevoflurane (sevo)) and five regressors of no interest/nuisance regressors (animal age (age), delay between anaesthesia induction and data acquisition (time), subject's median blood pressure (median BP), subject's heart rate (HR), and subject's individual MAC value (MAC)). The model uses four contrasts to tests four hypotheses:
Contrast 1 (C1): the mean isoflurane group effect is greater than zero
Contrast 2 (C2): the mean sevoflurane group effect is greater than zero
Contrast 3 (C3): the mean isoflurane group effect is greater than the mean isoflurane group effect
Contrast 4 (C54): the mean sevoflurane group effect is greater than the mean sevoflurane group effect
Contrast 5 (C5): the effect across all animals is greater than zero

8.6 Whole Brain Level Functional Connectivity Differences

Figure 8.5 Functional Connectivity Network of Isoflurane Compared to Sevoflurane in all Meaningful IC

For each of the 22 non-noisy IC, the results of the test for H_0: There is no difference between the mean isoflurane group effect and the mean sevoflurane group effect are represented by a t value map. Column 1 shows the result obtained with contrast Isoflurane - Sevoflurane (see Table 3.1) while column 2 presents the result obtained with contrast Sevoflurane – Isoflurane. The resulting maps are presented on the F99 template, thresholded at t=1 instead of t=0 for illustration purposes, so that voxel clusters (with no consideration of significance) would be more apparent to the reader. ICs are organised following the classification established in Chapter 3.3.
For legibility, Figure 8.5 is divided into four parts:
***A.** Figure 8.5 part 1: Visual IC* ***B.** Figure 8.5 part 2: Visual Association, DMN, Somatomotor IC* ***C.** Figure 8.5 part 3 Auditory, Insular, Frontal, Putamen.*

Figure 8.5 cont'd.

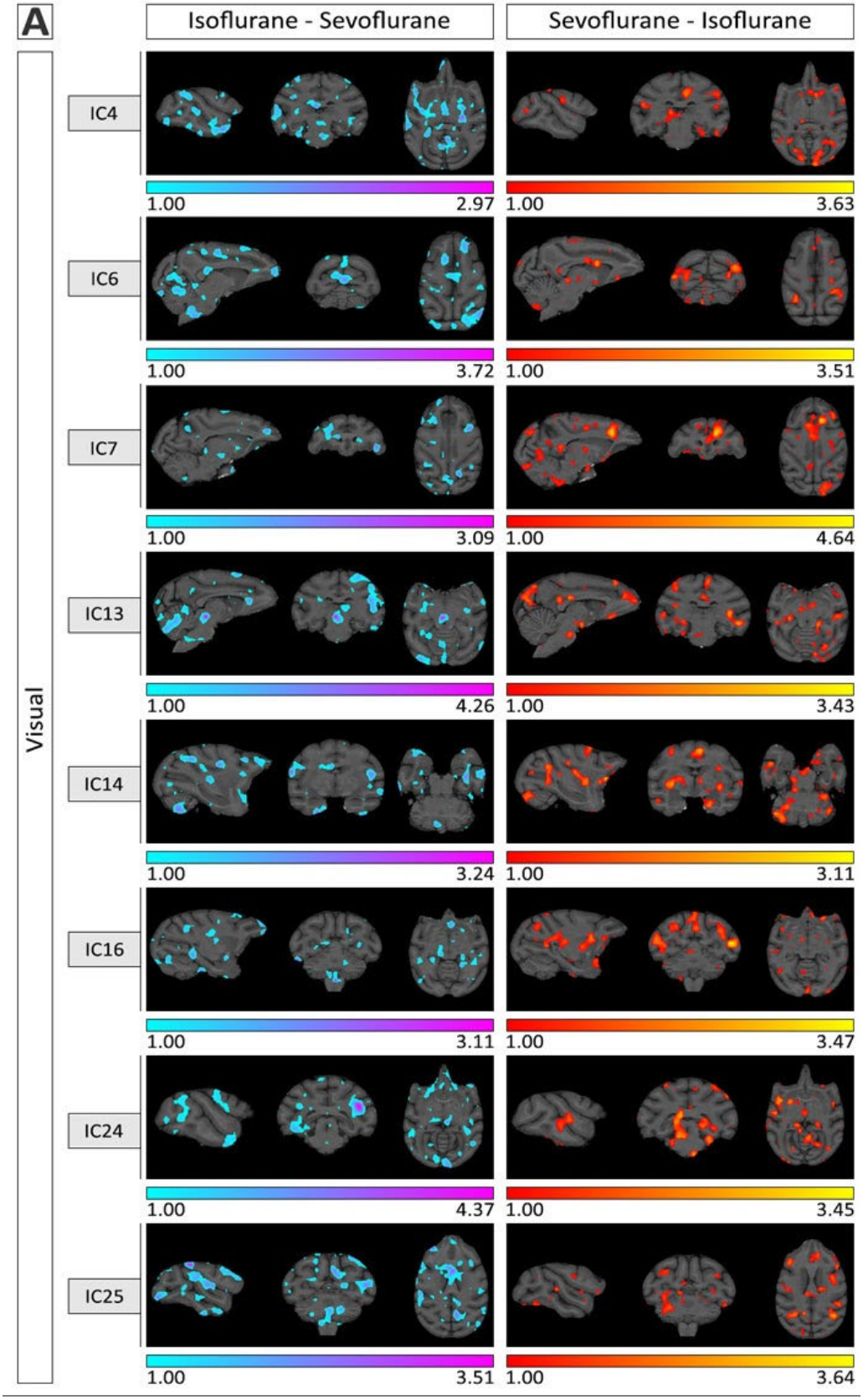


Figure 8.5 cont'd.

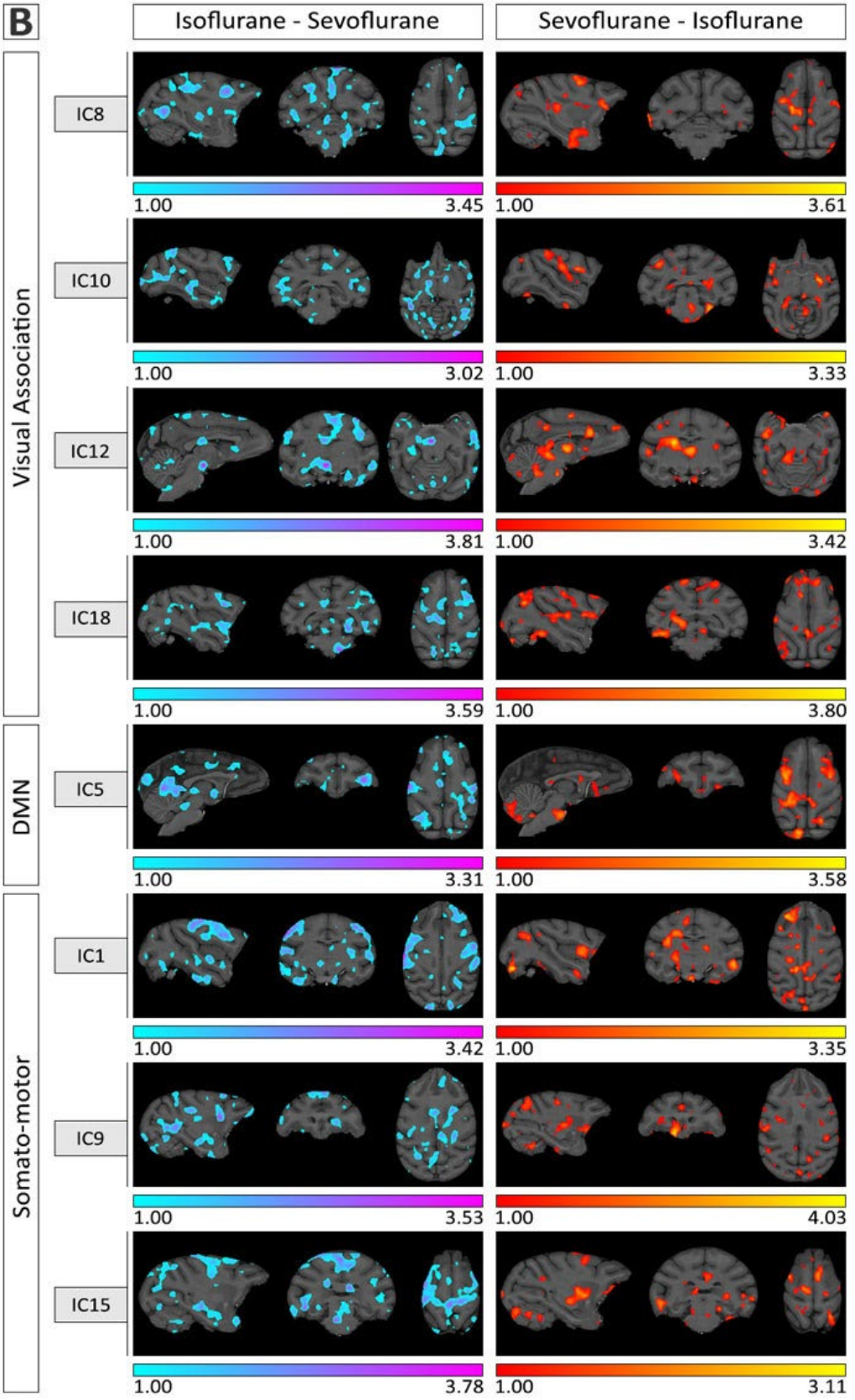
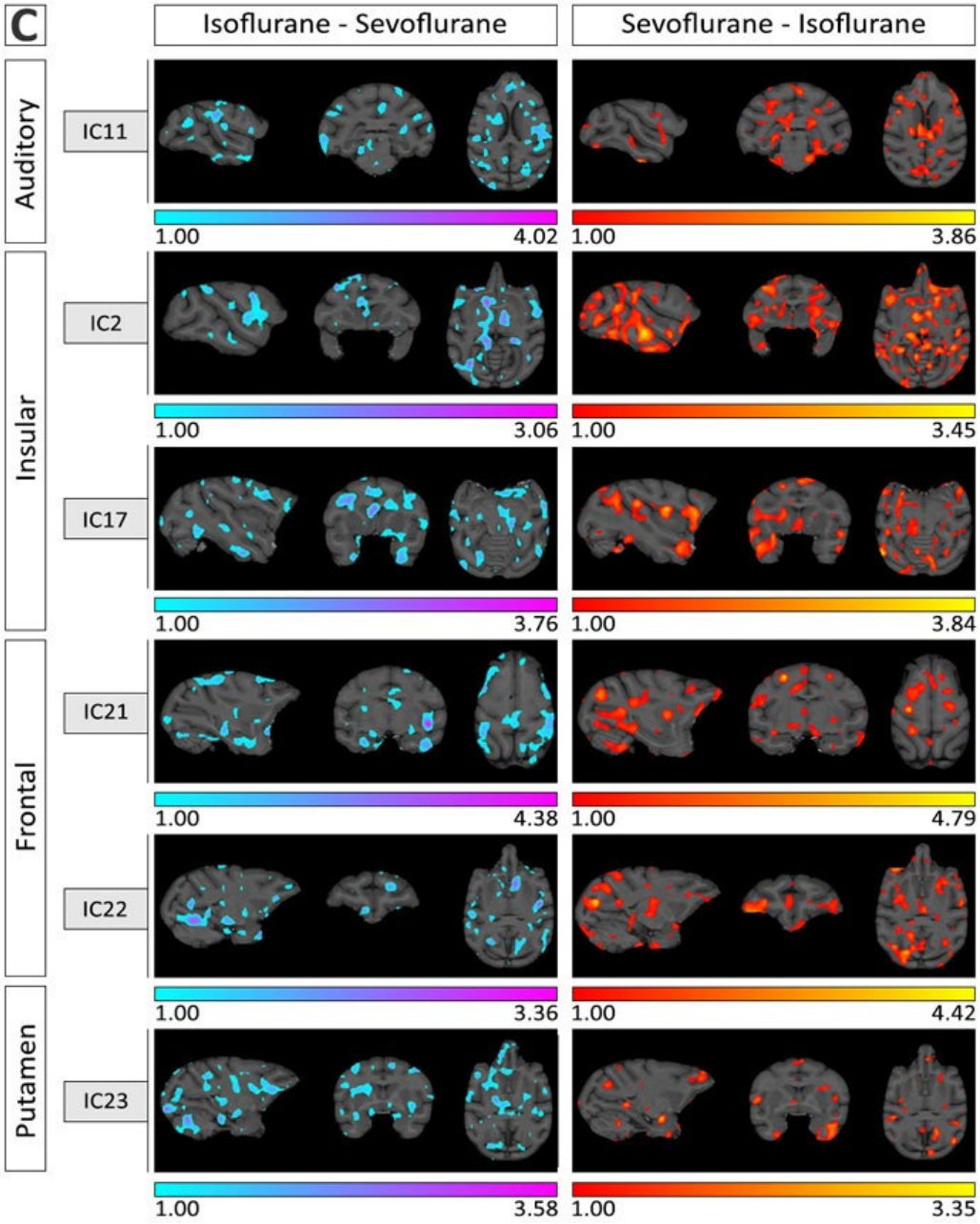
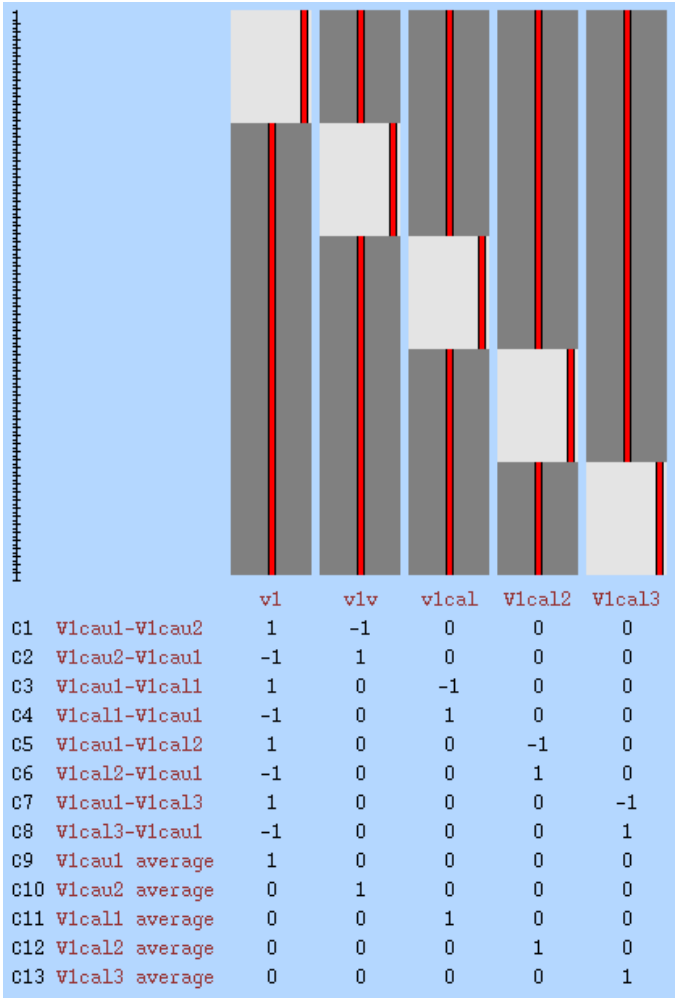


Figure 8.5 cont'd.



8.7 Functional Connectivity Comparisons Between the Calcarine Seeds: Part 1



		v1	v1v	v1cal	V1cal2	V1cal3
C1	V1cau1-V1cau2	1	-1	0	0	0
C2	V1cau2-V1cau1	-1	1	0	0	0
C3	V1cau1-V1cal1	1	0	-1	0	0
C4	V1cal1-V1cau1	-1	0	1	0	0
C5	V1cau1-V1cal2	1	0	0	-1	0
C6	V1cal2-V1cau1	-1	0	0	1	0
C7	V1cau1-V1cal3	1	0	0	0	-1
C8	V1cal3-V1cau1	-1	0	0	0	1
C9	V1cau1 average	1	0	0	0	0
C10	V1cau2 average	0	1	0	0	0
C11	V1cal1 average	0	0	1	0	0
C12	V1cal2 average	0	0	0	1	0
C13	V1cal3 average	0	0	0	0	1

Figure 8.6 GLME Design Matrix (1): Functional Connectivity Comparisons Between the Calcarine Seeds

The time series of each of the 5 primary visual cortex seed (2 in operculum, 3 in the calcarine), across the control animals are used as regressors. The model uses eleven contrasts to tests eight hypotheses:
Contrast 1 (C1): the mean correlation with the first operculum seed (V1cau1) is greater than the mean correlation with the second operculum seed (V1cau2)

Contrast 2 (C2): the mean correlation with V1cau2 is greater than the mean correlation with V1cau1
Contrast 3 (C3): the mean correlation with V1cau1 is greater than the mean correlation with V1cal1
Contrast 4 (C4): the mean correlation with V1cal1 is greater than the mean correlation with V1cau1
Contrast 5 (C5): the mean correlation with V1cau1 is greater than the mean correlation with V1cal2
Contrast 6 (C6): the mean correlation with V1cal2 is greater than the mean correlation with V1cau1
Contrast 7 (C7): the mean correlation with V1cau1 is greater than the mean correlation with V1cal3
Contrast 8 (C8): the mean correlation with V1cal3 is greater than the mean correlation with V1cau1
Contrast 9 (C9): the mean correlation with V1cau1 is greater than zero
Contrast 10 (C10): the mean correlation with V1cau2 is greater than zero (not presented)
Contrast 11 (C11): the mean correlation with V1cal1 is greater than zero (not presented)
Contrast 10 (C10): the mean correlation with V1cal2 is greater than zero (not presented)
Contrast 11 (C11): the mean correlation with V1cal3 is greater than zero

C1, C3, C5 and C7 were masked by C9. C2 was masked by C10, C4 by C11 and C8 by C13

8.8 Contrast Masking

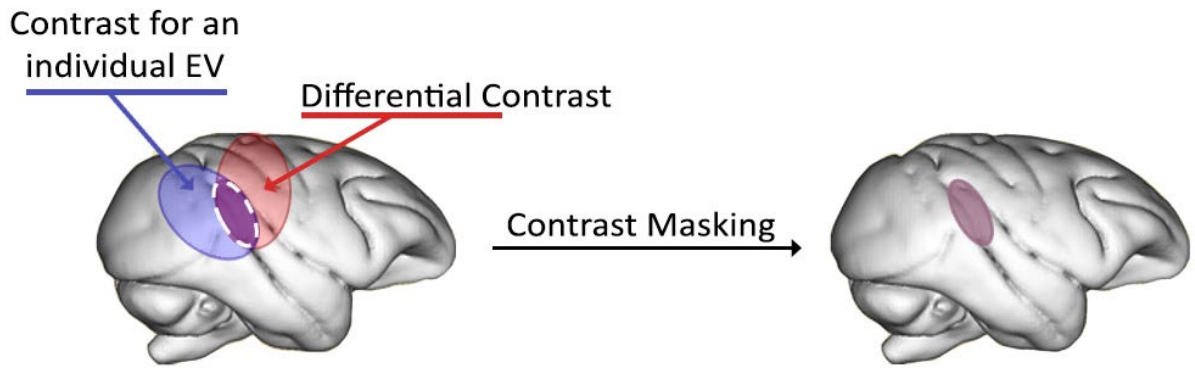


Figure 8.7 Contrast Masking

Contrast masking is a FSL FEAT feature preventing false positive when interpreting differential contrast. Blue: Contrast for an individual EV network, Red: Differential contrast network, purple: intersection/corrected for false positive differential network.

Contrast masking is a feature from FSL FEAT preventing false positive when interpreting differential contrast.
For example, if we have a set of contrasts for the following hypothesis:

- C1: The mean effect of A is greater than zero
- C2: The mean effect of B is greater than zero
- C3: the mean effect of A is greater than the mean effect of B.

C1 and C2 are contrast for an individual EV (blue on Figure 8.7 *Contrast Masking*). C3 is a differential contrast (red in Figure 8.7 *Contrast Masking*), it is obtained by subtracting B to A. So, if A and B happen to be both negative, the outputted value will show as being positive, what would be false positive.

In practice, this means that when a differential network is obtained, it is important to ensure that the areas involved in this differential network at a significance level α are also involved in the tested individual network at the same significance level. Contrast masking makes the thresholded at significance level α into a mask and uses it on the differential network thresholded at α, so only the intersection between the two networks is reported.

8.9 Lesion Animal Functional Connectivity at z≥2.3

Figure 8.8 Lesion Animal Functional Connectivity at z≥2.3

Functional connectivity maps were obtained by placing several seeds in the visual system (V1, V2d, V2m V4v. V4DP, V4d, MT), in areas associated to the visual system (FEF), and areas hypothesised to be relevant to blindsight (LGN, pulvinar, SC) in 2 macaques with a natural lesion in the primary visual cortex (Monkey S and Monkey Y).
The z-score maps obtained for each, in Monkey S and Monkey Y (titled respectively). The results obtained in the lesion animals are presented on their structural image, at the significance level (z≤2.3). A mask was applied to eliminate any correlations inside the lesions.
Colour bars represent the range of positive z-scores from the significance level in each case. Voxels with z values superior to 50 are represented under the same colour (yellow). For illustration purposes this figure is split over the next three pages

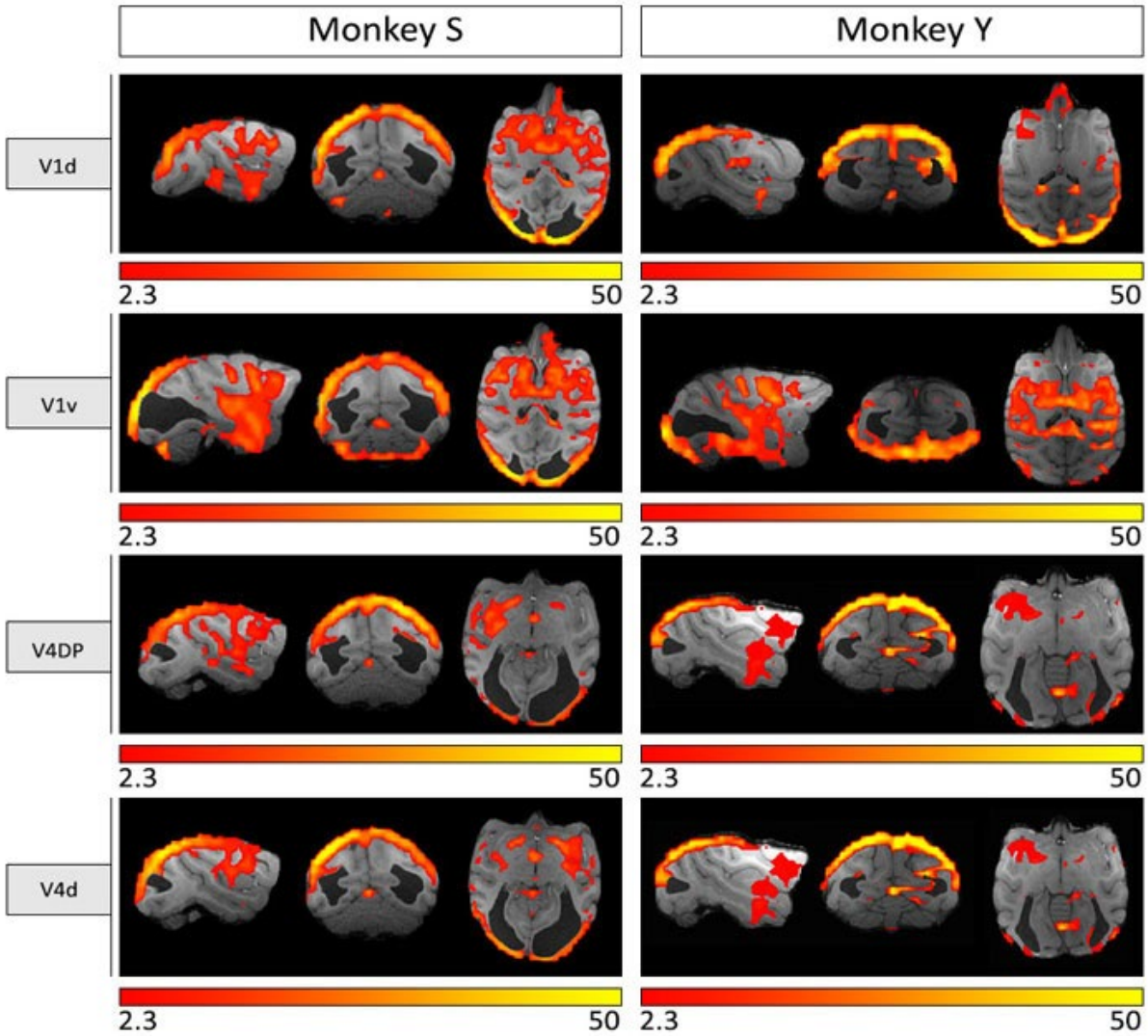


Figure 8.9 cont'd.

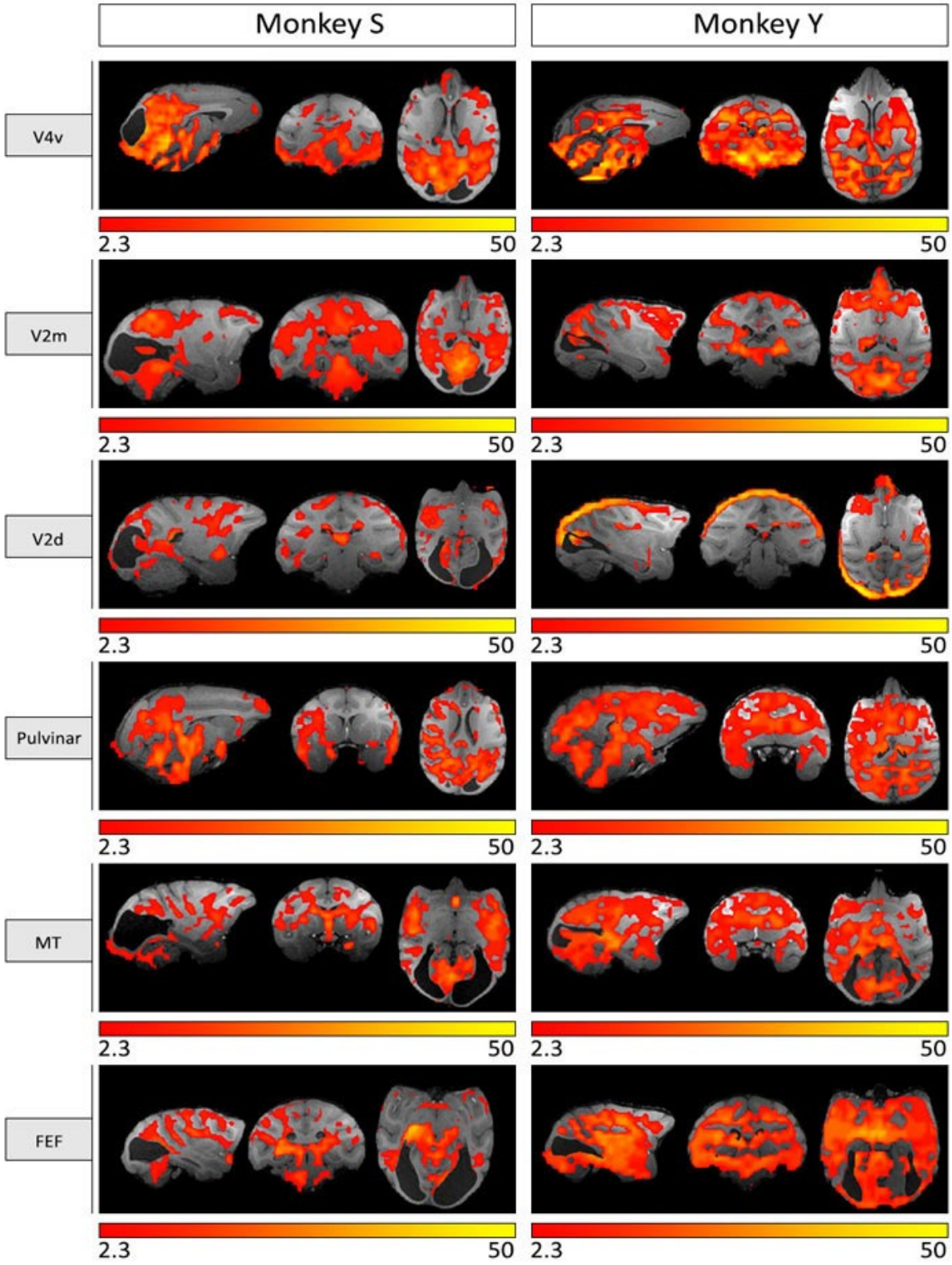


Figure 8.9 cont'd.

